Torus and Simple Surface Intersection Based on a Configuration Space Approach

Ku-Jin Kim
Department of Computer Science and Engineering
POSTECH
San 31, Hyoja-Dong
Pohang 790-784, Korea

Contents

List of Figures

Abstract

This thesis proposes efficient and robust geometric algorithms that classify and detect all possible topological types of the intersection curve of a torus and a simple surface (i.e., a plane, natural quadric, or another torus), including all degenerate conic sections and singular intersections. Given a torus and a simple surface, we treat one surface as the envelope surface of a moving ball, and the other surface as an obstacle. In this case, the *Configuration space* (*C-space*) obstacle is the same as the constant radius offset of the original obstacle, where the radius of the moving ball is taken as the offset distance. Based on the intersection between the *C-space* obstacle and the trajectory of the moving ball's center, all the intersection loops and singular contact point/curve of the original surfaces can be detected. Moreover, this thesis proposes simple geometric methods that detect and compute all degenerate conic sections (circles) in the torus/plane, torus/natural-quadric, and torus/torus intersection curves.

Chapter 1

Introduction

Plane, natural quadrics (sphere, cylinder, and cone), and torus form the so-called CSG primitives in solid modeling systems. They have been frequently used in modeling simple mechanical parts. In the Boolean operations (union, intersection, and difference) of CSG solid objects, we need to compute the intersection curves of these simple surfaces.

Many algorithms have been developed for intersecting two freeform surfaces represented in parametric and/or implicit forms. (See References [9, 19, 23] for surveys on surface intersection algorithms). In principle, they can be used for intersecting two simple surfaces. Unfortunately, there has been no single algorithm that can compute the intersection curve of two general surfaces accurately, robustly, and efficiently, while requiring no user intervention (see Chapter 12 of Hoschek and Lasser [9] for more details). In particular, when two surfaces have singular intersections, general algorithms have serious drawbacks in robustness. Even if we restrict the application of general algorithms to simple surfaces only, we cannot expect significant improvement. Therefore, general surface intersection algorithms are not appropriate for intersecting simple surfaces (such as plane, natural quadrics, and torus).

For intersecting two quadric surfaces, there are many specialized algorithms [6, 12, 13, 16, 18, 20, 26, 28, 29] that provide better solutions (in efficiency and robustness) than general surface intersection algorithms. Algebraic methods [6, 12, 13, 26, 29] (based on symbolic manipulation of surface equations) are general in the sense that they can handle all types of quadric surfaces. However, when the

algebraic algorithms are implemented using floating-point arithmetic, it is very difficult to ensure their robustness. Numerical errors in algebraic quantities may result in incorrect geometric decisions, especially when two intersecting surfaces have a nearly degenerate/singular configuration. More seriously, surface coefficients have no clear geometric meaning, which makes consistent geometric treatment more difficult. Purely symbolic computations may be used to guarantee the robustness of these algebraic algorithms; however, the problem is then how to maintain the efficiency of these algorithms.

In the case of intersecting two natural quadrics, the situation is much better. There are reliable geometric algorithms that can intersect two natural quadrics efficiently and robustly [16, 18, 20, 28]. In particular, Miller and Goldman [18] classify necessary and sufficient geometric conditions that correspond to all possible types of degenerate/singular intersections. All computations employed in these algorithms have clear geometric meanings. Moreover, they can be carried out efficiently and robustly. Together with similar geometric algorithms for computing the planar sections of natural quadrics [11, 17], these algorithms [16, 18, 20, 28] can support efficient and robust Boolean operations for CSG objects constructed by planes and natural quadrics. A natural question is how to extend the geometric coverage to include torus.

There are algebraic methods for intersecting two arbitrary cyclides [5, 10, 15]. Plane, natural quadrics, and torus are special types of cyclide. Therefore, these algorithms can be used in intersecting a torus with other simple surfaces (plane, natural quadrics, and torus). Similarly to the case of intersecting two quadric surfaces, algebraic methods are general, but they have limitations in robustness. Therefore, we need to develop geometric algorithms that can guarantee efficiency and robustness at the same time.

This thesis proposes efficient and robust geometric algorithms that classify and detect all possible topological types of the intersection curve of a torus and a simple surface (i.e., a plane, a natural quadric, or another torus), and generate one starting point on each connected component (for torus/plane, torus/sphere, and torus/cylinder intersections), or generate a set of starting points which detects all connected components (for torus/cone and torus/torus intersections). Starting points and singular points are computed by using vector/distance computations or curve/surface intersections (see Table 4.1). By solving quadratic polynomial equa-

tions, we can compute/detect starting points and singular points in torus/plane and torus/sphere intersection curves. The solutions of at most fourth order polynomial equations are required in computing/detecting starting points and singular points in the intersection curve of a torus and a cylinder (or a cone or another torus). Since polynomial equations of degree up to four have closed-form solutions using radicals, all required computations can be implemented efficiently and robustly using floating-point arithmetic. (The torus/simple-surface intersection curve itself is then numerically approximated with a sequence of cubic curve segments [1, 3, 4].) Degenerate conic sections (circles) in a torus/simple-surface intersection curve can be detected/constructed using a few additional simple geometric tests/computations.

Each algorithm proposed in this thesis reduces the surface/surface intersection problem to a curve/surface intersection problem based on a geometric transformation that generates *Configuration space* (*C-space*) obstacles [2, 14]. In robotics, the C-space approach (proposed by Lozano-Pérez [14]) reduces the collision detection problem between a moving robot and an obstacle (i.e., the intersection between two solid objects) to a simpler problem of testing the containment of a point (called the reference point of the robot) in the C-space obstacle. In the case of a robot bounded/modeled by a sphere, the C-space obstacle with respect to the sphere (robot) is essentially the same as the offset of the original obstacle [2].

Given a torus and a simple surface, we treat one surface as an obstacle and the other surface as the envelope surface of a moving ball. The C-space obstacle is then computed by offsetting the original obstacle, where the radius of the moving ball is taken as the offset radius [2]. The intersection points between the C-space obstacle and the trajectory of the moving ball's center provide a simple way of detecting and classifying the topological type and possible singularities of the intersection curve. Chapter 4 has more details of the C-space approach.

Although the C-space approach detects all singularities and completely determines the topological type of a torus/simple-surface intersection curve, it does not provide a direct classification of all degenerate conic sections in the intersection curve. Thus, we present an approach that detects all degenerate conic sections in the intersection curve. In classical geometry, it is well known that circles are the only conic sections that can be embedded in a torus. Thus, all conic sections in the torus/simple-surface intersection curve must be circles. Based on the classification of circles embedded in a torus and a simple surface, this thesis presents simple and

efficient geometric algorithms that detect and compute all degenerate conic sections (circles) in the torus/plane, torus/natural-quadric, and torus/torus intersections.

The detection of degenerate circles in torus/simple-surface intersection is important since circles can be represented exactly and efficiently. In the case of torus/plane intersection (TPI) and torus/sphere intersection (TSI) curves, degenerate circles and singular intersection curves are all rational. The real, affine TPI and TSI curves are the same as the intersection curves of two quadric surfaces. Farouki et al. [6] showed that all degenerate conic sections and singular intersections between two quadric surfaces are rational curves. Moreover, Shene and Johnstone [28] discussed the importance of conic sections in blending two natural quadrics using cyclides. We have a similar advantage in torus/simple-surface intersection. Let T_d be the offset of a torus and S_d be the offset of the other surface with respect to the offset distance d. When the offset surfaces T_d and S_d intersect in a degenerate circle of radius R, the torus and the other surface can be blended using a torus with a major radius R and a minor radius d (see Rossignac and Requicha [24, 25]).

The computation of torus/simple-surface intersection curves proceeds as follows (see Figure 1.1). In the first step, we detect and compute all degenerate circles in the intersection curve. After that, we detect and compute other components which are not circles using the C-space approach.

This thesis is organized as follows. In Chapter 2, we define some basic notations and present an elementary proof that circles are the only conic sections that can be embedded in a torus. Chapter 3 shows simple geometric algorithms that detect and compute all degenerate conic sections (circles) in a torus/simple-surface intersection curve. In Chapter 4, we explain the basic idea of the Configuration-space (C-space) approach in computing torus/simple-surface intersection curves, and compare the C-space approach with other methods. In Chapters 5–9, all possible types of intersection curves of a torus with a plane, sphere, cylinder, cone, and another torus are classified, respectively. Each chapter presents an efficient and robust geometric algorithm that detects and constructs the intersection curve (including degenerate circles) of a torus and a simple surface. Finally, in Chapter 10, we conclude this thesis and discuss possible further extensions of this thesis.

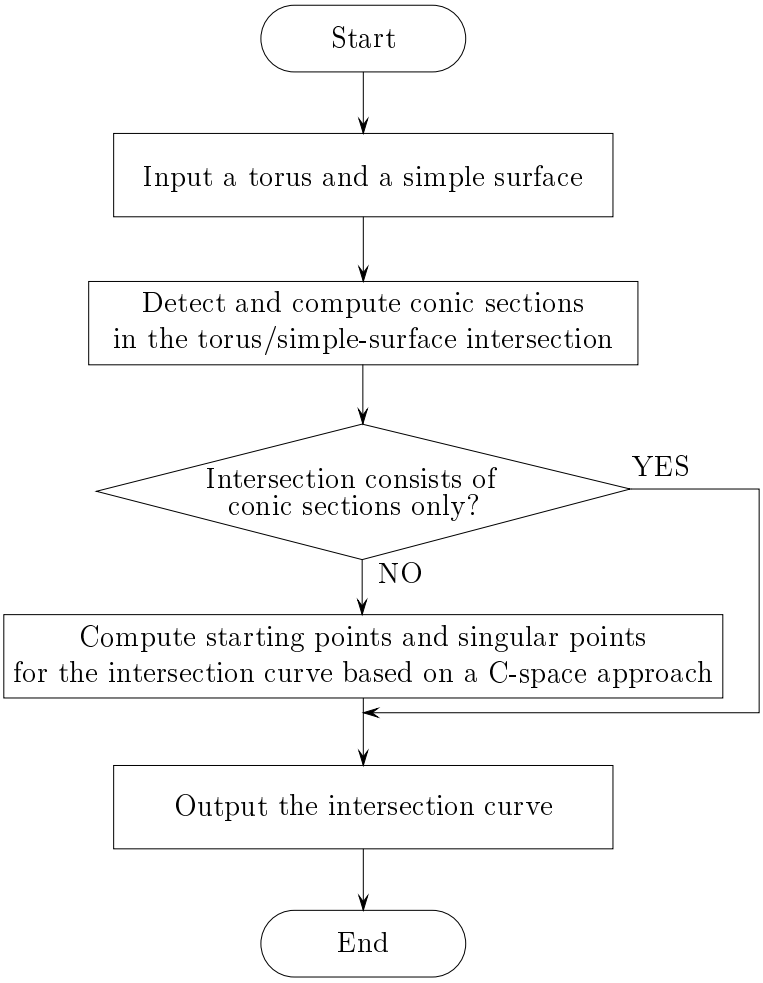

Figure 1.1: Flow chart for the torus/simple-surface intersection algorithm.

Chapter 2

Mathematical Preliminaries

In this chapter, we introduce some basic notations and background materials useful in understanding the concepts and algorithms presented in later chapters. In Section 2.1, we introduce notations for geometric primitives that will be used in this thesis. Section 2.2 presents an elementary proof that circles are the only conic sections that can be embedded in a torus. Moreover, Section 2.2 classifies the circles embedded in a torus as three special types: (i) profile circles, (ii) cross-sectional circles, and (iii) Yvone-Villarceau circles.

2.1 Notations for Geometric Primitives

Notations for basic geometric primitives are summarized in Table 2.1, where 3D points/vectors are represented in boldface.

When we assume that the torus is given in a standard form $T_{r,R}((0,0,0),\mathbf{e}_3)$, the torus can be constructed by rotating the circle $C_r((R,0,0),\mathbf{e}_2)$ about the z-axis (see Figure 2.1). At this time, r and R are the minor and major radii of the torus, respectively. Moreover, the circle $C_R((0,0,0),\mathbf{e}_3)$ (which is constructed by rotating the point $(R,0,0)$ about the z-axis) is called the main circle of the torus, and the plane which contains the main circle is called the main plane of the torus.

Note that the torus $T_{r,R}(\mathbf{p},\mathbf{N})$ is the boundary of the sweeping volume $\cup_{\mathbf{q}\in C_R(\mathbf{p},\mathbf{N})} B_r(\mathbf{q})$. When the ball center $\mathbf{q}$ is located on the main circle of the torus (i.e., $\mathbf{q}\in C_R(\mathbf{p},\mathbf{N})$), the torus $T_{r,R}(\mathbf{p},\mathbf{N})$ and the ball $B_r(\mathbf{q})$ share a cross-sectional circle $C_r(\mathbf{q},\mathbf{N_q})$, where $\mathbf{N_q}=\mathbf{N}\times\frac{\mathbf{q}-\mathbf{p}}{\|\mathbf{q}-\mathbf{p}\|}$. Figure 2.2 shows three different types of tori

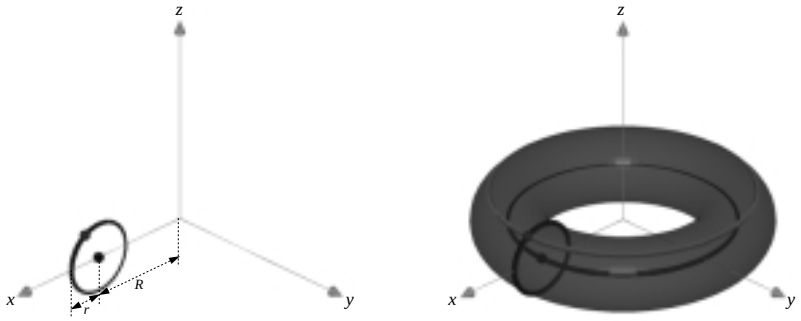

(a) (b)

Figure 2.1: Torus in a standard form.

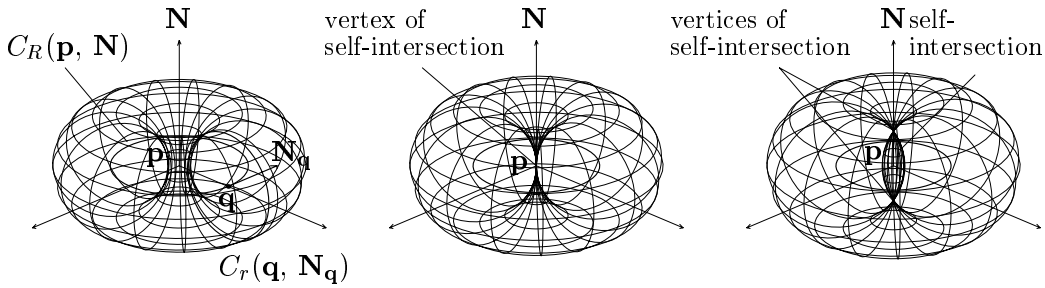

(a) $T_{r,R}(\mathbf{p},\mathbf{N})$ with $r < R$ (b)$T_{r,R}(\mathbf{p},\mathbf{N})$ with $r = R$ (c)$T_{r,R}(\mathbf{p},\mathbf{N})$ with $r > R$

Figure 2.2: The three types of tori.

$T_{r,R}(\mathbf{p}, \mathbf{N})$: for (a) $r < R$, (b) $r = R$, and (c) $r > R$. In this paper, we assume that the input torus is always of the first type; that is, we assume $0 < r < R$. However, when we offset the torus for the generation of a C-space obstacle, the resulting C-space torus may be of the type (b) or (c).

In this thesis, we consider four topological types of a surface patch: (i) a disk type, (ii) a degenerate disk type, (iii) a cylindrical type, and (iii) a degenerate cylindrical type. A surface patch of disk type represents a continuous surface without an interior hole, i.e., the boundary curve consists of a closed loop (Figure 2.3(a)). A surface patch of degenerate disk type represents a continuous surface with a self intersection point on the boundary curve (Figure 2.3(b)). A surface patch of cylindrical type represents a continuous surface with an interior hole, i.e., the boundary curve consists of two closed loops with no self-intersection (Figure 2.3(c)). A surface patch of degenerate cylindrical type represents a continuous surface with an interior hole and the boundary curve consists of an 8-figured loop (Figure 2.3(d)).

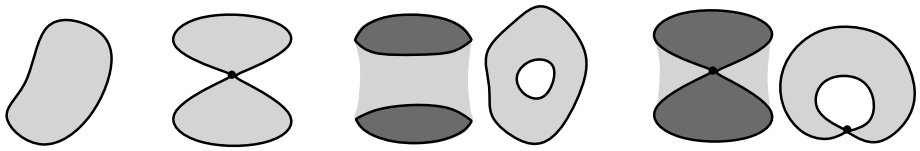

Figure 2.3: The topological types of a surface patch.

We define Bdr as the boundary of a closed (volumetric) region in $\mathbb{R}^3$. For example, $Bdr(\cup B_r(C(t)))$ means the envelope surface of a moving ball (with radius r) along a center trajectory $C(t)$. For the sake of simplicity, we use the notation $\cup B_r(C_i)$ (or $\cup S_r(C_i)$) instead of $\cup_{\mathbf{q} \in C_i} B_r(\mathbf{q})$ (or $\cup_{\mathbf{q} \in C_i} S_r(\mathbf{q})$), for a connected segment C_i.

2.2 Degenerate Conic Sections Embedded in a Torus

In this subsection, we show that conic sections that can be embedded in a torus must be circles. Since conic sections are planar curves, each conic section embedded in a torus must be in the intersection of the torus with a plane. Therefore, we show that all conic sections in the Torus/Plane Intersection (TPI) curves must be circles. We

$\mathbf{e}_1, \mathbf{e}_2, \mathbf{e}_3 \in S^2$	standard unit vectors: $\mathbf{e}_1 = (1,0,0), \mathbf{e}_2 = (0,1,0), \mathbf{e}_3 = (0,0,1)$
$\mathbf{p}, \mathbf{q} \in I\!R^3$	3D points
$\mathbf{N} \in S^2$	unit vector
$\mathbf{N_p}, \mathbf{N_q} \in S^2$	unit vectors with tails at $\mathbf{p}$ and $\mathbf{q}$, respectively
$L(\mathbf{p}, \mathbf{N})$	the plane that contains $\mathbf{p}$ and is normal to $\mathbf{N}$
$l^+(\mathbf{p}, \mathbf{N})$	infinite half-line: $\{ \mathbf{p} + t\mathbf{N} \in I\!R^3 \mid t \geq 0 \}$
$l(\mathbf{p}, \mathbf{N})$	infinite line: $\{ \mathbf{p} + t\mathbf{N} \in I\!R^3 \mid t \in I\!R \}$
$B_\delta(\mathbf{p})$	the ball with center $\mathbf{p}$ and radius δ: $\{ \mathbf{q} \in I\!R^3 \mid \|\mathbf{q} - \mathbf{p}\| \leq \delta \}$
$S_\delta(\mathbf{p})$	the sphere with center $\mathbf{p}$ and radius δ: $\{ \mathbf{q} \in I\!R^3 \mid \|\mathbf{q} - \mathbf{p}\| = \delta \}$
$C_d(\mathbf{p}, \mathbf{N})$	the circle with radius d and center $\mathbf{p}$, and contained in the plane $L(\mathbf{p}, \mathbf{N})$
$Y_\delta(\mathbf{p}, \mathbf{N})$	the cylinder with radius δ and axis $l(\mathbf{p}, \mathbf{N})$
$K_\theta(\mathbf{p}, \mathbf{N})$	the cone with vertex $\mathbf{p}$ and the unit direction vector $\mathbf{N}$, and half angle θ
$K_{r,\theta}(\mathbf{p}, \mathbf{N})$	the cone which is an envelope surface of moving ball along center trajectory $l(t) = \mathbf{p} + t\mathbf{N}$ $(t \geq 0)$ with radius function $\lvert r + \|l(t)\| \sin\theta \rvert$
$T_{r,R}(\mathbf{p}, \mathbf{N})$	the torus with minor radius r, major radius R, center $\mathbf{p}$, and main circle $C_R(\mathbf{p}, \mathbf{N})$

Table 2.1: Notations for geometric primitives.

show that, if the TPI curve is factorized into two conic sections, each conic section must be a circle.

Let's assume that a torus T intersects with a plane L. By applying translation and rotation if necessary, we may assume that the torus T is given in a standard position and its main circle is contained in the xy-plane: $T = T_{r,R}(\mathbf{0}, \mathbf{e}_3)$, where $r > 0$, $R > 0$, $\mathbf{0} = (0, 0, 0)$, and $\mathbf{e}_3 = (0, 0, 1)$. Note that the given plane L must be one of the following three types:

$$\begin{aligned} &z = b, \\ &y = b, \\ &z = ay + b, \ (a \neq 0). \end{aligned}$$

For each of above cases, we classify the conic sections in the TPI curve.

2.2.1 The Case of $L : z = b$

In this case, the plane L is parallel to the xy-plane. Thus, if T and L intersect, the TPI curve is composed of one or two profile circles.

2.2.2 The Case of $L : y = b$

An implicit surface equation of the torus T is given as follows:

$$(x^2 + y^2 + z^2 + R^2 - r^2)^2 - 4R^2(x^2 + y^2) = 0.$$

The intersection curve between T and $L : y = b$ is represented as:

$$(x^2 + z^2 + b^2 + R^2 - r^2)^2 - 4R^2(x^2 + b^2) = 0,$$

and equivalently:

$$\begin{aligned} x^4 + 2x^2z^2 + z^4 + 2(b^2 - r^2 - R^2)x^2 + 2(b^2 - r^2 + R^2)z^2 \\ +(b^2 - r^2 + R^2)^2 - 4b^2R^2 = 0. \end{aligned} \tag{2.1}$$

If the intersection curve between T and L includes one or two conic sections, Equation (2.1) is factorized as follows:

$$(Ax^2 + Bz^2 + Cxz + Dx + Ez + F)(Gx^2 + Hz^2 + Ixz + Jx + Kz + M) = 0. \tag{2.2}$$

By multiplying each term by a constant if necessary, we may assume that $A = G = 1$:

$$(x^2 + Bz^2 + Cxz + Dx + Ez + F)(x^2 + Hz^2 + Ixz + Jx + Kz + M) = 0. \quad (2.3)$$

Equation (2.3) is expanded as follows:

$$x^4 + (C + I)x^3z + (B + CI + H)x^2z^2 + (BI + CH)xz^3 + BHz^4 + \cdots = 0. \quad (2.4)$$

Comparing Equations (2.1) and (2.4), we obtain the following results:

$$\begin{array}{lll} & B, H \neq 0, & \\ \text{from } x^3z \text{ term}: & C + I = 0, & I = -C, \\ \text{from } z^4 \text{ term}: & BH = 1, & H = \dfrac{1}{B}, \\ \text{from } x^2z^2 \text{ term}: & CI + B + H = 2, & C^2 = \frac{(B-1)^2}{B}, \\ \text{from } xz^3 \text{ term}: & CH + BI = 0, & C(H - B) = C\frac{1-B^2}{B} = 0. \end{array}$$

From the relation $C\frac{1-B^2}{B} = 0$, we have: $C = 0$ or $B = \pm 1$.

Let's consider three cases: $C = 0$, $B = 1$, and $B = -1$.

- If $C = 0$, then $C^2 = \frac{(B-1)^2}{B} = 0$; thus $B = 1$.
- If $B = 1$, then $C^2 = \frac{(B-1)^2}{B} = 0$; thus $C = 0$.
- If $B = -1$, then $C^2 = \frac{(B-1)^2}{B} = -4$, which is impossible.

Thus, we have

$$B = 1, \quad C = 0, \quad H = 1, \quad \text{and} \quad I = 0.$$

Equation (2.3) is reformulated as:

$$(x^2 + z^2 + Dx + Ez + F)(x^2 + z^2 + Jx + Kz + M) = 0, \quad (2.5)$$

and equivalently:

$$\begin{array}{l} x^4 + 2x^2z^2 + z^4 + (D + J)x^3 + (E + K)x^2z + (D + J)xz^2 + (E + K)z^3 \\ +(DJ + F + M)x^2 + (DK + EJ)xz + (EK + F + M)z^2 \\ +(DM + FJ)x + (EM + FK)z + FM = 0. \end{array} \quad (2.6)$$

Comparing x^3 and x^2z terms of Equation (2.1) and (2.6), we obtain that:

$$\begin{aligned} D + J = 0, \quad J = -D, \\ E + K = 0, \quad K = -E. \end{aligned}$$

Thus, Equation (2.5) is reformulated as follows:

$$(x^2 + z^2 + Dx + Ez + F)(x^2 + z^2 - Dx - Ez + M) = 0, \tag{2.7}$$

and equivalently:

$$\begin{aligned} &x^4 + 2x^2z^2 + z^4 + (F - D^2 + M)x^2 + (F - E^2 + M)z^2 - 2DExz \\ &+D(M - F)x + E(M - F)z + FM = 0. \end{aligned} \tag{2.8}$$

Comparing xz term of Equations (2.1) and (2.8), we obtain:

$$DE = 0,$$

thus, $D = 0$ or $E = 0$.

Claim 2.2.1 *$E = 0$:*

Proof: Suppose $E \neq 0$. Then we must have $D = 0$. The difference between the z^2 and x^2 terms in Equations (2.1) and (2.8) is

$$\begin{aligned} 2(b^2 - r^2 + R^2) - 2(b^2 - r^2 - R^2) = 4R^2, \\ (F - E^2 + M) - (F - D^2 + M) = D^2 - E^2. \end{aligned} \tag{2.9}$$

We derive that $D^2 - E^2 = -E^2 = 4R^2 > 0$. This is a contradiction. □

From Equation (2.9) and the fact $E = 0$, we have

$$D^2 - E^2 = D^2 = 4R^2,$$

thus $D = \pm 2R$.

Comparing the x terms of Equations (2.1) and (2.8), we obtain the following relation

$$\begin{aligned} &D(M - F) = 0, \\ &\pm 2R(M - F) = 0, \\ &M = F. \end{aligned} \tag{2.10}$$

Comparing the x^2 terms of Equations (2.1) and (2.8), we have

$$\begin{aligned} 2F - D^2 = 2F - 4R^2 &= 2(b^2 - r^2 - R^2), \\ F &= b^2 - r^2 + R^2. \end{aligned} \tag{2.11}$$

Equation (2.7) is reformulated as follows:

$$\begin{aligned} &(x^2 + z^2 + 2Rx + F)(x^2 + z^2 - 2Rx + F) = 0, \\ &((x+R)^2 + z^2 + F - R^2)((x-R)^2 + z^2 + F - R^2) = 0, \\ &((x+R)^2 + z^2 + b^2 - r^2)((x-R)^2 + z^2 + b^2 - r^2) = 0, \end{aligned} \tag{2.12}$$

and equivalently:

$$x^4 + 2x^2z^2 + z^4 + 2(b^2 - r^2 - R^2)x^2 + 2(b^2 - r^2 + R^2)z^2 + (b^2 - r^2 + R^2)^2 = 0. \tag{2.13}$$

Comparing the constant term of Equations (2.1) and (2.13),

$$\begin{aligned} (b^2 - r^2 + R^2)^2 &= (b^2 - r^2 + R^2)^2 - 4b^2R^2, \\ 4b^2R^2 &= 0, \\ b &= 0. \end{aligned} \tag{2.14}$$

Equation (2.12) is reformulated as follows:

$$((x+R)^2 + z^2 - r^2)((x-R)^2 + z^2 - r^2) = 0. \tag{2.15}$$

When given plane L is $y = b$, T and L intersect in conic sections if and only if $b = 0$. In the intersection curve between T and L, the conic sections are composed of two circles on xz-plane, whose radii are r and centered at $(R, 0, 0)$ and $(-R, 0, 0)$, respectively.

2.2.3 The Case of $L : z = ay + b, (a \neq 0)$

The implicit surface equation of T is as follows:

$$(x^2 + y^2 + z^2 + R^2 - r^2)^2 - 4R^2(x^2 + y^2) = 0.$$

We may represent L as a parametric form: $\mathbf{p} + s\mathbf{v}_1 + t\mathbf{v}_2$, where $\mathbf{p} = (0, 0, b)$, $\mathbf{v}_1 = (1, 0, 0)$, and $\mathbf{v}_2 = \left(0, \frac{1}{\sqrt{1+a^2}}, \frac{a}{\sqrt{1+a^2}}\right)$. The xyz-values of an arbitrary

point on the plane L are represented as st-values as follows:

$$\begin{aligned} x &= p_x + sv_{1x} + tv_{2x} = s, \\ y &= p_y + sv_{1y} + tv_{2y} = \frac{t}{\sqrt{1+a^2}}, \\ z &= p_z + sv_{1z} + tv_{2z} = \frac{at}{\sqrt{1+a^2}} + b, \end{aligned} \tag{2.16}$$

where $\mathbf{v}_1 = (v_{1x}, v_{1y}, v_{1z})$ and $\mathbf{v}_2 = (v_{2x}, v_{2y}, v_{2z})$. By substituting xyz-values of Equation (2.16) for xyz-values of the implicit surface equation of T, we obtain the TPI curve on L as follows:

$$\left(s^2 + t^2 + \frac{2ab}{\sqrt{1+a^2}}t + b^2 - r^2 + R^2\right)^2 - 4R^2\left(s^2 + \frac{t^2}{1+a^2}\right) = 0. \tag{2.17}$$

and equivalently:

$$\begin{aligned} &s^4 + 2s^2t^2 + t^4 + \frac{4ab}{\sqrt{1+a^2}}s^2t + \frac{4ab}{\sqrt{1+a^2}}t^3 + 2(b^2 - r^2 - R^2)s^2 \\ &+ \left[2(b^2 - r^2 + R^2) + \frac{4(a^2b^2 - R^2)}{1+a^2}\right]t^2 + \frac{4ab(b^2 - r^2 + R^2)}{\sqrt{1+a^2}}t + (b^2 - r^2 + R^2)^2 = 0. \end{aligned} \tag{2.18}$$

If the TPI curve includes conic sections, then Equation (2.18) is factorized as follows:

$$(As^2 + Bt^2 + Cst + Ds + Et + F)(Gs^2 + Ht^2 + Ist + Js + Kt + M) = 0. \tag{2.19}$$

Comparing s^4, s^3t, t^4, s^2t^2, st^3, and s^3 terms of Equations (2.18) and (2.19), under the same derivation in Section 2.2.2, we obtain that

$$A = 1, \quad B = 1, \quad C = 0, \quad G = 1, \quad H = 1, \quad I = 0, \quad \text{and} \quad J = -D.$$

Equation (2.19) is reformulated as:

$$(s^2 + t^2 + Ds + Et + F)(s^2 + t^2 - Ds + Kt + M) = 0, \tag{2.20}$$

and equivalently:

$$\begin{aligned} &s^4 + 2s^2t^2 + t^4 + (E+K)s^2t + (E+K)t^3 + (F - D^2 + M)s^2 \\ &+D(K-E)st + (EK + F + M)t^2 + D(M-F)s + (EM + FK)t + FM = 0. \end{aligned} \tag{2.21}$$

Comparing st and s terms of Equations (2.18) and (2.21), we obtain:

$$\begin{aligned} D(K-E) &= 0, \\ D(M-F) &= 0. \end{aligned} \tag{2.22}$$

Claim 2.2.2 *$D \neq 0$:*

Proof: Suppose that $D = 0$. Equation (2.21) is reformulated as follows:

$$\begin{aligned} &s^4 + 2s^2t^2 + t^4 + (E+K)s^2t + (E+K)t^3 + (F+M)s^2 \\ &+(EK+F+M)t^2 + (EM+FK)t + FM = 0. \end{aligned} \tag{2.23}$$

Comparing s^2t, s^2, and t^2 terms of Equations (2.18) and (2.23), we have

$$E + K = \frac{4ab}{\sqrt{1+a^2}}, \tag{2.24}$$

$$F + M = 2(b^2 - r^2 - R^2), \tag{2.25}$$

$$EK + F + M = 2(b^2 - r^2 + R^2) + \frac{4(a^2b^2 - R^2)}{1+a^2}. \tag{2.26}$$

Then we have

$$\begin{aligned} EK &= (EK + F + M) - (F + M) \\ &= 4R^2 + \frac{4(a^2b^2 - R^2)}{1+a^2} = \frac{4a^2(R^2+b^2)}{1+a^2}, \end{aligned} \tag{2.27}$$

and

$$\begin{aligned} (E-K)^2 &= (E+K)^2 - 4EK, \\ &= \frac{16a^2b^2}{1+a^2} - \frac{16a^2(R^2+b^2)}{1+a^2}, \\ &= -\frac{16a^2R^2}{1+a^2} < 0, \end{aligned} \tag{2.28}$$

which is impossible. Therefore, we must have $D \neq 0$. □

From Equation (2.22) and the fact that $D \neq 0$, we have

$$K = E, \quad \text{and} \quad M = F.$$

Equation (2.20) is reformulated as follows:

$$(s^2 + t^2 + Ds + Et + F)(s^2 + t^2 - Ds + Et + F) = 0, \tag{2.29}$$

and equivalently:

$$s^4 + 2s^2t^2 + t^4 + 2Es^2t + 2Et^3 + (2F - D^2)s^2 + (2F + E^2)t^2 + 2EFt + F^2 = 0. \tag{2.30}$$

Comparing s^2t, s^2, t^2, t, and constant terms of Equations (2.18) and (2.30),

$$\begin{aligned}
2E &= \frac{4ab}{\sqrt{1+a^2}}, && (2.31)\\
2F - D^2 &= 2(b^2 - r^2 - R^2), && (2.32)\\
2F + E^2 &= 2(b^2 - r^2 + R^2) + \frac{4(a^2b^2 - R^2)}{1+a^2}, && (2.33)\\
2EF &= \frac{4ab(b^2 - r^2 + R^2)}{\sqrt{1+a^2}}, && (2.34)\\
F^2 &= (b^2 - r^2 + R^2)^2. && (2.35)
\end{aligned}$$

Claim 2.2.3 *$b = 0$:*

Proof: Assume $b \neq 0$. Since we know that $a \neq 0$, from Equations (2.31) and (2.34),

$$\begin{aligned}
2E &= \frac{4ab}{\sqrt{1+a^2}} \neq 0,\\
F &= \frac{2EF}{2E} = b^2 - r^2 + R^2.
\end{aligned}$$

From Equations (2.31) and (2.33),

$$\begin{aligned}
2F + E^2 &= 2(b^2 - r^2 + R^2) + \frac{4a^2b^2}{1+a^2}\\
&= 2(b^2 - r^2 + R^2) + \frac{4(a^2b^2 - R^2)}{1+a^2}, && (2.36)\\
\frac{-4R^2}{1+a^2} &= 0,
\end{aligned}$$

which is impossible. Thus, we must have b = 0. □

In the proof of Claim 2.2.3, we know that $F \neq b^2 - r^2 + R^2$. Thus, from Equation (2.35) and the fact $b = 0$ we obtain

$$F = -(b^2 - r^2 + R^2) = r^2 - R^2.$$

From Equation (2.32) and the facts $b = 0$ and $F = r^2 - R^2$,

$$D = \pm 2r.$$

From Equation (2.31) and the fact $b = 0$, we obtain

$$E = 0.$$

From Equation (2.33), we obtain:

$$\begin{aligned} 2(r^2 - R^2) &= R^2 - r^2 - \frac{4R^2}{1 + a^2}, \\ a &= \pm \frac{r}{\sqrt{R^2 - r^2}}, \end{aligned}$$

where $R > r > 0$.

Equation (2.29) is reformulated as:

$$\begin{aligned} &(s^2 + t^2 + 2rs + r^2 - R^2)(s^2 + t^2 - 2rs + r^2 - R^2) = 0, \\ &((s + r)^2 + t^2 - R^2)((s - r)^2 + t^2 - R^2) = 0. \end{aligned} \tag{2.37}$$

When L has the form $z = ay + b$, where $a \neq 0$, the TPI curve includes conic sections if and only if the case of

$$\begin{aligned} a &= \pm \frac{r}{\sqrt{R^2 - r^2}}, \\ b &= 0, \end{aligned}$$

where $R > r > 0$.

2.2.4 Classification of the Conic Sections on a Torus

The only conic section which can be embedded in a torus $T = T_{r,R}(\mathbf{p}, \mathbf{N})$ is a circle, and the circle belongs to one of the following classes:

- profile circles of T
- cross sectional circles of T
- Yvone-Villarceau circles of T

Chapter 3

Conic Sections in Torus and Simple Surface Intersections

In this chapter, we present efficient and robust geometric algorithms that can detect and compute all conic sections in Torus/Plane Intersection (TPI), Torus/natural-Quadric Intersection (TQI), and Torus/Torus Intersection (TTI). These algorithms are based on a simple classification of all conic sections that can be embedded in a torus. That is, they must be circles of special types: (i) profile circles, (ii) cross-sectional circles, and (iii) Yvone-Villarceau circles. Based on this classification, we formulate all necessary and sufficient conditions (except one condition in the torus-cone case and one in the torus-torus case) in algebraic and semi-algebraic constraints.

Let Γ_T and Γ_Q denote the sets of all circles that can be embedded in a torus T and a natural-quadric Q, respectively. The two surfaces T and Q intersect in circles if and only if the two sets Γ_T and Γ_Q of circles have a non-empty intersection: $\Gamma_T \cap \Gamma_Q \neq \emptyset$; that is, there are some circles that can be embedded in T and Q simultaneously.

In Section 3.1, we will show that the set Γ_T can be decomposed into five disjoint subsets: Γ_T^i $(i = 1, \ldots, 5)$, each of which is given as a one-parameter family of circles. Let $C(t) \in \Gamma_T^i$ be a one-parameter family of circles that are embedded in the torus T with their centers at $p(t)$, radius $r(t)$, and each contained in the plane with normal $N(t)$. Using the circle information: $p(t), r(t), N(t)$, we can derive the conditions for some circles $C(t)$ to be embedded in Q (i.e., $C(t) \in \Gamma_Q$).

The rest of this chapter is organized as follows. Sections 3.1 and 3.2 classify

all circles that can be embedded in a torus, sphere, cylinder, and cone. Based on this classification, Sections 3.3–3.7 present geometric algorithms that can detect and compute all conic sections in the torus/plane, torus/natural-quadric, and torus/torus intersection curves.

3.1 Circles on a Torus

Conic sections embedded in a torus must be circles of special types (see Figure 3.1): (i) profile circles, (ii) cross-sectional circles, and (iii) Yvone-Villarceau circles. This classification is a well-known result in classical geometry [22]. In Section 2.2, we proved this fact based on deriving elementary formulae. We present illustrative examples of these special types of circles.

(a) Profile circles (b) Cross-sectional circles (c) Yvone-Villarceau circles

Figure 3.1: Circles on a torus.

3.1.1 Profile Circles

For the sake of simplicity, we assume that the torus is given in a standard form $T_{r,R}((0,0,0),\mathbf{e}_3)$ (see Figure 2.1 in Section 2.1):

$$(x^2+y^2+z^2+R^2-r^2)^2-4R^2(x^2+y^2)=0,$$

where r and R are the minor and major radii of the torus. Note that the torus can be constructed by rotating the circle $C_r((R,0,0),\mathbf{e}_2)$ about the z-axis. Thus, it can be represented in a parametric form using two angular parameters θ and ϕ:

$$((R+r\cos\theta)\cos\phi,(R+r\cos\theta)\sin\phi,r\sin\theta).$$

Each profile circle is obtained by the rotational sweep of a point on the circle $C_r((R,0,0),\mathbf{e}_2)$ about the z-axis. Two concentric profile circles are obtained by intersecting the torus with a plane parallel to the xy-plane (see Figure 3.2(a)). The set of centers of profile circles forms a line segment on the z-axis:

$$\gamma_T^p = \{(0,0,z_0) \mid -r \leq z_0 \leq r\}.$$

To each center point $(0,0,z_0) \in \gamma_T^p$, there correspond two profiles circles of radii: $R \pm \sqrt{r^2 - z_0^2}$, both of which are contained in the plane $z = z_0$. Therefore, the set of all profiles circles of T is given as follows:

$$\Gamma_T^p = \{C_{R\pm\sqrt{r^2-z_0^2}}((0,0,z_0),\mathbf{e}_3) \mid -r \leq z_0 \leq r\}.$$

The set Γ_T^p can be represented as a disjoint union of the following two sets of circles, each of which is a one-parameter family of circles:

$$\Gamma_T^{p,-} = \{C_{R-\sqrt{r^2-z_0^2}}((0,0,z_0),\mathbf{e}_3) \mid -r \leq z_0 < r\},$$
$$\Gamma_T^{p,+} = \{C_{R+\sqrt{r^2-z_0^2}}((0,0,z_0),\mathbf{e}_3) \mid -r < z_0 \leq r\}.$$

The sets of centers of circles contained in $\Gamma_T^{p,-}$ and $\Gamma_T^{p,+}$ are given as follows:

$$\gamma_T^{p,-} = \{(0,0,z_0) \mid -r \leq z_0 < r\},$$
$$\gamma_T^{p,+} = \{(0,0,z_0) \mid -r < z_0 \leq r\}.$$

3.1.2 Cross-Sectional Circles

Each cross-sectional circle is obtained by rotating the circle $C_r((R,0,0),\mathbf{e}_2)$ by an angle ϕ_0 about the z-axis:

$$\begin{aligned} &C_r((R\cos\phi_0, R\sin\phi_0, 0), (-\sin\phi_0, \cos\phi_0, 0)) \\ =\ &\{((R + r\cos\theta)\cos\phi_0, (R + r\cos\theta)\sin\phi_0, r\sin\theta) | 0 \leq \theta < 2\pi\}. \end{aligned}$$

The set of all cross-sectional circles is:

$$\Gamma_T^c = \{C_r((R\cos\phi_0, R\sin\phi_0, 0), (-\sin\phi_0, \cos\phi_0, 0)) |\ 0 \leq \phi_0 < 2\pi\}.$$

The set of centers of cross-sectional circles is the same as the major circle of the torus T:

$$\gamma_T^c = \{(R\cos\phi_0, R\sin\phi_0, 0) \mid 0 \leq \phi_0 < 2\pi\} = C_R((0,0,0),\mathbf{e}_3).$$

Two coplanar cross-sectional circles are obtained by intersecting the torus with a plane containing the z-axis (see Figure 3.2(b)).

3.1.3 Yvone-Villarceau Circles

When the major radius R is larger than the minor radius r, the plane L_0 defined by an implicit equation:

$$rx + \left(\sqrt{R^2 - r^2}\right) z = 0$$

intersects with the torus T in two circles called Yvone-Villarceau circles (see Figure 3.2(c)).

The plane L_0 has a unit normal vector:

$$\left(\frac{r}{R}, 0, \frac{\sqrt{R^2 - r^2}}{R}\right).$$

The torus T and the plane L_0 intersect tangentially at two points:

$$\left(\pm\frac{R^2 - r^2}{R}, 0, \mp\frac{r}{R}\sqrt{R^2 - r^2}\right),$$

which are also the intersection points of two Yvone-Villarceau circles contained in the plane L_0. The whole y-axis ($x = z = 0$) is contained in the plane L_0. When we intersect the y-axis: $\{(0, t, 0) \mid t \in \mathbb{R}\}$ with the torus T, we get the following four solutions of t:

$$\begin{aligned}
(t^2 + R^2 - r^2)^2 - 4R^2t^2 &= 0, \\
(t^2 + R^2 - r^2) \pm 2Rt &= 0, \\
(t \pm R)^2 - r^2 &= 0, \\
t &= \pm R \pm r
\end{aligned}$$

Based on these four values of t and the relative configuration of two Yvone-Villarceau circles on the plane L_0, we can easily tell that the points $(0, -R-r, 0)$ and $(0, R - r, 0)$ are two extreme points (along the y-direction) of one Yvone-Villarceau circle. This circle has center $(0, -r, 0)$ and radius R. Moreover, the two extreme points of the circle along the x-direction are given as follows:

$$\left(\pm\sqrt{R^2 - r^2}, -r, \mp r\right).$$

Similarly, the points $(0, -R + r, 0)$ and $(0, R + r, 0)$ are two extreme points of the other Yvone-Villarceau circle with center $(0, r, 0)$ and radius R. The two extreme points along the x-direction are given as follows:

$$\left(\pm\sqrt{R^2 - r^2}, r, \mp r\right).$$

When we rotate the plane L_0 by angle ϕ_0 around the z-axis while maintaining the same slope with the xy-plane, we obtain a plane L_{ϕ_0} with a unit normal vector:

$$\left(\frac{r}{R}\cos\phi_0, \frac{r}{R}\sin\phi_0, \frac{\sqrt{R^2-r^2}}{R}\right).$$

Therefore, the plane L_{ϕ_0} has an implicit equation:

$$(r\cos\phi_0)x + (r\sin\phi_0)y + \left(\sqrt{R^2-r^2}\right)z = 0.$$

This plane L_{ϕ_0} also intersects with the torus T in two Yvone-Villarceau circles of radius R. The center of one Yvone-Villarceau circle is obtained by rotating $(0,-r,0)$ by angle ϕ_0 in the xy-plane:

$$(r\sin\phi_0, -r\cos\phi_0, 0).$$

The center of the other Yvone-Villarceau circle is obtained by rotating $(0,r,0)$:

$$(-r\sin\phi_0, r\cos\phi_0, 0).$$

As we rotate the plane L_{ϕ_0}, the center of one Yvone-Villarceau circle traces out a circle of radius r:

$$\gamma_T^{YV,-} = \{(r\sin\phi_0, -r\cos\phi_0, 0) \mid 0 \le \phi_0 < 2\pi\}.$$

The center of the other Yvone-Villarceau circle traces out another circle of radius r:

$$\gamma_T^{YV,+} = \{(-r\sin\phi_0, r\cos\phi_0, 0) \mid 0 \le \phi_0 < 2\pi\}.$$

The corresponding sets of Yvone-Villarceau circles of T are given as follows:

$$\begin{aligned}
\Gamma_T^{YV,-} &= \{C_R((rs_{\phi_0}, -rc_{\phi_0}, 0), (ac_{\phi_0}, as_{\phi_0}, \sqrt{1-a^2}))\mid 0 \le \phi_0 < 2\pi\},\\
\Gamma_T^{YV,+} &= \{C_R((-rs_{\phi_0}, rc_{\phi_0}, 0), (ac_{\phi_0}, as_{\phi_0}, \sqrt{1-a^2}))\mid 0 \le \phi_0 < 2\pi\},
\end{aligned}$$

where $c_{\phi_0} = \cos\phi_0$, $s_{\phi_0} = \sin\phi_0$, and $a = r/R$.

3.2 Circles on Natural Quadrics

In this section, we classify all circles that can be embedded in natural quadrics. By comparing these circles with those embedded in a torus, we can detect and compute all conic sections (i.e., circles) in the intersection curve of a torus and a natural quadric.

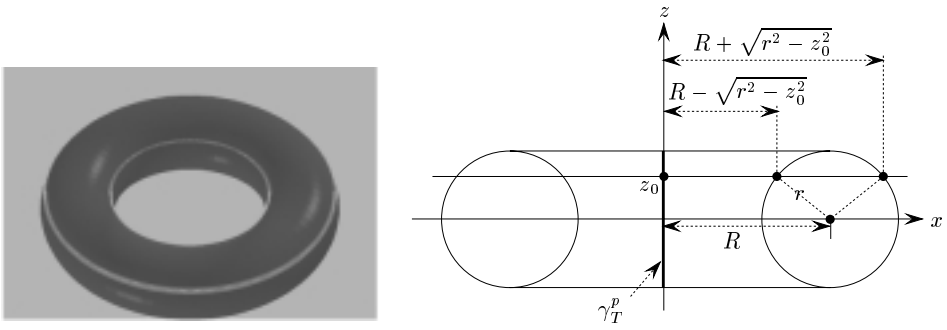

(a) Profile circles in TPI

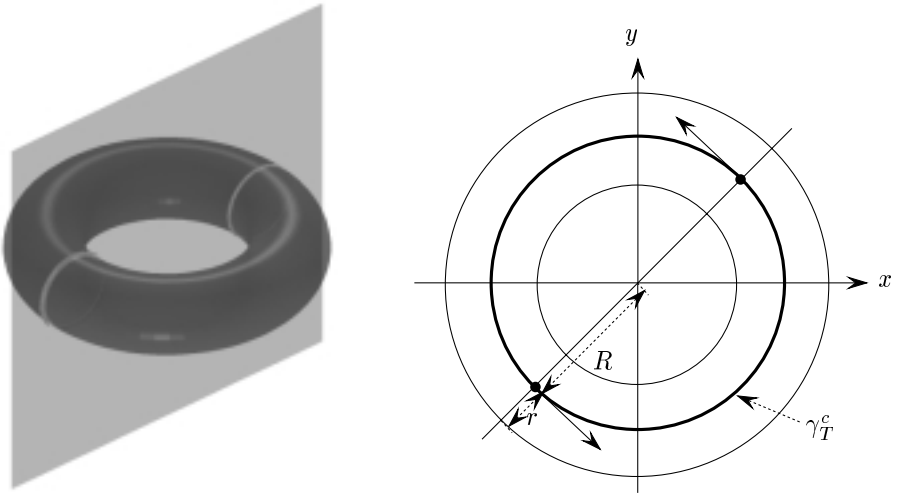

(b) Cross-sectional circles in TPI

Figure 3.2: Circles in TPI.

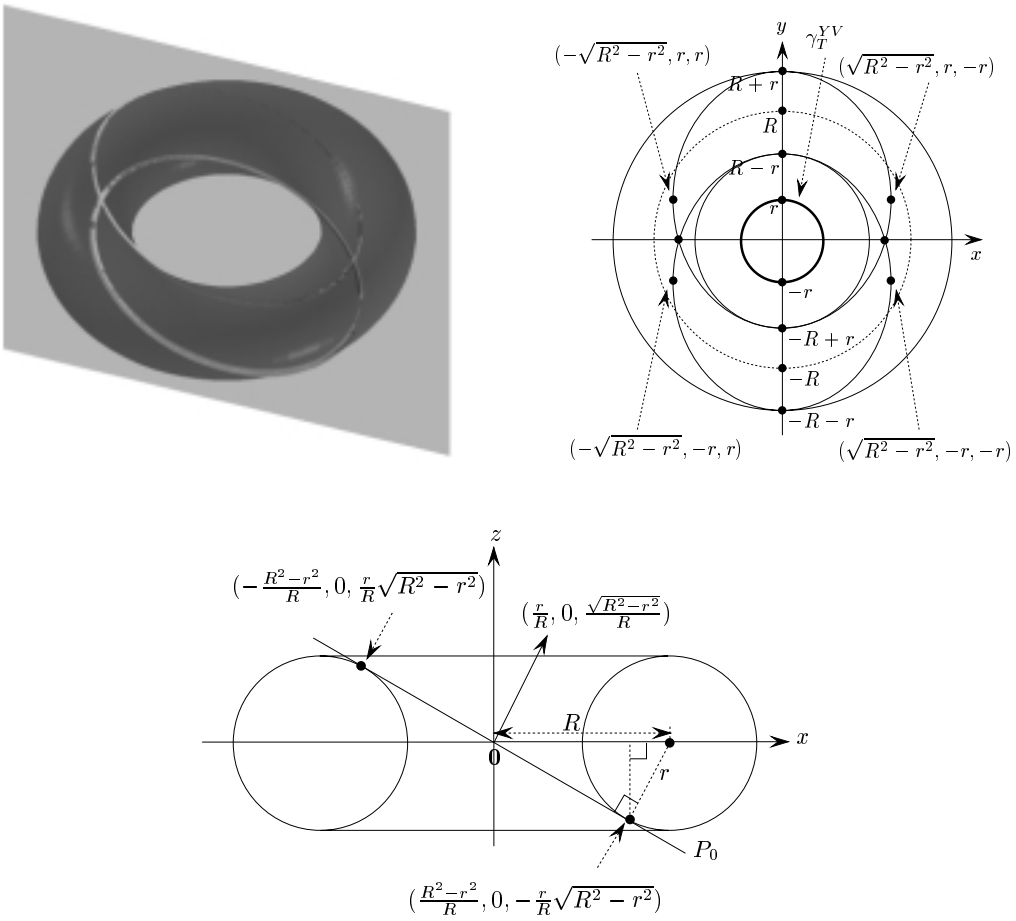

(c) Yvone-Villarceau circles in TPI

Figure 3.2: (*cont.*)

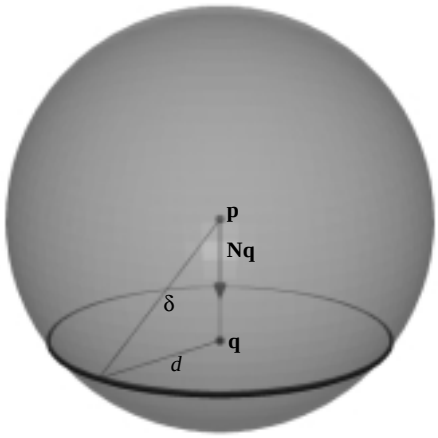

(a) Circles on a sphere

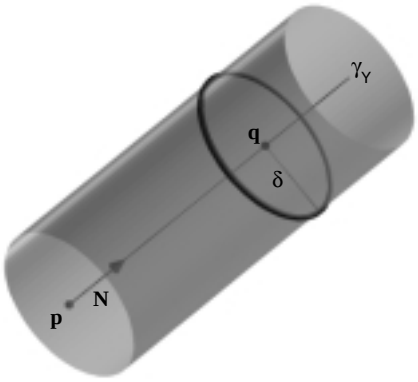

(b) Circles on a cylinder

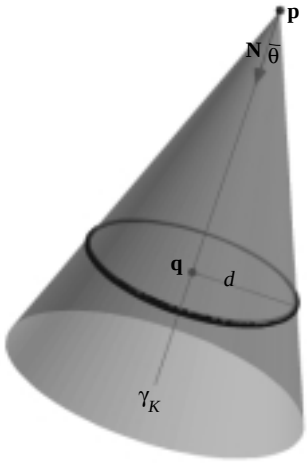

(c) Circles on a cone

Figure 3.3: Circles on a natural quadric.

3.2.1 Circles on a Sphere

For a sphere $S = S_\delta(\mathbf{p})$ with center $\mathbf{p}$ and radius δ, any point in the ball $B_\delta(\mathbf{p})$ can be the center of a circle embedded in the sphere S. Thus, we have

$$\gamma_S = B_\delta(\mathbf{p}).$$

To each point $\mathbf{q} \in B_\delta(\mathbf{p})$, there corresponds a unique circle with center $\mathbf{q}$ and embedded in the sphere $S_\delta(\mathbf{p})$. The circle has radius $\sqrt{\delta^2 - \|\mathbf{q}-\mathbf{p}\|^2}$. It is also contained in the plane $L(\mathbf{q}, \mathbf{N_q})$, where $\mathbf{N_q} = \frac{\mathbf{q}-\mathbf{p}}{\|\mathbf{q}-\mathbf{p}\|}$ (see Figure 3.3(a)). Therefore, the set Γ_S of all circles embedded in the sphere S can be represented as follows:

$$\Gamma_S = \left\{ C_d(\mathbf{q}, \mathbf{N_q}) \mid d = \sqrt{\delta^2 - \|\mathbf{q}-\mathbf{p}\|^2},\ \mathbf{q} \in B_\delta(\mathbf{p}),\ \text{and } \mathbf{N_q} = \frac{\mathbf{q}-\mathbf{p}}{\|\mathbf{q}-\mathbf{p}\|} \right\}. \quad (3.1)$$

3.2.2 Circles on a Cylinder

For a cylinder $Y = Y_\delta(\mathbf{p}, \mathbf{N})$, the centers of all circles embedded in the cylinder Y generate an infinite line:

$$\gamma_Y = l(\mathbf{p}, \mathbf{N}).$$

The circles embedded in the cylinder Y form a one-parameter family of circles (see Figure 3.3(b)):

$$\Gamma_Y = \{ C_\delta(\mathbf{q}, \mathbf{N}) \mid \mathbf{q} \in l(\mathbf{p}, \mathbf{N}) \}. \quad (3.2)$$

3.2.3 Circles on a Cone

For a cone $K = K_\theta(\mathbf{p}, \mathbf{N})$, the centers of all circles embedded in the cone K generate an infinite half-line:

$$\gamma_K = l^+(\mathbf{p}, \mathbf{N}).$$

The circles embedded in the cone K form a one-parameter family of circles (see Figure 3.3(c)):

$$\Gamma_K = \{ C_d(\mathbf{q}, \mathbf{N}) \mid \mathbf{q} \in l^+(\mathbf{p}, \mathbf{N}) \text{and } d = \|\mathbf{q}-\mathbf{p}\| \tan\theta \}. \quad (3.3)$$

3.3 Circle Detection in TPI

Circles in a torus/plane intersection curve must be of the following special types: (i) profile circles, (ii) cross-sectional circles, and (iii) Yvone-Villarceau circles. Given a torus $T = T_{r,R}(\mathbf{p}_1, \mathbf{N}_1)$ and a plane $L = L(\mathbf{p}_2, \mathbf{N}_2)$, we present geometric algorithms that detect and compute the circles of these special types in the TPI curve.

3.3.1 Profile Circles in TPI

The torus T intersects with the plane L in profile circles if and only if

1. The plane L is orthogonal to the main axis $l(\mathbf{p}_1, \mathbf{N}_1)$ of T (i.e., $\mathbf{N}_1$ and $\mathbf{N}_2$ are parallel or opposite to):

$$\mathbf{N}_1 \times \mathbf{N}_2 = \mathbf{0}.$$

2. The distance between two planes $L(\mathbf{p}_1, \mathbf{N}_1)$ and $L(\mathbf{p}_2, \mathbf{N}_2)$ is less than or equal to r:

$$\langle \mathbf{p}_2 - \mathbf{p}_1, \mathbf{N}_1 \rangle^2 \leq r^2.$$

When the above two conditions are satisfied, the two profile circles are given as follows:

$$C_{R \pm \delta}(\mathbf{q}, \mathbf{N}_1),$$

where

$$\begin{aligned} \delta &= \sqrt{r^2 - \langle \mathbf{p}_2 - \mathbf{p}_1, \mathbf{N}_1 \rangle^2} \\ \mathbf{q} &= \mathbf{p}_1 + \langle \mathbf{p}_2 - \mathbf{p}_1, \mathbf{N}_1 \rangle \, \mathbf{N}_1. \end{aligned}$$

When $\delta = 0$ (i.e., the signed distance $\langle \mathbf{p}_2 - \mathbf{p}_1, \mathbf{N}_1 \rangle$ between $L(\mathbf{p}_1, \mathbf{N}_1)$ and $L(\mathbf{p}_2, \mathbf{N}_2)$ is equal to $\pm r$), the two profile circles overlap in an identical circle of radius R.

3.3.2 Cross-Sectional Circles in TPI

The torus T intersects with the plane L in cross-sectional circles if and only if the plane L contains the main axis $l(\mathbf{p}_1, \mathbf{N}_1)$ of T; namely, $\mathbf{N}_1$ and $\mathbf{N}_2$ are orthogonal and the plane L contains the central point $\mathbf{p}_1$ of T:

$$\langle \mathbf{N}_1, \mathbf{N}_2 \rangle = 0, \text{ and } \langle \mathbf{p}_1 - \mathbf{p}_2, \mathbf{N}_2 \rangle = 0.$$

The two cross-sectional circles are given as follows:

$$C_r(\mathbf{p}_1 \pm R(\mathbf{N}_1 \times \mathbf{N}_2), \mathbf{N}_2).$$

3.3.3 Yvone-Villarceau Circles in TPI

The torus T intersects with the plane L in Yvone-Villarceau circles if and only if the plane L has two tangential intersection points with T; namely, the plane L contains the central point $\mathbf{p}_1$ of T and the two normals $\mathbf{N}_1$ and $\mathbf{N}_2$ make angle $\theta = \arcsin(r/R)$:

$$\begin{aligned} \langle \mathbf{p}_1 - \mathbf{p}_2, \mathbf{N}_2 \rangle &= 0, \\ \langle \mathbf{N}_1, \mathbf{N}_2 \rangle^2 &= \cos^2\theta = 1 - \frac{r^2}{R^2}. \end{aligned}$$

The two Yvone-Villarceau circles are given as follows:

$$C_R\left(\mathbf{p}_1 \pm \frac{r}{\sin\theta}(\mathbf{N}_1 \times \mathbf{N}_2), \mathbf{N}_2\right) = C_R\left(\mathbf{p}_1 \pm R(\mathbf{N}_1 \times \mathbf{N}_2), \mathbf{N}_2\right).$$

Note that the vector $\frac{1}{\sin\theta}(\mathbf{N}_1 \times \mathbf{N}_2)$ is a unit vector orthogonal to both $\mathbf{N}_1$ and $\mathbf{N}_2$.

3.4 Profile Circles in TQI

Given a torus $T = T_{r,R}(\mathbf{p}_1, \mathbf{N}_1)$ and a natural quadric Q ($= S_\delta(\mathbf{p}_2)$, $Y_\delta(\mathbf{p}_2, \mathbf{N}_2)$, or $K_\theta(\mathbf{p}_2, \mathbf{N}_2)$), we present geometric algorithms that detect and compute all profile circles in the TQI curve. We consider the set of all profile circles embedded in the torus $T = T_{r,R}(\mathbf{p}_1, \mathbf{N}_1)$:

$$\Gamma_T^p = \{ C_{R \pm \sqrt{r^2 - \alpha^2}}(\mathbf{p}_1 + \alpha \mathbf{N}_1, \mathbf{N}_1) \mid -r \le \alpha \le r \}. \tag{3.4}$$

3.4.1 Profile Circles in TSI

Assume that a profile circle $C \in \Gamma_T^p$ is also embedded in the sphere $S = S_\delta(\mathbf{p}_2)$ (i.e., $C \in \Gamma_T^p \cap \Gamma_S$). The set Γ_S of circles given in Equation (3.1) can be reformulated as follows:

$$\Gamma_S = \left\{ C_d(\mathbf{q}, \mathbf{N_q}) \mid d = \sqrt{\delta^2 - \|\mathbf{q} - \mathbf{p}_2\|^2},\ \mathbf{q} \in B_\delta(\mathbf{p}_2),\ \text{and } \mathbf{N_q} = \frac{\mathbf{q} - \mathbf{p}_2}{\|\mathbf{q} - \mathbf{p}_2\|} \right\} \tag{3.5}$$

Comparing the two sets Γ_T^p and Γ_S in Equations (3.4)–(3.5), we derive the following relations:

$$\mathbf{N_q} = \pm\mathbf{N}_1 \tag{3.6}$$

$$\mathbf{p}_1 + \alpha\mathbf{N}_1 = \mathbf{p}_2 + \beta\mathbf{N}_1 \tag{3.7}$$

$$R \pm \sqrt{r^2 - \alpha^2} = \sqrt{\delta^2 - \beta^2}, \tag{3.8}$$

for some α and β such that $-r \leq \alpha \leq r$ and $-\delta \leq \beta \leq \delta$.

Equation (3.7) implies that

$$k = \alpha - \beta = \langle(\alpha - \beta)\mathbf{N}_1, \mathbf{N}_1\rangle = \langle\mathbf{p}_2 - \mathbf{p}_1, \mathbf{N}_1\rangle$$

is a fixed constant which represents the signed distance from $\mathbf{p}_1$ to $\mathbf{p}_2$ along the direction of $\mathbf{N}_1$. Substituting $\beta = \alpha - k$ into Equation (3.8), we obtain

$$R \pm \sqrt{r^2 - \alpha^2} = \sqrt{\delta^2 - (\alpha - k)^2}. \tag{3.9}$$

Figure 3.4 shows that the solution of this equation is given as the intersection of a circle of radius r and a half circle of radius δ. In fact, the torus T and the sphere S are obtained by rotating the circle and the half circle of Figure 3.4(b) about the α-axis. Figure 3.4(b) shows the cross-sectional circles of T and S which are obtained by intersecting T and S with a plane containing the infinite line $l(\mathbf{p}_1, \mathbf{N}_1)$. Note that the circles C_δ and C_r^+ (or C_r^-) in Figure 3.4(b) intersect if and only if

$$\sqrt{k^2 + R^2} - r \ \leq \delta \leq \ \sqrt{k^2 + R^2} + r.$$

Consequently, necessary and sufficient conditions for the torus T and the sphere S to intersect in profile circles are:

$$\mathbf{N}_1 \times \mathbf{N_q} = \mathbf{0} \tag{3.10}$$

$$\|\mathbf{p}_1 - \mathbf{p}_2\|^2 = \langle\mathbf{p}_1 - \mathbf{p}_2, \mathbf{N}_1\rangle^2 \tag{3.11}$$

$$(\delta - r)^2 \ \leq k^2 + \ R^2 \leq \ (\delta + r)^2. \tag{3.12}$$

When these three conditions are met, the TSI circles are constructed as follows:

$$C_{R\pm\sqrt{r^2-\alpha^2}}(\mathbf{p}_1 + \alpha\mathbf{N}_1, \mathbf{N}_1),$$

where

$$\alpha = \frac{-B \pm \sqrt{B^2 - 4AC}}{2A},$$

and

$$\begin{aligned} A &= k^2 + R^2, \\ B &= k\ (\delta^2 - k^2 - r^2 - R^2), \\ C &= (k^2 - \delta^2)r^2 + \frac{1}{4}(R^2 - \delta^2 + k^2 - r^2)^2. \end{aligned}$$

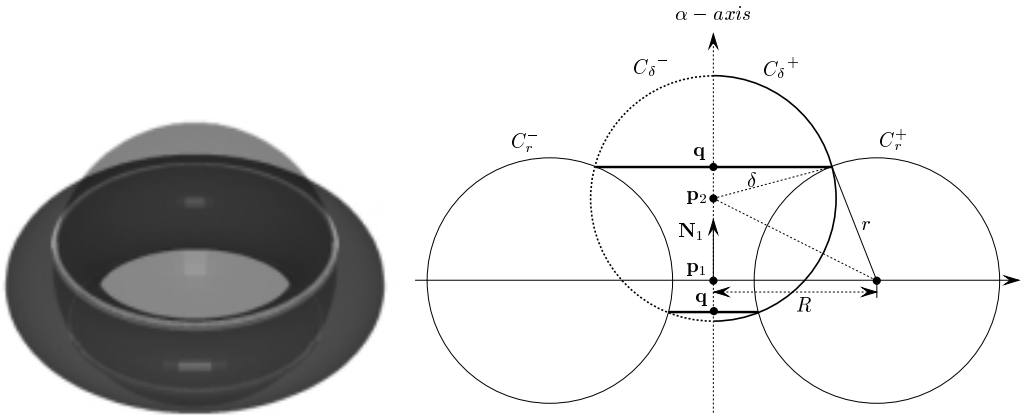

(a) (b)

Figure 3.4: Profile circles in TSI.

3.4.2 Profile Circles in TYI

Assume that a profile circle $C \in \Gamma_T^p$ is also embedded in the cylinder $Y = Y_\delta(\mathbf{p}_2, \mathbf{N}_2)$ (i.e., $C \in \Gamma_T^p \cap \Gamma_Y$). The set Γ_Y of circles given in Equation (3.2) can be reformulated as follows:

$$\Gamma_Y = \{C_\delta(\mathbf{p}_2 + \beta\mathbf{N}_2, \mathbf{N}_2) \mid \beta \in I\!R\ \}. \tag{3.13}$$

Comparing the two sets Γ_T^p and Γ_Y in Equations (3.4) and (3.13), we can derive the following relations:

$$\mathbf{N}_2 = \pm\mathbf{N}_1 \tag{3.14}$$

$$\mathbf{p}_1 + \alpha\mathbf{N}_1 = \mathbf{p}_2 + \beta\mathbf{N}_1 \tag{3.15}$$

$$R \pm \sqrt{r^2 - \alpha^2} = \delta, \tag{3.16}$$

for some α and β such that $-r \leq \alpha \leq r$ and $-\infty \leq \beta \leq \infty$.

The right-hand side of Equation (3.16) is a constant function of α. Figure 3.5(b) shows that there are solutions of α for Equation (3.16) if and only if $R-r \leq \delta \leq R+r$. Moreover, the corresponding values of α are given as follows:

$$\alpha = \pm\sqrt{r^2 - (R-\delta)^2}.$$

The torus T and the cylinder Y are obtained by rotating the circle and the line of Figure 3.5 about the α-axis. Figure 3.5(b) shows the cross-sectional circles of T and the profile lines of Y which are obtained by intersecting T and Y with a plane containing the infinite line $l(\mathbf{p}_1, \mathbf{N}_1)$.

Necessary and sufficient conditions for the torus T and the cylinder Y to intersect in profile circles are:

$$\mathbf{N}_1 \times \mathbf{N}_2 = \mathbf{0} \tag{3.17}$$

$$\|\mathbf{p}_1 - \mathbf{p}_2\|^2 = \langle \mathbf{p}_1 - \mathbf{p}_2, \mathbf{N}_1 \rangle^2 \tag{3.18}$$

$$R - r \leq \delta \leq R + r. \tag{3.19}$$

When these three conditions are met, the TYI circles are constructed as follows:

$$C_\delta(\mathbf{p}_1 \pm \sqrt{r^2 - (R-\delta)^2}\mathbf{N}_1, \mathbf{N}_1).$$

3.4.3 Profile Circles in TKI

Assume that a profile circle $C \in \Gamma_T^p$ is also embedded in the cone $K = K_\theta(\mathbf{p}_2, \mathbf{N}_2)$ (i.e., $C \in \Gamma_T^p \cap \Gamma_K$). The set Γ_K of circles given in Equation (3.3) can be reformulated as follows:

$$\Gamma_K = \{C_{\beta \tan\theta}(\mathbf{p}_2 + \beta\mathbf{N}_2, \mathbf{N}_2) \mid \beta \geq 0\}. \tag{3.20}$$

Comparing the two sets Γ_T^p and Γ_K in Equations (3.4) and (3.20), we can derive the following relations:

$$\mathbf{N}_2 = \pm\mathbf{N}_1 \tag{3.21}$$

$$\mathbf{p}_1 + \alpha\mathbf{N}_1 = \mathbf{p}_2 + \beta\mathbf{N}_1 \tag{3.22}$$

$$R \pm \sqrt{r^2 - \alpha^2} = \beta \tan\theta, \tag{3.23}$$

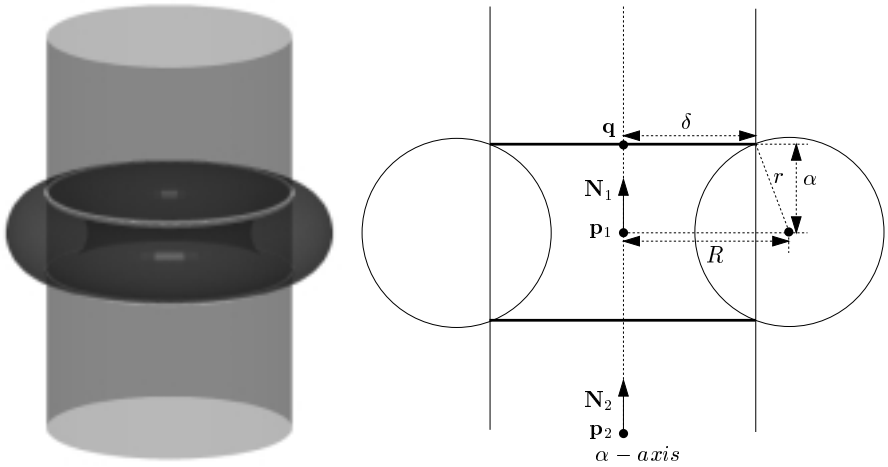

(a) (b)

Figure 3.5: Profile circles in TYI.

for some α and β such that $-r \leq \alpha \leq r$ and $\beta \geq 0$.

Let $\bar{k} = \langle \mathbf{p}_1 - \mathbf{p}_2, \mathbf{N}_2 \rangle$ be the signed distance from $\mathbf{p}_2$ to $\mathbf{p}_1$ along the direction of $\mathbf{N}_2$. Figure 3.6 shows that there are solutions of α for Equation (3.23) if and only if

$$\arctan(R/\bar{k}) - \arcsin\left(\frac{r}{\sqrt{R^2+\bar{k}^2}}\right) \leq \theta \leq \arctan(R/\bar{k}) + \arcsin\left(\frac{r}{\sqrt{R^2+\bar{k}^2}}\right) \quad (3.24)$$

The torus T and the cone K are obtained by rotating the circle and the line of Figure 3.6(b) about the α-axis. Figure 3.6(b) shows the cross-sectional circles of T and the profile lines of K which are obtained by intersecting T and Y with a plane containing the infinite line $l(\mathbf{p}_1, \mathbf{N}_1)$. Note that the profile lines of the cone K consist of two half-infinite lines, each of which makes angle θ with the half-infinite line $l^+(\mathbf{p}_1, \mathbf{N}_1)$.

Necessary and sufficient conditions for the torus T and the cone K to intersect in profile circles are:

$$\mathbf{N}_1 \times \mathbf{N}_2 = \mathbf{0} \quad (3.25)$$

$$\|\mathbf{p}_1 - \mathbf{p}_2\|^2 = \langle \mathbf{p}_1 - \mathbf{p}_2, \mathbf{N}_1 \rangle^2, \quad (3.26)$$

and the constraint given in Equation (3.24). When these three conditions are met, the TKI circles are constructed as follows:

$$C_{(\alpha \pm \bar{k}) \tan\theta}(\mathbf{p}_1 + \alpha \mathbf{N}_1, \mathbf{N}_1),$$

where $-r \leq \alpha \leq r$ and the value of α is given as follows:

$$\alpha = \frac{-B \pm \sqrt{B^2 - AC}}{A},$$

and

$$\begin{aligned}
A &= 1 + \tan^2\theta \\
B &= \begin{cases} \tan\theta\ (\bar{k}\tan\theta - R), & \text{if } \beta = \alpha + \bar{k}, \\ -\tan\theta\ (\bar{k}\tan\theta + R), & \text{if } \beta = \alpha - \bar{k} \end{cases} \\
C &= \begin{cases} \bar{k}\tan\theta\ (\bar{k}\tan\theta - 2R) + R^2 - r^2, & \text{if } \beta = \alpha + \bar{k}, \\ \bar{k}\tan\theta\ (\bar{k}\tan\theta + 2R) + R^2 - r^2, & \text{if } \beta = \alpha - \bar{k}. \end{cases}
\end{aligned}$$

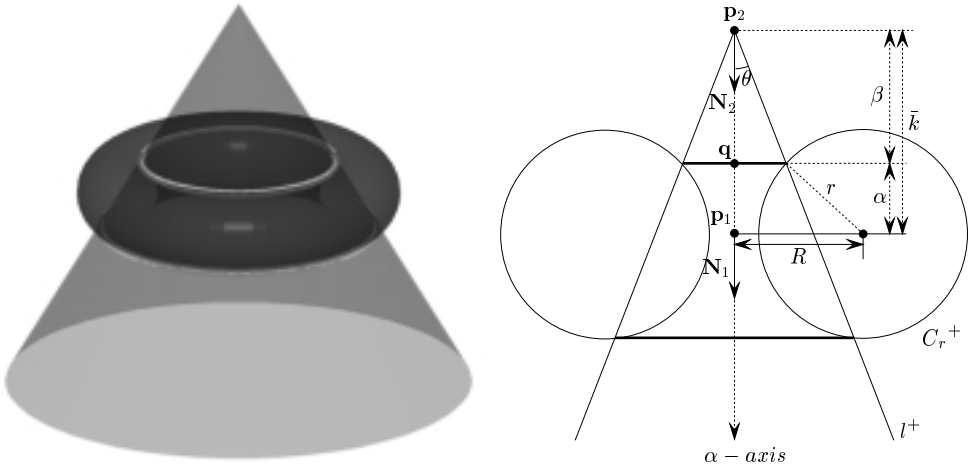

(a) (b)

Figure 3.6: Profile circles in TKI.

3.5 Cross-Sectional Circles in TQI

We consider the set of all cross-sectional circles embedded in the torus $T = T_{r,R}(\mathbf{p}_1, \mathbf{N}_1)$:

$$\Gamma_T^c = \{C_r(\mathbf{q}, \mathbf{N_q}) \mid \mathbf{q} \in C_R(\mathbf{p}_1, \mathbf{N}_1) \text{ and } \mathbf{N_q} = \frac{\mathbf{N}_1 \times (\mathbf{q} - \mathbf{p}_1)}{\|\mathbf{N}_1 \times (\mathbf{q} - \mathbf{p}_1)\|} \}. \quad (3.27)$$

Note that $\mathbf{N_q}$ is a unit tangent vector of the main circle $C_R(\mathbf{p}_1, \mathbf{N}_1)$ of T at $\mathbf{q}$.

3.5.1 Cross-Sectional Circles in TSI

Assume that a cross-sectional circle $C \in \Gamma_T^c$ is also embedded in the sphere $S = S_\delta(\mathbf{p}_2)$ (i.e., $C \in \Gamma_T^c \cap \Gamma_S$). The set Γ_S of circles given in Equation (3.1) can be reformulated as follows:

$$\Gamma_S = \left\{ C_d(\mathbf{q}, \bar{\mathbf{N}}_\mathbf{q}) \mid d = \sqrt{\delta^2 - \|\mathbf{q} - \mathbf{p}_2\|^2},\ \mathbf{q} \in B_\delta(\mathbf{p}_2), \text{ and } \bar{\mathbf{N}}_\mathbf{q} = \frac{\mathbf{q} - \mathbf{p}_2}{\|\mathbf{q} - \mathbf{p}_2\|} \right\} \quad (3.28)$$

Comparing $\mathbf{N_q}$ and $\bar{\mathbf{N}}_\mathbf{q}$ in Equations (3.27)–(3.28), we can notice that the vector $\mathbf{q} - \mathbf{p}_2$ is orthogonal to both $\mathbf{N}_1$ and $\mathbf{q} - \mathbf{p}_1$:

$$\langle \mathbf{q} - \mathbf{p}_2, \mathbf{N}_1 \rangle = 0 \text{ and } \langle \mathbf{q} - \mathbf{p}_2, \mathbf{q} - \mathbf{p}_1 \rangle = 0. \quad (3.29)$$

Since $\langle \mathbf{q} - \mathbf{p}_1, \mathbf{N}_1 \rangle = 0$, we have $\mathbf{q} = \mathbf{p}_1 + \mathbf{v}$, for some $\mathbf{v}$ such that $\langle \mathbf{v}, \mathbf{N}_1 \rangle = 0$ and $\|\mathbf{v}\| = R$. Therefore, Equation (3.29) can be reformulated as follows:

$$\langle \mathbf{p}_1 - \mathbf{p}_2, \mathbf{N}_1 \rangle = 0 \text{ and } \langle \mathbf{q} - \mathbf{p}_2, \mathbf{q} - \mathbf{p}_1 \rangle = 0. \quad (3.30)$$

Therefore, the point $\mathbf{p}_2$ (i.e., the center of the sphere $S = S_\delta(\mathbf{p}_2)$) must be contained in the plane $L(\mathbf{p}_1, \mathbf{N}_1)$. Moreover, the point $\mathbf{p}_2$ must be in the tangent line of the circle $C_R(\mathbf{p}_1, \mathbf{N}_1)$ at the point $\mathbf{q}$. There are one or two such points $\mathbf{q} \in C_R(\mathbf{p}_1, \mathbf{N}_1)$ if and only if $\mathbf{p}_2 \in L(\mathbf{p}_1, \mathbf{N}_1)$ and $\|\mathbf{p}_2 - \mathbf{p}_1\| \geq R$.

Note that (see Figure 3.7(b)):

$$\|\mathbf{q} - \mathbf{p}_2\|^2 = \|\mathbf{p}_1 - \mathbf{p}_2\|^2 - R^2.$$

Comparing the radii of the circles in Equations (3.27)–(3.28), we have

$$r^2 = \delta^2 - \|\mathbf{q} - \mathbf{p}_2\|^2 \quad (3.31)$$

$$r^2 = \delta^2 - \|\mathbf{p}_2 - \mathbf{p}_1\|^2 + R^2 \quad (3.32)$$

$$\|\mathbf{p}_2 - \mathbf{p}_1\|^2 = R^2 + \delta^2 - r^2. \quad (3.33)$$

In the last condition, note that $\|\mathbf{p}_2 - \mathbf{p}_1\| \geq R$ if and only if $\delta \geq r$.

Necessary and sufficient conditions for the torus T and the sphere S to intersect in cross-sectional circles are:

$$\delta \geq r \tag{3.34}$$

$$\langle \mathbf{p}_1 - \mathbf{p}_2, \mathbf{N}_1 \rangle = 0 \tag{3.35}$$

$$\|\mathbf{p}_2 - \mathbf{p}_1\|^2 = R^2 + \delta^2 - r^2. \tag{3.36}$$

When these three conditions are met, the TSI circles are constructed as follows:

$$C_r(\mathbf{q}, \mathbf{N}_\mathbf{q}),$$

where

$$\mathbf{q} = \mathbf{p}_1 + \frac{R^2}{\sqrt{R^2 + \delta^2 - r^2}} \frac{\mathbf{p}_2 - \mathbf{p}_1}{\|\mathbf{p}_2 - \mathbf{p}_1\|} \pm \frac{R\sqrt{\delta^2 - r^2}}{\sqrt{R^2 + \delta^2 - r^2}} \frac{\mathbf{N}_1 \times (\mathbf{p}_2 - \mathbf{p}_1)}{\|\mathbf{p}_2 - \mathbf{p}_1\|}.$$

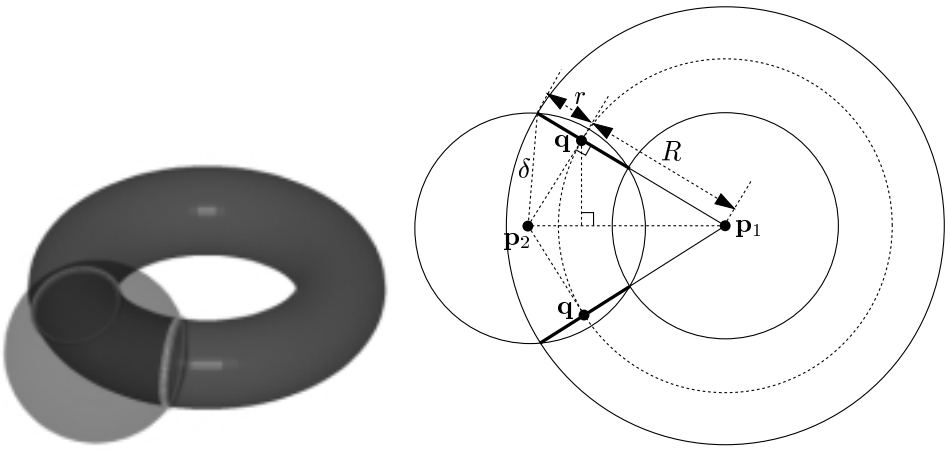

(a) (b)

Figure 3.7: Cross-sectional circles in TSI.

3.5.2 Cross-Sectional Circles in TYI

Assume that a cross-sectional circle $C \in \Gamma_T^c$ is also embedded in the cylinder $Y = Y_\delta(\mathbf{p}_2, \mathbf{N}_2)$ (i.e., $C \in \Gamma_T^c \cap \Gamma_Y$). The set Γ_Y of circles given in Equation (3.2) can be

reformulated as follows:

$$\Gamma_Y = \{C_\delta(\mathbf{p}_2 + \beta\mathbf{N}_2, \mathbf{N}_2) \mid \beta \in I\!R \}. \tag{3.37}$$

Necessary and sufficient conditions for the torus T and the cylinder Y to intersect in cross-sectional circles are:

$$\delta = r \tag{3.38}$$

$$\langle \mathbf{N}_1, \mathbf{N}_2 \rangle = 0 \tag{3.39}$$

$$\langle \mathbf{p}_1 - \mathbf{p}_2, \mathbf{N}_1 \rangle = 0 \tag{3.40}$$

$$\|\mathbf{p}_2 - \mathbf{p}_1\|^2 = \langle \mathbf{p}_1 - \mathbf{p}_2, \mathbf{N}_2 \rangle^2 + R^2. \tag{3.41}$$

When all these conditions are met, the TYI circles are constructed as follows:

$$C_r(\mathbf{p}_2 + \langle \mathbf{p}_1 - \mathbf{p}_2, \mathbf{N}_2 \rangle \mathbf{N}_2, \mathbf{N}_2).$$

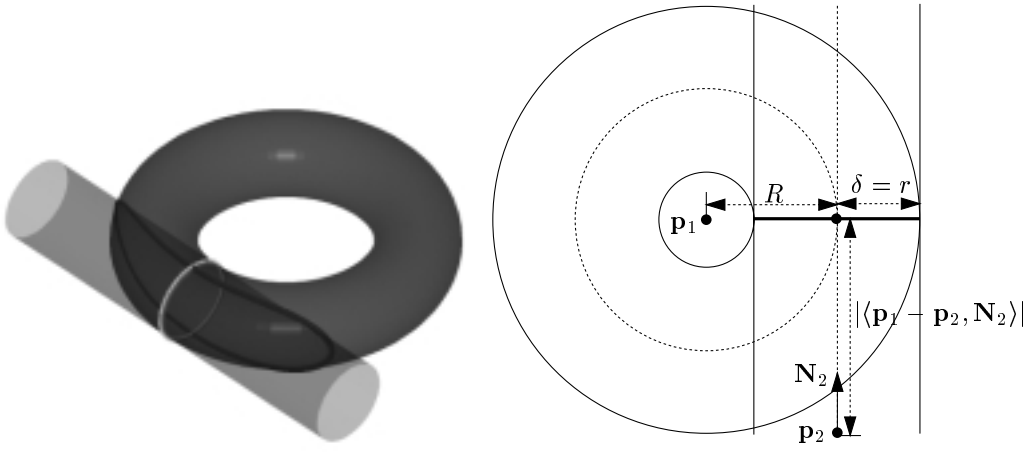

(a) (b)

Figure 3.8: Cross-sectional circles in TYI.

3.5.3 Cross-Sectional Circles in TKI

Assume that a cross-sectional circle $C \in \Gamma_T^c$ is also embedded in the cone $K = K_\theta(\mathbf{p}_2, \mathbf{N}_2)$ (i.e., $C \in \Gamma_T^c \cap \Gamma_K$). The set Γ_K of circles given in Equation (3.3) can

be reformulated as follows:

$$\Gamma_K = \{C_{\beta \tan\theta}(\mathbf{p}_2 + \beta \mathbf{N}_2, \mathbf{N}_2) \mid \beta \geq 0\}. \tag{3.42}$$

Necessary and sufficient conditions for the torus T and the cone K to intersect in cross-sectional circles are:

$$\tan\theta \ \langle \mathbf{p}_1 - \mathbf{p}_2, \mathbf{N}_2 \rangle = r \tag{3.43}$$

$$\langle \mathbf{N}_1, \mathbf{N}_2 \rangle = 0 \tag{3.44}$$

$$\langle \mathbf{p}_1 - \mathbf{p}_2, \mathbf{N}_1 \rangle = 0 \tag{3.45}$$

$$\|\mathbf{p}_2 - \mathbf{p}_1\|^2 = \langle \mathbf{p}_1 - \mathbf{p}_2, \mathbf{N}_2 \rangle^2 + R^2. \tag{3.46}$$

When all these conditions are met, the TYI circles are constructed as follows:

$$C_r(\mathbf{p}_2 + \langle \mathbf{p}_1 - \mathbf{p}_2, \mathbf{N}_2 \rangle \mathbf{N}_2, \mathbf{N}_2).$$

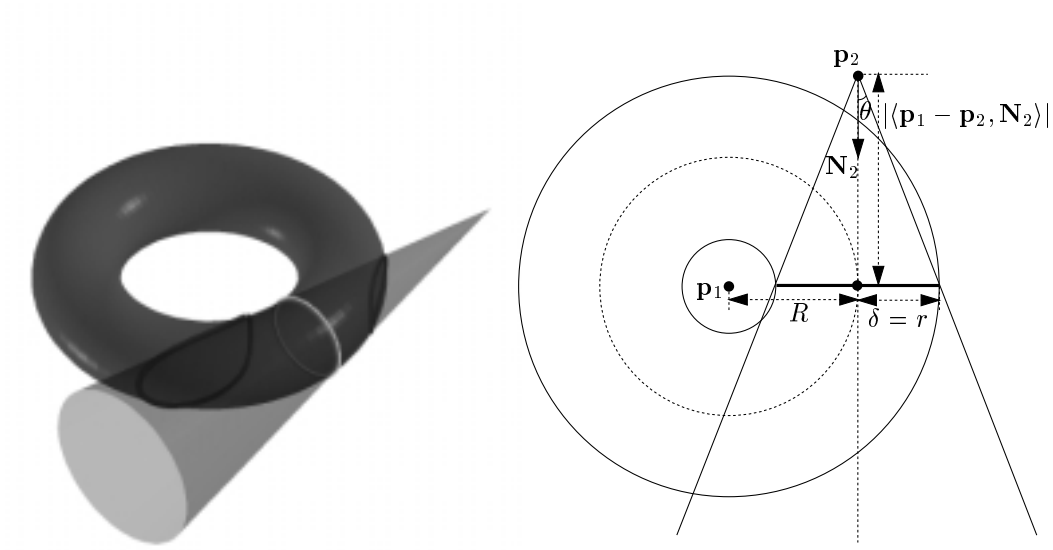

(a) (b)

Figure 3.9: Cross-sectional circles in TKI.

3.6 Yvone-Villarceau Circles in TQI

We consider the set of all Yvone-Villarceau circles embedded in the torus $T = T_{r,R}(\mathbf{p}_1, \mathbf{N}_1)$:

$$\Gamma_T^{YV,\pm} = \{C_R(\mathbf{q}, \mathbf{N_q}) \mid \mathbf{q} \in C_r(\mathbf{p}_1, \mathbf{N}_1)\ \}, \tag{3.47}$$

where

$$\mathbf{N_q} = \pm\frac{r}{R}\frac{(\mathbf{q}-\mathbf{p}_1)\times\mathbf{N}_1}{\|\mathbf{q}-\mathbf{p}_1\|} + \sqrt{1-\frac{r^2}{R^2}}\,\mathbf{N}_1.$$

Consider the set of lines $l(\mathbf{q}, \mathbf{N_q})$:

$$H_T^{YV,\pm} = \cup_{\mathbf{q}\in C_r(\mathbf{p}_1,\mathbf{N}_1)} l(\mathbf{q}, \mathbf{N_q}).$$

This set generates a ruled surface that forms a hyperboloid of one sheet. When the main plane of T is contained in the xy-plane, the direction vector $\mathbf{N}_1$ is parallel to the z-axis and the ruled surface is represented in an implicit equation:

$$x^2 + y^2 - \frac{r^2 z^2}{R^2 - r^2} = r^2. \tag{3.48}$$

Note that both $H_T^{YV,+}$ and $H_T^{YV,-}$ can be represented using the same implicit equation.

3.6.1 Yvone-Villarceau Circles in TSI

Given a sphere $S = S_\delta(\mathbf{p}_2)$ with radius δ and center $\mathbf{p}_2$, we can test whether this center belongs to the ruled surface $H_T^{YV,\pm}$ by first transforming the point $\mathbf{p}_1$ and the direction vector $\mathbf{N}_1$ into the origin and the z-direction, respectively, and then testing the resulting coordinate of $\mathbf{p}_2$ (under transformation) with respect to Equation (3.48). Since an explicit transformation is quite cumbersome, we compute the terms $x^2 + y^2$ and z^2 as follows:

$$\begin{aligned} z^2 &= |\,\langle \mathbf{p}_2 - \mathbf{p}_1, \mathbf{N}_1\rangle\,|^2 \\ x^2 + y^2 &= ||\mathbf{p}_2 - \langle \mathbf{p}_2 - \mathbf{p}_1, \mathbf{N}_1\rangle\,\mathbf{N}_1||^2. \end{aligned}$$

Substituting these two expressions into Equation (3.48), we obtain:

$$||\mathbf{p}_2 - \langle \mathbf{p}_2 - \mathbf{p}_1, \mathbf{N}_1\rangle\,\mathbf{N}_1||^2 - \frac{r^2}{R^2 - r^2}|\,\langle \mathbf{p}_2 - \mathbf{p}_1, \mathbf{N}_1\rangle\,|^2 = r^2. \tag{3.49}$$

When the sphere center $\mathbf{p}_2$ is contained in the ruled surface $H_T^{YV,\pm}$, this point belongs to a line $l(\mathbf{q}, \mathbf{N_q})$. The point $\mathbf{q} \in C_r(\mathbf{p}_1, \mathbf{N}_1)$ can be computed as follows:

$$\begin{aligned} \mathbf{q} &= \mathbf{p}_2 + \alpha \mathbf{N_q}, \\ \langle \mathbf{q} - \mathbf{p}_1, \mathbf{N}_1 \rangle &= 0, \\ \langle \mathbf{p}_2 - \mathbf{p}_1 + \alpha \mathbf{N_q}, \mathbf{N}_1 \rangle &= 0, \end{aligned}$$

where α is given as follows:

$$\alpha = \frac{\langle \mathbf{p}_1 - \mathbf{p}_2, \mathbf{N}_1 \rangle}{\langle \mathbf{N_q}, \mathbf{N}_1 \rangle} = \frac{R}{\sqrt{R^2 - r^2}} \langle \mathbf{p}_1 - \mathbf{p}_2, \mathbf{N}_1 \rangle .$$

Consequently, we have

$$\mathbf{q} = \mathbf{p}_2 + \frac{R \langle \mathbf{p}_1 - \mathbf{p}_2, \mathbf{N}_1 \rangle}{\sqrt{R^2 - r^2}} \mathbf{N_q}.$$

From the condition: $\mathbf{q} \in C_r(\mathbf{p}_1, \mathbf{N}_1)$, we have

$$\left\| \mathbf{p}_2 - \mathbf{p}_1 + \frac{R \langle \mathbf{p}_1 - \mathbf{p}_2, \mathbf{N}_1 \rangle}{\sqrt{R^2 - r^2}} \mathbf{N_q} \right\|^2 = r^2. \tag{3.50}$$

Finally, we have the following constraint on the radius δ of the sphere $S_\delta(\mathbf{p}_2)$:

$$R^2 + \frac{R^2}{R^2 - r^2} \langle \mathbf{p}_1 - \mathbf{p}_2, \mathbf{N}_1 \rangle^2 = \delta^2. \tag{3.51}$$

Necessary and sufficient conditions for the intersection curve of T and S to have degenerate Yvone-Villarceau circles are Equations (3.49)–(3.51). The circle itself is constructed as follows:

$$C_R(\mathbf{q}, \mathbf{N_q}),$$

where $\mathbf{q}$ and $\mathbf{N_q}$ are given as above.

3.6.2 Yvone-Villarceau Circles in TYI

Necessary and sufficient conditions for the torus T and the cylinder $Y = Y_\delta(\mathbf{p}_2)$ to intersect in an Yvone-Villarceau circle are:

$$\delta = R, \tag{3.52}$$

and the constraints of Equations (3.49)–(3.50). When all these conditions are met, the TYI circle is constructed as follows:

$$C_R(\mathbf{p}_2 + \langle \mathbf{p}_1 - \mathbf{p}_2, \mathbf{N}_2 \rangle \mathbf{N}_2, \mathbf{N}_2).$$

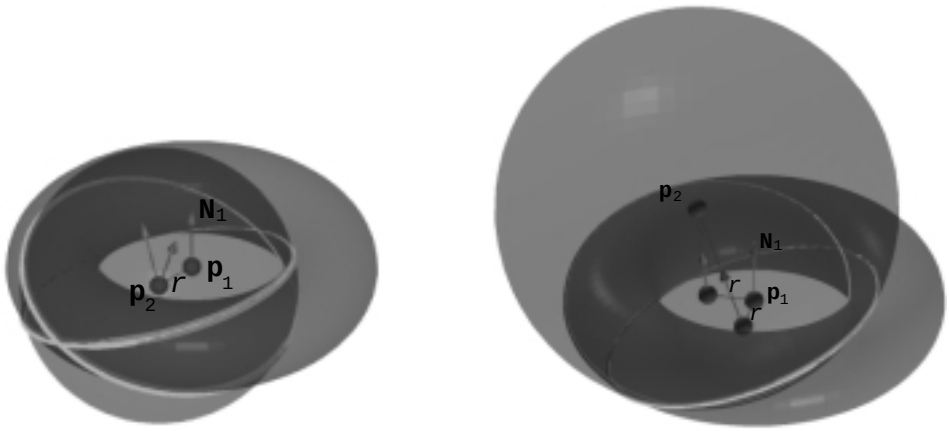

(a) (b)

Figure 3.10: Yvone-Villarceau circles in TSI.

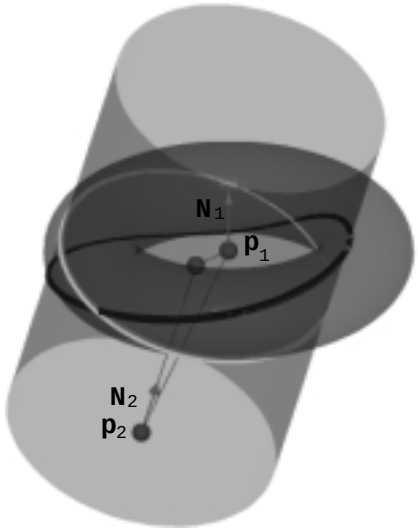

Figure 3.11: Yvone-Villarceau circle in TYI.

3.6.3 Yvone-Villarceau Circles in TKI

Necessary and sufficient conditions for the torus T and the cone K to intersect in an Yvone-Villarceau circle are:

$$|\langle \mathbf{p}_1 - \mathbf{p}_2, \mathbf{N}_2 \rangle| \tan\theta = R, \tag{3.53}$$

and the constraints of Equations (3.49)–(3.50). When all these conditions are met, the TKI circle is constructed as follows:

$$C_R(\mathbf{p}_2 + \langle \mathbf{p}_1 - \mathbf{p}_2, \mathbf{N}_2 \rangle \mathbf{N}_2, \mathbf{N}_2).$$

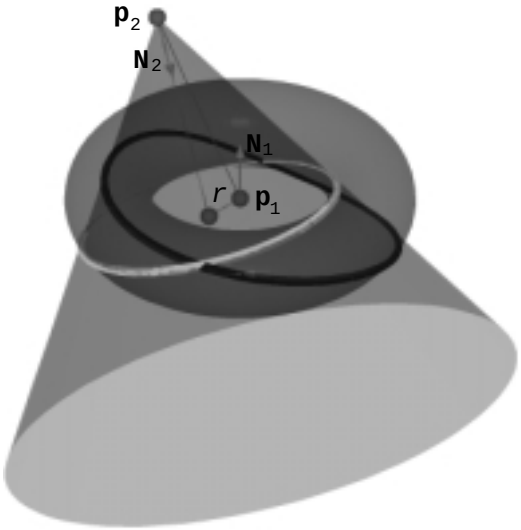

Figure 3.12: Yvone-Villarceau circle in TKI.

3.7 Circle Detection in TTI

Given two tori $T_1 = T_{r_1,R_1}(\mathbf{p}_1, \mathbf{N}_1)$ and $T_2 = T_{r_2,R_2}(\mathbf{p}_2, \mathbf{N}_2)$, we present geometric algorithms that detect and compute all degenerate circles in the TTI curve. The algorithm to detect degenerate circles in $\Gamma^c_{T_1} \cap \Gamma^p_{T_2}$ is essentially the same as that for $\Gamma^p_{T_1} \cap \Gamma^c_{T_2}$. Thus, we do not consider the case of $\Gamma^c_{T_1} \cap \Gamma^p_{T_2}$. Similarly, we do not consider the cases of $\Gamma^{YV}_{T_1} \cap \Gamma^p_{T_2}$ and $\Gamma^{YV}_{T_1} \cap \Gamma^c_{T_2}$.

3.7.1 Profile Circles of T_1 and other Circles of T_2

We consider the set of all profile circles embedded in the torus $T_1 = T_{r_1,R_1}(\mathbf{p}_1, \mathbf{N}_1)$:

$$\Gamma^p_{T_1} = \{C_{R_1 \pm \sqrt{r_1^2-\alpha^2}}(\mathbf{p}_1 + \alpha\mathbf{N}_1, \mathbf{N}_1) \mid -r_1 \leq \alpha \leq r_1 \}. \tag{3.54}$$

Profile Circles of T_2

The set of all profile circles embedded in the torus $T_2 = T_{r_2,R_2}(\mathbf{p}_2, \mathbf{N}_2)$ is given as follows:

$$\Gamma^p_{T_2} = \{C_{R_2 \pm \sqrt{r_2^2-\beta^2}}(\mathbf{p}_2 + \beta\mathbf{N}_2, \mathbf{N}_2) \mid -r_2 \leq \beta \leq r_2 \}. \tag{3.55}$$

Comparing the two sets $\Gamma^p_{T_1}$ and $\Gamma^p_{T_2}$ in Equations (3.54) and (3.55), we derive the following relations:

$$\mathbf{N}_1 = \pm\mathbf{N}_2 \tag{3.56}$$

$$\mathbf{p}_1 + \alpha\mathbf{N}_1 = \mathbf{p}_2 + \beta\mathbf{N}_1 \tag{3.57}$$

$$R_1 \pm \sqrt{r_1^2 - \alpha^2} = R_2 \pm \sqrt{r_2^2 - \beta^2}, \tag{3.58}$$

for some α and β such that $-r_1 \leq \alpha \leq r_1$ and $-r_2 \leq \beta \leq r_2$.

By solving Equations (3.57) and (3.58), the values of α and β are given as follows:

$$\begin{cases} \alpha &= \beta + A \\ \beta &= \dfrac{-D \pm \sqrt{D^2 - 4CE}}{2C} \end{cases} \quad \text{or} \quad \begin{cases} \alpha &= \beta - A \\ \beta &= \dfrac{D \pm \sqrt{D^2 - 4CE}}{2C}, \end{cases}$$

where

$$\begin{aligned} A &= ||\mathbf{p}_1 - \mathbf{p}_2||^2 \\ B &= (R_1 - R_2)^2 - (r_1^2 + r_2^2) \\ C &= 4(A^2 + B + r_1^2 + r_2^2) \\ D &= 4A(A^2 + B + 2r_2^2) \\ E &= B^2 + A^4 + 2BA^2 - 4r_1^2 r_2^2 + 4r_2^2 A^2. \end{aligned}$$

Figure 3.13(a) shows the case in which T_1 and T_2 intersect in two profile circles.

Cross-Sectional Circles of T_2

We consider the set of all cross-sectional circles embedded in the torus $T_2 = T_{r_2,R_2}(\mathbf{p}_2, \mathbf{N}_2)$:

$$\Gamma^c_{T_2} = \left\{ C_{r_2}(\mathbf{q}, \mathbf{N_q}) \mid \mathbf{q} \in C_{R_2}(\mathbf{p}_2, \mathbf{N}_2) \text{ and } \mathbf{N_q} = \frac{\mathbf{N}_2 \times (\mathbf{q} - \mathbf{p}_2)}{\|\mathbf{N}_2 \times (\mathbf{q} - \mathbf{p}_2)\|} \right\}. \quad (3.59)$$

Note that $\mathbf{N_q}$ is a unit tangent vector of the main circle $C_{R_2}(\mathbf{p}_2, \mathbf{N}_2)$ of T_2 at $\mathbf{q}$.

Comparing the two sets $\Gamma^p_{T_1}$ and $\Gamma^c_{T_2}$ in Equations (3.54) and (3.59), we derive the following relations:

$$\mathbf{N}_1 = \pm \mathbf{N_q} \quad (3.60)$$

$$\mathbf{p}_1 + \alpha \mathbf{N}_1 = \mathbf{q} \quad (3.61)$$

$$R_1 \pm \sqrt{r_1^2 - \alpha^2} = r_2 \quad (3.62)$$

for some α and $\mathbf{q}$ such that $-r_1 \leq \alpha \leq r_1$ and $\mathbf{q} \in C_{R_2}(\mathbf{p}_2, \mathbf{N}_2)$.

By solving Equation (3.62), we derive the value of α as follows:

$$\alpha = \pm \sqrt{r_1^2 - (r_2 - R_1)^2}.$$

Thus, from the value of α and Equation (3.61),

$$\mathbf{q} = \mathbf{p}_1 \pm \sqrt{r_1^2 - (r_2 - R_1)^2} \mathbf{N}_1.$$

When $\mathbf{q}$ satisfies Equation (3.60), the TTI curve contains a degenerate circle that is a profile circle of T_1 as well as a cross-sectional circle of T_2. Figure 3.13(b) shows a profile circle of T_1 and a cross-sectional circle of T_2 that are coincident in the TTI curve.

Yvone-Villarceau Circles of T_2

We consider the set of all Yvone-Villarceau circles embedded in the torus $T_2 = T_{r_2,R_2}(\mathbf{p}_2, \mathbf{N}_2)$:

$$\Gamma^{YV}_{T_2} = \{ C_{R_2}(\mathbf{q}, \mathbf{N_q}) \mid \mathbf{q} \in C_{r_2}(\mathbf{p}_2, \mathbf{N}_2) \}, \quad (3.63)$$

where

$$\mathbf{N_q} = \pm \frac{r_2}{R_2} \frac{(\mathbf{q} - \mathbf{p}_2) \times \mathbf{N}_2}{\|\mathbf{q} - \mathbf{p}_2\|} + \sqrt{1 - \frac{r_2^2}{R_2^2}}\ \mathbf{N}_2.$$

Comparing the two sets $\Gamma^p_{T_1}$ and $\Gamma^{YV}_{T_2}$ in Equations (3.54) and (3.63), we derive the following relations:

$$\mathbf{N}_1 = \pm\mathbf{N}_\mathbf{q} \tag{3.64}$$

$$\mathbf{p}_1 + \alpha\mathbf{N}_1 = \mathbf{q} \tag{3.65}$$

$$R_1 \pm \sqrt{r_1^2 - \alpha^2} = R_2 \tag{3.66}$$

for some α and $\mathbf{q}$ such that $-r_1 \leq \alpha \leq r_1$ and $\mathbf{q} \in C_{r_2}(\mathbf{p}_2, \mathbf{N}_2)$.

By solving Equation (3.66), we derive the value of α as follows:

$$\alpha = \pm\sqrt{r_1^2 - (R_2 - R_1)^2}.$$

Thus, from the value of α and Equation (3.65),

$$\mathbf{q} = \mathbf{p}_1 \pm \sqrt{r_1^2 - (R_2 - R_1)^2}\mathbf{N}_1.$$

When $\mathbf{q}$ satisfies Equation (3.64), the TTI curve contains a degenerate circle that is a profile circle of T_1 as well as an Yvone-Villarceau circle of T_2. Figure 3.13(c) shows a profile circle of T_1 and an Yvone-Villarceau circle of T_2 that are coincident in the TTI curve.

3.7.2 Cross-Sectional Circles of T_1 and other Circles of T_2

We consider the set of all cross-sectional circles embedded in the torus $T_1 = T_{r_1,R_1}(\mathbf{p}_1, \mathbf{N}_1)$:

$$\Gamma^c_{T_1} = \left\{ C_{r_1}(\mathbf{q}_1, \mathbf{N}_{1,\mathbf{q}_1}) \mid \mathbf{q}_1 \in C_{R_1}(\mathbf{p}_1, \mathbf{N}_1), \text{ and } \mathbf{N}_{1,\mathbf{q}_1} = \frac{\mathbf{N}_1 \times (\mathbf{q}_1 - \mathbf{p}_1)}{\|\mathbf{N}_1 \times (\mathbf{q}_1 - \mathbf{p}_1)\|} \right\}. \tag{3.67}$$

Cross-Sectional Circles of T_2

We consider the set of all cross-sectional circles embedded in the torus $T_2 = T_{r_2,R_2}(\mathbf{p}_2, \mathbf{N}_2)$:

$$\Gamma^c_{T_2} = \left\{ C_{r_2}(\mathbf{q}_2, \mathbf{N}_{2,\mathbf{q}_2}) \mid \mathbf{q}_2 \in C_{R_2}(\mathbf{p}_2, \mathbf{N}_2), \text{ and } \mathbf{N}_{2,\mathbf{q}_2} = \frac{\mathbf{N}_2 \times (\mathbf{q}_2 - \mathbf{p}_2)}{\|\mathbf{N}_2 \times (\mathbf{q}_2 - \mathbf{p}_2)\|} \right\}. \tag{3.68}$$

Comparing the two sets $\Gamma^c_{T_1}$ and $\Gamma^c_{T_2}$ in Equations (3.67) and (3.68), we derive the following relations:

$$\mathbf{N}_{1,\mathbf{q}_1} = \pm\mathbf{N}_{2,\mathbf{q}_2} \tag{3.69}$$

$$\mathbf{q}_1 = \mathbf{q}_2 \tag{3.70}$$

$$r_1 = r_2 \tag{3.71}$$

for some $\mathbf{q}_1$ and $\mathbf{q}_2$ such that $\mathbf{q}_1 \in C_{R_1}(\mathbf{p}_1, \mathbf{N}_1)$ and $\mathbf{q}_2 \in C_{R_2}(\mathbf{p}_2, \mathbf{N}_2)$.

Let $\mathbf{q}$ denote the center point of a circle in $\Gamma^c_{T_1} \cap \Gamma^c_{T_2}$. The point $\mathbf{q}$ is in $C_{R_1}(\mathbf{p}_1, \mathbf{N}_1) \cap C_{R_2}(\mathbf{p}_2, \mathbf{N}_2)$, and $\mathbf{N}_{1,\mathbf{q}} = \pm\mathbf{N}_{2,\mathbf{q}}$ should be satisfied. The vector $\mathbf{N}_{1,\mathbf{q}}$ is parallel with the tangent vector of $C_{R_1}(\mathbf{p}_1, \mathbf{N}_1)$ at $\mathbf{q}$, and the vector $\mathbf{N}_{2,\mathbf{q}}$ is parallel with the tangent vector of $C_{R_2}(\mathbf{p}_2, \mathbf{N}_2)$; thus, $\mathbf{q}$ is a tangential intersection point between $C_{R_1}(\mathbf{p}_1, \mathbf{N}_1)$ and $C_{R_2}(\mathbf{p}_2, \mathbf{N}_2)$. We can compute $C_{R_1}(\mathbf{p}_1, \mathbf{N}_1) \cap C_{R_2}(\mathbf{p}_2, \mathbf{N}_2)$ according to the cases : (i) $\mathbf{N}_1 \times \mathbf{N}_2 \neq \mathbf{0}$ and (ii) $\mathbf{N}_1 \times \mathbf{N}_2 = \mathbf{0}$.

Let $\mathbf{N}_\mathbf{q}$ be a vector which is identical to $\mathbf{N}_{1,\mathbf{q}} (= \pm\mathbf{N}_{2,\mathbf{q}})$. When $\mathbf{N}_1 \times \mathbf{N}_2 \neq \mathbf{0}$, if there is a point $\mathbf{q} \in C_{R_1}(\mathbf{p}_1, \mathbf{N}_1) \cap C_{R_2}(\mathbf{p}_2, \mathbf{N}_2)$, $l(\mathbf{q}, \mathbf{N}_\mathbf{q})$ is a line which is embedded in the intersection of main planes of two tori T_1 and T_2; thus $\mathbf{N}_\mathbf{q}$ is parallel with $\mathbf{N}_1 \times \mathbf{N}_2$. From Equations (3.67) and (3.68), we derive that $\mathbf{N}_\mathbf{q}$ is orthogonal to $\mathbf{p}_1 - \mathbf{q}$ and $\mathbf{p}_2 - \mathbf{q}$. Since $\mathbf{N}_\mathbf{q}$ is parallel with $\mathbf{N}_1 \times \mathbf{N}_2$, and $\mathbf{N}_\mathbf{q}$ is orthogonal to $\mathbf{p}_1 - \mathbf{q}$, $\mathbf{q}$ is a point in the set:

$$\{\mathbf{q} \mid \mathbf{q} \in \mathbf{p}_1 \pm R_1((\mathbf{N}_1 \times \mathbf{N}_2) \times \mathbf{N}_1)\}. \tag{3.72}$$

Moreover, $\mathbf{q}$ is a point on the circle $C_{R_2}(\mathbf{p}_2, \mathbf{N}_2)$; thus the following equations should be satisfied:

$$||\mathbf{p}_2 - \mathbf{q}||^2 = {R_2}^2 \tag{3.73}$$

$$\langle \mathbf{q} - \mathbf{p}_2, \mathbf{N}_2 \rangle = 0 \tag{3.74}$$

We derive the following condition by replacing $\mathbf{q}$ with $\mathbf{p}_1 \pm R_1((\mathbf{N}_1 \times \mathbf{N}_2) \times \mathbf{N}_1)$ in Equation (3.73):

$$||\mathbf{p}_2 - \mathbf{p}_1 \pm R_1((\mathbf{N}_1 \times \mathbf{N}_2) \times \mathbf{N}_1)||^2 = {R_2}^2. \tag{3.75}$$

When $\mathbf{N}_1 \times \mathbf{N}_2 \neq \mathbf{0}$, the TTI curve contains a degenerate circle $C_{r_1}(\mathbf{q}, \mathbf{N}_\mathbf{q})$, where $\mathbf{q} = \mathbf{p}_1 \pm R_1((\mathbf{N}_1 \times \mathbf{N}_2) \times \mathbf{N}_1)$ and $\mathbf{N}_\mathbf{q} = \dfrac{\mathbf{N}_1 \times (\mathbf{q} - \mathbf{p}_1)}{\|\mathbf{N}_1 \times (\mathbf{q} - \mathbf{p}_1)\|}$ (that is a cross-sectional

circle of T_1 as well as that of T_2) if and only if $r_1 = r_2$ and conditions (3.74) and (3.75) are satisfied.

When $\mathbf{N}_1 \times \mathbf{N}_2 = \mathbf{0}$, if there is an intersection point $\mathbf{q} \in C_{R_1}(\mathbf{p}_1, \mathbf{N}_1) \cap C_{R_2}(\mathbf{p}_2, \mathbf{N}_2)$, $\mathbf{p}_2$ should be on the plane $L(\mathbf{p}_1, \mathbf{N}_1)$; thus the following condition is derived:

$$\langle \mathbf{p}_1 - \mathbf{p}_2, \mathbf{N}_1 \rangle = 0. \tag{3.76}$$

From Equations (3.67) and (3.68), we derive that $\mathbf{N_q}$ is orthogonal to $\mathbf{p}_1 - \mathbf{q}$ and $\mathbf{p}_2 - \mathbf{q}$, and $\mathbf{q}$ is a point in the set:

$$\left\{ \mathbf{q} \mid \mathbf{q} \in \mathbf{p}_1 \pm R_1 \frac{\mathbf{p}_2 - \mathbf{p}_1}{||\mathbf{p}_2 - \mathbf{p}_1||} \right\}. \tag{3.77}$$

Moreover, $\mathbf{q}$ is a point on the circle $C_{R_2}(\mathbf{p}_2, \mathbf{N}_2)$; thus the following equation should be satisfied:

$$||\mathbf{p}_2 - \mathbf{q}||^2 = {R_2}^2 \tag{3.78}$$

We derive the following condition by replacing $\mathbf{q}$ with $\mathbf{p}_1 \pm R_1 \frac{\mathbf{p}_2 - \mathbf{p}_1}{||\mathbf{p}_2 - \mathbf{p}_1||}$ in Equation (3.78):

$$\left\| \mathbf{p}_2 - \mathbf{p}_1 \pm R_1 \frac{\mathbf{p}_2 - \mathbf{p}_1}{||\mathbf{p}_2 - \mathbf{p}_1||} \right\|^2 = {R_2}^2. \tag{3.79}$$

When $\mathbf{N}_1 \times \mathbf{N}_2 = \mathbf{0}$, the TTI curve contains a degenerate circle $C_{r_1}(\mathbf{q}, \mathbf{N_q})$, where $\mathbf{q} = \mathbf{p}_1 \pm R_1 \frac{\mathbf{p}_2 - \mathbf{p}_1}{||\mathbf{p}_2 - \mathbf{p}_1||}$ and $\mathbf{N_q} = \frac{\mathbf{N}_1 \times (\mathbf{q} - \mathbf{p}_1)}{\|\mathbf{N}_1 \times (\mathbf{q} - \mathbf{p}_1)\|}$ (that is a cross-sectional circle of T_1 as well as that of T_2) if and only if $r_1 = r_2$ and the condition (3.79) is satisfied.

Figure 3.13(d) shows a cross-sectional circle of T_1 and a cross-sectional circle of T_2 that are coincident in the TTI curve.

Yvone-Villarceau Circles of T_2

We consider the set of all Yvone-Villarceau circles embedded in the torus $T_2 = T_{r_2,R_2}(\mathbf{p}_2, \mathbf{N}_2)$:

$$\Gamma_{T_2}^{YV,\pm} = \{ C_{R_2}(\mathbf{q}_2, \mathbf{N}_{2,\mathbf{q}_2}) \mid \mathbf{q}_2 \in C_{r_2}(\mathbf{p}_{2,}\mathbf{N}_2) \}, \tag{3.80}$$

where

$$\mathbf{N}_{2,\mathbf{q}_2} = \pm \frac{r_2}{R_2} \frac{(\mathbf{q}_2 - \mathbf{p}_2) \times \mathbf{N}_2}{\|\mathbf{q}_2 - \mathbf{p}_2\|} + \sqrt{1 - \frac{r_2^2}{R_2^2}}\, \mathbf{N}_2.$$

Comparing the two sets $\Gamma^c_{T_1}$ and $\Gamma^{YV}_{T_2}$ in Equations (3.67) and (3.80), we derive the following relations:

$$\mathbf{N}_{1,\mathbf{q}_1} = \pm\mathbf{N}_{2,\mathbf{q}_2} \tag{3.81}$$

$$\mathbf{q}_1 = \mathbf{q}_2 \tag{3.82}$$

$$r_1 = R_2 \tag{3.83}$$

for some $\mathbf{q}_1$ and $\mathbf{q}_2$ such that $\mathbf{q}_1 \in C_{R_1}(\mathbf{p}_1, \mathbf{N}_1)$ and $\mathbf{q}_2 \in C_{r_2}(\mathbf{p}_2, \mathbf{N}_2)$.

Given two tori T_1 and T_2, the TTI curve contains a degenerate circle that is a cross-sectional circle of T_1 as well as an Yvone-Villarceau circle of T_2, if and only if $r_1 = R_2$ and there is $\mathbf{q} \in C_{R_1}(\mathbf{p}_1, \mathbf{N}_1) \cap C_{r_2}(\mathbf{p}_2, \mathbf{N}_2)$ such that $\mathbf{N}_{1,\mathbf{q}} = \mathbf{N}_{2,\mathbf{q}}$. Figure 3.13(e) shows a cross-sectional circle of T_1 and an Yvone-Villarceau circle of T_2 that are coincident in the TTI curve.

3.7.3 Yvone-Villarceau Circles of T_1 and T_2

We consider the set of all Yvone-Villarceau circles embedded in the torus $T_1 = T_{r_1,R_1}(\mathbf{p}_1, \mathbf{N}_1)$:

$$\Gamma^{YV}_{T_1} = \{C_{R_1}(\mathbf{q}_1, \mathbf{N}_{1,\mathbf{q}_1}) \mid \mathbf{q}_1 \in C_{r_1}(\mathbf{p}_1, \mathbf{N}_1)\ \}, \tag{3.84}$$

where

$$\mathbf{N}_{1,\mathbf{q}_1} = \pm\frac{r_1}{R_1}\frac{(\mathbf{q}_1 - \mathbf{p}_1) \times \mathbf{N}_1}{\|\mathbf{q}_1 - \mathbf{p}_1\|} + \sqrt{1 - \frac{r_1^2}{R_1^2}}\,\mathbf{N}_1.$$

We consider the set of all Yvone-Villarceau circles embedded in the torus $T_2 = T_{r_2,R_2}(\mathbf{p}_2, \mathbf{N}_2)$:

$$\Gamma^{YV}_{T_2} = \{C_{R_2}(\mathbf{q}_2, \mathbf{N}_{2,\mathbf{q}_2}) \mid \mathbf{q}_2 \in C_{r_2}(\mathbf{p}_2, \mathbf{N}_2)\ \}, \tag{3.85}$$

where

$$\mathbf{N}_{2,\mathbf{q}_2} = \pm\frac{r_2}{R_2}\frac{(\mathbf{q}_2 - \mathbf{p}_2) \times \mathbf{N}_2}{\|\mathbf{q}_2 - \mathbf{p}_2\|} + \sqrt{1 - \frac{r_2^2}{R_2^2}}\,\mathbf{N}_2.$$

Comparing the two sets $\Gamma^{YV}_{T_1}$ and $\Gamma^{YV}_{T_2}$ in Equations (3.84)–(3.85), we derive the following relations:

$$\mathbf{N}_{1,\mathbf{q}_1} = \pm\mathbf{N}_{2,\mathbf{q}_2} \tag{3.86}$$

$$\mathbf{q}_1 = \mathbf{q}_2 \tag{3.87}$$

$$R_1 = R_2 \tag{3.88}$$

for some $\mathbf{q}_1$ and $\mathbf{q}_2$ such that $\mathbf{q}_1 \in C_{r_1}(\mathbf{p}_1, \mathbf{N}_1)$ and $\mathbf{q}_2 \in C_{r_2}(\mathbf{p}_2, \mathbf{N}_2)$.

Given two tori T_1 and T_2, the TTI curve contains a degenerate circle that is an Yvone-Villarceau circle of T_1 as well as that of T_2, if and only if $R_1 = R_2$ and there is $\mathbf{q} \in C_{r_1}(\mathbf{p}_1, \mathbf{N}_1) \cap C_{r_2}(\mathbf{p}_2, \mathbf{N}_2)$ such that $\mathbf{N}_{1,\mathbf{q}} = \mathbf{N}_{2,\mathbf{q}}$. Figure 3.13(e) shows an Yvone-Villarceau circle of T_1 and an Yvone-Villarceau circle of T_2 that are coincident in the TTI curve.

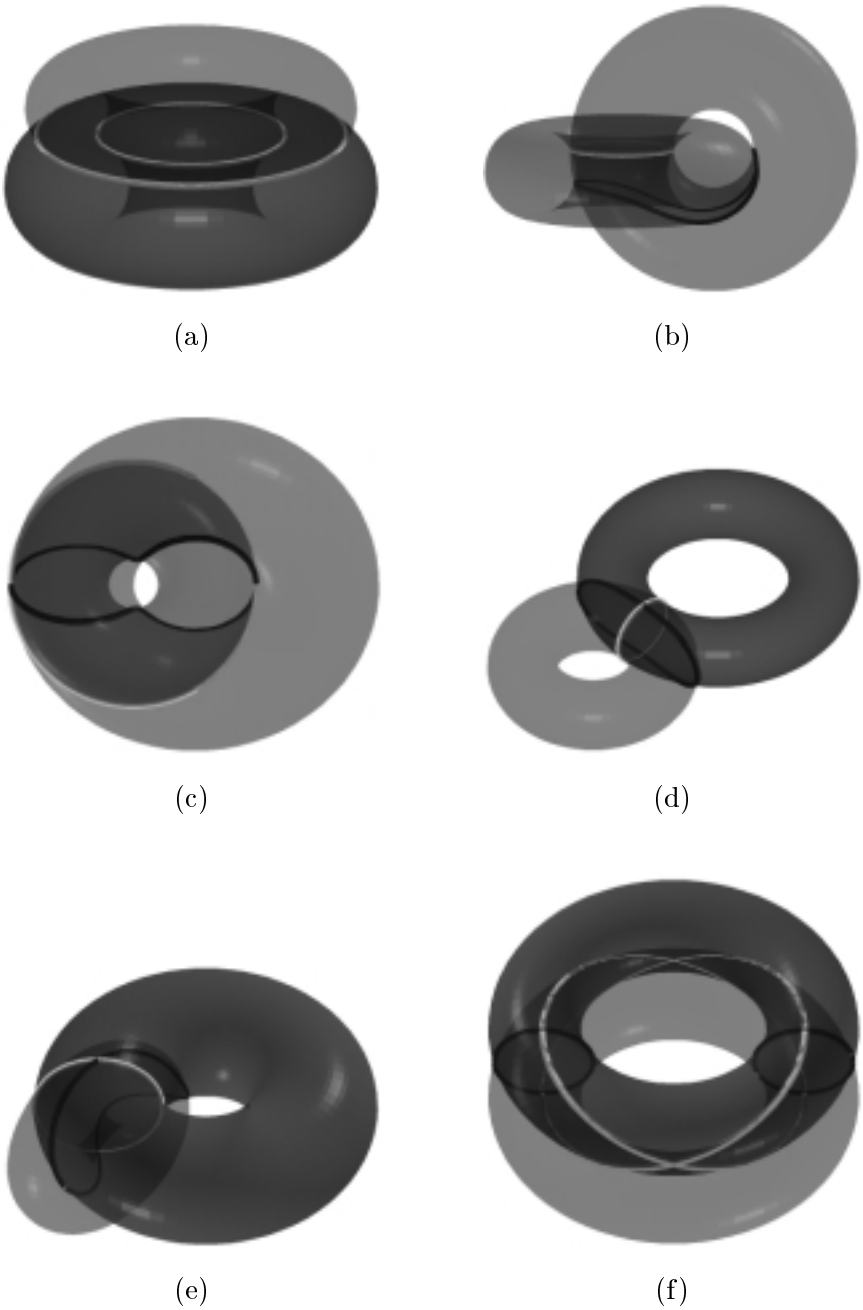

(a) (b)

(c) (d)

(e) (f)

Figure 3.13: Circles in the TTI curve.

Chapter 4

Configuration Space Approach and Related Previous Work

This chapter explains the basic idea of the C-space approach to detect and compute torus/simple-surface intersections and compares the C-space approach with other methods.

4.1 Configuration Space Approach

For the sake of simplicity, we consider torus/sphere intersection (TSI). When we consider the sphere as an obstacle and the torus as an envelope surface of a moving ball along a circular trajectory, the C-space obstacle of the sphere is bounded by the inner and outer offsets of the sphere (which are two concentric spheres). Intersecting the trajectory circle of the moving ball with the C-space obstacle (bounded by two spheres), we can effectively classify the topological type of the TSI curve and construct the TSI curve with all its singularities detected properly.

Given a torus T and a sphere S, in each of the first three cases shown in Figure 4.1, the toroidal volume bounded by T and the ball bounded by S intersect in a single connected (volumetric) component. However, their boundary surfaces T and S intersect in two closed loops (Figure 4.1(a)), in an 8-figured loop with self-intersection (Figure 4.1(b)), and in a single loop (Figure 4.1(c)), respectively. The last case shown in Figure 4.1(d) is related to a singular tangential intersection point. Note that the bold dots represent the center positions of the sweeping ball (inside

the torus T), each corresponding to a tangential contact with the sphere S. In Figure 4.2, these dots correspond to the intersection points between the main circle C (of the torus T) and the C-space obstacle boundary (composed of two concentric spheres). Note that the circle C is also the circular trajectory of the sweeping ball's center.

The classification of each possible type of intersection loop(s) can be made considerably easier when we do the C-space transformation. That is, in Figure 4.2, the sphere S is expanded to a volume bounded by two spheres S^I and S^O, and the torus is shrunk to its main circle C. In Figure 4.2(a), the intersection between the circle C and the volume (bounded by S^I and S^O) has two connected components (i.e., two circular arcs). Each component corresponds to a closed loop in the intersection curve between T and S. Moreover, in Figure 4.2(c), the intersection (in the C-space) has only one connected component. Therefore, the intersection curve of T and S has a single closed loop. Figure 4.2(b) shows an interesting degenerate case in which the intersection (between C and the C-space obstacle) may be considered as two components connected at the tangential intersection point with the inner sphere S^I. The corresponding intersection curve of T and S is an 8-figured curve which may be considered as two intersection loops connected at a singular intersection point (on the sphere S).

Based on a C-space approach, the torus/simple-surface intersection problem is reduced to a simpler problem of intersecting the C-space obstacle (which consists of two offset surfaces of the obstacle surface) with the trajectory of the moving ball's center. The torus/plane intersection (TPI) problem is reduced to that of intersecting a circle with two parallel planes. The torus/sphere intersection (TSI) problem is reduced to: either (i) classifying the relative position of a point with respect to the regions bounded by two tori, or (ii) intersecting a circle with two concentric spheres. The torus/cylinder intersection (TYI) problem is reduced to: either (i) intersecting a line with two tori, or (ii) intersecting a circle with two co-axial cylinders. The torus/torus intersection (TTI) problem is reduced to that of intersecting a circle with two tori.

Compared with other cases, the torus/cone intersection (TKI) problem needs special treatment. In the TKI problem, we always consider the cone as an obstacle, and the torus as the envelope surface of a moving ball. We may interpret a cone as the envelope surface of a moving ball (with a linear radius function $r(t)$) along

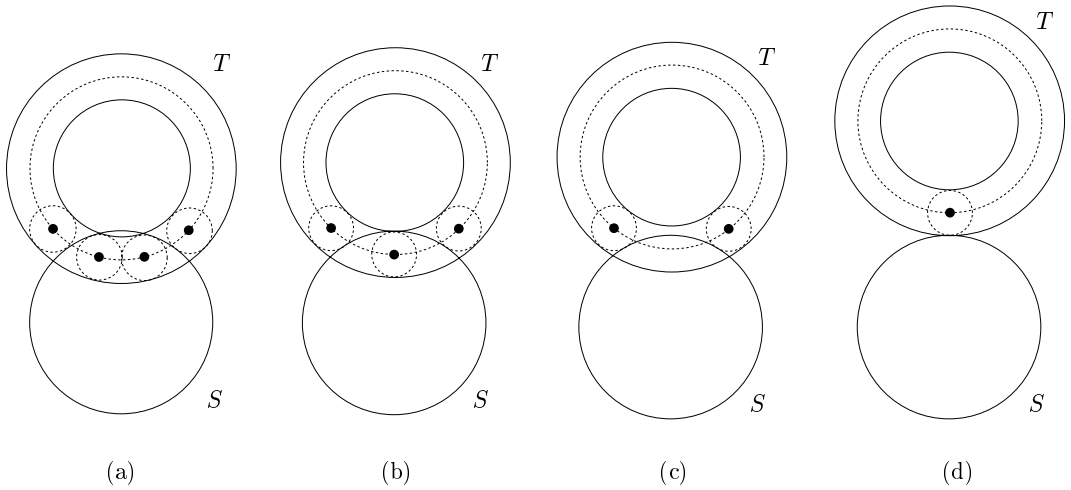

Figure 4.1: Intersections between a torus T and a sphere S

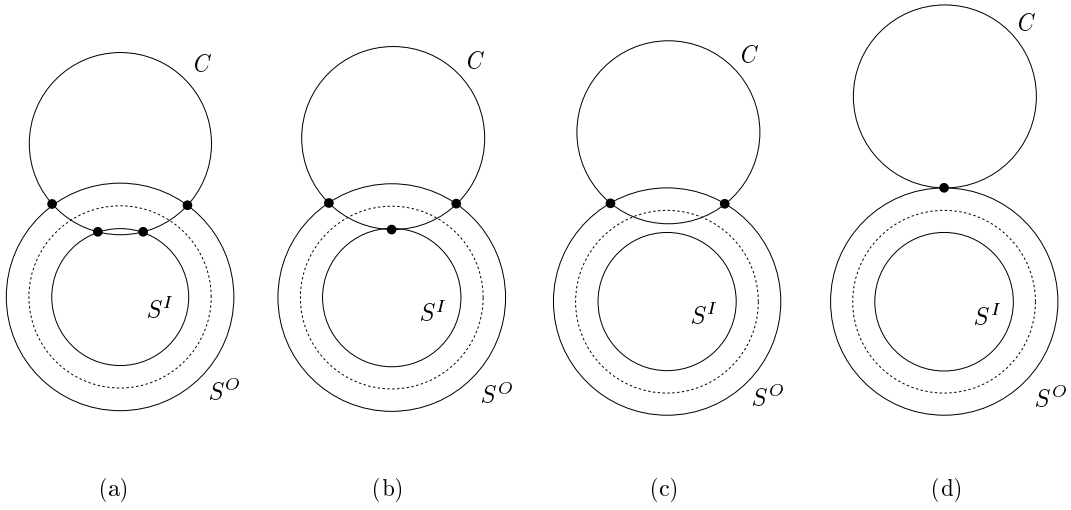

Figure 4.2: Intersections between the main circle of T and the C-space obstacle of S

a half-infinite line $l(t)$, where $t \geq t_0$ for some t_0. Generally speaking, a cone is the envelope surface of the moving ball $B_{r(t)}(\mathbf{q})$ with a linear radius function $r(t)$ (with $r(t_0) = 0$) and the ball center $\mathbf{q}$ moving along a line $l(t)$ with a uniform speed. The d-offset surface of a cone is also a cone which is given as the envelope surface of a moving ball $B_{r(t)+d}(\mathbf{q})$ with its center $\mathbf{q}$ moving along the same line $l(t)$ and its radius function given as $r(t) + d$, where $t \geq t_0$. The offset surface of the cone has a spherical patch attached at an end instead of a vertex. The TKI problem is then reduced to that of intersecting a circle with two such co-axial cones (with attached spherical patches).

Intersections between the C-space obstacle and the trajectory of the moving ball's center provide an effective way of computing singular points and starting points for closed loops in the intersection curve. Table 4.1 shows all computations required in detecting singularities and computing starting points (for numerical curve tracing). The circle/cone, circle/ellipse, circle/torus, and line/torus intersection points can be computed by solving polynomial equations of degree at most four. In computing the starting points and singular points, all other required computations are vector/distance computations which are significantly easier to compute than polynomial equations of degree four. All computations listed in Table 4.1 can be implemented efficiently and robustly using floating-point arithmetic. The intersection curve itself (in general, a quartic space curve for TPI or TSI, and an algebraic space curve of degree eight for TYI, TKI, and TTI) is traced numerically as a sequence of cubic curve segments [1, 3, 4].

4.2 Related Previous Work

We briefly review two other approaches that can be needed in computing torus/simple-surface intersection curves: i) an algebraic method for intersecting two cyclides and ii) a subdivision method.

Cyclide is the envelope surface of a sphere with varying radii, which is tangent to three given fixed spheres. Simple surfaces (plane, natural quadrics, and torus) are special types of cyclide. Therefore, general algebraic methods [5, 10, 15] for intersecting two cyclides may be used in computing the intersection curves of a torus and a simple surface.

de Pont [5] and Martin et al. [15] proposed an algebraic method that computes

Torus/Plane Intersection	(i) circle/plane intersection (ii) vector/distance computation
Torus/Sphere Intersection	(i) circle/circle intersection (ii) vector/distance computation
Torus/Cylinder Intersection	(i) circle/ellipse intersection (ii) line/torus intersection (iii) circle/torus intersection (iv) vector/distance computation
Torus/Cone Intersection	(i) circle/cone intersection (ii) line/torus intersection (iii) vector/distance computation
Torus/Torus Intersection	(i) circle/torus intersection (ii) vector/distance computation

Table 4.1: Operations for computing starting points and singular points

the cyclide/plane, cyclide/quadric, and cyclide/cyclide intersections. The algebraic method computes the intersection curve by substituting the parametric equation of one cyclide into the implicit equation of another cyclide. For example, the intersection curve of a cyclide and a quadric (or a plane) can be represented by the following implicit equation:

$$C(u,v) = (c_0u^2 + c_1u + c_2)v^2 + (c_3u^2 + c_4u + c_5)v + (c_6u^2 + c_7u + c_8) = 0.$$

For a fixed value of u, this is a quadratic equation of v, the solution of which can be represented exactly using radicals. There is a real solution of v if and only if

$$\Delta = (c_3u^2 + c_4u + c_5)^2 - 4(c_0u^2 + c_1u + c_2)(c_6u^2 + c_7u + c_8) \geq 0.$$

The cyclide/cyclide intersection curve $C(u,v) = 0$ is derived as follows:

$$C(u,v) \;=\; [\; u^4 \quad u^3 \quad u^2 \quad u \quad 1 \;]\; [\; M \;] \begin{bmatrix} v^4 \\ v^3 \\ v^2 \\ v \\ 1 \end{bmatrix} = 0,$$

where $[M]$ is a 5×5 matrix with constant elements. For a fixed value of u (respectively, v), the intersection points are computed by solving a quartic polynomial equation of v (respectively, u).

Johnstone [10] presented an intersection algorithm between a cyclide and a ringed surface, where a ringed surface is the sweep surface of a circle. By decomposing the ringed surface into a set of circles, and then performing several steps of inversion, the cyclide/ringed-surface intersection problem is reduced to a cyclide/ruled-surface intersection problem. Since the intersection between a cyclide and a line is computed by solving a polynomial equation of degree at most four, the intersection between a cyclide and a ruling line has a closed-form solution. The intersection curve for the original cyclide/ringed-surface is computed by performing the inversion for the intersection points of a cyclide and ruling lines.

As we have discussed in Section 1, the algebraic methods are general, but they have limitations in robustness. Moreover, it is not easy to determine the topology of the intersection curve. In the torus/plane and torus/quadric intersections, the

double points and the range of the parameter value over which the intersection curve exists can be computed. However, these informations are not enough to know the number of closed loops and singular curves in the intersection curve. It is also hard to determine that a connected component in the intersection curve is singular or regular. Moreover, for the case of torus/torus intersection, the location of double points and the range of the real part of the intersection curve cannot be computed. Without knowing the parameter ranges over which the intersection curve exists, it is hard to detect small closed loops in the intersection curve.

The subdivision method is an approach which recursively subdivides given surfaces until detect all closed loops. Sederberg et al. [27] showed that, if two non-singular surface patches intersect at a closed loop, and the dot product between any normal vector on one surface and any other normal vector on either surface is never zero, and the normal vector is uniquely defined at every point on each surface region, there exists a line which is perpendicular to both surface patches simultaneously. Using this fact and by comparing Gaussian maps of a given torus and a simple surface, we can subdivide given surfaces to detect closed loops in the intersection curve. For the case of a plane, a cylinder, or a cone, the Gaussian map is a point, a great circle, and a circle, respectively, in the unit sphere. For the case of a sphere or a torus, the Gaussian map is a unit sphere. If two surfaces have a closed loop, their Gaussian maps are overlap. When we subdivide the two surfaces until their Gaussian maps do not overlap, all the closed loops can be detected.

The subdivision method has a disadvantage. That is, when the two surfaces intersect almost tangentially, the subdivision may repeat almost indefinitely. Because of round-off errors, it becomes very difficult to connect (with correct topology) the small intersection curve segments of subdivided surface patches.

The C-space approach reduces a surface/surface intersection problem to a curve/surface intersection problem. The topological types of the intersection curve are determined by curve/surface intersection efficiently and robustly. The starting points and the singularities in the torus/simple-surface intersection are exactly computed, by constant number of computing curve/surface intersection and vector/distance computations. Since exact starting points and singular points are given, the intersection curve itself can be traced accurately and robustly.

Chapter 5

Torus and Plane Intersection

This chapter introduces a method to compute the TPI curve based on a C-space approach. Given a torus $T = T_{r,R}(\mathbf{p}_1, \mathbf{N}_1)$ and a plane $L = L(\mathbf{p}_2, \mathbf{N}_2)$, we consider the plane L as an obstacle and the torus T as the envelope surface of a moving ball $B_r(C(t))$. That is, $T = Bdr(\cup B_r(C(t)))$, where $C(t)$ is a circle of radius R.

5.1 Case Analysis for TPI Curve

By applying translation and rotation if necessary, we may assume that the torus T is given in a standard position and orientation; that is, its center is at the origin and its main circle is contained in the xy-plane: $T = T_{r,R}(\mathbf{0}, \mathbf{e}_3)$, where $\mathbf{0} = (0,0,0)$ and $\mathbf{e}_3 = (0,0,1)$. The plane L is given in an arbitrary position: $L = L(\mathbf{p}, \mathbf{N})$.

The C-space obstacle of the plane L (with respect to the moving ball $B_r(C(t))$ of radius r) is bounded by the $\pm r$-offsets of the plane L: that is, two offset planes $L^O = L(\mathbf{p}+r\mathbf{N}, \mathbf{N})$ and $L^I = L(\mathbf{p}-r\mathbf{N}, \mathbf{N})$. Let L^O_- and L^O_+ denote the open regions (of $\mathbb{R}^3$) $\{\mathbf{q} \mid \mathbf{q} = \mathbf{q}_i + s\mathbf{N}, \text{ for } \mathbf{q}_i \in L, \text{ and } s > 0\}$ and $\{\mathbf{q} \mid \mathbf{q} = \mathbf{q}_i + s\mathbf{N}, \text{ for } \mathbf{q}_i \in L, \text{ and } s < 0\}$, respectively, that are separated by L^O. L^I_- and L^I_+ are defined in a similar way.

The two planes L^O and L^I separate the space $\mathbb{R}^3$ into three open regions: L^O_+, $L^O_- \cap L^I_+$, and L^I_-. Consider the case in which the ball $B_r(C(t))$ moves, while its center $C(t)$ is located in the open region $L^O_- \cap L^I_+$, only for $t_1 \le t \le t_2$. The ball $B_r(C(t))$ $(t_1 \le t \le t_2)$ intersects with the plane $L = L(\mathbf{p}, \mathbf{N})$ in a circular disc $D(t)$.

We have the following relation (see Figure 5.1):

$$\begin{aligned} D(t) &= B_r(C(t)) \cap L \subset L \\ \cup D(t) &= \cup(B_r(C(t)) \cap L) = (\cup B_r(C(t))) \cap L \subset L. \end{aligned}$$

The TPI curve $T \cap L$ is the boundary curve of the region $\cup D(t)$ on the plane L (Figure 5.1(b)). Moreover, it is the envelope curve of the one-parameter family of circular discs $D(t)$ on the plane L. With the exception of some degenerate cases, each $D(t)$ contributes two points, $\gamma_-(t)$ and $\gamma_+(t)$, to the envelope curve. These two points are the same as the two intersection points of the cross-sectional circle $C_r(C(t), \mathbf{N}_{C(t)})$ with the plane L, where $\mathbf{N}_{C(t)} = \dfrac{||C'(t)||}{C'(t)}$ (Figure 5.1(c)).

Assume that the ball $B_r(C(t))$ intersects with the plane L, for $t_1 \leq t \leq t_2$, and there is no intersection between $B_r(C(t))$ and L, for $t_1 - \epsilon < t < t_1$ and $t_2 < t < t_2 + \epsilon$, where $\epsilon > 0$ is an arbitrarily small positive number. Then, there are some values of $\hat{t}_1$ and $\hat{t}_2$ such that (Figure 5.1)

- $t_1 < \hat{t}_1 < \hat{t}_2 < t_2$.
- $C_r(C(t), \mathbf{N}_{C(t)}) \cap L = \emptyset$, for $t_1 < t < \hat{t}_1$ or $\hat{t}_2 < t < t_2$.
- $C_r(C(t), \mathbf{N}_{C(t)}) \cap L = \{\gamma_-(t) = \gamma_+(t)\}$, for $t = \hat{t}_1, \hat{t}_2$.
- $C_r(C(t), \mathbf{N}_{C(t)}) \cap L = \{\gamma_-(t), \gamma_+(t)\}$, with $\gamma_-(t) \neq \gamma_+(t)$, for $\hat{t}_1 < t < \hat{t}_2$.

The boundary curve of the region $\cup_{t_1 \leq t \leq t_2} D(t)$ (on the plane L) is the same as the union

$$\cup_{\hat{t}_1 \leq t \leq \hat{t}_2} \left(C_r(C(t), \mathbf{N}_{C(t)}) \cap L \right).$$

Since the cross-sectional circles $C_r(C(t), \mathbf{N}_{C(t)})$ are all disjoint, no boundary point of $\cup_{t_1 \leq t \leq t_2} D(t)$ can be shared by two different instances of $C_r(C(t), \mathbf{N}_{C(t)})$, for $\hat{t}_1 \leq t \leq \hat{t}_2$. Therefore, the two curves $\gamma_-(t)$ and $\gamma_+(t)$ have no intersection, for $\hat{t}_1 < t < \hat{t}_2$. They have no self-intersection, either. Moreover, these two curves are connected at two common end points: $\gamma_-(\hat{t}_1) = \gamma_+(\hat{t}_1)$ and $\gamma_-(\hat{t}_2) = \gamma_+(\hat{t}_2)$. The resulting boundary curve of $\cup D(t)$ thus forms a closed loop on the plane L.

In the above discussion, we showed that: when the circle $C(t)$ intersects with $L_-^O \cap L_+^I$, but is not totally contained in the open region $L_-^O \cap L_+^I$, each connected component of the intersection $C(t) \cap (L_-^O \cap L_+^I)$ produces a closed loop in the TPI

(a) $T \cap L$

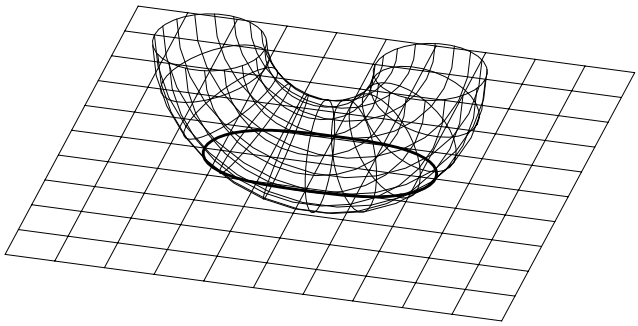

(b) $\cup_{t_1 \le t \le t_2} D(t)$

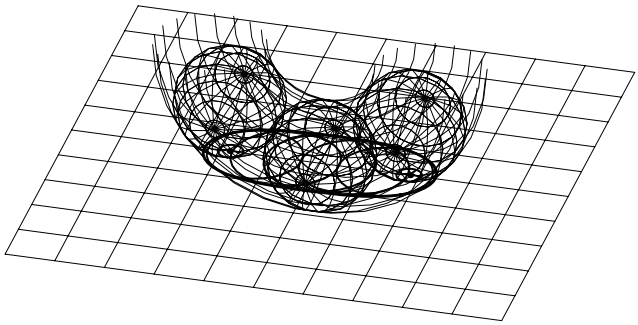

(c) $\cup_{\hat{t}_1 \le t \le \hat{t}_2} \dot{\left(C_r(C(t), \mathbf{N}_{C(t)}) \cap L\right)}$

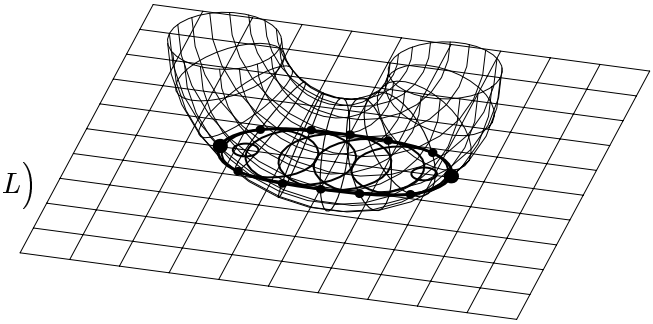

(d) $\gamma_-(t)$ and $\gamma_+(t)$

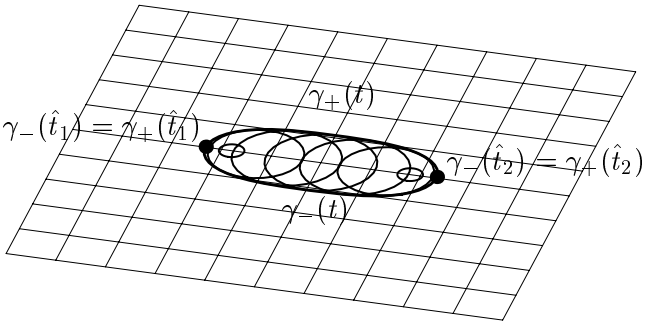

Figure 5.1: $\gamma_-(t)$ and $\gamma_+(t)$ which generate $T \cap L$

curve. We can easily show that there are at most two connected components in the intersection $C(t) \cap (L_-^O \cap L_+^I)$. This is because the circle $C(t)$ may intersect with the plane L^I at no more than two points. Similarly, the circle $C(t)$ may intersect with the plane L^O at no more than two points.

The figures in the left columns of Figures 5.2–5.5 illustrate the relative position of the main circle $C_R(\mathbf{0}, \mathbf{e}_3)$ of the torus T in the C-space of the plane L; the figures in the right columns of Figures 5.2–5.5 illustrate the corresponding relative configurations of T and L.

When the circle $C(t)$ is totally contained in the open region L_+^O or L_-^I, there is no TPI curve since no ball $B_r(C(t))$ intersects with the plane L (Figure 5.2(a)). Next, we consider the case in which the circle $C(t)$ is totally contained in the open region $L_+^I \cap L_-^O$. In this case, each cross-sectional circle $C_r(C(t), \mathbf{N}_{C(t)})$ intersects with the plane L at two different points: $\gamma_-(t)$ and $\gamma_+(t)$. As the cross-sectional circle $C_r(C(t), \mathbf{N}_{C(t)})$ sweeps out the entire torus T, the two points, $\gamma_-(t)$ and $\gamma_+(t)$, generate two smooth curves that bound the connected region $\cup D(t)$ on the plane L. Therefore, the TPI curve consists of two closed loops (Figure 5.2(b)). The starting points to detect $T \cap L$ can be computed by intersecting the plane L with an arbitrary cross-sectional circle of T.

If $C(t)$ is embedded in L^I (or L^O), then the TPI curve is a singular circle with multiplicity two. In this case, this singular circle is a profile circle of T.

The necessary and sufficient condition for the TPI curve to have the singularity at a point $\mathbf{q}_L \in L$ is that $C(t)$ intersects with L^I or L^O at a point $C(t_1)$, and $C_r(C(t_1), \mathbf{N}_{C(t_1)})$, intersects with L at $\mathbf{q}_L$ tangentially. If the circle $C(t)$ has a tangential contact (at a point $\mathbf{q}$) with either L^I or L^O, then the TPI curve contains a singular point $\mathbf{q}_L$, where $\mathbf{q} = \mathbf{q}_L + r\mathbf{N}$ if $\mathbf{q} \in L^O$, or $\mathbf{q} = \mathbf{q}_L - r\mathbf{N}$ if $\mathbf{q} \in L^I$. If $C(t)$ is not embedded in $L^I \cup L^O$ and $C(t)$ has no tangential contact with $L^I \cup L^O$, then there is no singular point in the TPI curve.

If the circle $C(t)$ has a tangential contact (at a point $\mathbf{q}$) with either L^I or L^O, and the circular arc $(C(t) - \mathbf{q})$ is totally contained in the region $L_+^I \cap L_-^O$, then the two closed loops in the TPI curve have a contact at $\mathbf{q}_L$, forming an 8-figured loop (Figure 5.3(a)), where $\mathbf{q} = \mathbf{q}_L + r\mathbf{N}$ if $\mathbf{q} \in L^O$, or $\mathbf{q} = \mathbf{q}_L - r\mathbf{N}$ if $\mathbf{q} \in L^I$. When the circle $C(t)$ has a tangential contact (at a point $\mathbf{q}$) with either L^I or L^O, and $(C(t) - \mathbf{q}) \cap (L_+^I \cap L_-^O)$ consists of two circular arcs, then the two closed loops in the TPI curve have a contact at $\mathbf{q}_L$, forming an 8-figured loop (Figure 5.3(b)). In

Figure 5.3(c), $C(t)$ has a tangential intersection with L^I at a point $\mathbf{q} \in L^I$. The corresponding TPI curve is a tangent isolated point $\mathbf{q}_L$, where $\mathbf{q} = \mathbf{q}_L - r\mathbf{N}$.

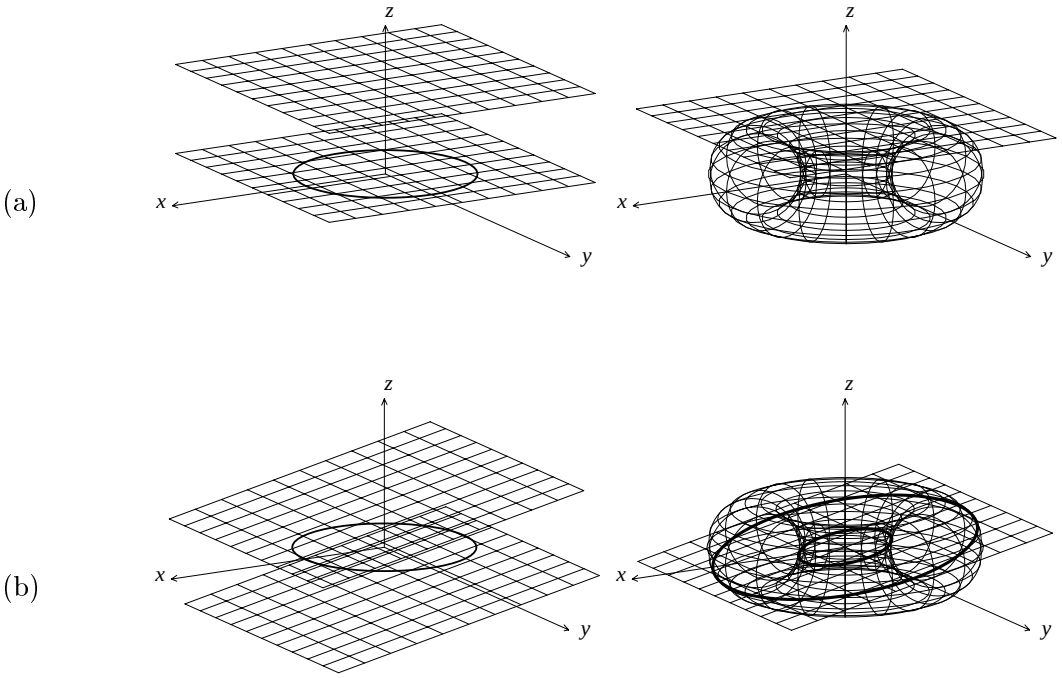

Figure 5.2: Regular TPI curves

Figures 5.4–5.5 show the cases in which the intersection $C(t) \cap (L^O_- \cap L^I_+)$ has one and two connected component(s). The corresponding TPI curve consists of one and two closed loop(s).

Figures 5.6(a)–(c) show degenerate cases in which the circle $C(t)$ has two tangential intersections with $L^I \cup L^O$. Each tangential intersection generates a singularity in the corresponding TPI curve. Therefore, there are two singular points in the TPI curve. Being a self-intersection point of the TPI curve, each singular point has multiplicity two. When we pass a plane L through the two singular points, the plane L cannot intersect with any other point of the TPI curve since the plane L already intersects with the TPI curve (of degree four) at four points (counting the multiplicity

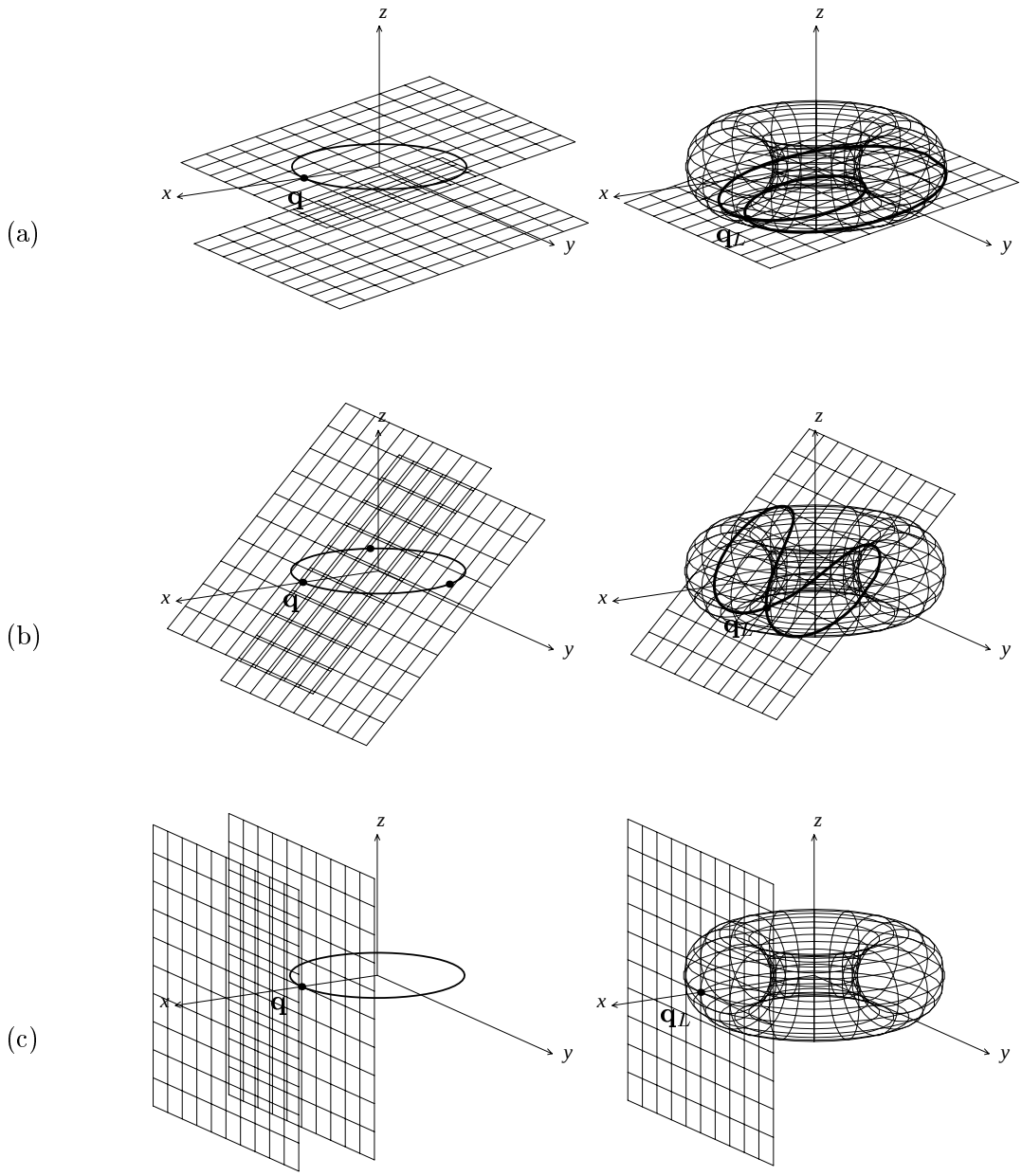

Figure 5.3: Singular TPI curves

properly). The only exception is the case in which the plane L completely contains the TPI curve. This means that each component of the singular TPI curve is a planar curve. That is, this curve must be a circle. In fact, in this case, the TPI curve consists of two Yvone-Villarceau circles of T. Consequently, the TPI curve consists of two circles when there are two singular points. Each singularity can be easily detected from a tangential intersection of $C(t)$ with the two offset planes $L^O \cup L^I$.

5.2 Algorithm: Torus_Plane_Intersection

Algorithm: Torus_Plane_Intersection of Appendix A.1 summarizes the algorithm discussed in this section. We assume that two curve tracing routines: Trace_Singular _TPI_Curve (T, L, P) and Trace_Regular_TPI_Curve(T, L, P), are available, where T is a torus, L is a plane, and P is the set of starting points (one for each closed loop of the TPI curve). Each singular intersection curve can be traced starting from its singular point (see also Piegl [20, 21]), the details of which are given in the routine: Trace_Singular_TPI_Curve. To deal with the cases in which T and L have no tangential intersection point, a starting point must be generated on each closed loop of the TPI curve. After that, each curve component is traced using the routine: Trace_Regular_TPI_Curve.

In Lines (1), (2), and (4), we assume that the routines computing degenerate circles of the TPI curve are available (see Section 3.3 and Figure 3.2). Line (3) corresponds to the case shown in Figure 5.4. Assume that the ball $B_r(C(t))$ intersects with the plane L, only for $t_1 \le t \le t_2$, (i.e., $C(t_1) = \mathbf{p}_1$ and $C(t_2) = \mathbf{p}_2$), and the cross-sectional circle $C_r(C(t), \mathbf{N}_{C(t)})$ intersects with the plane L, for $t_1 < \hat{t}_1 \le t \le \hat{t}_2 < t_2$. Since the TPI curve is symmetric with respect to both T and L, we have the following relation:

$$t_1 < \hat{t}_1 \le \frac{t_1 + t_2}{2} \le \hat{t}_2 < t_2.$$

Note that the middle point $\mathbf{q}$ in Line (3) is the same as $C(\frac{t_1+t_2}{2})$. Therefore, the cross-sectional circle $C_r(\mathbf{q}, \mathbf{N_q})$ intersects with the plane L at two different points. We take only one of them as a starting point for numerical curve tracing.

Line (5) corresponds to the case shown in Figures 5.5(a)–(c). Let $C(t_i) = \mathbf{p}_i$, for $i = 1, 2, 3, 4$. Note that the ball $B_r(C(\frac{t_1+t_2}{2}))$ is totally contained in L^-, and the ball $B_r(C(\frac{t_3+t_4}{2}))$ is totally contained in L^+, where L^+ and L^- are two half-spaces separated by the plane L. Then any profile circle of the torus T will intersect with the

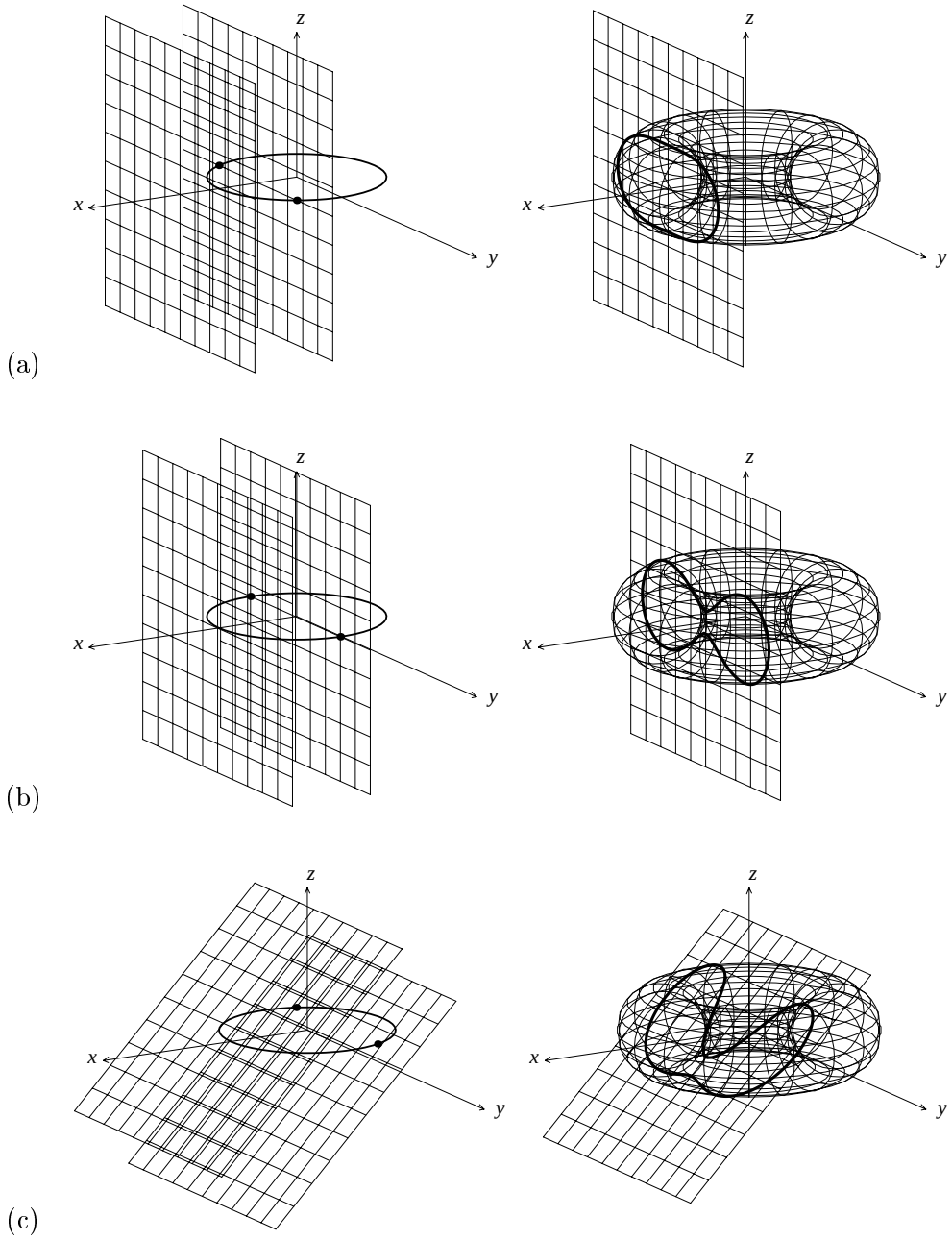

Figure 5.4: The TPI curve which consists of one intersection loop

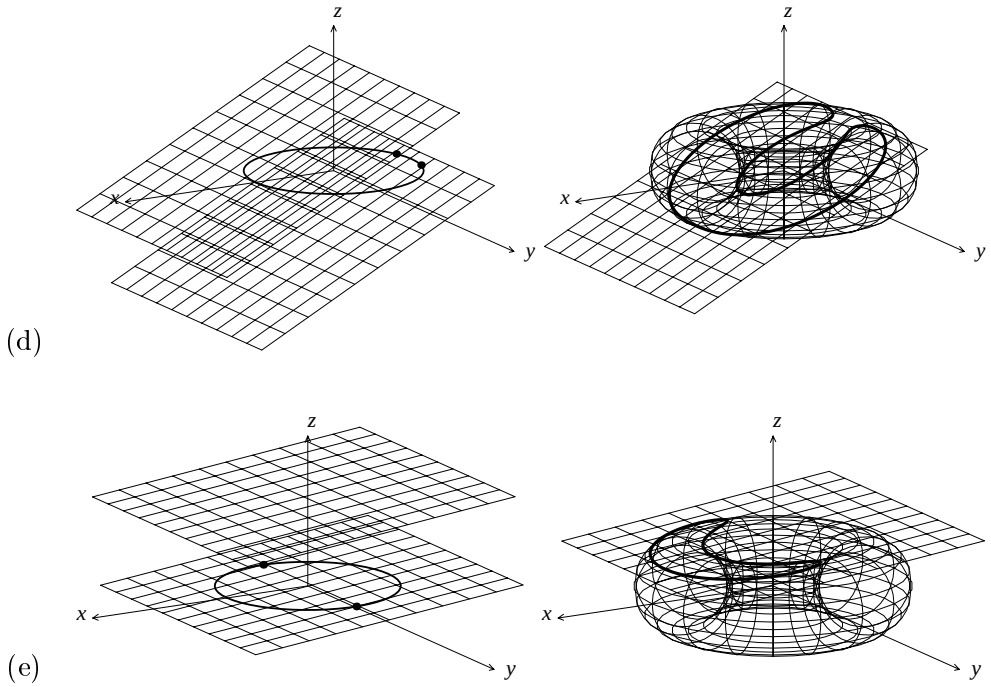

Figure 5.4: (*cont.*)

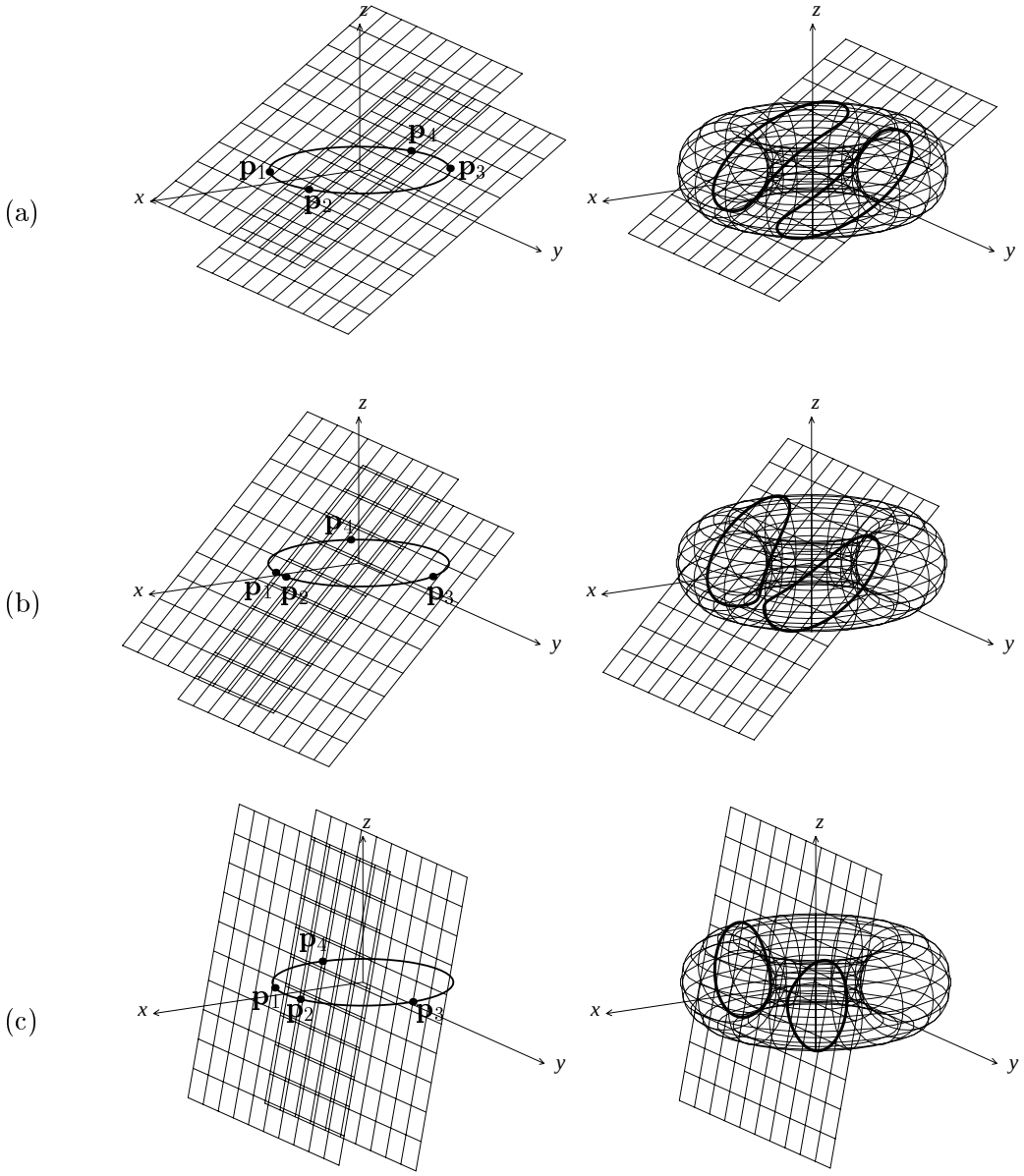

Figure 5.5: The TPI curve which consists of two intersection loops

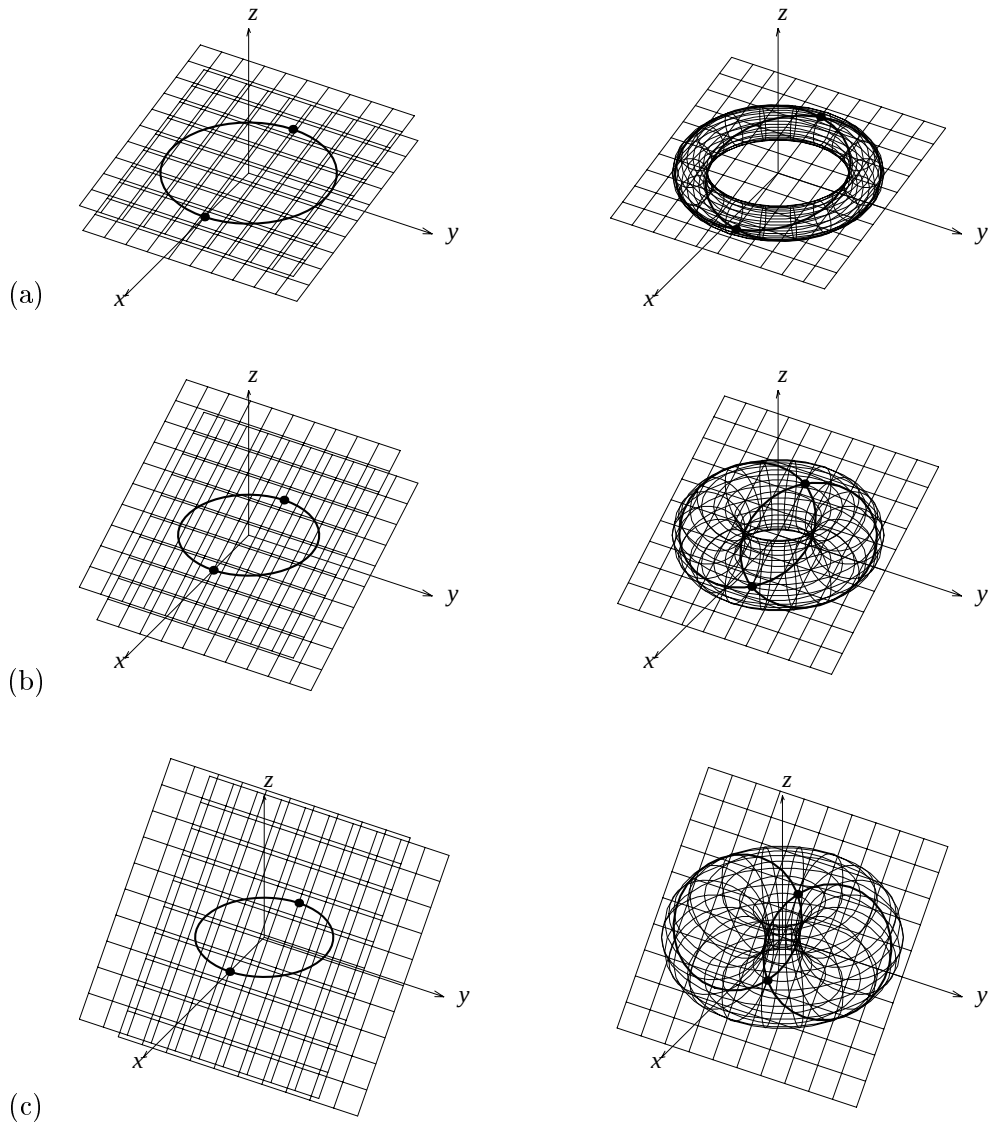

Figure 5.6: Yvone-Villarceau circles in TPI

plane L at two different points (see Figure 3.1(a) for profile circles). Moreover, each intersection point belongs to a different component of the TPI curve. In Line (5), we take the profile circle $C_{R+r}(\mathbf{0}, \mathbf{e}_3)$ of the largest radius. The two intersection points in $L \cap C_{R+r}(\mathbf{0}, \mathbf{e}_3)$ are used as the starting points for the two closed loops in the TPI curve.

Chapter 6

Torus and Sphere Intersection

This chapter shows that the TSI curve is a quartic space curve, and then introduces two methods of computing the TSI curve based on a C-space approach. Given a torus $T = T_{r,R}(\mathbf{p}_1, \mathbf{N})$ and a sphere $S = S_\delta(\mathbf{p}_2)$, the first method considers the case of $0 < \delta \leq r$, and the second method considers the case of $0 < r < \delta$. In the first method, the relative position of the sphere center $\mathbf{p}_2$ with respect to the torus T determines the TSI curve. In the second method, the relative position of the main circle $C_R(\mathbf{p}_1, \mathbf{N})$ with respect to the sphere S determines the TSI curve. The C-space approach is useful in classifying the relative positions.

6.1 TSI as a Quartic Curve

We show that the real, affine TSI curve is the same as the intersection curve of a sphere and a quadric surface. Thus, the algebraic degree of a real, affine TSI curve is four at most. By applying translation and rotation if necessary, we may assume that the torus T is given in a standard position and orientation; that is, its center is at the origin and its main circle is contained in the xy-plane: $T = T_{r,R}(\mathbf{0}, \mathbf{e}_3)$, where $\mathbf{0} = (0, 0, 0)$ and $\mathbf{e}_3 = (0, 0, 1)$. The sphere S is in an arbitrary position: $S = S_\delta((\alpha, \beta, \gamma))$.

The implicit equation of the torus $T = T_{r,R}(\mathbf{0}, \mathbf{e}_3)$ is given as follows:

$$(x^2 + y^2 + z^2 + R^2 - r^2)^2 - 4R^2(x^2 + y^2) = 0. \tag{6.1}$$

Moreover, the implicit equation of the sphere $S = S_\delta((\alpha, \beta, \gamma))$ is given by

$$(x-\alpha)^2 + (y-\beta)^2 + (z-\gamma)^2 - \delta^2 = 0,$$

equivalently,

$$x^2 + y^2 + z^2 = \delta^2 - \alpha^2 - \beta^2 - \gamma^2 + 2\alpha x + 2\beta y + 2\gamma z. \tag{6.2}$$

By substituting Equation (6.2) to Equation (6.1), we obtain

$$(2\alpha x + 2\beta y + 2\gamma z + E)^2 - 4R^2(x^2 + y^2) = 0, \tag{6.3}$$

where $E = R^2 - r^2 + \delta^2 - \alpha^2 - \beta^2 - \gamma^2$. This equation can be reformulated as a quadric surface as follows:

$$\begin{aligned} & 4(\alpha^2 - R^2)x^2 + 4(\beta^2 - R^2)y^2 + 4\gamma^2 z^2 + 8(\alpha\beta)xy + 8(\beta\gamma)yz + 8(\gamma\alpha)zx \\ + \quad & 4(\alpha E)x + 4(\beta E)y + 4(\gamma E)z + E^2 = 0. \end{aligned} \tag{6.4}$$

The TSI curve is the same as the intersection curve of the sphere S and the quadric surface defined by Equation (6.4). But, the quadric surface of Equation (6.4) is not a natural quadric. For example, when $(\alpha, \beta, \gamma) = (1, 0, 0)$, $R = 3$, $r = 1$, and $\delta = 3$, Equation (6.4) represents an elliptic cylinder. When $(\alpha, \beta, \gamma) = (3, 0, 0)$, $R = 2$, $r = 0.5$, and $\delta = 3$, Equation (6.4) represents a hyperbolic cylinder. Therefore, we cannot use the intersection algorithms for natural quadrics to solve the TSI problem [16, 18, 20, 26, 28]. Although there are algebraic algorithms for intersecting two general quadrics [6, 12, 13, 29], they have limitations in numerical stability (see References [16, 18] for related discussions). Therefore, we need to develop an efficient and robust geometric method to compute the TSI curve. In this paper, we present such an algorithm using a geometric transformation that reduces the torus/sphere intersection problem to a simpler problem of: either (i) classifying the containment of a point in an open region bounded by two toroidal surfaces, or (ii) intersecting a circle with two concentric spheres. Using a few vector/distance computations, we can reduce this problem to: either (i) classifying the containment of a point in a circular region, or (ii) intersecting two circles in the same plane. These computations can be implemented in an efficient and robust way using floating-point arithmetic. We discuss this in more detail in following sections.

6.2 The Case of $0 < \delta \leq r$

In this case, we consider the torus T as an obstacle and compute its C-space obstacle with respect to the sphere S. By applying a simple translation, we may assume that the torus T has its center at the origin: $T = T_{r,R}(\mathbf{0}, \mathbf{N})$, and the sphere S is given as: $S = S_\delta(\mathbf{p})$. The C-space obstacle of T is bounded by the $\pm\delta$-offsets of the torus: i.e., the inner offset torus $T^I = T_{r-\delta,R}(\mathbf{0}, \mathbf{N})$ and the outer offset torus $T^O = T_{r+\delta,R}(\mathbf{0}, \mathbf{N})$.

6.2.1 Case Analysis for Singular Intersections

When $r + \delta \geq R$, the outer torus T^O self-intersects. Let T^D denote the self-intersected part of T^O (see Figures 2.2(b)–(c)). (In the case of $r + \delta < R$, T^O has no self-intersection; thus we have $T^D = \emptyset$.) Based on the relative position of $\mathbf{p}$ with respect to T^I, T^O, and T^D, we can classify all possible topological types of the TSI curves. The TSI curve has singularity (i.e., the torus T and the sphere S have a tangential intersection at $\mathbf{p}_T \in T \cap S$) if and only if the center $\mathbf{p}$ of S is on the boundary of T^I, T^O, or T^D, where $\mathbf{p}_T$ is an orthogonal projection of $\mathbf{p}$ onto the surface T. Note that $\mathbf{p}$ is also the $\pm\delta$-offset point of $\mathbf{p}_T \in T$ (see Figure 6.1). There are five different cases to consider (for singular intersections):

1. $\mathbf{p} \in T^O \setminus T^D$: the TSI curve degenerates into a point $\mathbf{p}_T$ (Figure 6.1(a)).
2. $\mathbf{p} \in T^D$ and $\mathbf{p}$ is a vertex of T^D: the TSI curve degenerates into a circle (Figure 6.1(b)).
3. $\mathbf{p} \in T^D$ and $\mathbf{p}$ is not a vertex: the TSI curve is a quartic space curve with singularity at $\mathbf{p}_T$ (Figure 6.1(c)).
4. $\mathbf{p} \in T^I$ and $0 < \delta < r$: the TSI curve degenerates into a point $\mathbf{p}_T$ (Figure 6.1(d)).
5. $\mathbf{p} \in T^I$ and $0 < \delta = r$: the TSI curve degenerates into a circle (Figure 6.1(e)).

The figures in the left columns of Figures 6.1–6.2 illustrate the relative positions of $\mathbf{p}$ in the C-space of the torus T; the figures in the right columns of Figures 6.1–6.2 illustrate the corresponding relative configurations of T and S.

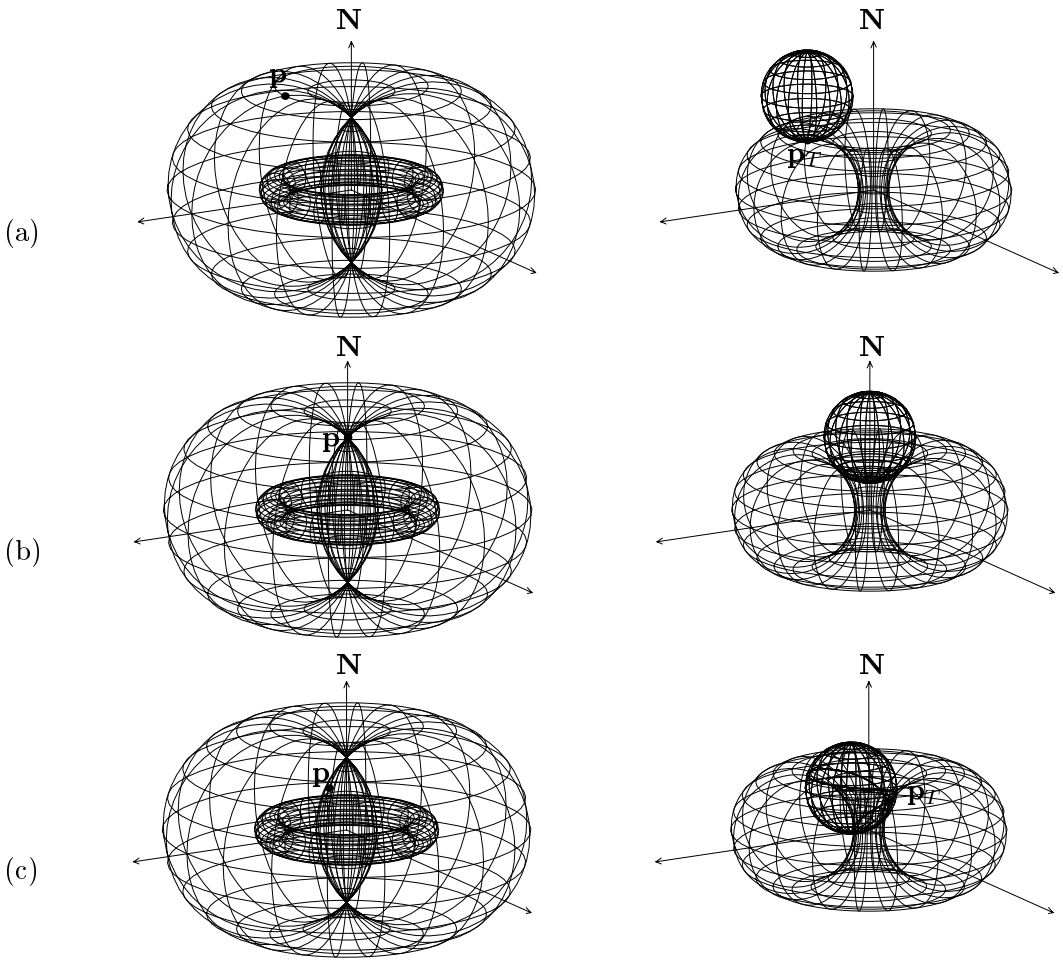

Figure 6.1: Degenerate or singular TSI curves.

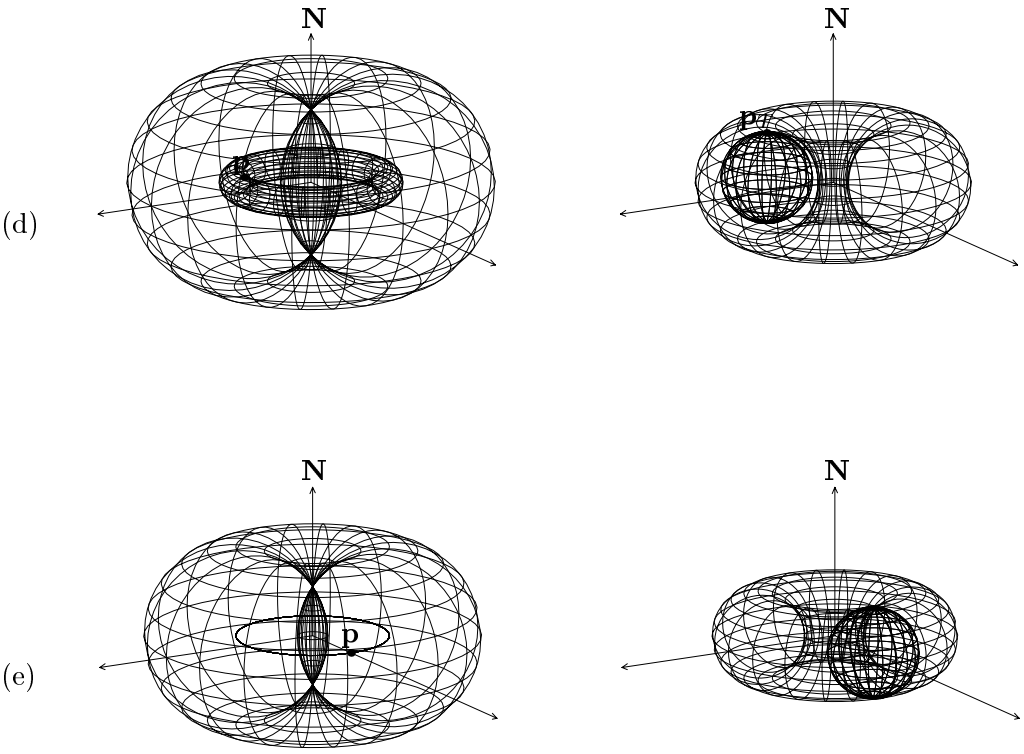

Figure 6.1: (*cont.*)

In case 2 considered above, the torus and the sphere touch along a degenerate circle. When we enlarge the radius δ of the sphere S slightly, the sphere S will intersect with the torus T in two different circles. Therefore, the degenerate circle of Figure 6.1(b) may be considered as the limit of these two converging circles. When the limiting circle is interpreted as an overlap of two identical circles, the singular degenerate circle has a total algebraic degree of four. Therefore, it is clear that there is no other loop in the TSI curve.

In case 3 considered above, the TSI curve has degree four and the curve has four branches at the singular point (i.e., at the tangential intersection point of T and S). (In algebraic geometry, two opposite branch directions are counted as a single branch; however, in this paper, we count them separately to make the counting scheme more intuitive for the engineering community.) We can easily compute these four branches by comparing the Dupin indicatrices of the torus T and the sphere S at their tangential intersection point (see also Piegl [21]). The whole TSI curve can be detected by tracing along only two appropriate branches at the singular point. Using the result of Farouki et al. [6], we can also represent the TSI curve (with a singular point) exactly as a rational quartic space curve. The fact that there is no other loop in the TSI curve will become clear when we discuss the relationship between the number of intersection loops and the winding number assigned to each 3D (volumetric) open region bounded by T^I, T^O, and T^D.

In case 5, when we enlarge the radius δ of the sphere S slightly, the sphere S will intersect with the torus T in an irreducible quartic space curve. But, when we relocate the center $\mathbf{p}$ of S in the main plane of T and at a distance $\sqrt{R^2+\delta^2-r^2}$ from the center of T, the sphere S will intersect with the torus T in two degenerate circles (see Figure 3.7). As the radius δ of S converges to the minor radius r of T, the two degenerate circles converge to the singular degenerate circle of case 5 shown in Figure 6.1(e). Therefore, we can apply an argument similar to that of case 2 and conclude that there is no other loop in the TSI curve.

6.2.2 Case Analysis for Non-Singular Intersections

The TSI curve has a singularity if and only if the center $\mathbf{p}$ of S is located on the toroidal surface T^I, T^O, or T^D. Let T^I_- and T^I_+ denote the interior and exterior open regions of $\mathbb{R}^3$ separated by the closed surface T^I. T^D_- and T^D_+ are defined similarly.

T_-^O and T_+^O are the open regions separated by the closed surface $T^O \setminus T^{D^o}$, where T^{D^o} denotes T^D except two vertices of T^D. There are four different cases to consider (for non-singular intersections):

1. $\mathbf{p} \in T_+^O$: the TSI curve is empty (Figure 6.2(a)).
2. $\mathbf{p} \in T_-^I$: the TSI curve is empty (Figure 6.2(b)).
3. $\mathbf{p} \in T_-^O \cap T_+^I \cap T_+^D$: the TSI curve has only one loop (Figure 6.2(c)).
4. $\mathbf{p} \in T_-^D$: the TSI curve has two loops (Figure 6.2(d)).

Note that each point $\mathbf{p} \notin T^I \cup T^O \cup T^D$ (i.e., $\mathbf{p}$ is not located on any of the toroidal surfaces T^I, T^O, and T^D) must belong to one of the four open regions enumerated in the above classification. In case 4 considered above, each loop of the TSI curve may degenerate into a circle when the point $\mathbf{p}$ is located on the main axis of the torus T (see Section 3.5 and Figure 3.4).

6.2.3 Winding Number Theory

The number of closed loops in the TSI curve is closely related to the winding number of the two toroidal surfaces T^O and T^I around the center $\mathbf{p}$ of the sphere S. When we give the normal orientations of the surfaces T^O and T^D as the outward directions (i.e., pointing to the regions T_+^O and T_+^D, respectively) and that of the surface T^I as the inward direction (i.e., pointing to the region T_-^I), the winding numbers assigned to the open regions T_+^O and T_-^I are both zero. Moreover, the winding number assigned to $T_-^O \cap T_+^I \cap T_+^D$ is one and that assigned to T_-^D is two. A formal definition of winding number can be found in a standard textbook of differential topology [8]. But there is a simple way to compute the winding number assigned to an open region. That is, when we cut the space $\mathbb{R}^3$ by a plane L that passes through a point $\mathbf{p}$, the toroidal surfaces T^I and T^O will intersect with the plane in some closed planar curves. These closed curves bound the planar open regions: $T_+^O \cap L$, $T_-^I \cap L$, $(T_-^O \cap T_+^I \cap T_+^D) \cap L$, and $T_-^D \cap L$ in the plane L. When we trace each curve so that the curve normal (inherited from the surface normal orientation) is always to the right-hand side of the curve advancing direction, we can determine the winding number of the planar curves around the selected point $\mathbf{p}$. Figure 6.3 shows two examples of planar cuts, in which the plane L is taken so that it contains the point

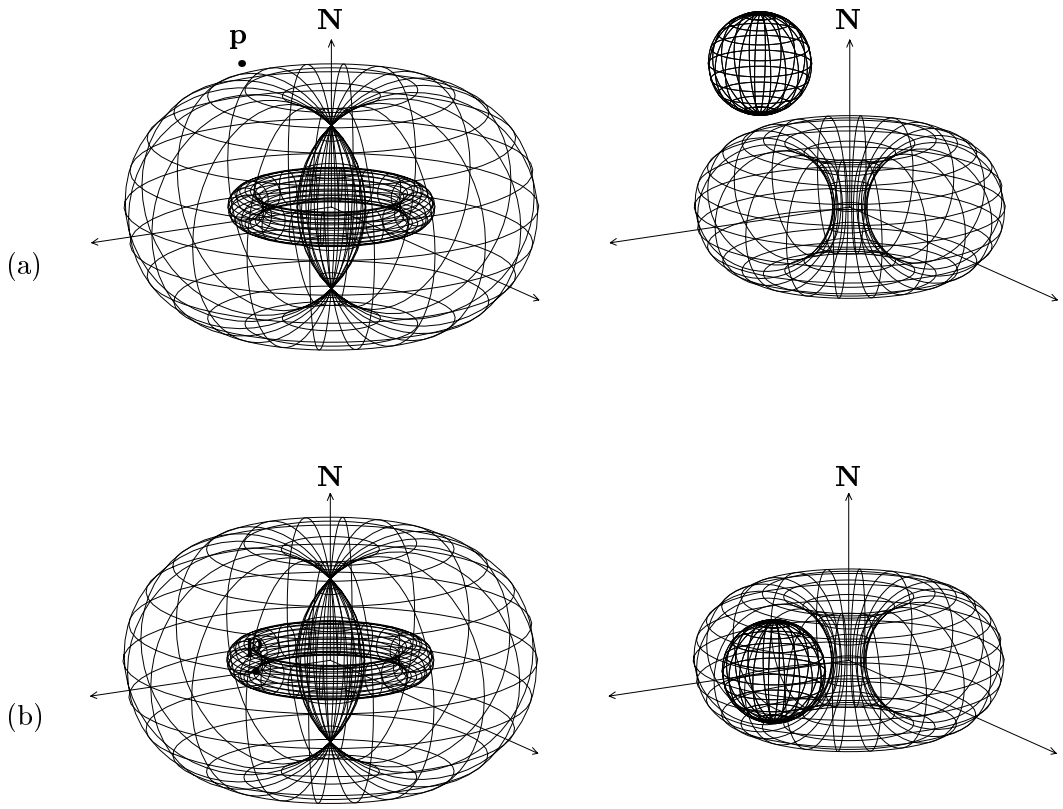

Figure 6.2: Regular TSI curves.

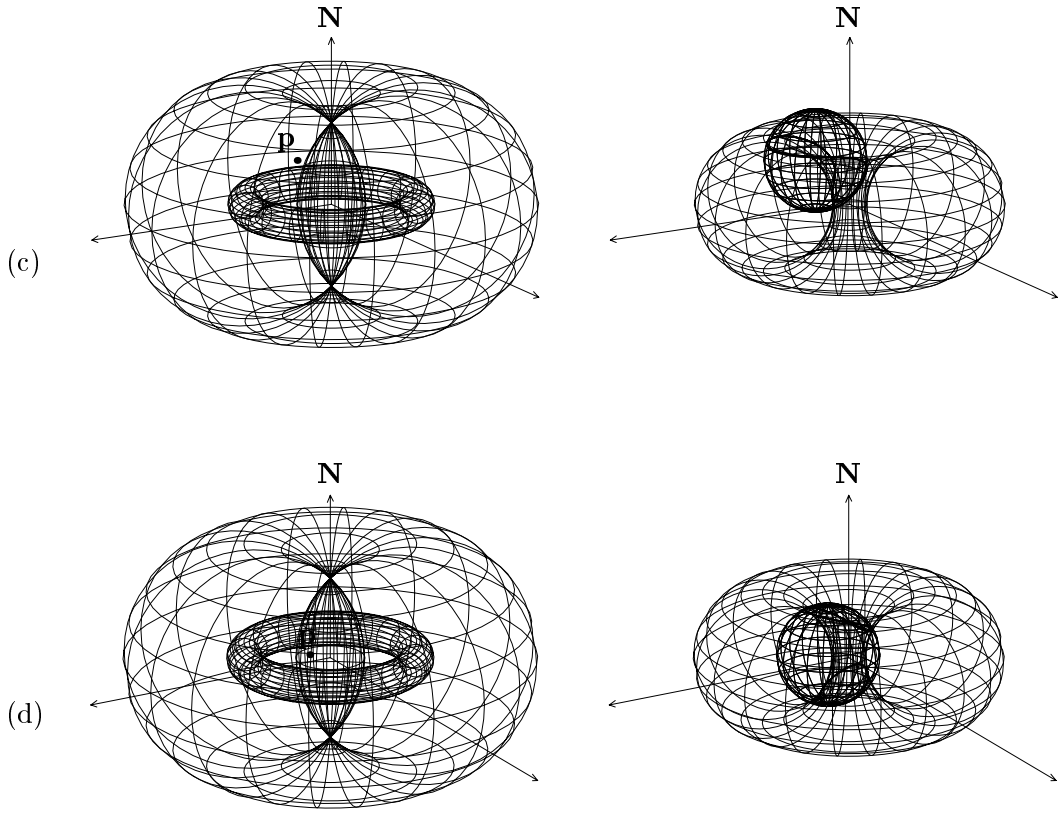

Figure 6.2: (*cont.*)

$\mathbf{p}$ and is orthogonal to the normal vector $\mathbf{N}$. Figure 6.3(a) is the result of a planar cut applied to the example shown in Figure 6.2(c). Note that the winding number of two oriented circles around $\mathbf{p}$ is one. Figure 6.3(b) shows a similar result applied to the example of Figure 6.2(d). The winding number of four oriented circles around $\mathbf{p}$ is two. One can also show that the winding number is unique as long as $\mathbf{p}$ is selected in the same open region: T_+^O, T_-^I, $T_-^O \cap T_+^I \cap T_+^D$, or T_-^D.

When we consider the sphere $S = S_\delta(\mathbf{p})$ as a moving sphere, as the sphere S passes through a touching configuration with the torus T, the number of closed loops in the TSI curve $T \cap S$ increases/decreases. That is, when the center $\mathbf{p}$ of S passes through T^I, T^O, or T^D, the number of TSI loops increases/decreases depending on the winding numbers of the corresponding open regions bounded by the toroidal surfaces T^I, T^O, and T^D. A case-by-case analysis of each of the four different cases possible (enumerated in Figure 6.2) will show that the winding number of each open region properly classifies the number of closed loops in the TSI curve. In general, an argument based on the Jordan-Brouwer Separation Theorem will provide a rigorous proof for the relation between the winding number and the number of closed loops in the TSI curve [8]. We skip the details here.

Guibas et al. [7] showed an application of the winding number (defined for planar closed loops which may self-intersect) in computing the number of connected components in the intersection of two planar objects. However, they did not consider an intersected volume with interior holes (e.g., an object with genus 1) such as the volume bounded by T and S in Figure 6.2(d).

6.2.4 Algorithm: Torus_Sphere_Intersection_I

Algorithm: Torus_Sphere_Intersection_I of Appendix A.2 summarizes the TSI algorithm based on the above case analyses. In this algorithm, we assume that cubic curve tracing routines: Trace_Singular_TSI_Curve(T, S, P) and Trace_Regular_TSI_Curve(T, S, P), are available, where T is a torus, S is a sphere, and P is the set of starting points (exactly one point for each closed loop of the TSI curve). Each singular intersection curve can be traced starting from its singular point (see also Piegl [21]), the details of which are given in the routine: Trace_Singular_TSI_Curve. One may also use the technique of Farouki et al. [6] for an exact rational parametrization of the singular quartic space curve. To deal with the case in which T and S have

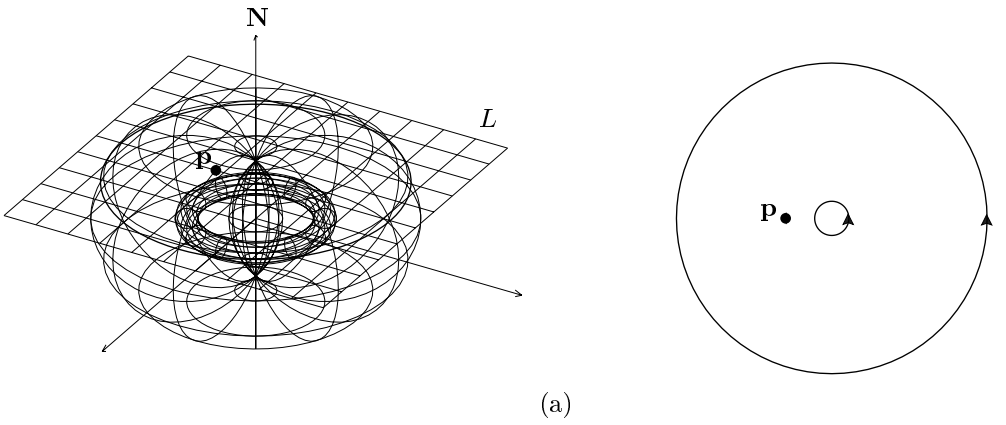

(a)

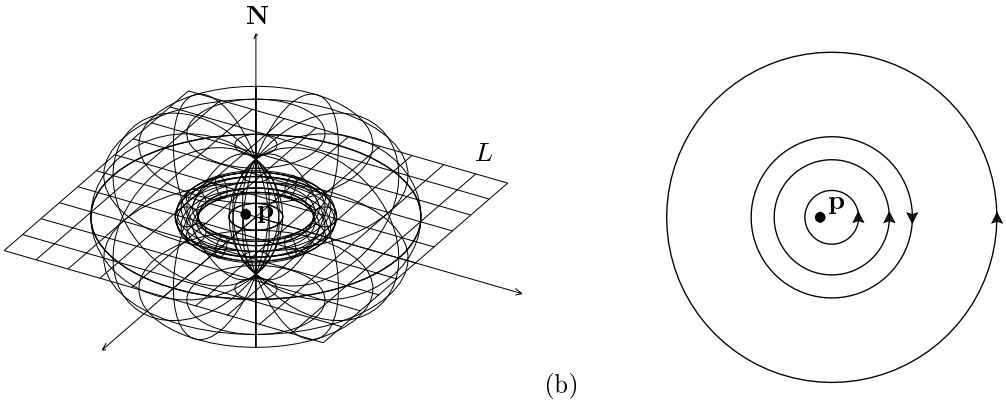

(b)

Figure 6.3: Counting winding numbers using planar cuts

no tangential intersection point, a starting point must be generated on each closed loop of the TSI curve. After that, each curve component is traced using the routine: Trace_Regular_TSI_Curve. Our implementation of the two curve tracing routines is based on customizing the general SSI procedures of Choi [4] to the special case of intersecting a torus with a sphere (see also Bajaj et al. [1, 3]).

Lines (1)–(3) compute orthogonal projections of $\mathbf{p}$ onto the torus T. Given a point $\mathbf{p}$ (not located on the main axis of the torus T), the closest point $\mathbf{p}_c$ of the main circle $C_R(\mathbf{0}, \mathbf{N})$ to the point $\mathbf{p}$ is computed as follows:

$$\mathbf{p}_c = R \, \frac{\mathbf{p} - \langle \mathbf{p}, \mathbf{N} \rangle \, \mathbf{N}}{\| \mathbf{p} - \langle \mathbf{p}, \mathbf{N} \rangle \, \mathbf{N} \|}.$$

Similarly, the farthest point $\mathbf{p}_f$ is given by:

$$\mathbf{p}_f = -R \, \frac{\mathbf{p} - \langle \mathbf{p}, \mathbf{N} \rangle \, \mathbf{N}}{\| \mathbf{p} - \langle \mathbf{p}, \mathbf{N} \rangle \, \mathbf{N} \|}.$$

Line (4) considers the case in which there is only a single loop in the TSI curve. It is easy to show that the sphere S and the cross-sectional circle $C_r(\mathbf{p}_c, \mathbf{N}_{p_c})$ intersect at two different points. We take any one of the two points as a starting point for curve tracing. Line (6) handles the case in which the intersected volume bounded by T and S is an object with genus 1 (see Figure 6.2(d)). In this case, each cross-sectional circle $C_r(C(t), \mathbf{N}_{C(t)})$ intersects the sphere S at two different points. Moreover, each point belongs to a different loop in the TSI curve. Thus both intersection points can be used as starting points for numerical curve tracing.

In Line (5), we assume the availability of the routine: Compute_Profile_Circles (T,S), which computes two degenerate profile circles in the TSI curve. Each profile circle is contained in a plane that is orthogonal to the normal vector $\mathbf{N}$. The distance of the plane from the main plane of the torus and the radius of each profile circle can be computed by intersecting two circles (see Section 3.4 and Figure 3.4).

In Algorithm: Torus_Sphere_Intersection_I, except the procedures for numerical curve tracing, all the required computations are vector/distance computations and circle/circle intersections. The numerical errors in these operations can be measured geometrically. Moreover, the maximum distance between a cubic approximation curve segment and the torus (or the sphere) can be measured with high accuracy, utilizing the simple structure of the torus and the sphere. The geometric nature of these errors enables an efficient and robust implementation of our algorithm using floating-point arithmetic.

6.3 The Case of $0 < r < \delta$

In this case, we consider the sphere $S = S_\delta(\mathbf{p}_2)$ as an obstacle and the torus $T = T_{r,R}(\mathbf{p}_1, \mathbf{N}_1)$ as the envelope surface of a moving ball $B_r(C(t))$, where $C(t)$ is a parametrization of the main circle $C_R(\mathbf{p}_1, \mathbf{N}_1)$ of the torus T. That is, $T = Bdr(\cup B_r(C(t)))$, where Bdr means the boundary of a closed (volumetric) region in $\mathbb{R}^3$. By applying a translation, we may assume that the sphere S has its center at the origin: $S = S_\delta(\mathbf{0})$, and the torus T is given as: $T = T_{r,R}(\mathbf{p}, \mathbf{N})$. The C-space obstacle of the sphere S (with respect to the moving ball $B_r(C(t))$ of radius r) is bounded by the $\pm r$-offsets of the sphere S: that is, the inner offset sphere $S^I = S_{\delta - r}(\mathbf{0})$ and the outer offset sphere $S^O = S_{\delta + r}(\mathbf{0})$. Let S^I_- and S^I_+ denote the inner and outer open regions (of $\mathbb{R}^3$) that are separated by S^I. S^O_- and S^O_+ are defined in a similar way.

6.3.1 Counting the Number of Closed Loops

When we give the normal orientation of the outer sphere S^O as outward (i.e., into the direction pointing to the open region S^O_+), and that of the inner sphere S^I as inward (i.e., into the direction pointing to the open region S^I_-), the two spheres S^I and S^O separate the space $\mathbb{R}^3$ into three open regions: S^O_+, $S^O_- \cap S^I_+$, and S^I_-, with the corresponding winding numbers: zero, one, and zero, respectively. Consider the case in which the ball $B_r(C(t))$ moves, while its center $C(t)$ is located in the open region $S^O_- \cap S^I_+$, only for $t_1 \le t \le t_2$. The ball $B_r(C(t))$ $(t_1 \le t \le t_2)$ intersects with the sphere $S = S_\delta(\mathbf{0})$ in a circular disc $D(t)$. We have the following relation (see Figure 6.4):

$$\begin{aligned} D(t) &= B_r(C(t)) \cap S \subset S \\ \cup D(t) &= \cup (B_r(C(t)) \cap S) = (\cup B_r(C(t))) \cap S \subset S. \end{aligned}$$

The TSI curve $T \cap S$ is the boundary curve of the region $\cup D(t)$ on the sphere S (Figure 6.4(b)). Moreover, it is the envelope curve of the one-parameter family of circular discs $D(t)$ on the sphere S. With the exception of some degenerate cases, each $D(t)$ contributes two points, $\gamma_-(t)$ and $\gamma_+(t)$, to the envelope curve. These two points are the same as the two intersection points of the cross-sectional circle $C_r(C(t), \mathbf{N}_{C(t)})$ with the sphere S, where $\mathbf{N}_{C(t)} = \frac{C'(t)}{\|C'(t)\|}$ (Figure 6.4(c)).

(a) $T \cap S$

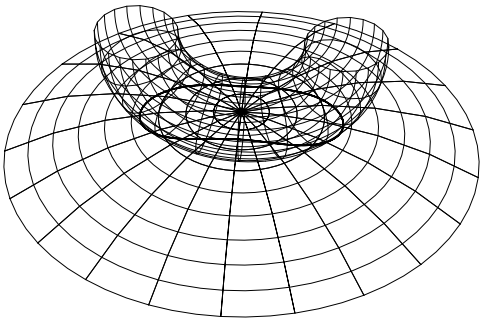

(b) $\cup_{t_1 \le t \le t_2} D(t)$

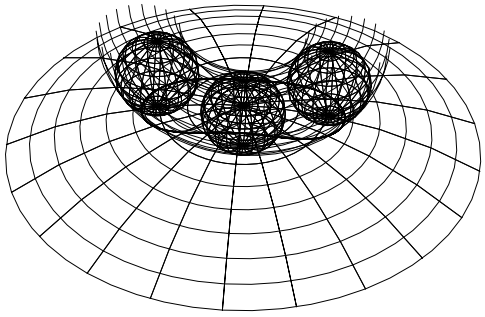

(c) $\cup_{\hat{t}_1 \le t \le \hat{t}_2} \left(C_r(C(t), \mathbf{N}_{C(t)}) \cap S \right)$

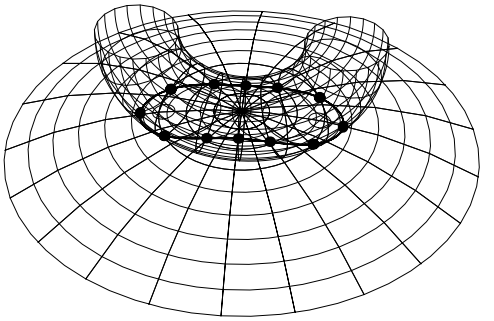

(d) $\gamma_-(t)$ and $\gamma_+(t)$

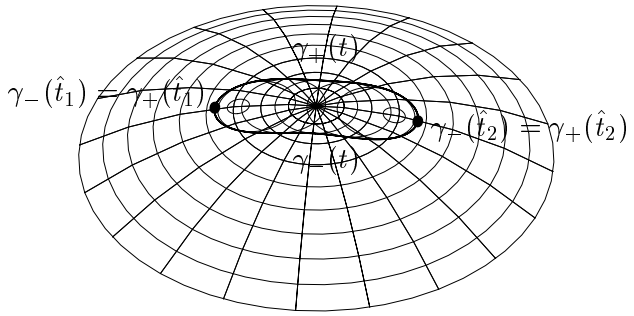

Figure 6.4: $\gamma_-(t)$ and $\gamma_+(t)$ which generate $T \cap S$

When the main circle $C_R(\mathbf{p}, \mathbf{N})$ is totally contained in the open region S_+^O or S_-^I, the TSI curve is empty since no ball $B_r(C(t))$ intersects with the sphere S. Next, we consider the case in which the main circle $C_R(\mathbf{p}, \mathbf{N})$ is totally contained in the open region $S_+^I \cap S_-^O$. In this case, each cross-sectional circle $C_r(C(t), \mathbf{N}_{C(t)})$ intersects with the sphere S at two different points: $\gamma_-(t)$ and $\gamma_+(t)$. As the cross-sectional circle $C_r(C(t), \mathbf{N}_{C(t)})$ sweeps out the entire torus T, the two points, $\gamma_-(t)$ and $\gamma_+(t)$, generate two smooth curves that bound the connected region $\cup D(t)$ on the sphere S. Therefore, the TSI curve consists of two closed loops (Figure 6.5(a)). When the main circle $C_R(\mathbf{p}, \mathbf{N})$ has a tangential contact (at a point $\mathbf{p}_0$) with either S^I or S^O, the two closed loops in the TSI curve have a contact at $\mathbf{p}_S$, forming an 8-figured loop (Figure 6.5(b)), where $\mathbf{p}_S$ is the orthogonal projection of $\mathbf{p}_0$ onto the sphere S. Note that $\mathbf{p}_0$ is the r-offset of $\mathbf{p}_S \in S$ if $\mathbf{p}_0 \in S^O$, or $\mathbf{p}_0$ is the $(-r)$-offset of $\mathbf{p}_S \in S$ if $\mathbf{p}_0 \in S^I$. The figures in the left columns of Figures 6.5–6.6 illustrate the relative position of the main circle $C_R(\mathbf{p}, \mathbf{N})$ of the torus T in the C-space of the sphere S; the figures in the right columns of Figures 6.5–6.6 illustrate the corresponding relative configurations of T and S.

Assume that the ball $B_r(C(t))$ intersects with the sphere S, for $t_1 \le t \le t_2$, and there is no intersection between $B_r(C(t))$ and S, for $t_1 - \epsilon < t < t_1$ and $t_2 < t < t_2 + \epsilon$, where $\epsilon > 0$ is an arbitrarily small positive number. Then, there are some values of $\hat{t}_1$ and $\hat{t}_2$ such that (Figure 6.4):

- $t_1 < \hat{t}_1 < \hat{t}_2 < t_2$.
- $C_r(C(t), \mathbf{N}_{C(t)}) \cap S = \emptyset$, for $t_1 < t < \hat{t}_1$ or $\hat{t}_2 < t < t_2$.
- $C_r(C(t), \mathbf{N}_{C(t)}) \cap S = \{\gamma_-(t) = \gamma_+(t)\}$, for $t = \hat{t}_1, \hat{t}_2$.
- $C_r(C(t), \mathbf{N}_{C(t)}) \cap S = \{\gamma_-(t), \gamma_+(t)\}$, with $\gamma_-(t) \neq \gamma_+(t)$, for $\hat{t}_1 < t < \hat{t}_2$.

The boundary curve of the region $\cup_{t_1 \le t \le t_2} D(t)$ (on the sphere S) is the same as the union

$$\cup_{\hat{t}_1 \le t \le \hat{t}_2} \left(C_r(C(t), \mathbf{N}_{C(t)}) \cap S \right).$$

Since the cross-sectional circles $C_r(C(t), \mathbf{N}_{C(t)})$ are all disjoint, no boundary point of $\cup_{t_1 \le t \le t_2} D(t)$ can be shared by two different instances of $C_r(C(t), \mathbf{N}_{C(t)})$, for $\hat{t}_1 \le t \le \hat{t}_2$. Therefore, the two curves $\gamma_-(t)$ and $\gamma_+(t)$ have no intersection, for $\hat{t}_1 < t < \hat{t}_2$. They have no self-intersection, either. Moreover, these two curves are

connected at two common end points: $\gamma_-(\hat{t}_1) = \gamma_+(\hat{t}_1)$ and $\gamma_-(\hat{t}_2) = \gamma_+(\hat{t}_2)$. The resulting boundary curve of $\cup D(t)$ thus forms a closed loop on the sphere S.

In the above discussion, we showed that: when the main circle $C_R(\mathbf{p}, \mathbf{N})$ intersects with $S_-^O \cap S_+^I$, but is not totally contained in the open region $S_-^O \cap S_+^I$, each connected component of the intersection $C_R(\mathbf{p}, \mathbf{N}) \cap (S_-^O \cap S_+^I)$ produces a closed loop in the TSI curve. We can easily show that there are at most two connected components in the intersection $C_R(\mathbf{p}, \mathbf{N}) \cap (S_-^O \cap S_+^I)$. This is because the main circle $C_R(\mathbf{p}, \mathbf{N})$ may intersect with the inner sphere S^I at no more than two points. (The plane L containing the main circle $C_R(\mathbf{p}, \mathbf{N})$ intersects with the sphere S^I in a circle; then this circle may intersect with $C_R(\mathbf{p}, \mathbf{N})$ at no more than two points.) Similarly, the main circle $C_R(\mathbf{p}, \mathbf{N})$ may intersect with the outer sphere S^O at no more than two points.

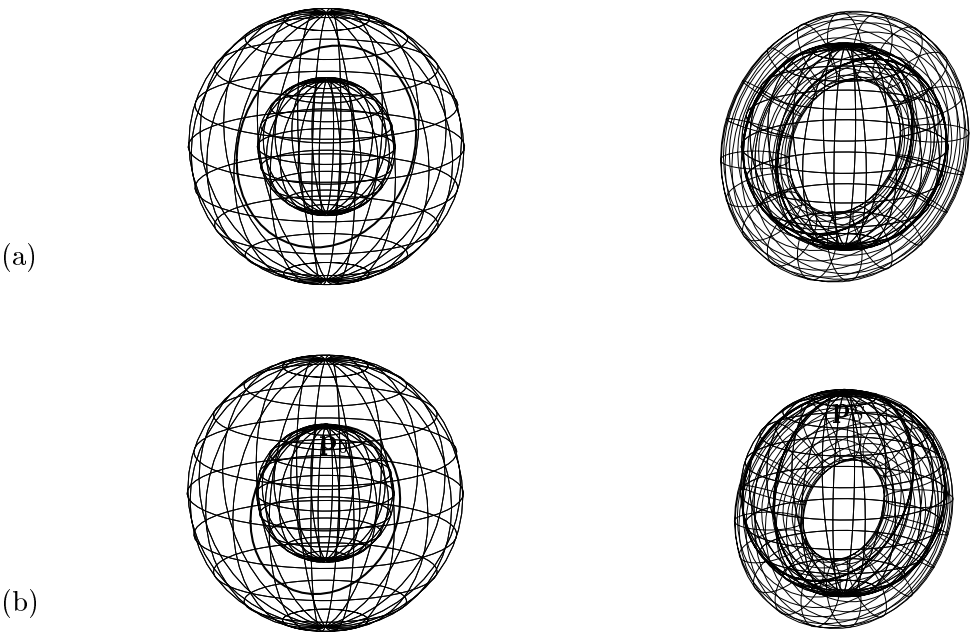

Figure 6.5: Regular or singular TSI curves.

(c)

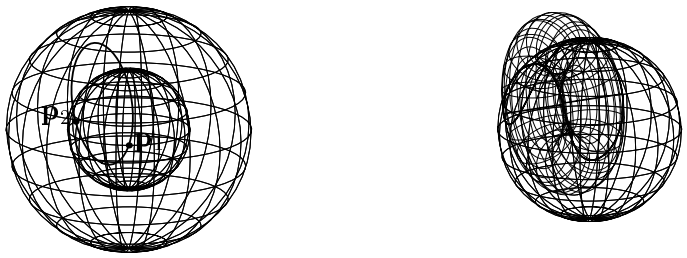

(d)

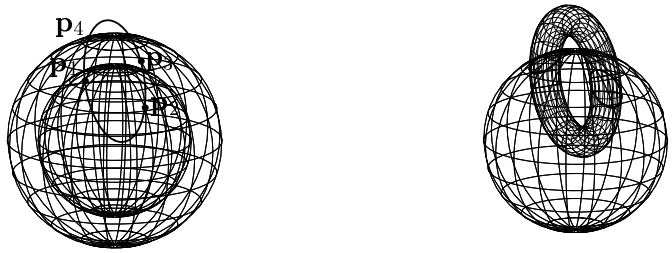

(e)

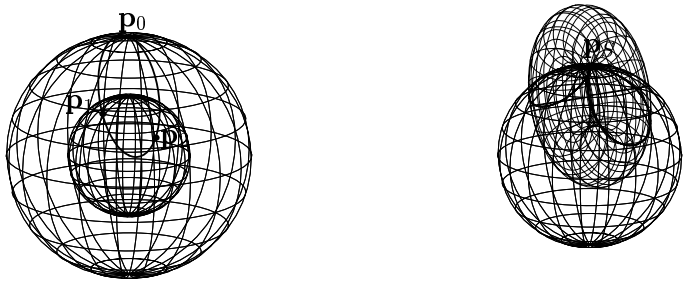

Figure 6.5: (*cont.*)

6.3.2 More Examples

Figures 6.5(c)–(d) show two cases in which the intersection $C_R(\mathbf{p}, \mathbf{N}) \cap (S_-^O \cap S_+^I)$ has one and two connected component(s), respectively. The corresponding TSI curve consists of one and two closed loop(s), respectively. In Figure 6.5(e), the circular arc $C_R(\mathbf{p}, \mathbf{N}) \cap (S_-^O \cap S_+^I)$ has a tangential intersection with S^O at a point $\mathbf{p}_0 \in S^O$. The corresponding TSI curve is an 8-figured curve with singularity at $\mathbf{p}_S \in S$, where $\mathbf{p}_S$ is the orthogonal projection of $\mathbf{p}_0$ onto the sphere S. Note that $\mathbf{p}_0$ is also the r-offset of $\mathbf{p}_S$.

Each closed loop of Figure 6.5(a) degenerates into a profile circle of the torus T if and only if the main axis of the torus T passes through the center of the sphere S, which can be detected by the condition: $\mathbf{p} \times \mathbf{N} = \mathbf{0}$ (see Section 3.4 and Figure 3.4). Moreover, each closed loop of Figure 6.5(d) degenerates into a cross-sectional circle of the torus T if and only if the center of the sphere S is contained in the main plane of the torus T (i.e., $\langle \mathbf{p}, \mathbf{N} \rangle = 0$) and the distance between the two centers of T and S (i.e., $\|\mathbf{p}\|$) satisfies the condition: $\|\mathbf{p}\|^2 = R^2 + \delta^2 - r^2$ (see Figure 3.7).

Figures 6.6(a)–(b) show singular degenerate cases in which the main circle $C_R(\mathbf{p}, \mathbf{N})$ has two tangential intersection points with $S^O \cup S^I$. Each tangential intersection point generates a singular point in the corresponding TSI curve. Therefore, there are two singular points in the TSI curve. Being a self-intersection point of the TSI curve, each singular point has multiplicity two. When we pass a plane L through the two singular points, the plane L cannot intersect with any other point of the TSI curve since the plane L already intersects with the TSI curve (of degree four) at four points (counting the multiplicity properly). The only exception is the case in which the plane L completely contains at least one component of the TSI curve. This means that each component of the singular TSI curve is a planar curve. Moreover, this planar curve is embedded in the sphere S. That is, this curve must be a circle. Consequently, the TSI curve consists of two circles (called Yvone-Villarceau circles) when there are two singular points (see also Piegl [21] and Figure 3.1(c)). Each singularity can be easily detected from a tangential intersection of the main circle $C_R(\mathbf{p}, \mathbf{N})$ with the two concentric spheres $S^O \cup S^I$.

Figures 6.6(c)–(d) show other degenerate cases in which the main circle $C_R(\mathbf{p}, \mathbf{N})$ is totally embedded in the sphere S^O or S^I. Then the torus T intersects with the sphere S tangentially along a circle. In this case, the intersection circle must be

considered to have multiplicity two; that is, as the limit of two converging circles, which produces an overlap of two identical circles. Therefore, there is no other loop in the TSI curve.

6.3.3 Algorithm: Torus_Sphere_Intersection_II

Algorithm: Torus_Sphere_Intersection_II of Appendix A.3 summarizes the algorithm discussed above. Similarly to Torus_Sphere_Intersection_I of Appendix A.2, we assume that the two curve tracing routines: Trace_Singular_TSI_Curve(T, S, P) and Trace_Regular_TSI_Curve(T, S, P) are available. Moreover, in Lines (1), (2), and (4), we assume that the routines computing degenerate circles of the TSI curve are available (see Chapter 3 and Figures 3.1–3.7).

Line (3) corresponds to the case shown in Figure 6.5(c). Assume that the ball $B_r(C(t))$ intersects with the sphere S, only for $t_1 \leq t \leq t_2$, (i.e., $C(t_1) = \mathbf{p}_1$ and $C(t_2) = \mathbf{p}_2$), and the cross-sectional circle $C_r(C(t), \mathbf{N}_{C(t)})$ intersects with the sphere S, for $t_1 < \hat{t}_1 \leq t \leq \hat{t}_2 < t_2$, (see also Section 6.3.1). Since the TSI curve is symmetric with respect to both T and S, we have the following relation:

$$t_1 < \hat{t}_1 \leq \frac{t_1 + t_2}{2} \leq \hat{t}_2 < t_2.$$

Note that the middle point $\mathbf{q}$ in Line (3) is the same as $C(\frac{t_1+t_2}{2})$. Therefore, the cross-sectional circle $C_r(\mathbf{q}, \mathbf{N_q})$ intersects with the sphere S at two different points. We take only one of them as a starting point for numerical curve tracing.

Line (5) corresponds to the case shown in Figure 6.5(d). Let $C(t_i) = \mathbf{p}_i$, for $i = 1, 2, 3, 4$. Note that the ball $B_r(C(\frac{t_1+t_2}{2}))$ is totally contained inside the sphere S, and the ball $B_r(C(\frac{t_3+t_4}{2}))$ is totally contained outside the sphere S. Then any profile circle of the torus T will intersect with the sphere S at two different points (see Figure 3.1(a) for profile circles). Moreover, each intersection point belongs to a different component of the TSI curve. In Line (5), we take the profile circle $C_{R+r}(\mathbf{p}, \mathbf{N})$ of the largest radius. The two intersection points in $S \cap C_{R+r}(\mathbf{p}, \mathbf{N})$ are used as the starting points for the two closed loops in the TSI curve.

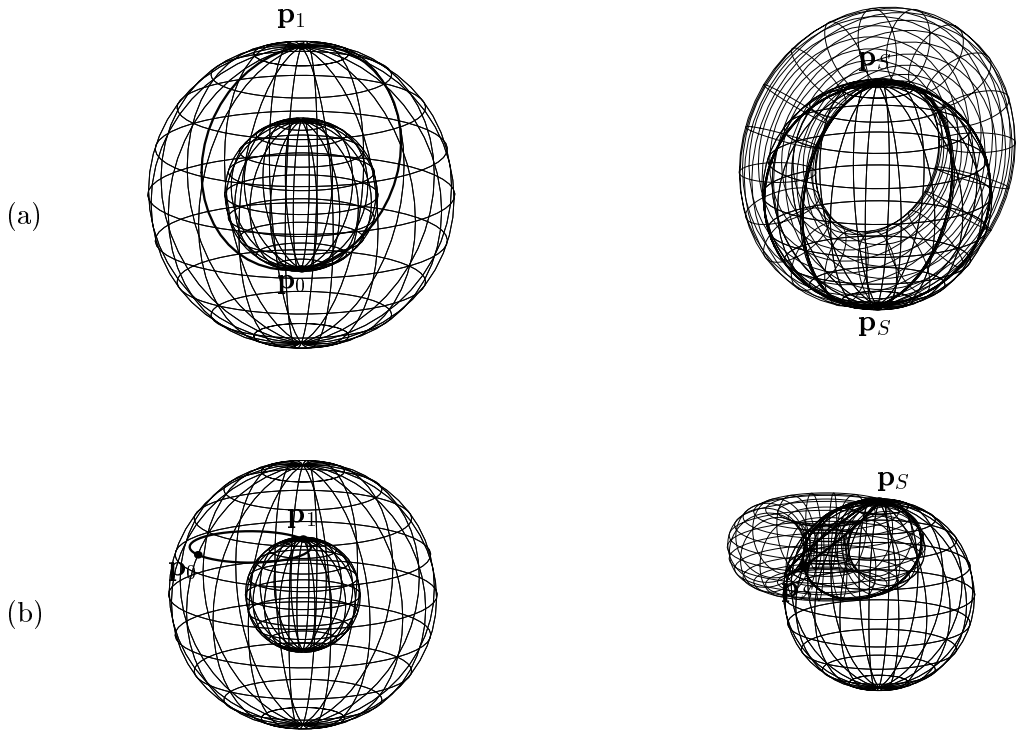

Figure 6.6: Degenerate TSI curves in circle(s).

(c)

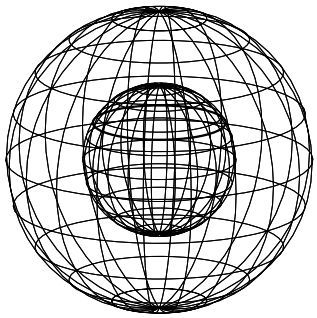

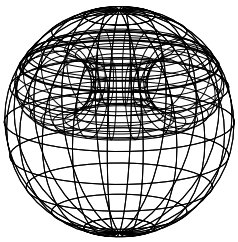

(d)

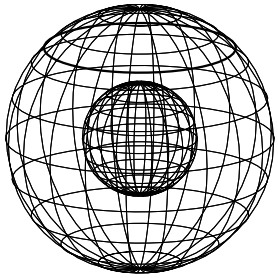

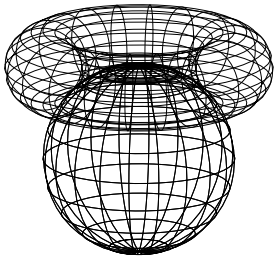

Figure 6.6: (*cont.*)

Chapter 7

Torus and Cylinder Intersection

This chapter introduces two methods that compute the TYI curve based on a C-space approach. Given a torus $T = T_{r,R}(\mathbf{p}_1, \mathbf{N}_1)$ and a cylinder $Y = Y_\delta(\mathbf{p}_2, \mathbf{N}_2)$, we consider two cases: (i) $0 < r \leq \delta$ and (ii) $0 < \delta < r$, separately. In the case of $0 < r \leq \delta$, we treat the cylinder as an obstacle and the torus as the envelope surface of a moving ball along a circular trajectory. That is, $T = Bdr(\cup B_r(C(t)))$, where $C(t)$ is a circle of radius R. In this case, the C-space obstacle of the cylinder is bounded by two cylinders (with the same axis, but with two different radii). In the case of $0 < \delta < r$, we treat the torus as an obstacle and the cylinder as the envelope surface of a moving ball along a linear trajectory. That is, $Y = Bdr(\cup B_\delta(l(t)))$, where $l(t)$ is a line. The C-space obstacle of the torus is bounded by two tori (with the same center and the same major radius, but with two different minor radii: $r \pm \delta$).

The intersection points between the C-space obstacle and the trajectory of a moving ball's center provide an efficient way to classify the topological type of the TYI curve and construct the TYI curve with all its singularities detected properly.

7.1 The Case of $0 < r \leq \delta$

Without loss of generality, we may assume that $T = T_{r,R}(\mathbf{0}, \mathbf{e}_3)$ and $Y = Y_\delta(\mathbf{p}, \mathbf{N})$. Let $C = C_R(\mathbf{0}, \mathbf{e}_3)$ denote the main circle of T. The C-space obstacle of the cylinder Y (with respect to the moving ball $B_r(C(t))$ of radius r) is bounded by $\pm r$-offsets of the cylinder: i.e., the inner offset cylinder $Y^I = Y_{\delta - r}(\mathbf{p}, \mathbf{N})$ and the outer offset

cylinder $Y^O = Y_{\delta+r}(\mathbf{p}, \mathbf{N})$. When $r = \delta$, Y^I degenerates into a line $l(\mathbf{p}, \mathbf{N})$. Let Y^I_- and Y^I_+ denote the inner and outer open regions (of $\mathbb{R}^3$) that are separated by Y^I. Y^O_- and Y^O_+ are defined in a similar way.

When we give the normal orientation of the outer cylinder Y^O as outward (i.e., into the direction pointing to the open region Y^O_+), and that of the inner cylinder Y^I as inward (i.e., into the direction pointing to the open region Y^I_-), the two cylinders Y^I and Y^O separate the space $\mathbb{R}^3$ into three open regions: Y^O_+, $Y^O_- \cap Y^I_+$, and Y^I_- with the corresponding winding numbers: zero, one, and zero, respectively (See Figure 7.1).

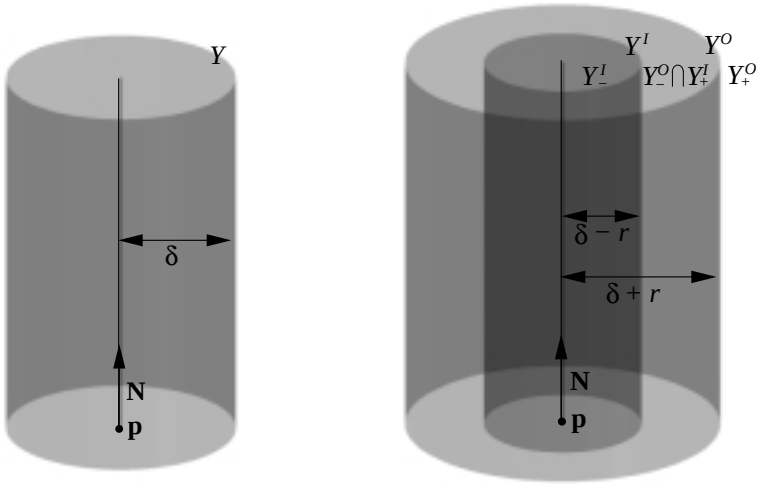

(a) (b)

Figure 7.1: The cylinder $Y = Y_\delta(\mathbf{p}, \mathbf{N})$ and the C-space obstacle of Y with respect to a ball with radius r.

The number of closed loops in the intersection curve of the cylinder Y and a sphere S (moving in the torus T) is determined by the winding number of the region to which the center of the sphere S belongs. If the center of S is located in the region with winding number one, Y and S intersect in a single closed loop. If the center of S is located in the region with winding number zero, Y and S has no intersection.

For an arbitrary point $\mathbf{q} \in Y^O_- \cap Y^I_+$ (that is, $\mathbf{q}$ belongs to the region with winding number one), the sphere $S_r(\mathbf{q})$ intersects with the cylinder Y in one closed loop, and the intersection $B_r(\mathbf{q}) \cap Y$ is a cylindrical surface patch of disk type. We can classify

the topological type of a TYI curve by intersecting the main circle of T, C, with the two cylinders $Y^I \cup Y^O$ based on the above consideration.

The intersection points between C and $Y^I \cup Y^O$ can be computed efficiently by utilizing the following fact:

$$C \cap (Y^I \cup Y^O) \equiv (C \cap L(\mathbf{0}, \mathbf{e}_3)) \cap (Y^I \cup Y^O) \equiv C \cap (L(\mathbf{0}, \mathbf{e}_3) \cap (Y^I \cup Y^O)),$$

where $L(\mathbf{0}, \mathbf{e}_3)$ is the main plane of the torus T and contains the circle C. $L(\mathbf{0}, \mathbf{e}_3) \cap (Y^I \cup Y^O)$ consists of two ellipses or four lines; thus, $C \cap (Y^I \cup Y^O)$ can be computed efficiently and robustly by computing circle/ellipse or circle/line intersections.

Let $C_n(t)$, $(t_0 < t < t_1)$, denote an open connected component of curve $C \cap (Y_+^O \cup Y_-^I)$. For each t, $(t_0 < t < t_1)$, $B_r(C_n(t))$ has no intersection with Y; thus $(\cup B_r(C_n(t))) \cap Y$ is an empty set. We can detect all closed loops and singular points/curves in the TYI curve by computing $Bdr(\cup B_r(C_i)) \cap Y$, for each C_i connected component curve of $C \cap \overline{(Y_-^O \cap Y_+^I)}$, where $\overline{Y_-^O \cap Y_+^I}$ denotes the closure of $Y_-^O \cap Y_+^I$, i.e., $\overline{Y_-^O \cap Y_+^I} = (Y_-^O \cap Y_+^I) \cup (Y^O \cup Y^I)$. Let C_i denote a closed connected component curve of $C \cap \overline{Y_-^O \cap Y_+^I}$.

7.1.1 Analysis for the Case of $0 < r < \delta$

The figures in the left columns of Figures 7.2, 7.5–7.7 illustrate the relative positions of C in the C-space of the cylinder Y; the figures in the right columns of Figures 7.2, 7.5–7.7 illustrate the corresponding relative configurations of T and Y.

Lemma 7.1 *If $C_i \neq C$ and C_i has no tangent intersection point with $Y^I \cup Y^O$, the intersection curve $Bdr(\cup B_r(C_i)) \cap Y$ consists of one single closed loop (see Figures 7.2(a)–(b)).*

Proof. To prove this lemma, we use two facts:

1. When $\mathbf{q}$ is an end point of C_i, the intersection $B_r(\mathbf{q}) \cap Y$ consists of one single contact point.

2. When $\mathbf{q} \in C_i$ and $\mathbf{q}$ is not an end point of C_i, the intersection $B_r(\mathbf{q}) \cap Y$ consists of a surface patch of disk type.

Since the cylinder can be thought as a torus with infinite major radius, these facts are proved by the result in Section 6.2.

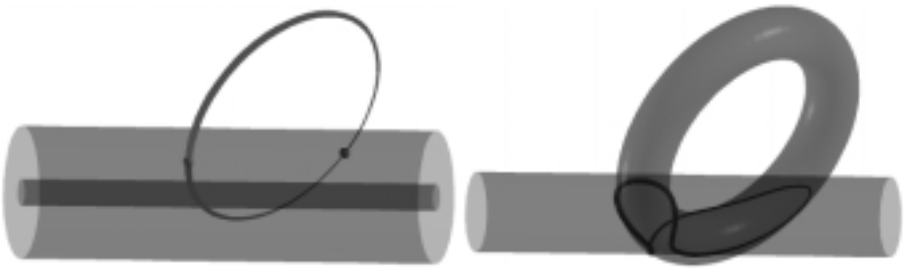

(a)

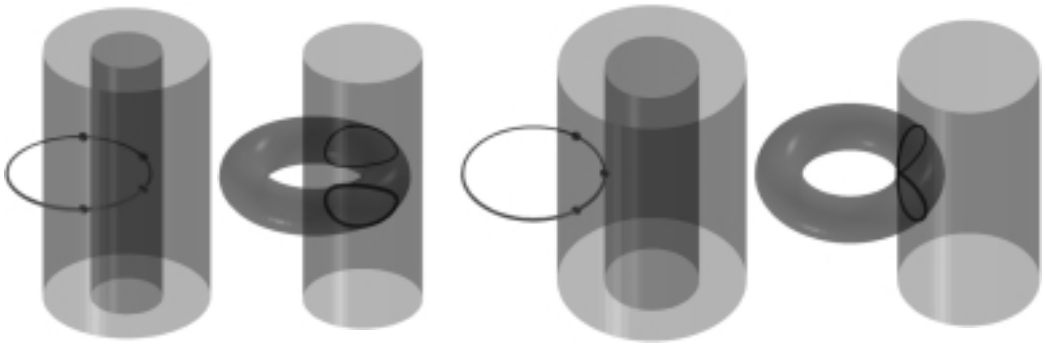

(b) (c)

Figure 7.2: Regular or singular TYI curves for the case of $0 < r < \delta$.

We prove this lemma by contradiction. The intersection curve $Bdr(\cup B_r(C_i)) \cap Y$ consists of two or more closed loops if and only if the intersection $(\cup B_r(C_i)) \cap Y$ consists of a surface patch with one or more holes on it, or two or more surface patches.

Let $C(t)$, $t_0 \leq t \leq t_1$, denote a parametrization of C_i. When we construct the intersection $(\cup B_r(C(t))) \cap Y$ by increasing the parameter t from t_0 to t_1, let A denote the intersection $(\cup_{t_0 \leq t < \bar{t}} B_r(C(t))) \cap Y$ which consists of the largest single surface patch of disk type. Let A_0 denote the surface patch $B_r(C(\bar{t})) \cap B_r(C(\bar{t} - \epsilon)) \cap Y$, which is the subpatch of A. Then $B_r(C(\bar{t})) \cap Y$ can be connected with A only through the patch A_0. Figure 7.3(a) shows examples of A and A_0.

First, let's assume that the intersection $(\cup B_r(C_i)) \cap Y$ consists of a surface patch with one or more holes on it. If the surface patch $A \cup (B_r(C(\bar{t})) \cap Y)$ contains a hole on it, $B_r(C(\bar{t})) \cap Y$ must be a surface patch of degenerate disk type or a surface patch of degenerate cylindrical type (see Figure 7.3(b)). This violates given facts.

Second, let's assume that the intersection $(\cup B_r(C_i)) \cap Y$ consists of two or more surface patches. If the surface patch $A \cup (B_r(C(\bar{t})) \cap Y)$ consists of two or more surface patches, $B_r(C(\bar{t})) \cap Y$ must be an empty set or consists of two or more surface patches. This also violates given facts.

Thus, we conclude that $(\cup B_r(C_i)) \cap Y$ consists of a surface patch of disk type, and the intersection curve $Bdr(\cup B_r(C_i)) \cap Y)$ consists of one single closed loop. □

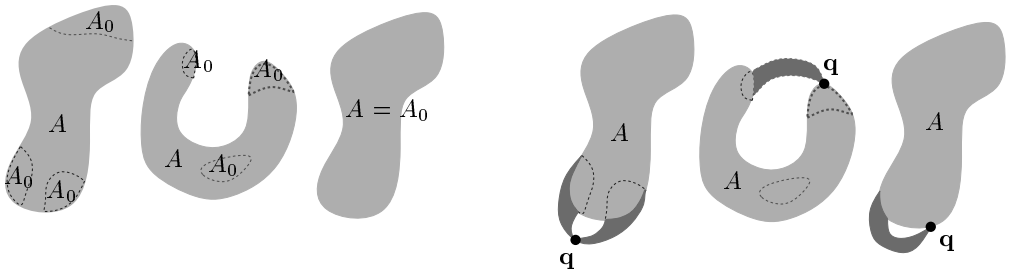

Figure 7.3: $\cup_{t_0 \leq t < \bar{t}} B_r(C(t)) \cap Y$ and $B_r(C(\bar{t})) \cap Y$.

- If $C_i \neq C$ and C_i has k tangential intersection points with $Y^I \cup Y^O$, $(\cup B_r(C_i)) \cap Y$ consists of $(k+1)$ disk-type surface patches which are connected at k points;

that is, the intersection curve has singularity at k points (see Figure 7.2(c)).

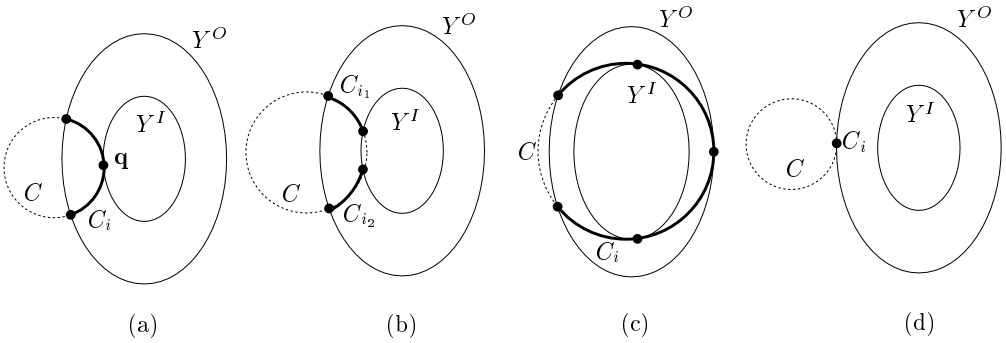

Figure 7.4: $C_R(\mathbf{0}, \mathbf{e}_3) \cap (Y^I \cup Y^O)$.

Let's assume that C_i intersects with $Y^I \cup Y^O$ tangentially at a point $\mathbf{q}$ (see Figure 7.4(a)). If we move C slightly so that C_i is split into two connected components C_{i_1} and C_{i_2}(see Figure 7.4(b)), the intersection curve consists of two closed loops, Therefore, when C_i intersects with $Y^I \cup Y^O$ tangentially at a point $\mathbf{q}$, the intersection curve has singularity at a point.

Similarly, if C_i has k tangential intersection points with $Y^I \cup Y^O$, the intersection curve has singularity at k points. When $C_i \neq C$, the maximum number of tangential intersection points between C_i and $Y^I \cup Y^O$ is three. In this case, the intersection curve has three singular points (see Figure 7.4(c)). If C_i is a point, the intersection curve itself is also a singular contact point (see Figure 7.4(d)).

- When $C_i = C$ and C has k tangential intersection points with $Y^I \cup Y^O$, the intersection curve $T \cap Y$ has k singular points (see Figures 7.5 (a)–(b)).

When $C_i = C$, the maximum number of tangential intersection points in $C_i \cap Y^I$ is two, and similarly that of $C_i \cap Y^O$ is also two. Consequently, the intersection curve $T \cap Y$ may have four singular points at most.

- When $C_i = C$ and C does not intersect with $Y^I \cup Y^O$, the intersection $T \cap Y$ consists of two closed loops (see Figures 7.6 (a)–(b)).

When $C \subset Y^O_- \cap Y^I_+$, $(\cup B_r(C)) \cap Y$ is a surface patch of cylindrical type. The intersection curve $T \cap Y$ is identical to the boundary curve of $(\cup B_r(C)) \cap Y$. Thus, the intersection curve $T \cap Y$ consists of two closed loops.

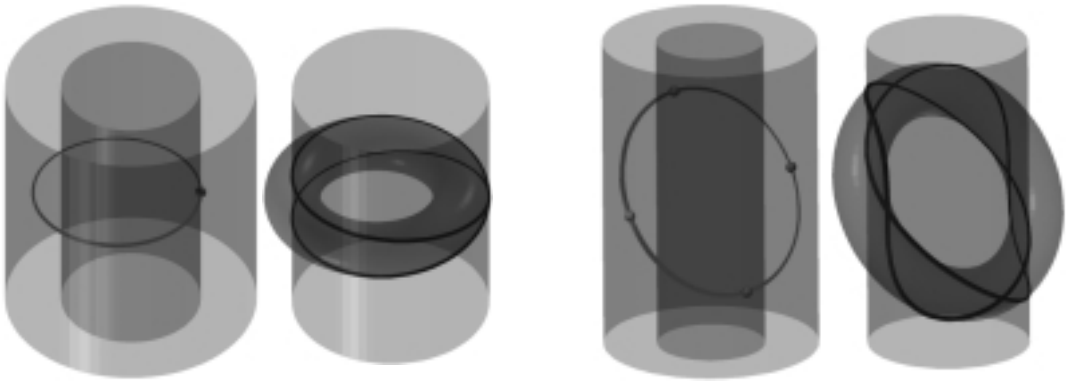

(a) (b)

Figure 7.5: The TYI curves for the case of $C \subset \overline{Y_-^O \cap Y_+^I}$.

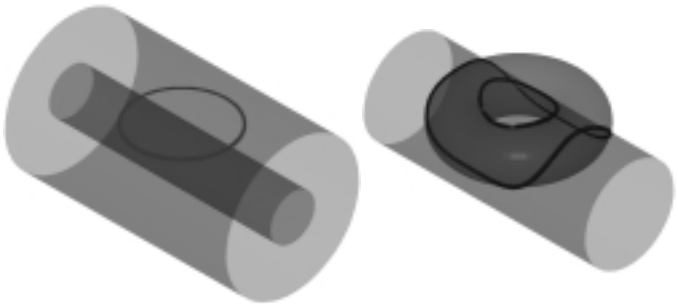

(a)

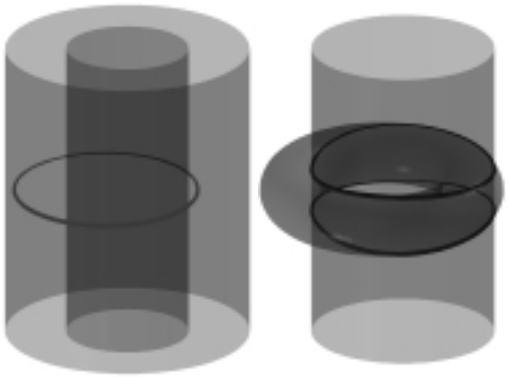

(b)

Figure 7.6: The TYI curves for the case of $C \subset (Y_-^O \cap Y_+^I)$.

- When C is embedded in the union $Y^I \cup Y^O$, the intersection curve consists of one singular circle.

When C is embedded in Y^I, T is inside Y and touches Y along a singular circle. When C is embedded in Y^O, T is outside Y and touches Y along a singular circle.

- When $C \subset Y^I_- \cup Y^O_+$, the intersection $T \cap Y$ is an empty set.

When C is in the open region $Y^I_- \cup Y^O_+$, no ball $B_r(C(t))$ intersects with the cylinder Y; thus, in this case, there is no TYI curve in the real, affine space.

7.1.2 Analysis for the Case of $0 < r = \delta$

When the minor radius of the torus T and the radius of the cylinder Y are the same, the inner offset surface of Y degenerates into a line: $Y^I = l(\mathbf{p}, \mathbf{N})$. Let C denote the main circle of T: $C = C_R(\mathbf{0}, \mathbf{e}_3)$. When there is no intersection between C and Y^I, we can apply the same methods as Section 7.1.1. Thus, we consider only the cases where C intersects with Y^I. $C \cap Y^I$ is a circle/line intersection; thus C may intersect with Y^I at two intersection points at most.

Let C_i denote a connected component of $C \cap (Y^O_- \cup Y^O)$, which intersects with Y^I. When C_i intersects with Y^I at a point $\mathbf{q}$, the intersection $Bdr(B_r(C_i)) \cap Y$ has singular points which can be computed by intersecting two cross-sectional circles centered at $\mathbf{q}$ on Y and T. These one cross-sectional circle of Y and the other cross-sectional circle of T are two great circles contained in the same sphere $S_\delta(\mathbf{q})$. Thus, there are only two cases to consider: either (i) two cross-sectional circles are coincident or (ii) they intersect at two points.

- When C_i tangentially intersects with Y^I at $\mathbf{q}$, the cross-sectional circle of T at $\mathbf{q}$ intersects with Y in a circle, where each point on the circle is singular. The intersection curve consists of a singular circle and a singular curve which intersects with the singular circle at two singular points: $\mathbf{q} + \delta\mathbf{e}_3$ and $\mathbf{q} - \delta\mathbf{e}_3$ (see Figure 3.8).

- Otherwise, when C_i transversally intersects with Y^I at k intersection points, and tangentially intersects with Y^O at l intersection points, the intersection curve has singularity at $2k + l$ points (see Figure 7.7).

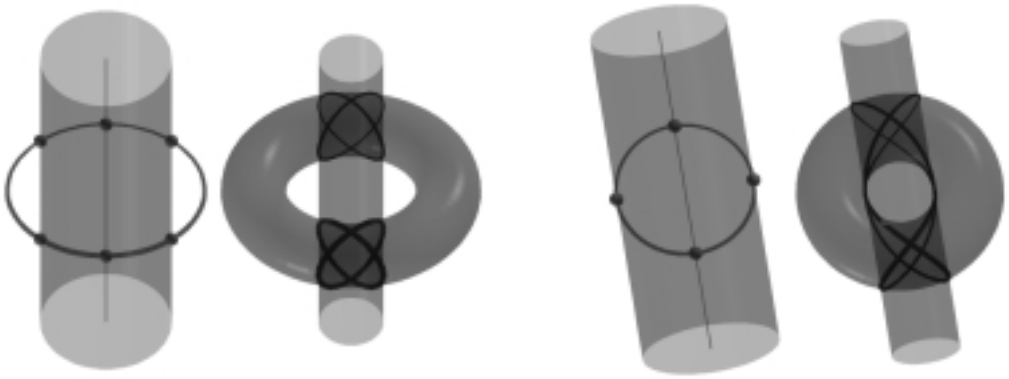

(a) (b)

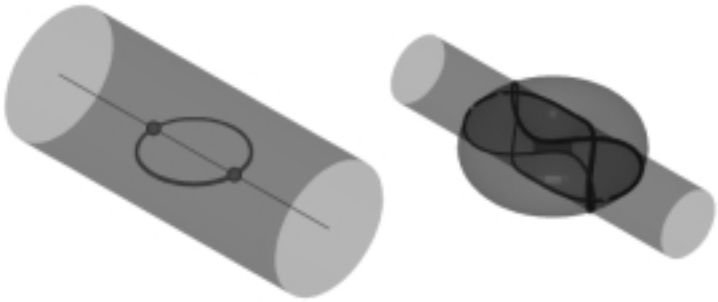

(c)

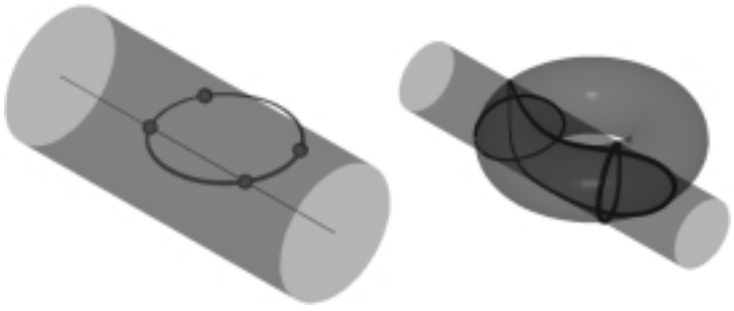

(d)

Figure 7.7: The TYI curves for the case of $0 < r = \delta$.

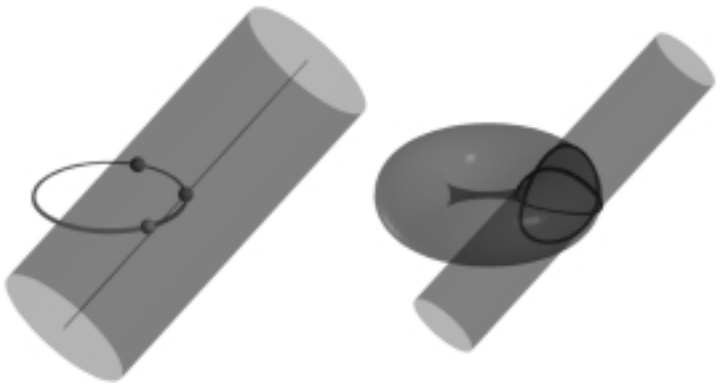

(e)

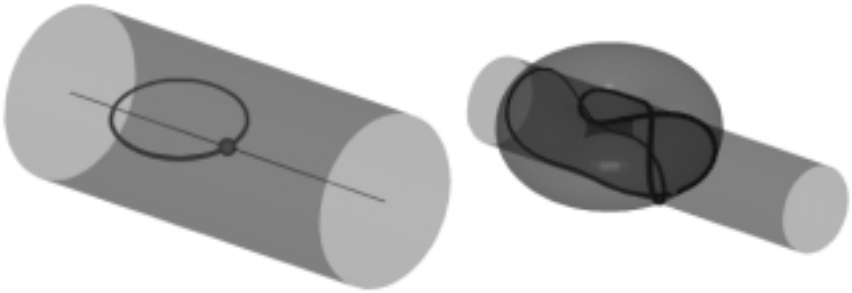

(f)

Figure 7.7: (*cont.*)

7.1.3 Algorithm: Torus_Cylinder_Intersection_I

Algorithm: Torus_Cylinder_Intersection_I of Appendix A.4 summarizes the TYI algorithm based on the above case analyses. In this algorithm, we assume that the following cubic curve tracing routines: Trace_Singular_TYI_Curve(T, Y, P) and Trace_Regular_TYI _Curve(T, Y, P), are available, where T is a torus, Y is a cylinder, and P is the set of starting points (exactly one point for each closed loop of the TYI curve). Each singular intersection curve can be traced starting from its singular point (see also Piegl [21]), the details of which are given in the routine: Trace_Singular_TYI_Curve.

To deal with the case in which the closed loops in the TYI curve have no tangent intersection point, a starting point must be generated on each closed loop of the TYI curve. After that, each curve component is traced using the routine: Trace_Regular_TYI_Curve. Our implementation of the two curve tracing routines is based on customizing the general SSI procedures of Choi [4] to the special case of intersecting a torus with a cylinder (see also Bajaj et al. [1, 3]).

Line (1) computes two starting points by intersecting Y with an arbitrary cross-sectional circle of T to trace the TYI curve. Line (2) computes the singular points in the TYI curve. DP includes singular points, if $C_R(\mathbf{0}, \mathbf{e}_3)$ intersects with $Y^I \cup Y^O$ tangentially or $C_R(\mathbf{0}, \mathbf{e}_3)$ intersects with Y^I when $Y^I = l(\mathbf{p}, \mathbf{N})$. Line (3) traces all singular curves in the TYI curve starting from the singular points in DP. Lines (4)–(8) compute the starting points for each regular closed loop in the TYI curve.

7.2 The Case of $0 < \delta < r$

Without loss of generality, we may assume that $T = T_{r,R}(\mathbf{0}, \mathbf{e}_3)$ and $Y = Y_\delta(\mathbf{p}, \mathbf{N})$. In this case, we consider the torus T as an obstacle. The C-space obstacle of the torus T (with respect to the moving ball $B_\delta(l(t))$ of radius δ) is bounded by the $\pm\delta$-offsets of the torus: i.e., the inner offset torus $T^I = T_{r-\delta,R}(\mathbf{0}, \mathbf{e}_3)$ and the outer offset torus $T^O = T_{r+\delta,R}(\mathbf{0}, \mathbf{e}_3)$.

When $r + \delta \geq R$, the outer torus T^O self-intersects. Let T^D denote the self-intersected part of T^O (see Figures 2.2(b)–(c)). (In the case of $r + \delta < R$, T^O has no self-intersection; thus we have $T^D = \emptyset$.) Let T^I_- and T^I_+ denote the interior and exterior open regions of $\mathbb{R}^3$ separated by the closed surface T^I. T^D_- and T^D_+ are

defined similarly. T_-^O and T_+^O are the open regions separated by the closed surface $T^O \setminus T^{D^o}$, where T^{D^o} denotes T^D except two vertices of T^D.

When we give the normal orientations of the surfaces T^O and T^D as the outward directions (i.e., pointing to the regions T_+^O and T_+^D, respectively) and that of the surface T^I as the inward direction (i.e., pointing to the region T_-^I), the winding numbers assigned to the open regions T_+^O and T_-^I are both zero. Moreover, the winding number assigned to $T_-^O \cap T_+^I \cap T_+^D$ is one and that assigned to T_-^D is two. Given a torus and a sphere, when the radius of the sphere is smaller than the minor radius of the torus, Chapter 6 showed that the number of closed loops in the torus/sphere intersection is zero, one, and two, when the sphere center is located in the region of winding number zero, one, and two, respectively. We classify the topological types of TYI curves by considering the relationship between the winding number and the number of closed loops in the intersection curve.

7.2.1 Case Analysis

Let $l = l(\mathbf{p}, \mathbf{N})$ denote the axis of the cylinder Y. Let $\overline{T_-^O \cap T_+^I \cap T_+^D}$ denote the closure of $T_-^O \cap T_+^I \cap T_+^D$, i.e., $\overline{T_-^O \cap T_+^I \cap T_+^D} = (T_-^O \cap T_+^I \cap T_+^D) \cup T^I \cup T^O$, and l_i denote a connected component of the intersection $l \cap \overline{T_-^O \cap T_+^I \cap T_+^D}$. Each l_i corresponds to a certain number of closed loops and/or singular points/curves in the TYI curve. We can classify all possible types of TYI curves based on the winding numbers of the open regions in which l_i is located.

For the case of $l_i \cap T^D = \emptyset$, we classify all possible subcases as follows:

- If l_i has no tangent intersection point with $T^I \cup T^O$, the intersection curve has only one closed loop (Figures 7.8(a)–(b)).
- If l_i intersects with $T^I \cup T^O$ at k tangential intersection points, the intersection curve has singularity at k points (Figures 7.8(c)–(d)).

The figures in the left columns of Figures 7.8, 7.9, 7.12, 7.14 illustrate the relative positions of l in the C-space of the torus T; the figures in the right columns of Figures 7.8, 7.9, 7.12, 7.14 illustrate the corresponding relative configurations of T and Y.

When $l_i \cap T^D = \emptyset$, l_i is located in the region of winding number one. If l_i has no tangent intersection point with $T^I \cup T^O$, $B_\delta(\mathbf{q}) \cap T$ forms a surface patch of disk

(a)

(b)

(c)

(d)

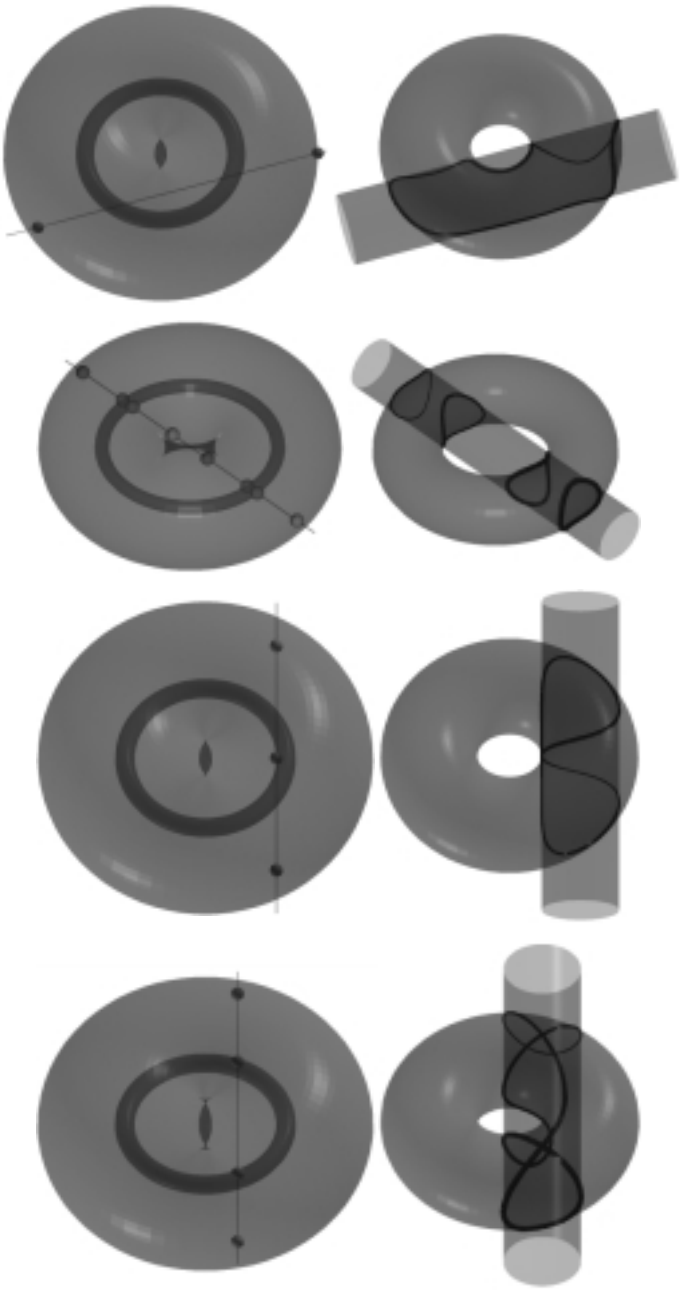

Figure 7.8: Regular or singular TYI curves for the case of $0 < \delta < r$.

type, for each point $\mathbf{q} \in l_i$ except two end points of l_i, and $(\cup B_\delta(l_i)) \cap T$ also forms a surface patch of disk type. If l_i has k tangential intersection points with $T^I \cup T^O$, $(\cup B_\delta(l_i)) \cap T$ consists of $(k+1)$ surface patches of disk type which are connected at k points; that is, the intersection curve has singularity at k points.

Let's consider the case where l_i passes through T^D_-. The number of the intersection points between a line and a torus is at most four. When l_i passes through T^D_-, l_i intersects with T^D at two points; thus there can be no tangential intersection point between l_i and T^O.

Lemma 7.2

If $l_i \cap T^D_- \neq \emptyset$ and l_i has no tangential intersection point with $T^I \cup T^O$, the intersection $(\cup B_\delta(l_i)) \cap T$ consists of a surface patch of cylindrical type, and the intersection curve $Bdr(\cup B_\delta(l_i)) \cap T$ consists of two closed loops (see Figure 7.9(a)).

(a)

(b)

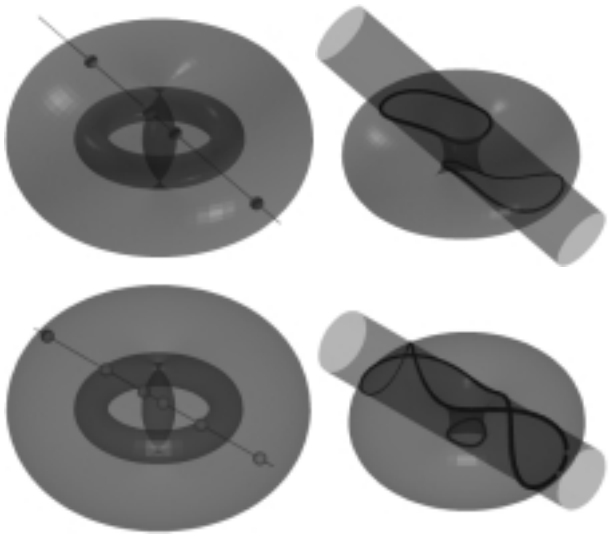

Figure 7.9: The TYI curves for the case of l_i passing through T^D_-.

Proof. To prove this lemma, we show that $(\cup B_\delta(l_i \cap (T^D_- \cup T^D))) \cap T$ consists of a surface patch of cylindrical type, first. Let l_j denote a connected component in the intersection $l_i \cap (T^D_- \cup T^D)$ (Figure 7.10(a)). We show that $(\cup B_\delta(l_j)) \cap T$ consists of

a surface patch of cylindrical type as follows (Figure 7.10(b)). Following two facts are given by the result in Section 6.2.

1. When $\mathbf{q}$ is an end point of l_j, the intersection $B_\delta(\mathbf{q}) \cap T$ consists of a surface patch of degenerate cylindrical type (Figure 7.10(c)).

2. When $\mathbf{q} \in l_j$ and $\mathbf{q}$ is not an end point of l_j, the intersection $B_\delta(\mathbf{q}) \cap T$ consists of a surface patch of cylindrical type (Figure 7.10(c)).

Let's assume that $(\cup B_\delta(l_j)) \cap T$ consists of two cylindrical-type surface patches. Then there must be a point $\mathbf{q} \in l_j$, such that $B_\delta(\mathbf{q}) \cap T$ consists of two cylindrical-type surface patches or $B_\delta(\mathbf{q}) \cap T = \emptyset$ (Figure 7.11(a)). This violates the given facts. Let's assume that $(\cup B_\delta(l_j)) \cap T$ consists of a surface patch with two or more holes on it. Then there must be a point $\mathbf{q} \in l_j$, such that $B_\delta(\mathbf{q}) \cap T$ consists of a surface patch with two or more holes on it, or $B_\delta(\mathbf{q}) \cap T$ is a surface patch of disk type (Figure 7.11(b)). This also violates the given facts. Thus, $(\cup B_\delta(l_j)) \cap T$ is a surface patch of cylindrical type.

Following two facts are given by the result in Section 6.2.

1. When $\mathbf{q}$ is an end point of l_i, the intersection $B_\delta(\mathbf{q}) \cap T$ consists of one single contact point.

2. When $\mathbf{q} \in (l_i \setminus l_j)$ and $\mathbf{q}$ is not an end point of l_i, the intersection $B_\delta(\mathbf{q}) \cap T$ consists of a surface patch of disk type.

Let l_k denote a connected component in $l_i \setminus l_j$. Similar to the proof for Lemma 7.1), we can prove that $(\cup B_\delta(l_k)) \cap T$ is a surface patch of disk type, and $(\cup B_\delta(l_i)) \cap T$ is a surface patch of cylindrical type. □

- If $l_i \cap T_-^D \neq \emptyset$ and l_i has k tangential intersection points with T^I, the intersection curve consists of two singular curves, or a closed loop and a singular curve (with k singular points on it) (see Figure 7.9(b)).

Let's consider the case where l_i intersects with T^{D^o} tangentially.

- When l_i has no tangential intersection point with T^I, the intersection curve has singularity at a point (Figure 7.12(a)).

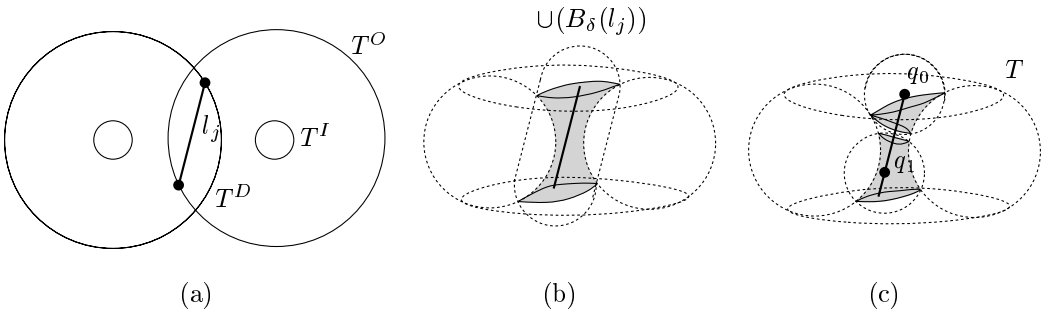

Figure 7.10: l_j and $(\cup B_\delta(l_j)) \cap T$.

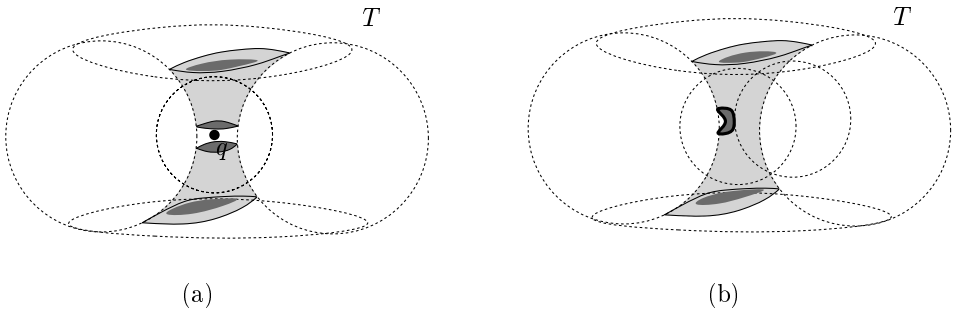

Figure 7.11: Contradictions to prove that $(\cup B_\delta(l_j)) \cap T$ consists of a surface patch of cylindrical type.

- When l_i has k tangential intersection points with T^I, the intersection curve has singularity at $k+1$ points (Figure 7.12(b)).

(a)

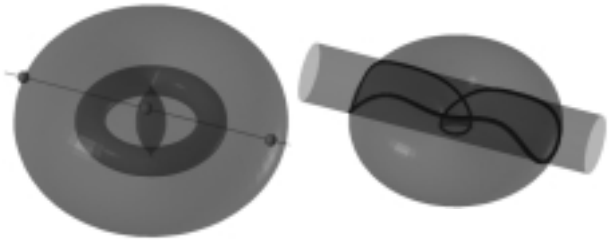

(b)

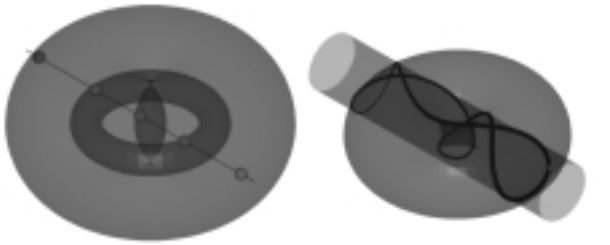

Figure 7.12: The TYI curves for the case of l_i intersecting with T^D tangentially.

Let $\mathbf{q}$ denote a vertex of T^D (except the case where T^D is a point). Let's consider the case where l_i passes through $\mathbf{q}$. Let K denote a cone which consists of tangent lines of cross-sectional circles of T^O at $\mathbf{q}$. Figure 7.13 shows the plane section of $T^I \cup T^O \cup T^D$ by the plane which contains l and z-axis. A line intersects with a torus at four regular points at most. Thus, if l intersects with T^D_-, and l passes through $\mathbf{q}$ (which is a point of multiplicity two), there is no other tangential intersection point between l and T^O.

- When l_i is in the inner open region of K, l_i always passes through T^D_-. If l_i has no tangent intersection point with T^I, the intersection curve consists of two closed loops. If l_i intersects with T^I at k tangential intersection points, the intersection curve consists of a closed loop and a singular curve with k singular points on it (see Figure 7.13(a) and Figure 7.14(a)).

- When l_i is on the surface of K, l_i has a tangential intersection point with T^D. If l_i has no tangential intersection point with T^I, the intersection curve

consists of a singular curve (with a singular point on it). If l_i intersects with T^I at k tangent intersection points, the intersection curve consists of a singular curve with $k+1$ singular points on it (see Figure 7.13(b) and Figure 7.14(b)).

- When l_i is in the outer region of K, l_i does not intersect with T^{D^o}. If l_i does not intersect with T^I tangentially, the intersection curve consists of a singular curve (with two singular points). If l_i intersects with T^I at k tangent intersection points, the intersection curve consists of a singular curve with $k+2$ singular points on it (see Figure 7.13(c) and Figure 7.14(c)).

Let's assume that T^D is a point and l_i passes through T^D. If l_i is parallel to $\mathbf{e}_3$ (i.e., the main plane normal of T), $T \cap Y$ consists of a singular circle. If l_i is not parallel to $\mathbf{e}_3$ and l_i has k tangential intersection points with T^I, the intersection curve consists of a singular curve with $k+2$ singular points on it (see Figure 7.14(d)). If l_i is not parallel to $\mathbf{e}_3$ and l_i has no tangent intersection point with T^I, the intersection curve consists of a singular curve with two singular points on it.

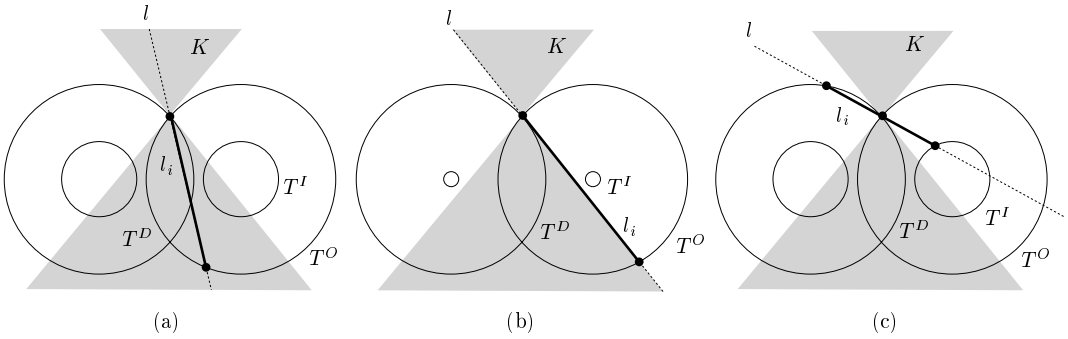

Figure 7.13: The cases of l_i passing through a vertex of T^D.

7.2.2 Algorithm: Torus_Cylinder_Intersection_II

Algorithm: Torus_Cylinder_Intersection_II of Appendix A.5 summarizes the TYI algorithm based on the above case analyses. Line (1) computes the singular points/circles in the TYI curve. Line (2) traces all singular curves in the TYI curve from singular point set DP. Lines (3)–(7) compute regular TYI curves when the trajectory of the moving ball's center does not pass through T^D_-. If $l(\mathbf{p}, \mathbf{N})$ passes through T^D_-

(a)

(b)

(c)

(d)

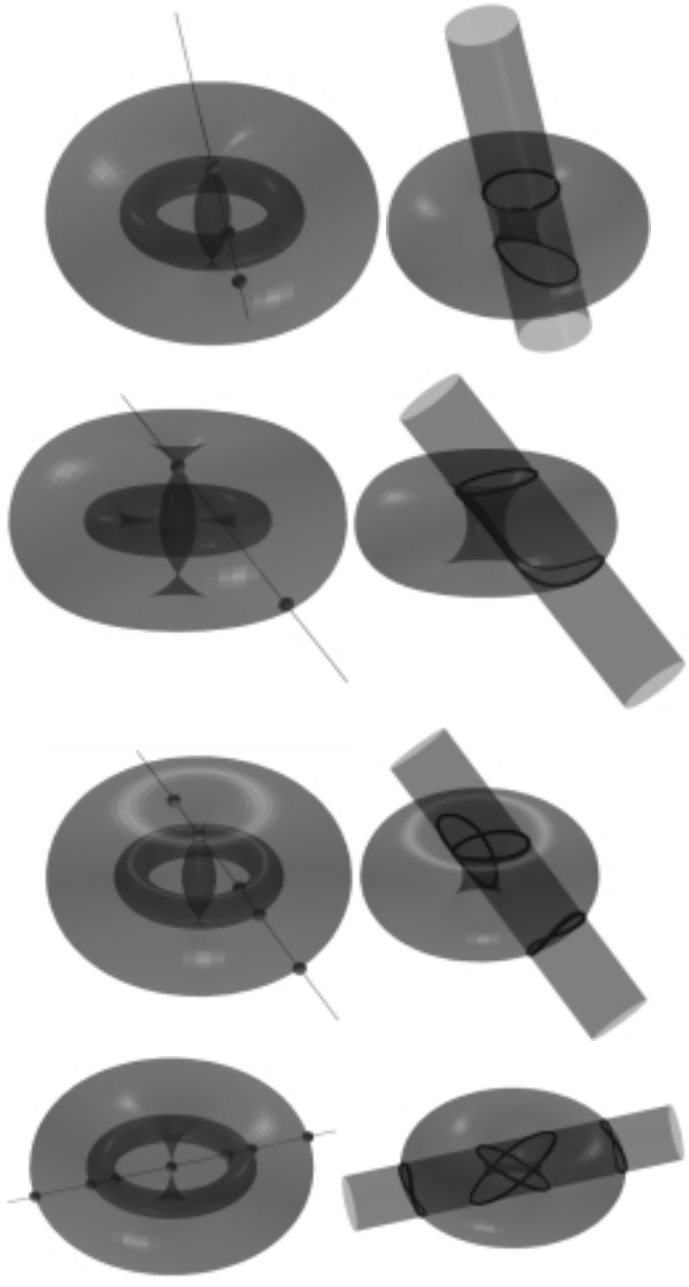

Figure 7.14: The TYI curves for the case of l_i passing through a vertex of T^D.

and $|DP| = 0$, there are two closed loops in the TYI curve. We can trace these closed loops from two starting points which are computed by intersecting an arbitrary cross-sectional circle of T and Y. Lines (8)–(12) compute two regular closed loops in the TYI curve for this case. If $l(\mathbf{p}, \mathbf{N})$ passes through T_{-}^{D} and $l(\mathbf{p}, \mathbf{N})$ has a tangent intersection point with T^{I}, $|DP| = 1$ and the TYI curve consists of a singular curve and a closed loop. If $l(\mathbf{p}, \mathbf{N})$ passes through T_{-}^{D} and $l(\mathbf{p}, \mathbf{N})$ has two tangent intersection points with T^{I}, $|DP| = 2$. At this time, if the z-values of points in DP have the same sign, the TYI curve consists of two singular curves. Otherwise, the TYI curve consists of a singular curve and a closed loop. Line (2) traces all singular curves starting from the points in DP, and Line (13) traces undetected closed loops starting from the points in IP.

Chapter 8

Torus and Cone Intersection

This chapter introduces a method of computing the TKI curve based on a C-space approach. Given a torus $T = T_{r,R}(\mathbf{p}_1, \mathbf{N}_1)$ and a cone $K = K_\theta(\mathbf{p}_2, \mathbf{N}_2)$, the relative position of the main circle $C_R(\mathbf{p}_1, \mathbf{N}_1)$ with respect to the cone K determines the TKI curve. The C-space approach is useful in classifying the relative positions.

We consider the cone $K = K_\theta(\mathbf{p}_2, \mathbf{N}_2)$ as an obstacle and the torus $T = T_{r,R}(\mathbf{p}_1, \mathbf{N}_1)$ as the envelope surface of a moving ball $B_r(C(t))$, where $C(t)$ is a parametrization of the main circle $C_R(\mathbf{p}_1, \mathbf{N}_1)$ of the torus T. That is, $T = Bdr(\cup B_r(C(t)))$, where Bdr means the boundary of a closed (volumetric) region in $\mathbb{R}^3$. By applying translation and rotation if necessary, we may assume that the torus T is given in a standard position and orientation; that is, its center is at the origin and its main circle is contained in the xy-plane: $T = T_{r,R}(\mathbf{0}, \mathbf{e}_3)$, where $\mathbf{0} = (0,0,0)$ and $\mathbf{e}_3 = (0,0,1)$. The cone K is in an arbitrary position: $K = K_\theta(\mathbf{p}, \mathbf{N})$ (Figure 8.1(a)).

The C-space obstacle of the cone K (with respect to the moving ball $B_r(C(t))$ of radius r) is bounded by the $\pm r$-offsets of the cone K: that is, the inner offset cone $K_{-r,\theta}(\mathbf{p}, \mathbf{N})$ and the outer offset cone $K_{r,\theta}(\mathbf{p}, \mathbf{N})$. Let K^O denote the outer offset cone $K_{r,\theta}(\mathbf{p}, \mathbf{N})$; that is, $Bdr(\cup_{t \geq 0} B_{\delta_O(t)}(l_O(t)))$, where $l_O(t) = \mathbf{p} + t\mathbf{N}$ and $\delta_O(t) = |r + ||l_O(t)|| \sin\theta|$, and K^B denote the sphere $S_r(\mathbf{p})$ (see Figure 8.1(c)). We separate the inner offset cone $K_{-r,\theta}(\mathbf{p}, \mathbf{N})$ into two parts: K^I and K^D. Let K^I denote the cone $K_\theta(\mathbf{p} + \frac{r}{\sin\theta}\mathbf{N}, \mathbf{N})$ (see Figure 8.1(d)). Let K^D denote the surface $Bdr(\cup_{0 \leq t \leq \frac{r}{\sin\theta}} B_{\delta_D(t)}(l_D(t)))$, where $l_D(t) = \mathbf{p} + t\mathbf{N}$ and $\delta_D(t) = |-r + ||l_D(t)|| \sin\theta|$, which is the surface $K_{-r,\theta}(\mathbf{p}, \mathbf{N}) \setminus K^I$, and K^V denote the apex of K^D (i.e., $K^V =$

$\mathbf{p} + \frac{r}{\sin\theta}\mathbf{N}$) (see Figure 8.1(e)).

Let K_-^I and K_+^I denote the inner and outer open regions (of $\mathbb{R}^3$) that are separated by K^I. K_-^D and K_+^D, K_-^O and K_+^O, K_-^B and K_+^B are defined in a similar way. The three cones K^I, K^D, K^O, and a sphere K^B separate the space $\mathbb{R}^3$ into five open regions: K_+^O, K_-^B, $K_-^D \cap K_+^B$, $K_-^O \cap K_+^I \cap K_+^D$, and K_-^I (Figure 8.1(b)). Let's consider the sphere $S = S_r(\mathbf{q})$, ($\mathbf{q} \in C_R(\mathbf{0}, \mathbf{e}_3)$), as a moving sphere. When the sphere S passes through a touching configuration with the cone K, the number of closed loops in the cone/sphere intersection curve $K \cap S$ increases/decreases. That is, when the center $\mathbf{q}$ of S passes through K^I, K^O, K^D, or K^B, the number of KSI loops increases/decreases.

The next section classifies cone/sphere intersection curves by classifying the containment of the center of the sphere in an open region bounded by three cones and a sphere. We classify the torus/cone intersection curve based on the classification of the cone/sphere intersection and the intersection of the moving ball's center trajectory and the C-space obstacle.

8.1 Case Analysis for Cone/Sphere Intersection

This section presents a method to classify the cone/sphere intersection based on a C-space approach. Given a cone $K = K_\theta(\mathbf{p}, \mathbf{N})$ and a sphere $S = S_r(\mathbf{q})$, based on the relative position of $\mathbf{q}$ with respect to K^I, K^O, K^B, and K^D, we can classify all possible topological types of the cone/sphere intersection (KSI) curves. The KSI curve has singularity (i.e., the cone K and the sphere S have a tangential/degenerate intersection at $\mathbf{q}_K \in K \cap S$) if and only if the center $\mathbf{q}$ of S is on the boundary of K^I, K^O, K^D, or K^B. When $\mathbf{q}$ is on the boundary sphere of K^B, $\mathbf{p}$ (i.e., the apex of K) is included in the KSI curve (see Figure 8.2). When $\mathbf{q}$ is on the boundary surface of K^I, K^O or $K^D \setminus K^B$, $\mathbf{q}_K$ is an orthogonal projection of $\mathbf{q}$ onto the surface K. Note that $\mathbf{q}$ is also the $\pm r$-offset point of $\mathbf{q}_K \in K$ (see Figure 8.3).

The figures in the left columns of Figures 8.5–8.6 illustrate the relative positions of C in the C-space of cone K; the figures in the right columns of Figures 8.5–8.6 illustrate the corresponding relative configurations of T and K.

For singular KSI intersections, there are four different cases to consider:

1. $\mathbf{q} \in K^B$: the KSI curve consists of point $\mathbf{p}$ (i.e., the apex of K), or a closed loop with point $\mathbf{p}$ on it, or a closed loop and point $\mathbf{p}$ (see Figure 8.2).

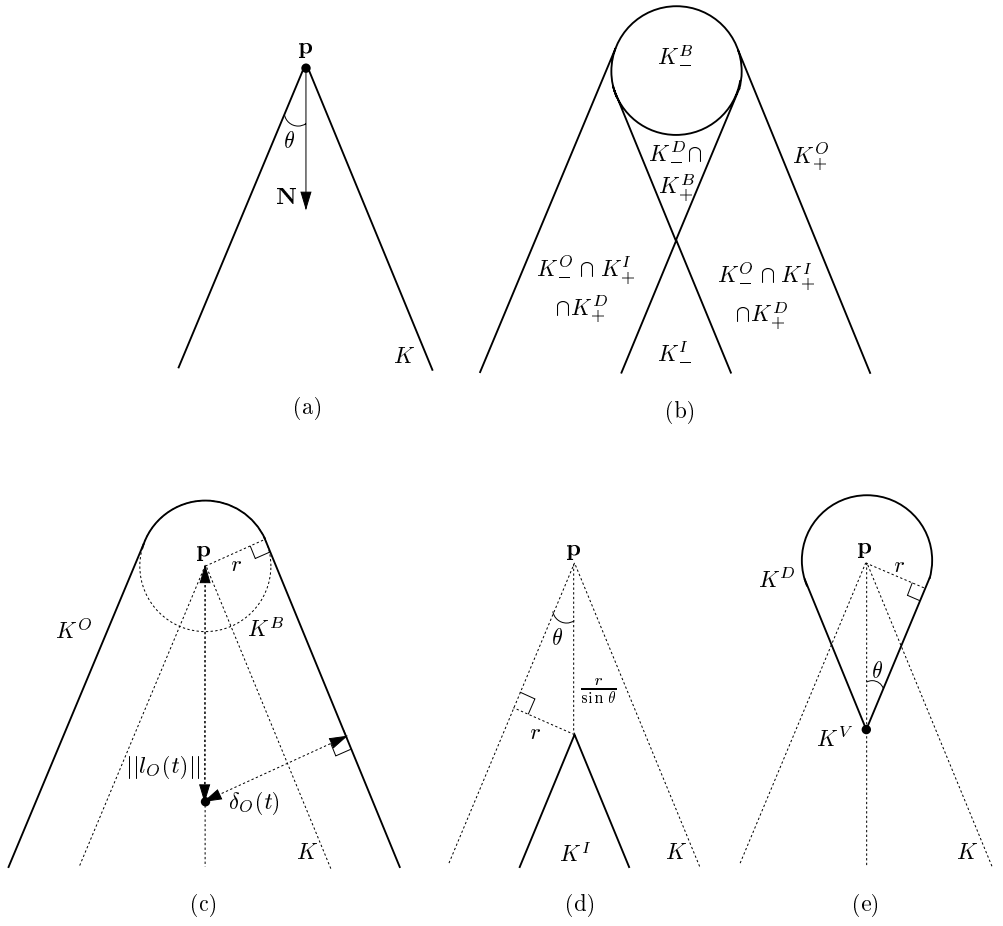

Figure 8.1: The cone $K = K_\theta(\mathbf{p}, \mathbf{N})$ and the C-space obstacle of K with respect to a ball with radius r.

2. $\mathbf{q} \in K^D \setminus (K^B \cup K^V)$: the KSI curve is a quartic space curve with singularity at $\mathbf{q}_K$ (Figure 8.3(b)).

3. $\mathbf{q} \in K^V$: the KSI curve degenerates into a circle (see Figure 8.3(c)).

4. $\mathbf{q} \in (K^I \setminus K^V) \cup (K^O \setminus K^B)$: the KSI curve degenerates into a point (see Figure 8.3(d)).

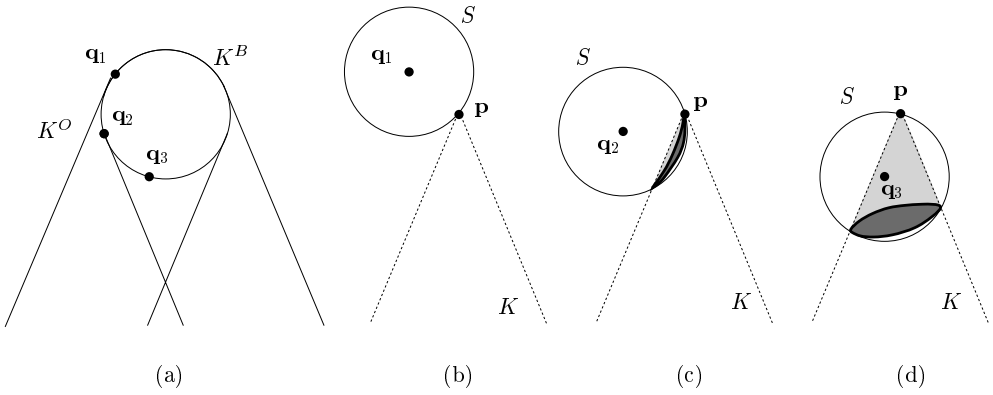

Figure 8.2: Singular KSI curve which includes $\mathbf{p}$.

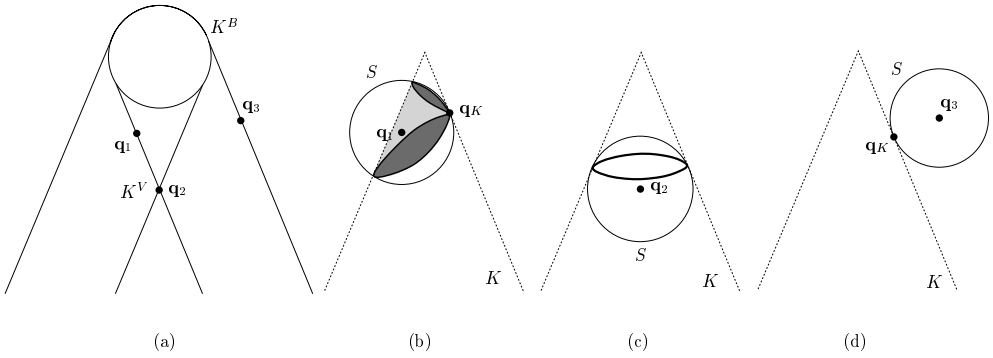

Figure 8.3: Singular KSI curve which does not include $\mathbf{p}$.

Figure 8.2(a) and Figure 8.3(a) illustrate the relative positions of the center $\mathbf{q}$ of S in the C-space of the cone K; Figures 8.2(b)–(d) and Figures 8.3(b)–(d) illustrate the corresponding relative configurations of K and S.

In case 1 considered above, $\mathbf{p}$, (i.e., the apex of K) is on the sphere S; thus, the KSI curve always contains $\mathbf{p}$. When $\mathbf{q}$ is on the surface $K^B \cap K^O$, K and S intersect at point $\mathbf{p}$, and $B_r(\mathbf{q}) \cap K$ also consists of point $\mathbf{p}$ (Figure 8.2(b)). When $\mathbf{q}$ is on the surface of $(K^B \cap K^D) \setminus K^O$, the KSI curve consists of a closed loop with point $\mathbf{p}$ on it, and $B_r(\mathbf{q}) \cap K$ is a surface patch of disk type with point $\mathbf{p}$ on its boundary (Figure 8.2(c)). When $\mathbf{q}$ is on the surface $K^B \setminus K^D$, the KSI curve consists of a closed loop and point $\mathbf{p}$, and $B_r(\mathbf{q}) \cap K$ is a surface patch of disk type (Figure 8.2(d)).

In case 2 considered above, the KSI curve has degree four and the curve has four branches at the singular point (i.e., at the tangential intersection point of K and S). In case 3 considered above, the cone and the sphere touch along a degenerate circle. When we enlarge the radius r of the sphere S slightly, the sphere S will intersect with the cone K in two different circles. Therefore, the degenerate circle of Figure 8.3(c) may be considered as the limit of these two converging circles. When the limiting circle is interpreted as an overlap of two identical circles, the singular degenerate circle has a total algebraic degree of four. $B_r(\mathbf{q}) \cap K$ also consists of a circle. In case 4 considered above, the sphere touches cone K at a point $\mathbf{q}_K$, where $\mathbf{q}_K$ is the orthogonal projection of $\mathbf{q}$ onto the surface of K.

For regular KSI intersections, there are three different cases to consider:

1. $\mathbf{q} \in K_-^B$: the KSI curve consists of a closed loop (Figure 8.4(b)).
2. $\mathbf{q} \in K_-^D \setminus (K^B \cup K_-^B)$: the KSI curve consists of two closed loops (Figure 8.4(c)).
3. $\mathbf{q} \in (K_-^O \cap K_+^I) \setminus (K_-^D \cup K^D)$: the KSI curve consists of a closed loop (Figure 8.4(d)).

Figure 8.4(a) illustrates the relative positions of $\mathbf{q}$ in the C-space of cone K; Figures 8.4(b)–(d) illustrate the corresponding relative configurations of K and S.

In case 1 considered above, the KSI curve is a closed loop, and $B_r(\mathbf{q}) \cap K$ is a surface of disk type with point $\mathbf{p}$ on it. In case 2 considered above, the KSI curve consists of two closed loops, and $B_r(\mathbf{q}) \cap K$ is a surface of cylindrical type. In case 3 considered above, the KSI curve is a closed loop, and $B_r(\mathbf{q}) \cap K$ is a surface of disk type.

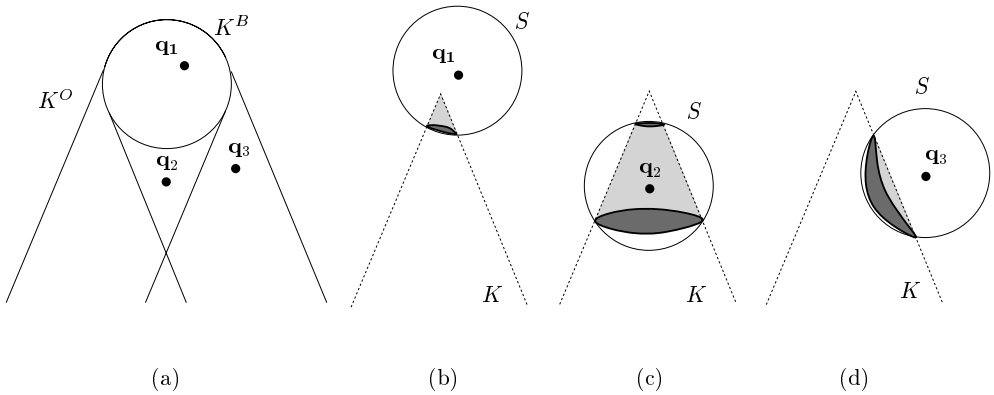

Figure 8.4: Regular KSI curves

8.2 Case Analysis for TKI Curve

When C is the main circle of T (that is, $C = C_R(\mathbf{0}, \mathbf{e}_3)$), let Q denote the set of points $\mathbf{q} \in C$, such that $S_r(\mathbf{q}) \cap K$ includes a tangent/degenerate intersection point/circle. The TKI curve has singularities if and only if the cross-sectional circle of T at $\mathbf{q}$, where $\mathbf{q} \in Q$, intersects with the tangent/degenerate intersection point/circle in $S_r(\mathbf{q}) \cap K$. We can detect the singular points in the TKI curve based on a C-space approach. The TKI curve has singularities if and only if:

1. C has tangent intersections with $K^I \cup K^O \cup K^D \cup K^B$.

2. C passes through K^V, and the cross-sectional circle of T at K^V has tangent intersection points with K.

The TKI curve is the same as the intersection of $Bdr(\cup B_r(C))$ and K. Let C_n denote a connected component in $C \cap (K_+^O \cup K_-^I)$. For an arbitrary point $\mathbf{q} \in C_n$, $B_r(\mathbf{q})$ does not intersect with K; thus, $(\cup B_r(C_n)) \cap K$ is an empty set. Due to the fact that $Bdr(\cup B_r(C_n)) \cap K$ is an empty set, we can detect the TKI curve by computing the set of intersection curves in $Bdr(\cup B_r(C_i)) \cap K$, where C_i is a connected component in $C \setminus (K_+^O \cup K_-^I)$.

Let C_i denote a connected component in $C \setminus (K_+^O \cup K_-^I)$. We consider two cases where $C_i \cap (K_-^D \cup K^D) = \emptyset$ and $C_i \cap (K_-^D \cup K^D) \neq \emptyset$.

8.2.1 The Case of $C_i \cap (K_-^D \cup K^D) = \emptyset$

When $C_i \cap (K_-^D \cup K^D) = \emptyset$, we can classify the topological types of the TKI curve as follows.

- If $C_i = C$ and C is embedded in $K^I \cup K^O$, the intersection curve consists of a singular circle.

If C is a circle embedded in K^I, T is inside K and touches K along a singular circle. If C is a circle embedded in K^O, T is outside K and touches K along a singular circle.

- If $C_i \neq C$ and C_i has no tangent intersection point with $K^I \cup K^O$, the intersection curve consists of a closed loop (see Figure 8.5(a)).

When $B_r(\mathbf{q})$ moves along the center trajectory C_i, for each point $\mathbf{q} \in C_i$, $B_r(\mathbf{q}) \cap K$ consists of a disk-type surface patch or one single contact point. $(\cup B_r(C_i)) \cap K$ is a surface patch of disk type (Refer to Lemma 7.1 in Section 7.1.1), and $Bdr(\cup B_r(C_i)) \cap K$ consists of a closed loop.

Let $\mathbf{q}_0$ denote an end point of C_i, and $\mathbf{q}_K$ denote a point on K at which $S_r(\mathbf{q}_0)$ touches K. We can trace the closed loop $Bdr(\cup B_r(C_i)) \cap K$ from the closest point from $\mathbf{q}_K$ in the set of intersection points between T and the profile line of K which passes through $\mathbf{q}_K$.

- If $C_i \neq C$ and C_i has k tangent intersection points with $K^I \cup K^O$, the intersection curve consists of a singular curve with k singular points on it (see Figures 8.5(b)–(c)).

For all $\mathbf{q} \in C_i$, each surface patch $B_r(\mathbf{q}) \cap K$ is of disk type except the case where $\mathbf{q}$ is a tangent intersection point of C_i and $K^I \cup K^O$. $(\cup B_r(C_i)) \cap K$ is a sequence of disk-type surface patches which are connected at k points. $Bdr(\cup B_r(C_i)) \cap K$ consists of a singular curve with k singular points on it. From k singular points, we can trace the singular curve.

- If $C_i = C$ and $C_i \cap (K^I \cup K^O)$ has k tangent intersection points, the intersection curve consists of a singular curve with k singular points on it (see Figures 8.5(d)–(e)).

(a)

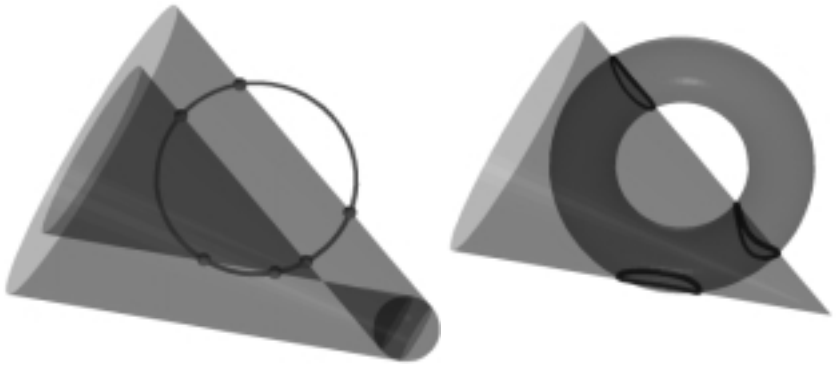

(b)

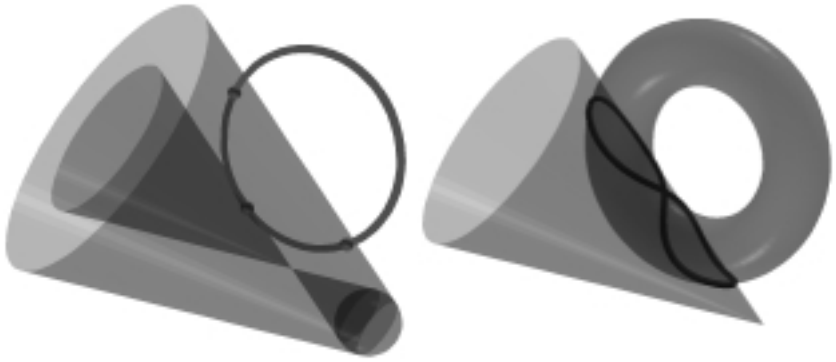

(c)

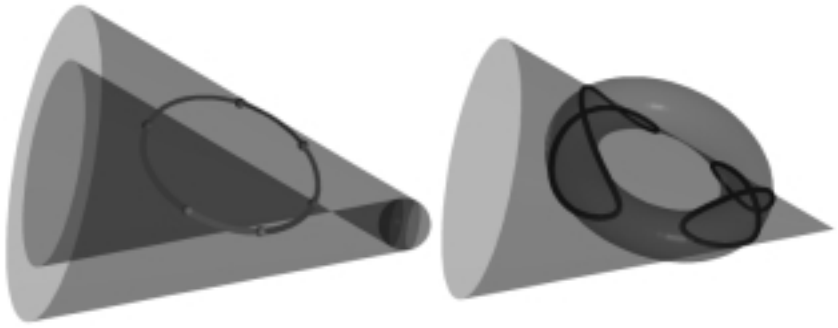

Figure 8.5: The TKI curves for the case of $C_i \cap (K_-^D \cup K^D) = \emptyset$

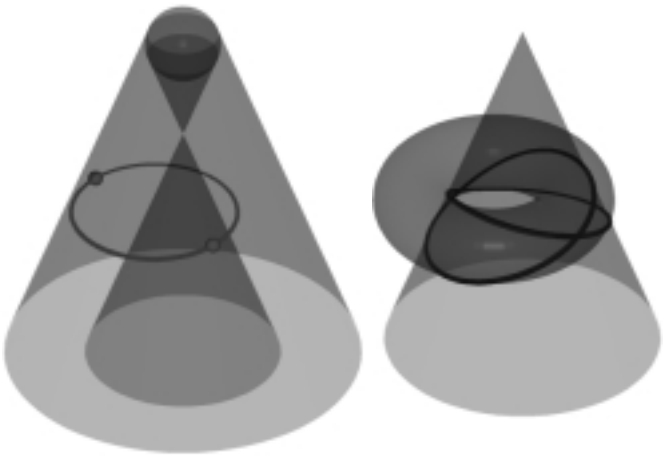

(d)

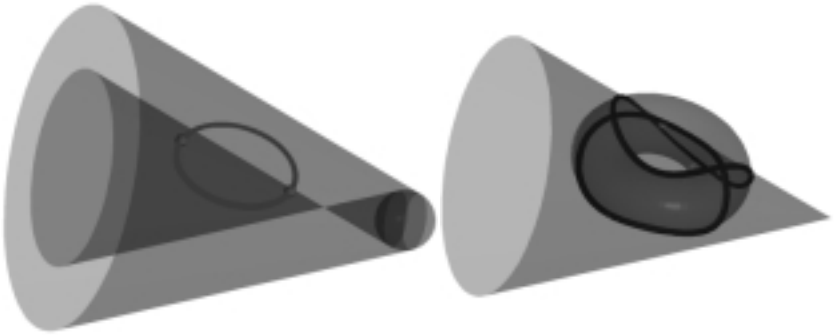

(e)

Figure 8.5: (*cont.*)

For all $\mathbf{q}$ in C_i, $B_r(\mathbf{q}) \cap K$ is a surface patch of disk type except the case where $\mathbf{q}$ is a tangent intersection point of C_i and $K^I \cup K^O$. When $\mathbf{q}$ is a tangent intersection point of C_i and $K^I \cup K^O$, $B_r(\mathbf{q}) \cap K$ consists of a singular point, and the cross-sectional circle of T at $\mathbf{q}$ intersects with the singular point. Thus, $(\cup B_r(C_i)) \cap K$ is a sequence of disk-type surfaces connected by k singular points, and whose whole shape is cylindrical. $Bdr(\cup B_r(C_i)) \cap K$ consists of a singular curve with k singular points on it. The TKI curve is traced from the singular points on it.

- If $C_i = C$ and C_i has no tangent intersection point with $K^I \cup K^O$, the intersection curve consists of two closed loops (see Figure 8.6).

For all $\mathbf{q} \in C_i$, the surface patch $B_r(\mathbf{q}) \cap K$ is of disk type. Due to the fact that $C_i = C$, $(\cup B_r(C_i)) \cap K$ consists of a surface patch of cylindrical type. The boundary of the surface patch of cylindrical type consists of two closed loops; thus, $Bdr(\cup B_r(C)) \cap K$ (that is, $T \cap K$) consists of two closed loops. In this case, an arbitrary cross-sectional circle of T intersects with K at two points. From these two intersection points, we can trace the TKI curve.

8.2.2 The Case of $C_i \cap (K^D_- \cup K^D) \neq \emptyset$

When $C_i \cap (K^D_- \cup K^D) \neq \emptyset$, we split the circular arc C_i into the set of circular arcs and/or points according to the regions in which C_i is located. For each split component C_j in C_i, we compute $(\cup B_r(C_j)) \cap K$, and by merging them, construct $(\cup B_r(C_i)) \cap K$. From the topological type of $(\cup B_r(C_i)) \cap K$, we can construct $Bdr(\cup B_r(C_i)) \cap K$ which is a subset of the TKI curve. C_i is split into connected components as in: (i) $C_i \cap (K^D_- \cup K^D)$, and (ii) $C_i \setminus (K^D_- \cup K^D)$. When C_i passes through K^V, more careful consideration is needed to classify the topological types of $Bdr(\cup B_r(C_i)) \cap K$ than other cases of C_i. Before classifying the types of C_i, we consider the cases where C_i passes through K^V first.

We classify the cases where C_i passes through K^V as follows. When C_j is a connected component in $C_i \cap (K^D_- \cup K^D)$, C_j can be a point K^V or a circular arc in $K^D_- \cup K^D$ which passes through K^V. Let l denote the tangent line of C_i at K^V. When l intersects with K^D tangentially along a profile line of K^D, there is one intersection point between the cross-sectional circle of T at K^V and $B_r(K^V) \cap K$. The intersection point is a singular point in the TKI curve (see Figures 8.7(a)–(b) and Figures 8.8(a)–(b)). When l passes through K^I_-, there is no intersection

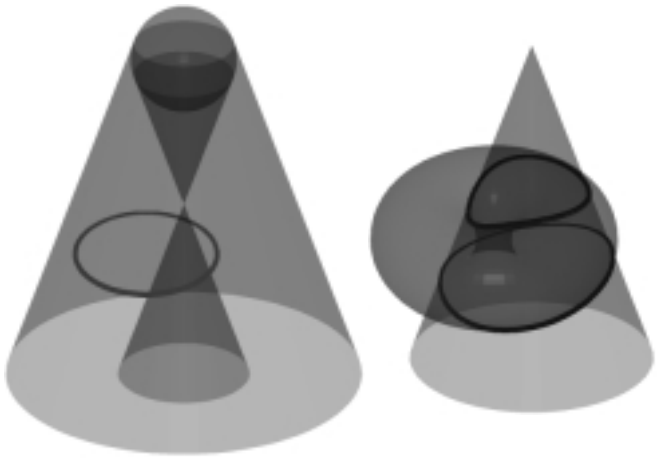

(a)

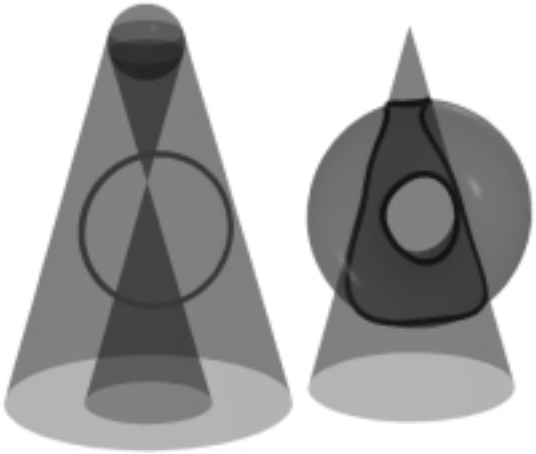

(b)

Figure 8.6: The TKI curves for the case of $C \cap (K_-^O \cap K_+^I \cap K_+^D) = C$

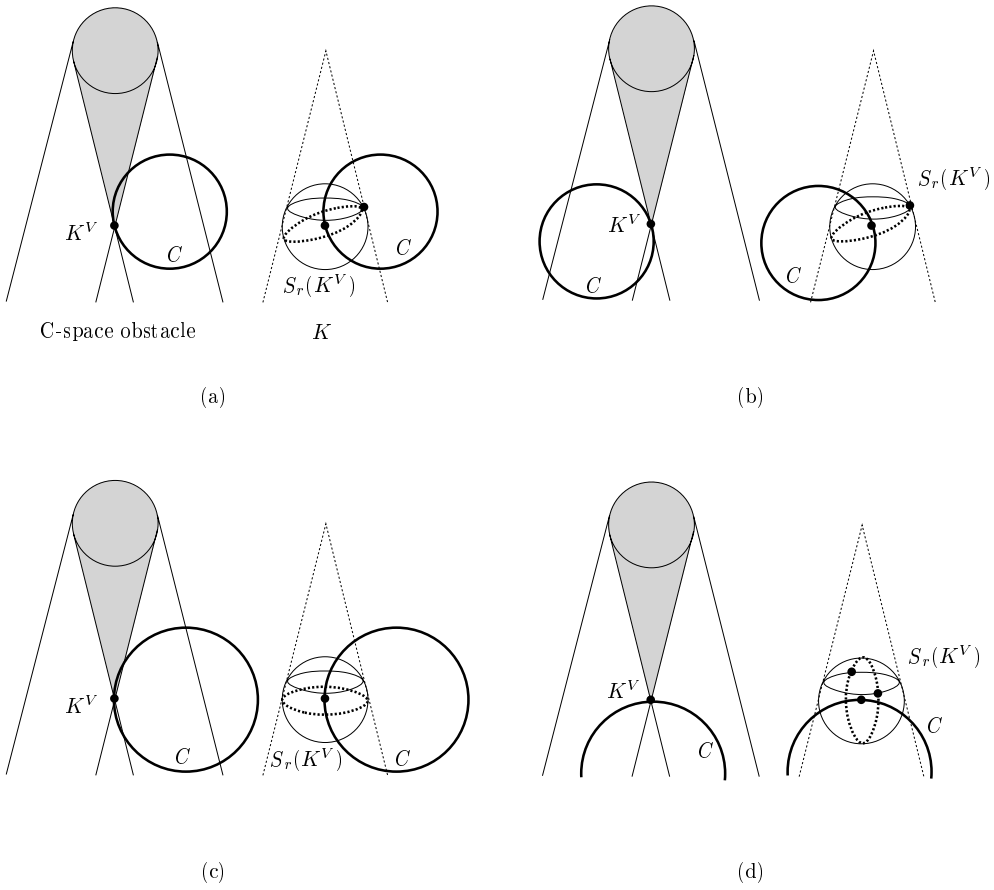

Figure 8.7: The cases of C_i passing through K^V.

between the cross-sectional circle of T at K^V and $B_r(K^V) \cap K$ (see Figure 8.7(c) and Figure 8.8(c)). When l passes through the region $K_-^O \cap K_+^I \cap K_+^D$, there are two intersection points between the cross-sectional circle of T at K^V and $B_r(K^V) \cap K$ (see Figure 8.7(d) and Figure 8.8(d)). In this case, two intersection points are singular points in the TKI curve, and each singular point has four branches.

The figures in the left columns of Figure 8.8 illustrate the relative positions of C in the C-space of the cone K; the figures in the right columns of Figure 8.8 illustrate the corresponding relative configurations of T and K.

Let C_j denote a connected component in $C_i \cap (K_-^D \cup K^D)$. $C_j \cap K^D$ includes a tangent intersection point in two cases: one case where C_j intersects with $K^D \setminus K^V$

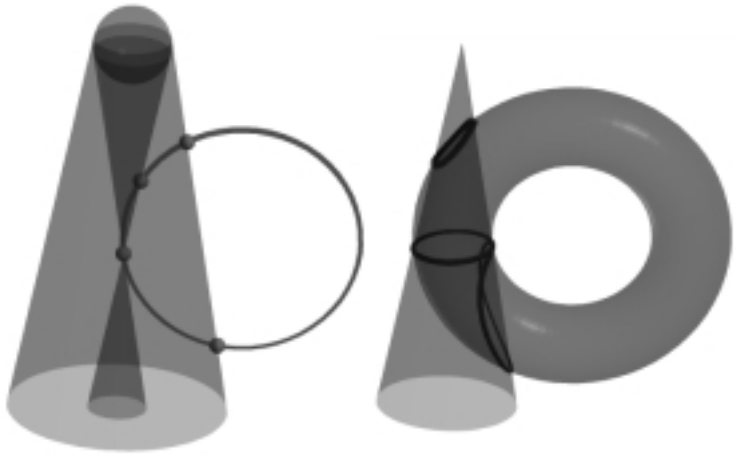

(a)

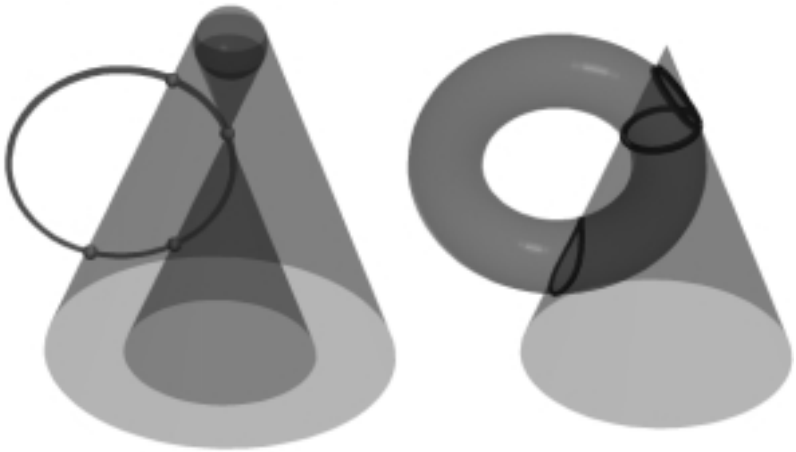

(b)

Figure 8.8: The TKI curves for the case of C_i passing through K^V

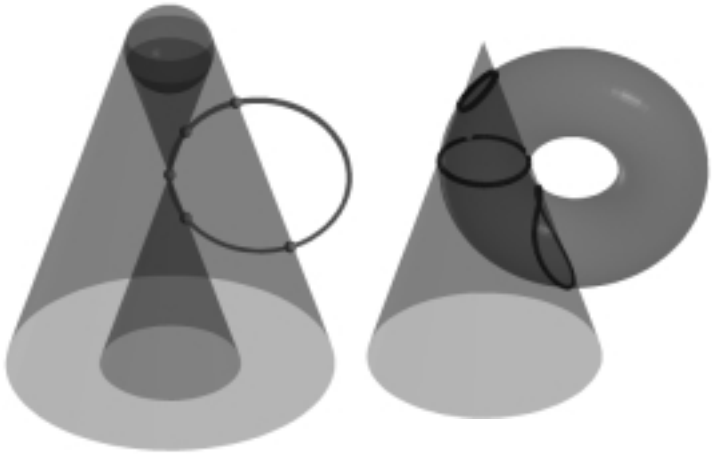

(c)

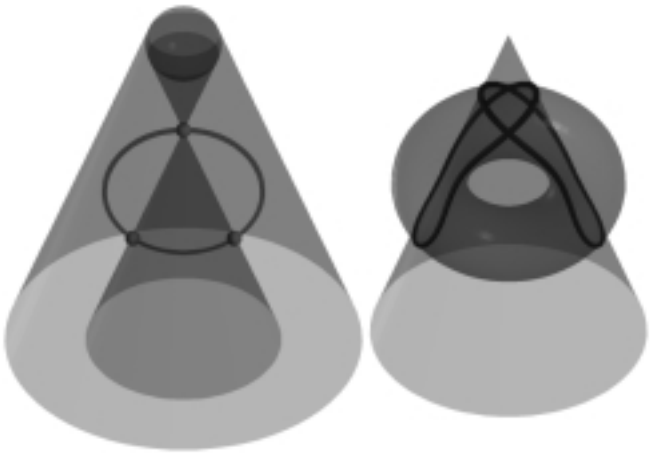

(d)

Figure 8.8: (*cont.*)

tangentially and the other case where C_j intersects with K^V tangentially. When C_j passes through K^V and the tangent line of C_j at K^V intersects with K^D tangentially along a profile line of K^D, we define that C_j intersects with K^V tangentially. Under this definition, we consider the seven types of C_j:

1. C_j is a point on K^D (Figures 8.2(b)–(c), and Figures 8.3(b)–(c)).
2. $C_j \cap K^B_- \neq \emptyset$ and C_j intersects with K^D tangentially (Figures 8.9(a)–(b)).
3. $C_j \cap K^B_- \neq \emptyset$ and $C_j \cap K^D$ does not include any tangent intersection point (Figure 8.9(c)).
4. C_j intersects with K^B tangentially, and $C_j \cap K^D$ includes a tangent intersection point (Figures 8.9(d)–(e)).
5. C_j intersects with K^B tangentially, and $C_j \cap K^D$ does not include any tangent intersection point (Figure 8.9(f)).
6. $C_j \cap K^B = \emptyset$ and $C_j \cap K^D$ includes a tangent intersection point (Figures 8.9(g)–(h)).
7. $C_j \cap K^B = \emptyset$ and $C_j \cap K^D$ does not include any tangent intersection point (Figure 8.9(i)).

There are four cases where C_j can be a point on K^D. If C_j is a point on $K^B \cap K^D$, $B_r(C_j) \cap K$ is the apex of K (Figure 8.2(b)). If C_j is a point on $(K^B \cap K^D) \setminus K^O$, $B_r(C_j) \cap K$ is a singular curve which contains the apex of K on it (Figure 8.2(c)). If C_j is a point on $K^D \setminus K^B$, $B_r(C_j) \cap K$ is a singular curve with a singular point on it (Figure 8.3(b)). If C_j is a point on K^V, $B_r(C_j) \cap K$ is a singular circle (Figure 8.3(c)).

When $C_j \cap K^B \neq \emptyset$ and $C_j \cap (K^D \setminus K^V)$ includes a tangent intersection point $\mathbf{q}$, $(\cup B_r(C_j)) \cap K$ is a surface patch of disk type, and $Bdr(\cup B_r(C_j)) \cap K$ consists of a closed loop (boundary curve of the disk-type surface), and a singular point (which is the tangent intersection point of K and a cross-sectional circle of T at $\mathbf{q}$) (see Figure 8.9(a)). If C_j intersects with K^V tangentially, $Bdr(\cup B_r(C_j)) \cap K$ consists of a singular curve with a singular point on it (see Figure 8.9(b)). The singular point is a tangent intersection point of K and a cross-sectional circle of T at K^V. When $C_j \cap K^B \neq \emptyset$ and $C_j \cap K^D$ does not include any tangent intersection point,

$(\cup B_r(C_j)) \cap K$ is a surface patch of disk type. $Bdr(\cup B_r(C_j)) \cap K$ consists of a closed loop (see Figure 8.9(c)).

When C_j intersects with K^B tangentially and $C_j \cap (K^D \setminus K^V)$ includes a tangent intersection point $\mathbf{q}$, $(\cup B_r(C_j)) \cap K$ is a disk-type surface, and $Bdr(\cup B_r(C_j)) \cap K$ consists of a closed loop (boundary curve of the disk-type surface), the apex of K, and a singular point, which is the tangent intersection point of K (see Figure 8.9(d)). If C_j intersects with K^V tangentially, $Bdr(\cup B_r(C_j)) \cap K$ consists of the apex of K and a singular curve with a singular point on it (see Figure 8.9(e)). The singular point is a tangent intersection point of K and a cross-sectional circle of T at K^V. When C_j intersects with K^B tangentially, and $C_j \cap K^D$ does not include any tangent intersection point, $(\cup B_r(C_j)) \cap K$ is a surface patch of disk type, and $Bdr(\cup B_r(C_j)) \cap K$ consists of a closed loop and the apex of K (see Figure 8.9(f)).

When $C_j \cap K^B = \emptyset$ and $C_j \cap (K^D \setminus K^V)$ includes a tangent intersection point $\mathbf{q}$, $(\cup B_r(C_j)) \cap K$ is a cylindrical-type surface, and $Bdr(\cup B_r(C_j)) \cap K$ consists of two closed loops (boundary curve of the cylindrical-type surface) and a singular point, which is the tangent intersection point of K and a cross-sectional circle of T at $\mathbf{q}$ (see Figure 8.9(g)). If C_j intersects with K^V tangentially, $Bdr(\cup B_r(C_j)) \cap K$ consists of a closed loop and a singular curve with a singular point on it (see Figure 8.9(h)). The singular point is a tangent intersection point of K and a cross-sectional circle of T at K^V. When $C_j \cap K^B = \emptyset$ and $C_j \cap K^D$ does not include any tangent intersection point, $(\cup B_r(C_j)) \cap K$ is a cylindrical-type surface, and $Bdr(\cup B_r(C_j)) \cap K$ consists of two closed loops (see Figure 8.9(i)).

Let C_k denote a connected component in $C_i \setminus (K_-^D \cup K^D)$. Then we consider three types of C_k:

1. C_k is a circular arc which has no tangent intersection point with $K^I \cup K^O$ (Figures 8.10(a)–(b)).

2. C_k is a circular arc which has m $(m > 0)$ tangent intersection points with $K^I \cup K^O$ (Figures 8.10(c)–(d)).

When C_k is a circular arc which has m $(m > 0)$ tangent intersection points with $K^I \cup K^O$, $(\cup B_r(C_k)) \cap K$ consists of several disk-type surface patches which are connected by m points. When C_k is a circular arc which has no tangent intersection point with $K^I \cup K^O$, $(\cup B_r(C_k)) \cap K$ consists of a surface patch of disk type.

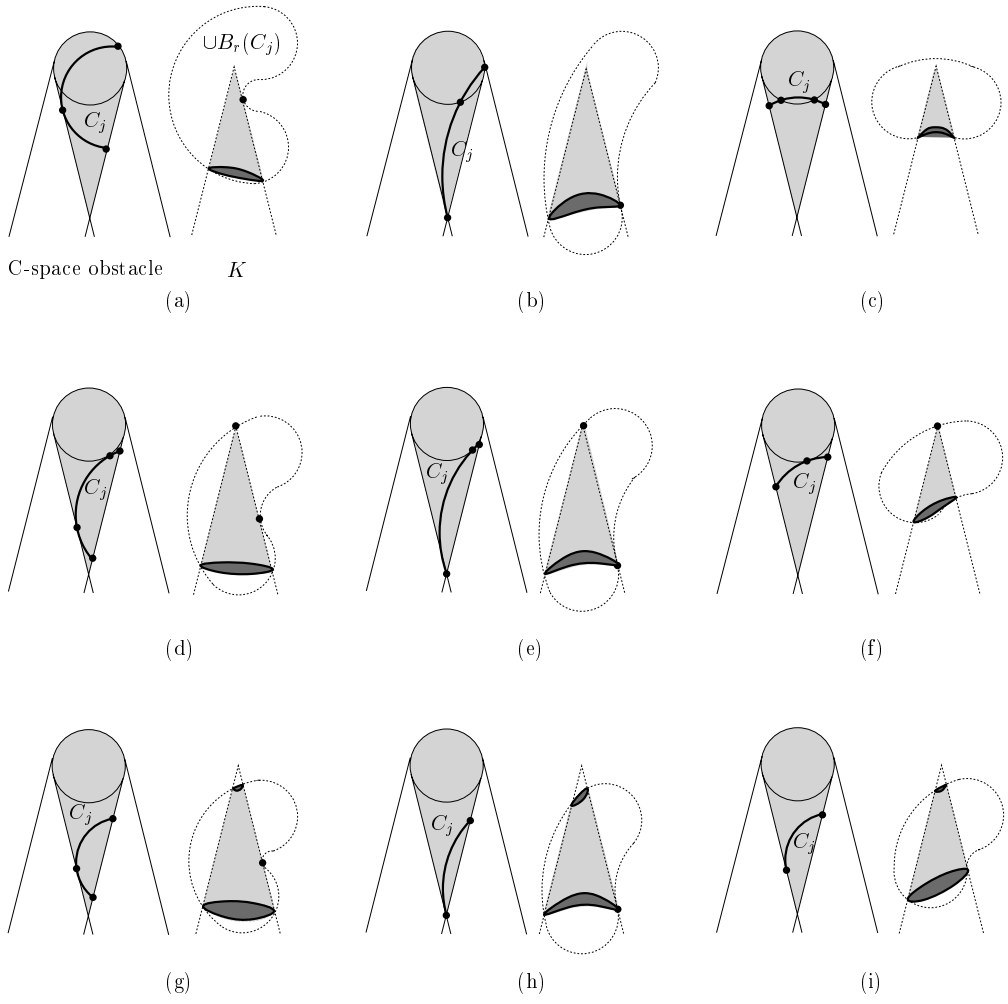

Figure 8.9: $(\cup B_r(C_j)) \cap K$ for the connected component C_j in $C_i \cap (K_-^D \cup K^D)$

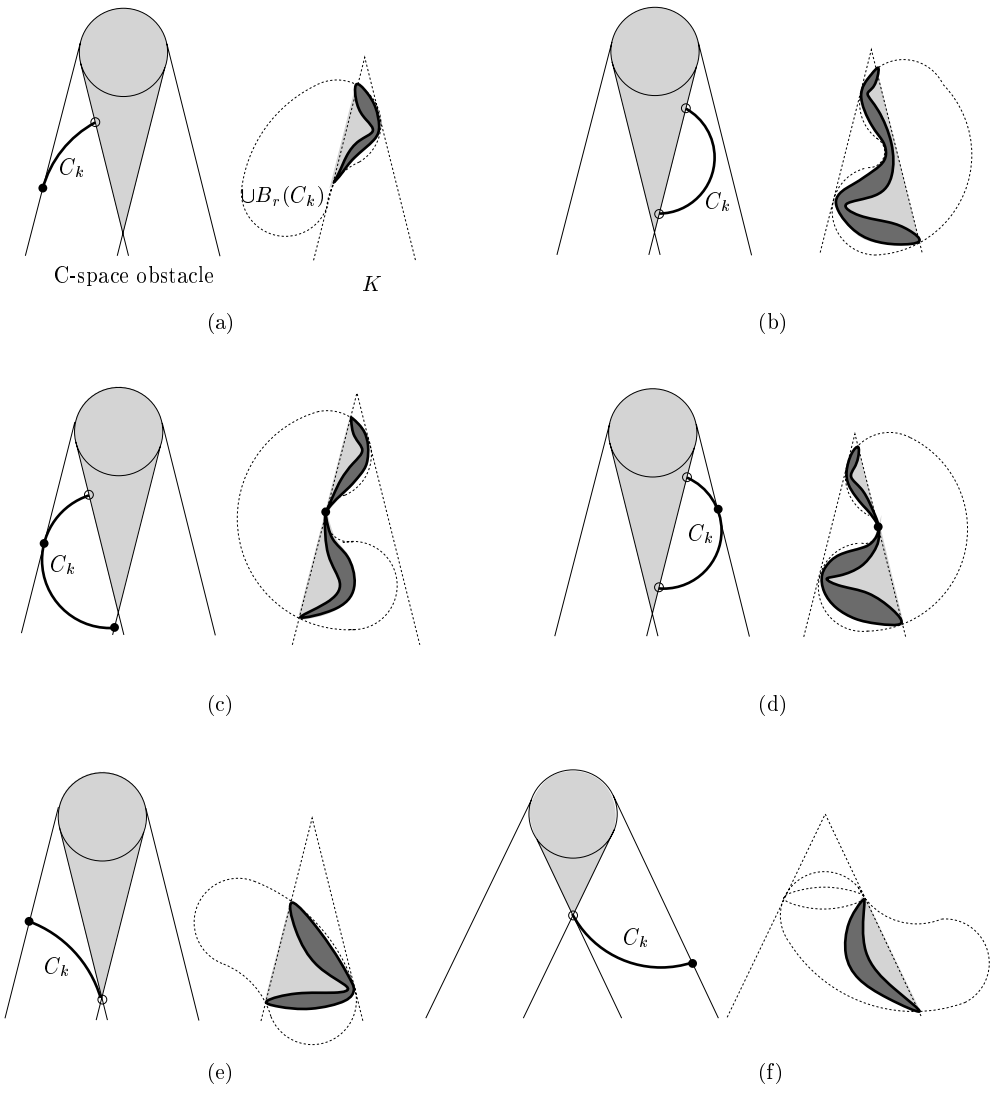

Figure 8.10: $(\cup B_r(C_k)) \cap K$ for the connected component C_k in $C_i \setminus (K_-^D \cup K^D)$

Let C_j denote a connected component in $C_i \cap (K_-^D \cup K^D)$, and C_k denote a connected component in $C_i \setminus (K_-^D \cup K^D)$. We classify the topological types of the intersection curve $Bdr(\cup B_r(C_i)) \cap K$ according to the number of connected components in $C_i \cap (K_-^D \cup K^D)$ and the connection type between C_js and C_ks. Figure 8.11 classifies the topological types of $(\cup B_r(C_j)) \cap K$ as Types (A) to (I).

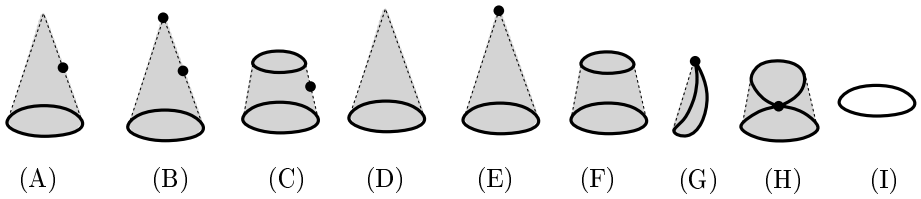

Figure 8.11: The topological types of $(\cup B_r(C_j)) \cap K$ for a connected component C_j in $C_i \cap (K_-^D \cup K^D)$

When the number of connected components in $C_i \cap (K_-^D \cup K^D)$ is one, there are two cases: $C_i \neq C$, or $C_i = C$. If $C_i \neq C$, C_j can be connected with one or two C_ks. When C_k does not have any tangent intersection point with $K^I \cup K^O$, the topological types of surface patches $(\cup B_r(C_j)) \cap K$ and $(\cup B_r(C_j \cup C_k)) \cap K$ are the same. We show examples for the case of the number of connected components in $C_i \cap (K_-^D \cup K^D)$ is one and $C_i \neq C$ in Figure 8.12. Figure 8.12(a) shows the case where the $\cup B_r(C_j)$ of Type (F) is connected with two surface patches of disk type $(\cup B_r(C_{k_1})) \cup K$ and $(\cup B_r(C_{k_2})) \cup K$, where an end point of C_{k_1} is on K^D and the other end point is on K^I, and an end point of C_{k_2} is on K^D and the other end point is on K^I. Thus, the topological type of $(\cup B_r(C_j \cup C_{k_1} \cup C_{k_2})) \cap K$ is same as that of $(\cup B_r(C_j)) \cap K$. Figure 8.12(b) shows the case where the $\cup B_r(C_j)$ of Type (H) is connected with two surface patches of disk type $(\cup B_r(C_{k_1})) \cap K$ and $(\cup B_r(C_{k_2})) \cap K$, where an end point of C_{k_1} is on K^D and the other end point is on K^I, and an end point of C_{k_2} is on K^D and the other end point is on K^I. Thus, the topological type of $(\cup B_r(C_j \cup C_{k_1} \cup C_{k_2})) \cap K$ is same as that of $(\cup B_r(C_j)) \cap K$. When C_k has m tangent intersection points with $K^I \cup K^O$, there are m singular points in $Bdr(\cup B_r(C_k)) \cap K$, and $(\cup B_r(C_j \cup C_k)) \cap K$ has m more singular points than $(\cup B_r(C_j)) \cap K$.

If $C_i = C$, C_j can be connected with one C_k which touches K^D at both end points. At this time, the topological type of surface patch $(\cup B_r(C_j \cup C_k)) \cap K$

is different from $(\cup B_r(C_j)) \cap K$. When C_i has no tangent intersection point with $K^I \cup K^O$, a closed loop is added. Figure 8.12(c) shows the case when C_i (such that $C_i = C$) consists of C_j and C_k, where $(\cup B_r(C_j)) \cap K$ is a surface patch of Type (F) and C_k has no tangent intersection point with $K^I \cup K^O$. When C_i has m tangent intersection points with $K^I \cup K^O$, one of the closed loops in $(\cup B_r(C_j)) \cap K$ is replaced by a singular curve with m singular points on it. Figure 8.12(d) shows the case when C_i (such that $C_i = C$) consists of C_j and C_k, where $(\cup B_r(C_j)) \cap K$ is a surface patch of Type (H) and C_k has one tangent intersection point with $K^I \cup K^O$.

When the number of connected components in $C_i \cap (K_-^D \cup K^D)$ is two, the connection types of two components are classified in Figure 8.13. Two connected components in $C_i \cap (K_-^D \cup K^D)$ are connected by two or three components in $C_i \setminus (K_-^D \cup K^D)$. When a component $C_k \subset C_i \setminus (K_-^D \cup K^D)$ connects two components C_{j_1} and C_{j_2} (which are two connected components in $C_i \cap (K_-^D \cup K^D)$), the topological types of $(\cup B_r(C_{j_1})) \cap K$ and $(\cup B_r(C_{j_2})) \cap K$ are merged into $(\cup B_r(C_i)) \cap K$. The boundary curves of $(\cup B_r(C_i)) \cap K$ are detected from the set of singular points, and by subdividing T at the cross-sectional circle of T at the middle point on circular arc C_k, and by subdividing K at an arbitrary profile line.

Figure 8.14 shows examples of the connection types between two connected components of Type (D) and Type (F) in $C_i \cap (K_-^D \cup K^D)$. In Figure 8.14(a), there are two connected components C_{j_1} and C_{j_2} in $C_i \cap (K_-^D \cup K^D)$, where $(\cup B_r(C_{j_1})) \cap K$ is of Type (D) and $(\cup B_r(C_{j_2})) \cap K$ is of Type (F). Figures 8.14(b)–(f) show the cases where C_{j_1} and C_{j_2} are connected with C_ks of various types. Figure 8.15 show the corresponding TKI curves.

8.3 Algorithm: Torus_Cone_Intersection

Previous sections classified the topological types of the TKI curve based on a C-space approach. Algorithm: Torus_Cone_Intersection of Appendix A.6 summarizes the TKI algorithm based on the above case analyses. In this algorithm, we assume that cubic curve tracing routines: Trace_Singular_TKI_Curve (T, K, DP) and Trace_Regular_TKI_Curve (T, K, IP), are available, where T is a torus and K is a cone, and DP, IP are a set of singular points and a set of starting points, respectively. Each singular intersection curve can be traced starting from its singular point (see also Piegl [21]), the details of which are given in the routine:

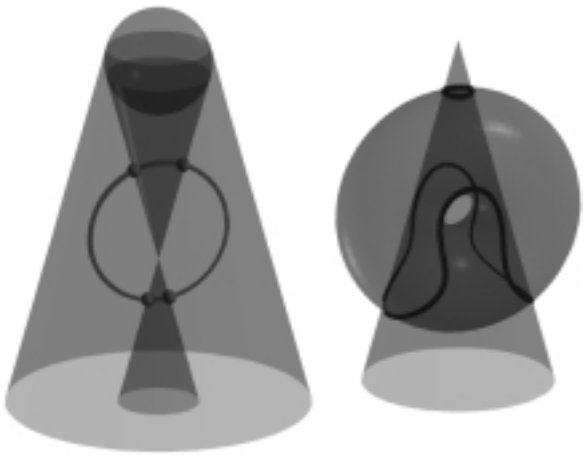

(a)

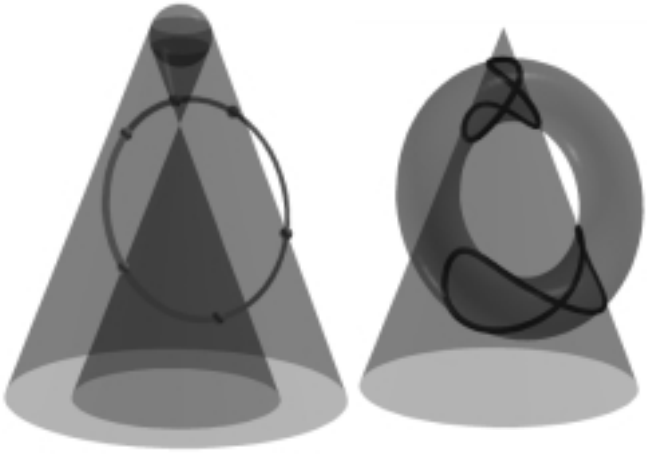

(b)

Figure 8.12: The TKI curves for the case of one connected component in $C_i \cap (K_-^D \cup K^D)$.

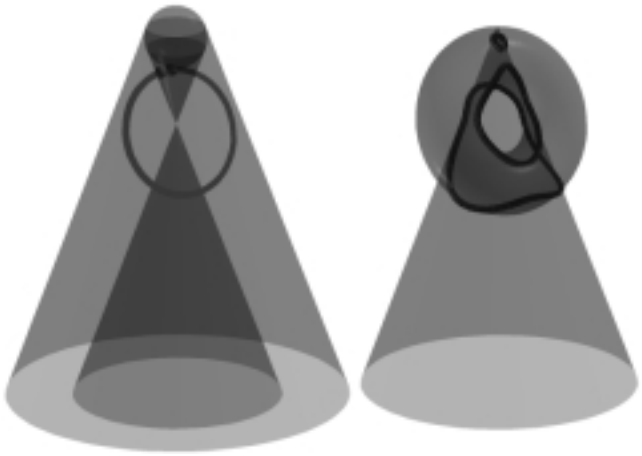

(c)

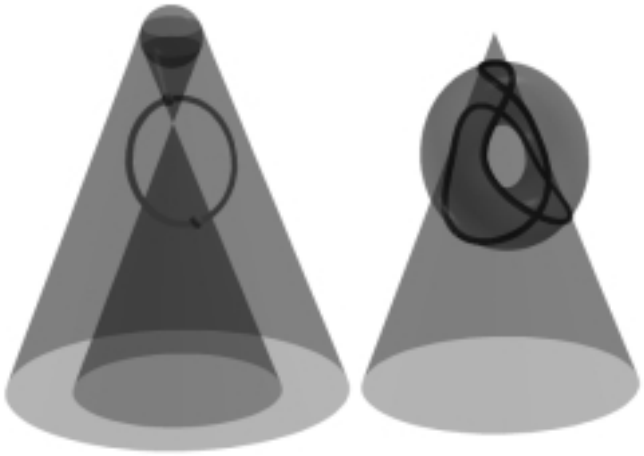

(d)

Figure 8.12: (*cont.*)

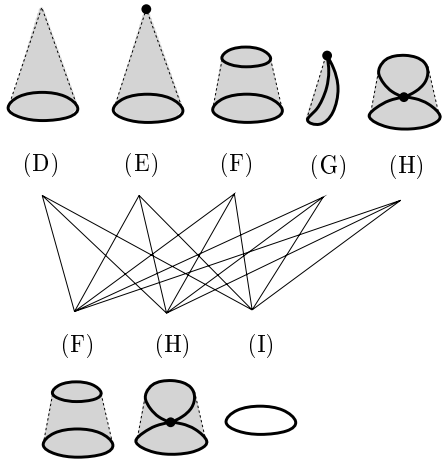

Figure 8.13: Possible pairs of types of $(\cup B_r(C_j)) \cap K$, where C_j is a connected component in $C_i \cap (K_-^D \cup K^D)$.

Trace_Singular_TKI_Curve. We assume that when a singular curve is traced, if the singular curve passes through a point in the set IP, the point is removed from IP.

In Line (1), we assume that the routine Detect_Circles_in_TKI(T, K), which detects and computes all degenerate circles in the TKI curve is available (See Chapter 3). Line (2) computes starting points of two closed loops when C is in $K_-^O \cap K_+^I \cap K_+^D$. By intersecting an arbitrary cross-sectional circle of T with K, the starting points are computed. Line (3) computes a starting point for a closed loop which corresponds to a connected component C_i such that $C_i \subset C \cap (K_-^O \cap K_+^I)$, and $C_i \cap (K_-^D \cup K^D) \neq \emptyset$. When $\mathbf{q}$ is an end point of C_i, and $\mathbf{q}_K$ denotes a point on K at which $S_r(\mathbf{q})$ touches K, let l denote a profile line of K which passes through $\mathbf{q}_K$. We can trace the closed loop $Bdr(\cup B_r(C_i)) \cap K$ from the closest point from $\mathbf{q}_K$ in the set of intersection points between T and l. Line (4) computes the starting points for the closed loop which corresponds to a connected component $C_i \subset K_-^O \cap K_+^I$, where $C_i \cap (K_-^D \cup K^D) \neq \emptyset$. Line (5) computes the starting points for closed loops, where each closed loop corresponds to C_k which is a connected component in $K_-^O \cap K_+^I$, and whose both end points are on K^D. By intersecting the cross-sectional circle of T at the middle point of C_k with K, the starting points are computed. In Line (6), all singular curves in the TKI curve are traced from DP which is a set of all singular

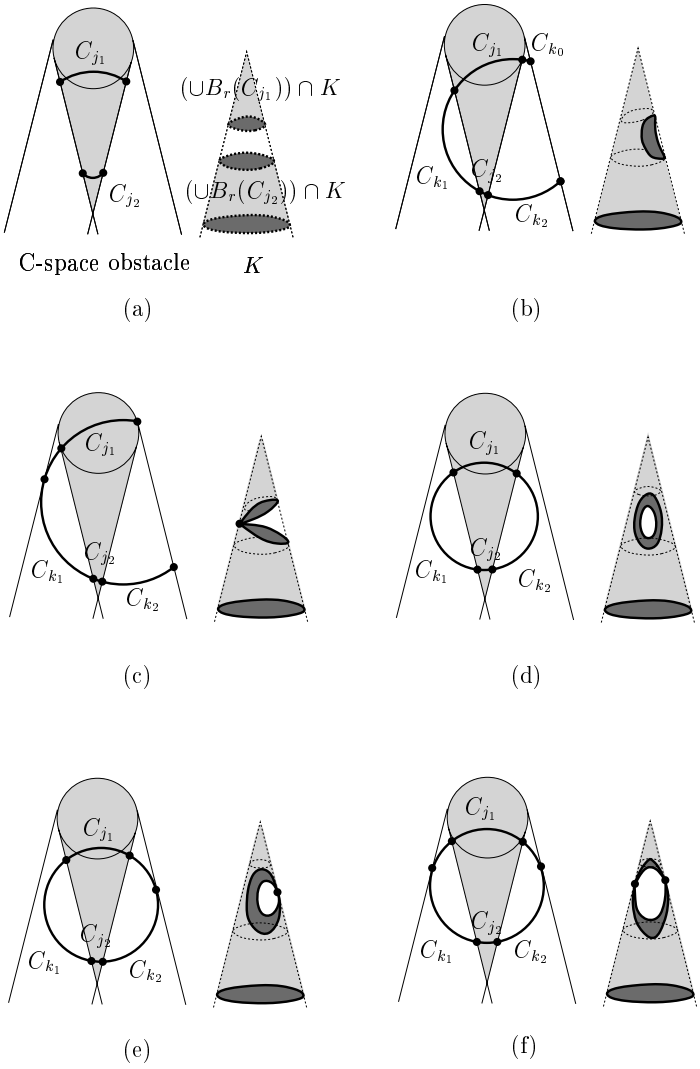

Figure 8.14: The connection types of two connected components in $C_i \cap (K_-^D \cup K^D)$

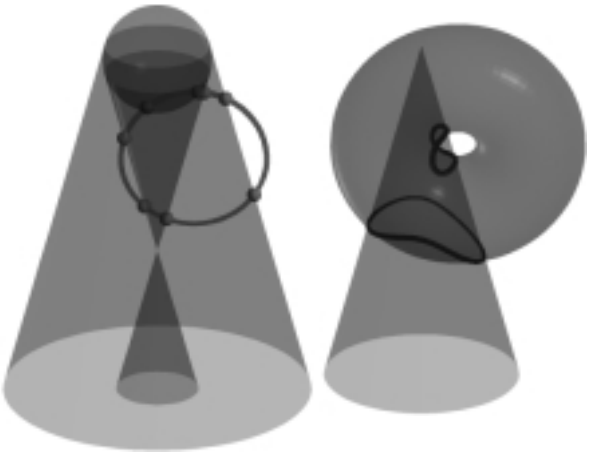

(a)

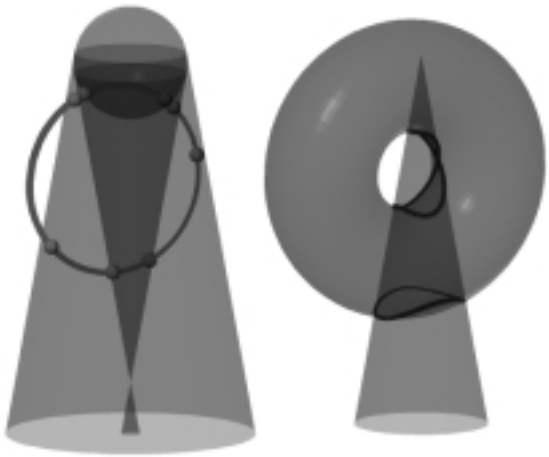

(b)

Figure 8.15: The TKI curves for the case of two connected components in $C_i \cap (K^D_- \cup K^D)$.

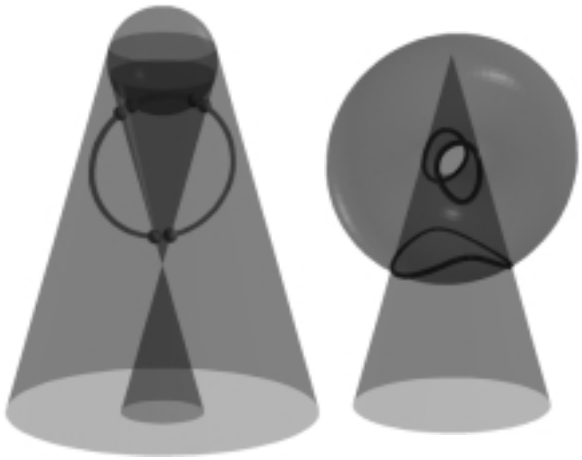

(c)

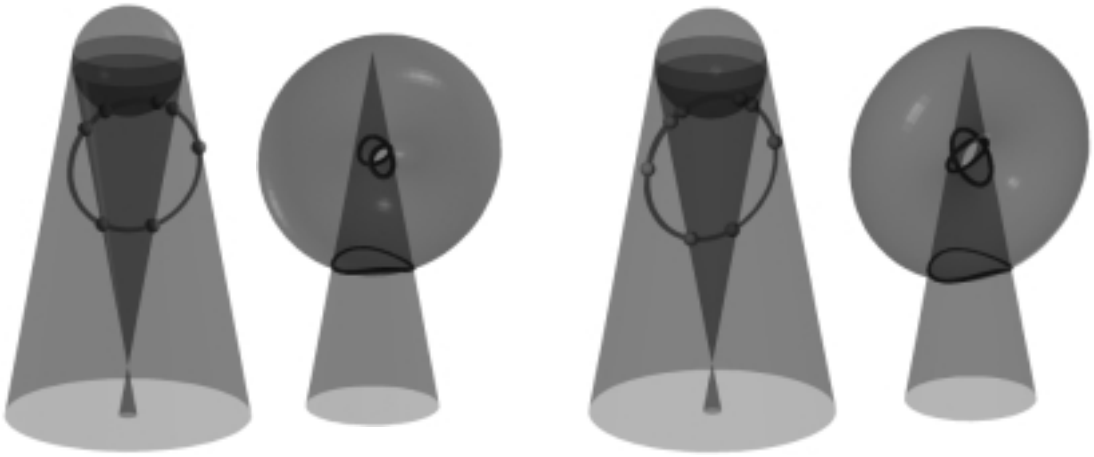

(d) (e)

Figure 8.15: (*cont.*)

points in the TKI curve. In Line (7), all closed loops in the TKI curve are traced from IP which is a set of starting points in the TKI curve.

Chapter 9

Torus and Torus Intersection

Given two tori $T_1 = T_{\delta,\Delta}(\mathbf{p}_1, \mathbf{N}_1)$ and $T_2 = T_{r,R}(\mathbf{p}_2, \mathbf{N}_2)$, we consider the torus with larger minor radius as an obstacle. Without loss of generality, we may assume that $0 < r \leq \delta$. That is, we treat the torus T_1 as an obstacle and the torus T_2 as the envelope surface of a moving ball along a circular trajectory: $T_2 = Bdr(\cup B_r(C(t)))$, where $C(t)$ is a circle of radius R. By applying translation and rotation if necessary, we may assume that the torus T_1 is in the standard position and orientation: $T_1 = T_{\delta,\Delta}(\mathbf{0}, \mathbf{e}_3)$, and the torus T_2 is in an arbitrary position and orientation: $T_2 = T_{r,R}(\mathbf{p}, \mathbf{N})$.

We compute the C-space obstacle of the torus T_1 with respect to the moving ball with radius r. The C-space obstacle of T_1 is bounded by the $\pm r$-offsets of T_1: i.e., the inner offset torus $T^I = T_{\delta-r,R}(\mathbf{0}, \mathbf{e}_3)$ and the outer offset torus $T^O = T_{\delta+r,R}(\mathbf{0}, \mathbf{e}_3)$. When $\delta + r \geq R$, the outer torus T^O self-intersects. Let T^D denote the self-intersected part of T^O (see Figures 2.2(b)–(c)). (In the case of $\delta + r < R$, T^O has no self-intersection; thus we have $T^D = \emptyset$.) Let T^I_- and T^I_+ denote the interior and exterior open regions of $\mathbb{R}^3$ separated by the closed surface T^I. T^D_- and T^D_+ are defined similarly. T^O_- and T^O_+ are the open regions separated by the closed surface $T^O \setminus T^{D^o}$, where T^{D^o} denotes T^D except two vertices of T^D.

When we give the normal orientations of the surfaces T^O and T^D as the outward directions (i.e., pointing to the regions T^O_+ and T^D_+, respectively) and that of the surface T^I as the inward direction (i.e., pointing to the region T^I_-), the winding numbers assigned to the open regions T^O_+ and T^I_- are both zero. Moreover, the winding number assigned to $T^O_- \cap T^I_+ \cap T^D_+$ is one and that assigned to T^D_- is two.

Section 6.2 classified the topological type of the intersection curve of a torus and a sphere according to the relative position of the sphere center with respect to the C-space obstacle of the torus. Given a sphere and a torus, where the radius of the sphere is smaller than or equal to the minor radius of the torus, the number of closed loops in the torus/sphere intersection is zero, one, and two, when the sphere center is contained in the region of the C-space with winding number zero, one, and two, respectively.

Let $\mathbf{q}$ denote a point on the main circle of T_2. For $\mathbf{q} \in T_-^O \cap T_+^I \cap T_+^D$ (that is, $\mathbf{q}$ belongs to the region of winding number one), the sphere $S_r(\mathbf{q})$ intersects with T_1 in one closed loop, and the surface patch $B_r(\mathbf{q}) \cap T_1 \subset T_1$ is of disk type. For $\mathbf{q} \in T_-^D$ (that is, $\mathbf{q}$ belongs to the region of winding number two), the sphere $S_r(\mathbf{q})$ intersects with T_1 in two closed loops, and the surface patch $B_r(\mathbf{q}) \cap T_1$ is of cylindrical type. For $\mathbf{q} \in T_+^O \cup T_-^I$ (that is, $\mathbf{q}$ belongs to the region of winding number zero), the sphere $S_r(\mathbf{q})$ has no intersection with T_1. If $\mathbf{q} \in T^I \cup T^O$ (that is, the boundary of the C-space obstacle), the intersection curve $S_r(\mathbf{q}) \cap T_1$ consists of a singular curve or a singular point. Based on this classification and the intersection of the C-space obstacle and the trajectory of the moving ball's center, we can classify all possible topological types of the closed loops and/or singular curves in the TTI curve.

The C-space obstacle consists of two tori, and the trajectory of the moving ball's center forms a circle; thus we can compute the intersection between the C-space obstacle and the trajectory circle by a torus/circle intersection. Torus/circle intersection is computed by solving a fourth order polynomial equation (see Appendix B).

Let C denote the main circle of T_2: $C = C_R(\mathbf{p}, \mathbf{N})$, and Q denote the set: $Q = \{\mathbf{q} \in C \mid S_r(\mathbf{q}) \cap T_1$ has a tangent intersection point/circle $\}$. The TTI curve has singularities if and only if the cross-sectional circle of T_1 at $\mathbf{q} \in Q$, intersects with the tangential intersection point/circle of $S_r(\mathbf{q}) \cap T_1$. We can detect the singular points in the TTI curve based on a C-space approach. The TTI curve has singularities if and only if one of the following conditions holds:

1. C has tangent intersections with $T^I \cup T^O$.

2. C passes through a vertex of T^D and the cross-sectional circle of T_2 at the vertex intersects with T_1.

3. C intersects with T^I, when $0 < r = \delta$.

The TTI curve is the same as the intersection of $Bdr(\cup B_r(C))$ and T_1. Let C_n denote a connected component in $C \cap (T_+^O \cup T_-^I)$. For an arbitrary point $\mathbf{q} \in C_n$, $B_r(\mathbf{q})$ does not intersect with T_1; thus, $(\cup B_r(C_n)) \cap T_1$ is an empty set. Due to the fact that $Bdr(\cup B_r(C_n)) \cap T_1$ is the subset of $(\cup B_r(C_n)) \cap T_1$, $Bdr(\cup B_r(C_n)) \cap T_1$ is an empty set.

We detect all closed loops and singular points/curves in the TTI curve by computing $Bdr(\cup B_r(C_i)) \cap T_1$, for all C_i which is a connected component in $C \setminus (T_+^O \cup T_-^I)$. Let C denote the main circle of the torus T_2 (i.e., $C = C_R(\mathbf{p}, \mathbf{N})$) and C_i denote a connected component in $C \cap ((T_-^O \cap T_+^I) \cup T^I \cup T^O)$. First, we consider the case of $0 < r < \delta$, and then we consider the case of $0 < r = \delta$.

9.1 Analysis for the Case of $0 < r < \delta$

We consider two cases of $C_i \cap (T_-^D \cup T^D) = \emptyset$ and $C_i \cap (T_-^D \cup T^D) \neq \emptyset$ separately.

9.1.1 The Case of $C_i \cap (T_-^D \cup T^D) = \emptyset$

The figures in the left columns of Figure 9.1 illustrate the relative positions of C in the C-space of the torus T_1; the figures in the right columns of Figure 9.1 illustrate the corresponding relative configurations of T_1 and T_2.

- If $C_i \neq C$ and C_i does not have any tangent intersection point with $T^I \cup T^O$, $(\cup B_r(C_i)) \cap T_1$ consists of a surface patch of disk type, and the intersection curve consists of one closed loop (see Figures 9.1(a)–(b)).

This can be proved in a similar way of proving Lemma 7.1 in Section 7.1.1.

- If $C_i \neq C$ and C_i has k tangent intersection points with $T^I \cup T^O$, $(\cup B_r(C_i)) \cap T_1$ consists of several disk-type surface patches which are connected by k singular points, and the intersection curve consists of a singular curve with k singular points on it(see Figure 9.1(c)).

Let's assume that C_i intersects with $T^I \cup T^O$ tangentially at a point $\mathbf{q}$. If we move C slightly for C_i to be split into two connected components C_{i_1} and C_{i_2}, $Bdr(\cup B_r(C_{i_1})) \cap T_1$ consists of a closed loop, and $Bdr(\cup B_r(C_{i_2})) \cap T_1$ consists of another closed loop. If C_{i_1} and C_{i_2} meet at a point on $T^I \cup T^O$, two closed loops

$Bdr(\cup B_r(C_{i_1})) \cap T_1$ and $Bdr(\cup B_r(C_{i_2})) \cap T_1$ are merged into a singular curve. When C_i intersects with $T^I \cup T^O$ tangentially at a point $\mathbf{q}$, $Bdr(\cup B_r(C_i)) \cap T_1$ consists of a singular curve with a singular point (which is the intersection point of T_1 and the cross-sectional circle of T_2 at $\mathbf{q}$) on it. Similarly, if C_i has k tangent intersection points with $T^I \cup T^O$, $Bdr(\cup B_r(C_i)) \cap T_1$ consists of a singular curve with k singular points on it.

- If $C_i = C$ and C_i consists of k tangent intersection points with $T^I \cup T^O$, $T_1 \cap T_2$ has a singular curve with k singular points (see Figure 9.1 (d)).

When $C_i = C$, the maximum number of the tangent intersection points in $C_i \cap T^I$ is two, and that of $C_i \cap T^O$ is two; thus, $T_1 \cap T_2$ can have a singular curve with a maximum of four singular points on it.

- If $C_i = C$ and C_i does not intersect with $T^I \cup T^O$, $T_1 \cap T_2$ has two closed loops (see Figure 9.1(e)).

When $C_i = C$ and $C \subset T^O_- \cap T^I_+ \cap T^D_+$, $(\cup B_r(C_i)) \cap T_1$ is a surface patch of cylindrical type. $Bdr(\cup B_r(C_i)) \cap T_1$, that is, $T_2 \cap T_1$, is identical to the boundary curve of $(\cup B_r(C_i)) \cap T_1$; thus $T_2 \cap T_1$ consists of two closed loops.

- If $C_i = C$ and C_i is embedded in $T^I \cup T^O$, $T_1 \cap T_2$ consists of a singular circle or a singular curve.

C_i is embedded in T^I (or T^O) if and only if C_i is a profile circle or a cross-sectional circle or an Yvone-Villarceau circle of T^I (or T^O). When C_i is a profile circle of T^I, T_2 is inside T_1, and T_2 intersects with T_1 tangentially along a profile circle of T_1. When C_i is a profile circle of T^O, T_2 is outside T_1, and T_2 intersects with T_1 tangentially along a profile circle of T_1.

When C_i is a cross-sectional circle of T^I, T_2 is inside T_1, and T_2 intersects with T_1 tangentially along a cross-sectional circle of T_1. If C_i is a cross-sectional circle of T^O, T_1 is outside T_1, and T_2 intersects with T_1 tangentially along a cross-sectional circle of T_1.

When C_i is an Yvone-Villarceau circle of T^I, T_2 is inside T_1, and T_2 intersects with T_1 tangentially along a singular quartic curve. When C_i is an Yvone-Villarceau circle of T^O, T_2 is outside T_1, and T_2 intersects with T_1 tangentially along a singular quartic curve.

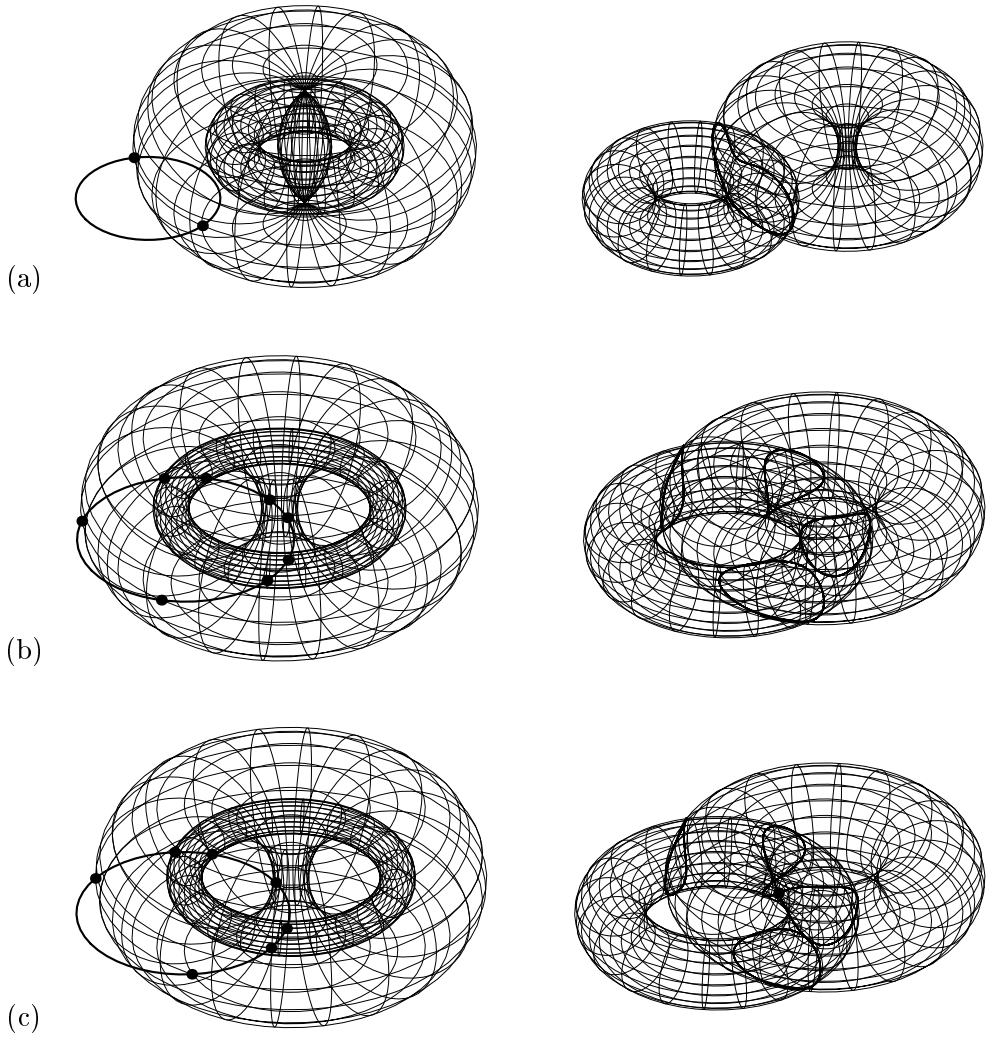

Figure 9.1: The TTI curves for the case of $C_i \cap (T_-^D \cup T^D) = \emptyset$.

(d)

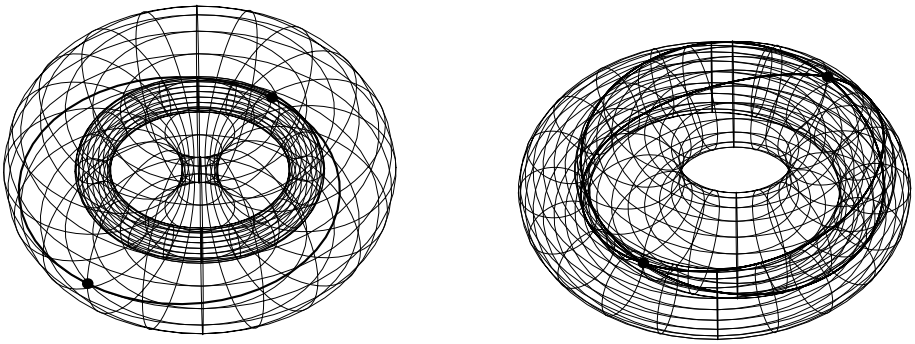

(e)

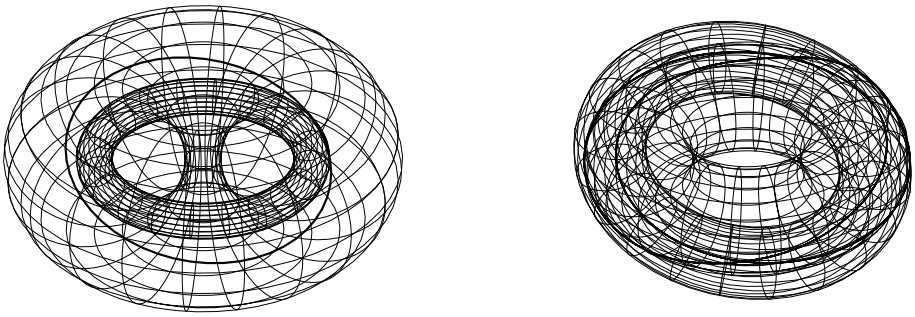

Figure 9.1: (*cont.*)

9.1.2 The Case of $C_i \cap (T_-^D \cup T^D) \neq \emptyset$

When $C_i \cap (T_-^D \cup T^D) \neq \emptyset$, we split the circular arc C_i into the set of circular arcs and/or points according to the region C_i passes through. C_i is split into connected components as in: (i) $C_i \cap (T_-^D \cup T^D)$, and (ii) $C_i \setminus (T_-^D \cup T^D)$. Let C_j denote a connected component in $C_i \cap (T_-^D \cup T^D)$, and C_k denote a connected component in $C_i \setminus (T_-^D \cup T^D)$. We classify the possible topological types of $(\cup B_r(C_j)) \cap T_1$ and $(\cup B_r(C_k)) \cap T_1$. The topological types of the intersection curve $Bdr(\cup B_r(C_i)) \cap T_1$ are classified according to the combination of topological types of $(\cup B_r(C_j)) \cap T_1$ and $(\cup B_r(C_k)) \cap T_1$.

We consider three types of C_j:

1. C_j is a point on T^D (see Figures 9.2(a)–(b)).
2. C_j is a circular arc which intersects with T^D tangentially (see Figures 9.2(c)–(d)).
3. C_j is a circular arc which does not intersect with T^D tangentially (see Figures 9.2(e)–(f)).

The figures in the left columns of Figures 9.2, 9.4–9.11, and 9.13–9.20 illustrate the relative positions of C_j or C_i in the C-space of the torus T_1; the figures in the right columns of Figures 9.2, 9.4–9.11, and 9.13–9.20 illustrate the corresponding relative configurations of $(\cup B_r(C_j)) \cap T_1$ or $(\cup B_r(C_i)) \cap T_1$.

There are two cases where C_j can be a point on T^D. If C_j is a point on a vertex of T^D, $S_r(C_j) \cap T_1$ is a singular circle (Figure 9.2(a)). If C_j is a point on T^{D^o} (where T^{D^o} denotes T^D except two vertices of T^D), $S_r(C_j) \cap T_1$ is a singular curve with a singular point on it (Figure 9.2(b)).

We define the tangent intersection of C_j and T^D as two cases: (i) C_j intersects with T^{D^o} tangentially, and (ii) C_j passes through $\mathbf{q}$ (which is a vertex of T^D) and there is a tangent line of a cross-sectional circle of T^O at $\mathbf{q}$ which is colinear with the tangent line of C_j at $\mathbf{q}$. When C_j is a circular arc and C_j intersects with T^{D^o} tangentially, $(\cup B_r(C_j)) \cap T_1$ is a surface patch of cylindrical type, and $Bdr(\cup B_r(C_j)) \cap T_1$ consists of a singular point and two closed loops (Figure 9.2(c)). When C_j intersects with a vertex of T^D tangentially, $(\cup B_r(C_j)) \cap T_1$ is a surface patch of cylindrical type, and $Bdr(\cup B_r(C_j)) \cap T_1$ consists of a singular curve (with a singular point on it) and a closed loop (Figure 9.2(d)).

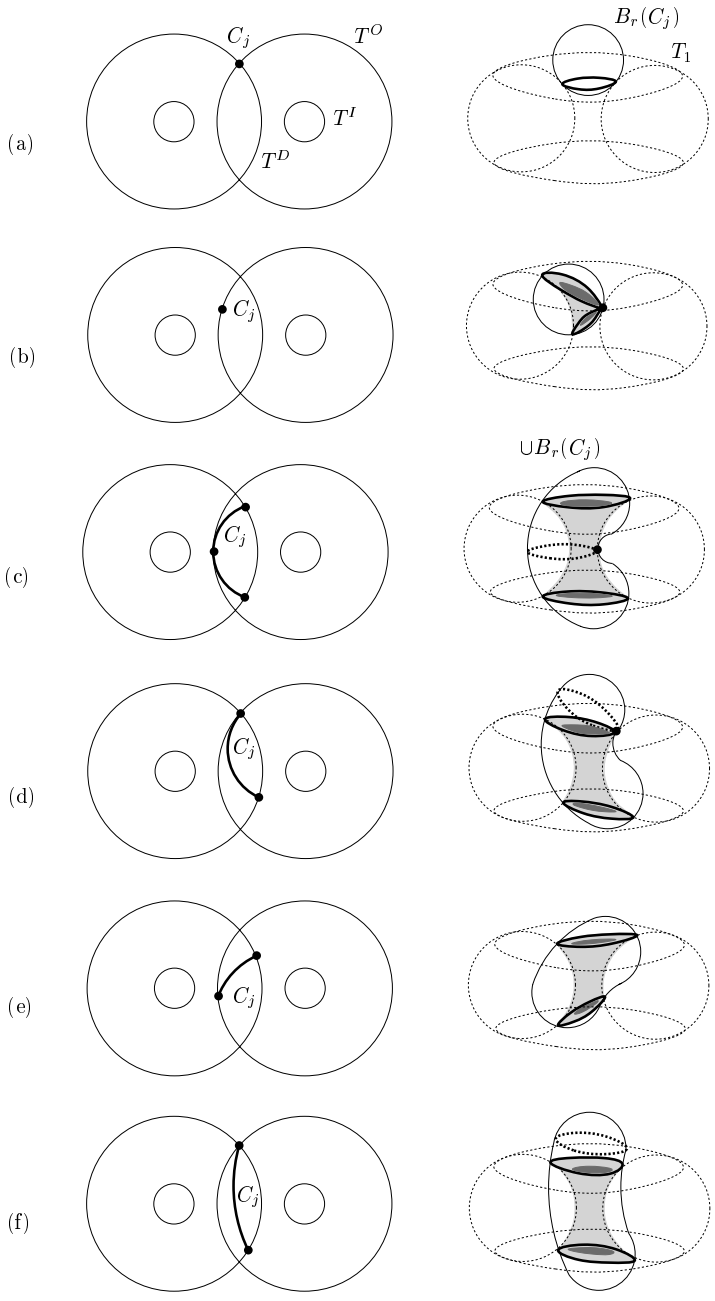

Figure 9.2: Types of $Bdr(\cup B_r(C_j)) \cap T_1$, where C_j is a connected component in $C_i \cap (T_-^D \cup T^D)$.

When C_j is a circular arc and C_j does not intersect with T^D tangentially, $B_r(\mathbf{q}) \cap T_1$ ($\mathbf{q} \in C_j$) is a surface patch of cylindrical type or degenerate cylindrical type. $(\cup B_r(C_j)) \cap T_1$ is equivalent to $\cup_{\mathbf{q} \in C_j}(B_r(\mathbf{q}) \cap T_1)$, and $(\cup B_r(C_j)) \cap T_1$ is a surface patch of cylindrical type (Figures 9.2(e)–(f)). Compare Figure 9.2(f) with Figure 9.2(d). Figure 9.2(f) shows the case when C_j passes through a vertex of T^D, but C_j does not intersect with the vertex tangentially. In this case, $Bdr(\cup B_r(C_j)) \cap T_1$ does not include a singular point.

When C_k is a connected component in $C_i \setminus (T_-^D \cup T^D)$, we consider two types of C_k:

- (Type 1) C_k is a circular arc whose one end point is on $(T^I \cup T^O) \setminus T^D$.
- (Type 2) C_k is a circular arc whose end points are on T^D.

When C_j denotes a connected component in $C_i \cap (T_-^D \cup T^D)$, $(\cup B_r(C_j)) \cap T_1$ has one of topological types : Type I, Type II, Type III, Type IV, and Type V (Figure 9.3). The topological type of $(\cup B_r(C_i)) \cap T_1$ is classified by the combination of C_j (of Types I–V) and C_k (of Types 1,2).

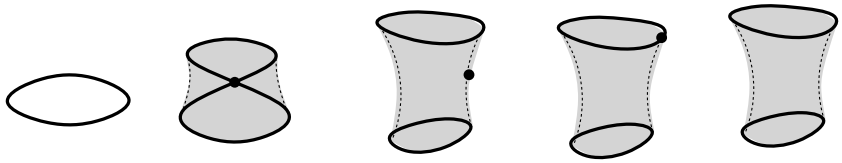

Figure 9.3: Types of $Bdr(\cup B_r(C_j)) \cap T_1$, where C_j is a connected component in $C_i \cap (T_-^D \cup T^D)$.

When the number of connected components in $C_i \cap (T_-^D \cup T^D)$ is one, let's consider the case when C_j has Type V. Let's assume that C_k has no tangent intersection with $T^I \cup T^O$. When both end points of C_j are connected to C_k of Type 1, $(\cup B_r(C_i)) \cap T_1$ is a surface patch of cylindrical type. In this case, the topological type of $(\cup B_r(C_i)) \cap T_1$ is inherited from that of $(\cup B_r(C_j)) \cap T_1$, and $Bdr(\cup B_r(C_i)) \cap T_1$ consists of two closed loops (Figure 9.4(a)). When C_k of Type 2 is added to C_j, $C_j \cup C_k$ is C. In this case, if the main circle of T_1 ($C_\Delta(\mathbf{0}, \mathbf{e}_3)$) passes through the inner area of C, $Bdr(\cup B_r(C)) \cap T_1$ consists of a closed loop (Figure 9.4(b)). Otherwise, $Bdr(\cup B_r(C)) \cap T_1$ consists of three closed loops (Figure 9.4(c)).

Let's assume that C_k has m ($m \geq 1$) tangent intersection points with $T^I \cup T^O$. Then $Bdr(\cup B_r(C_k)) \cap T_1$ includes m singular points. When both end points of C_j are connected to C_k of Type 1, $(\cup B_r(C_i)) \cap T_1$ is the union of a surface patch of cylindrical type and several surface patches of disk type which are connected by m singular points. $Bdr(\cup B_r(C_i)) \cap T_1$ consists of either (i) one singular curve and one closed loop, or (ii) two singular curves (Figure 9.4(d)). If C_k of Type 2 is added to C_j, $C_j \cup C_k$ is C. When the main circle of T_1 passes through the inner area of C, $Bdr(\cup B_r(C)) \cap T_1$ consists of a singular curve (Figure 9.4(e)), otherwise, $Bdr(\cup B_r(C)) \cap T_1$ consists of a singular curve and a closed loop (Figure 9.4(f)).

For the C_j of Type V, Figure 9.5 presents the examples of TTI Curves. Figures 9.5(a)–(b) show the TTI curves when C_j of Type V is connected with two C_ks of Type 1. In this case, $Bdr(\cup B_r(C_i)) \cap T_1$ consists of two closed loops. Figures 9.5(c)–(e) show the TTI curves when C_j of Type V is connected with a C_k of Type 2. When the main circle of T_1 passes through the inside area of C, the TTI curve consists of a closed loop (Figure 9.5(c)). When the main circle of T_1 does not pass through the inside area of C, the TTI curve consists of three closed loops (Figures 9.5(d)–(e)).

Figures 9.6–9.9 show $(\cup B_r(C_i)) \cap T_1$, when C_i includes C_j of Type I, II, III, and IV, respectively.

Figure 9.10 presents the TTI curves when C_j of Type I is included in C_i. When two C_ks are connected with C_j, $Bdr(\cup B_r(C_i)) \cap T_1$ consists of a singular curve with two singular points on it. In this case, the singular points are intersection points of T_1 and the cross-sectional circle of T_2 at C_j (Figure 9.10(a)). Figure 9.10(b) shows the case when C_j is connected with two C_ks of Type 1, where each C_k has a tangent intersection point with T^I. If C_j is of Type I and C is tangent to T^D at C_j, there can be only one C_k which is connected to C_j. In this case, $Bdr(\cup B_r(C_i)) \cap T_1$ consists of a singular curve with one singular point on it, and this singular point is an intersection point of T_1 and the cross-sectional circle of T_2 at C_j (Figure 9.10(c)).

Figure 9.11(a) shows the case when C_j of Type II is connected with two C_ks of Type 1. In this case, $Bdr(\cup B_r(C_i)) \cap T_1$ consists of a singular curve with a singular point on it. Figure 9.11(b) shows the case when C_j of Type III is connected with one C_k of Type 2. In this case, C_k has a tangent intersection point with T^I; thus $Bdr(\cup B_r(C_i)) \cap T_1$ consists of a singular point and a singular curve with a singular point on it. If C_k does not have a tangent intersection point with $T^I \cup T^O$,

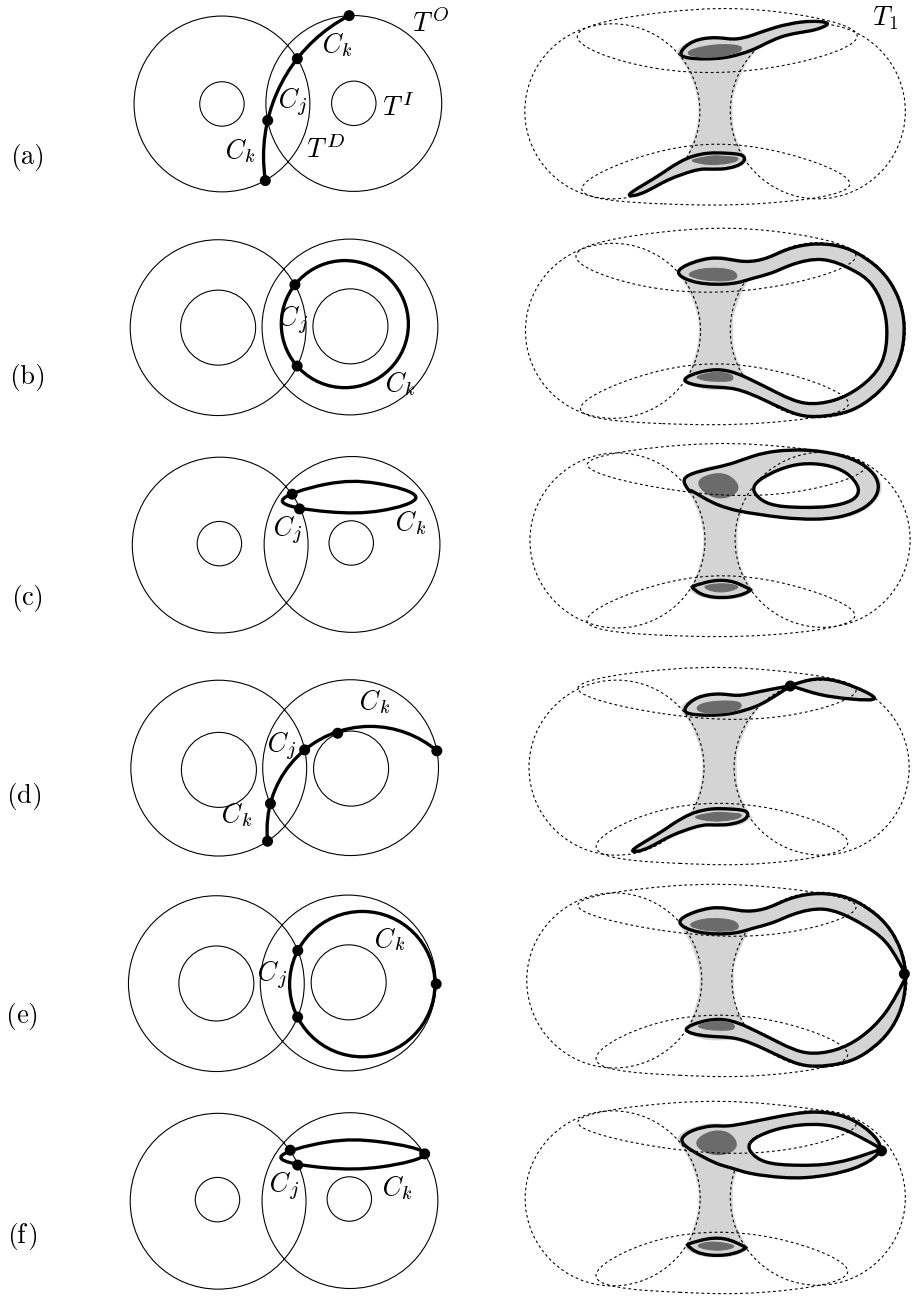

Figure 9.4: $Bdr(\cup B_r(C_j \cup C_k)) \cap T_1$ for C_j of Type V.

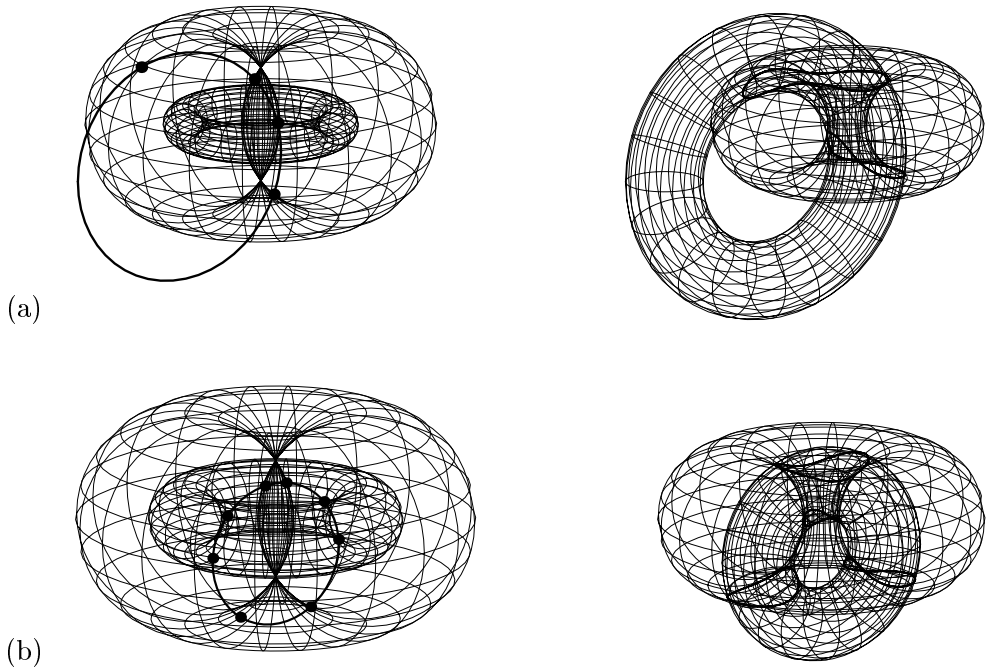

Figure 9.5: The TTI curves when a C_j of Type V is in C_i.

(c)

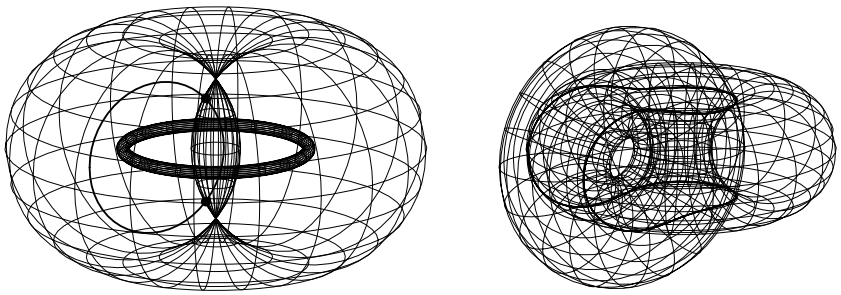

(d)

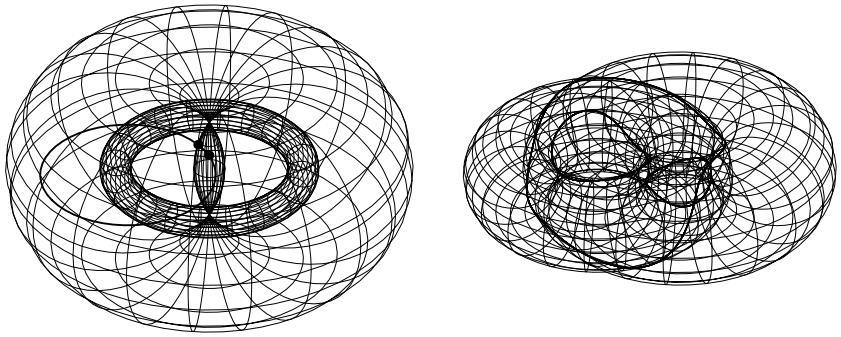

(e)

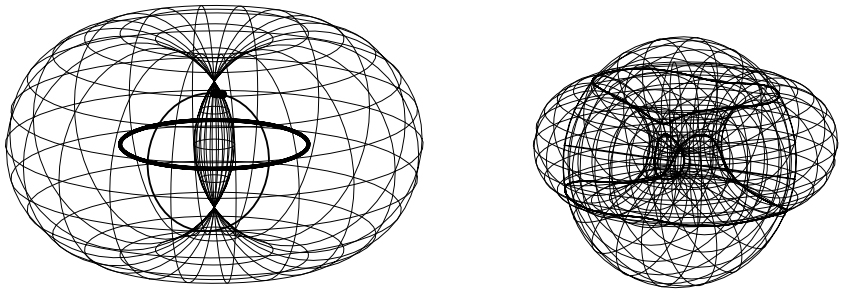

Figure 9.5: (*cont.*)

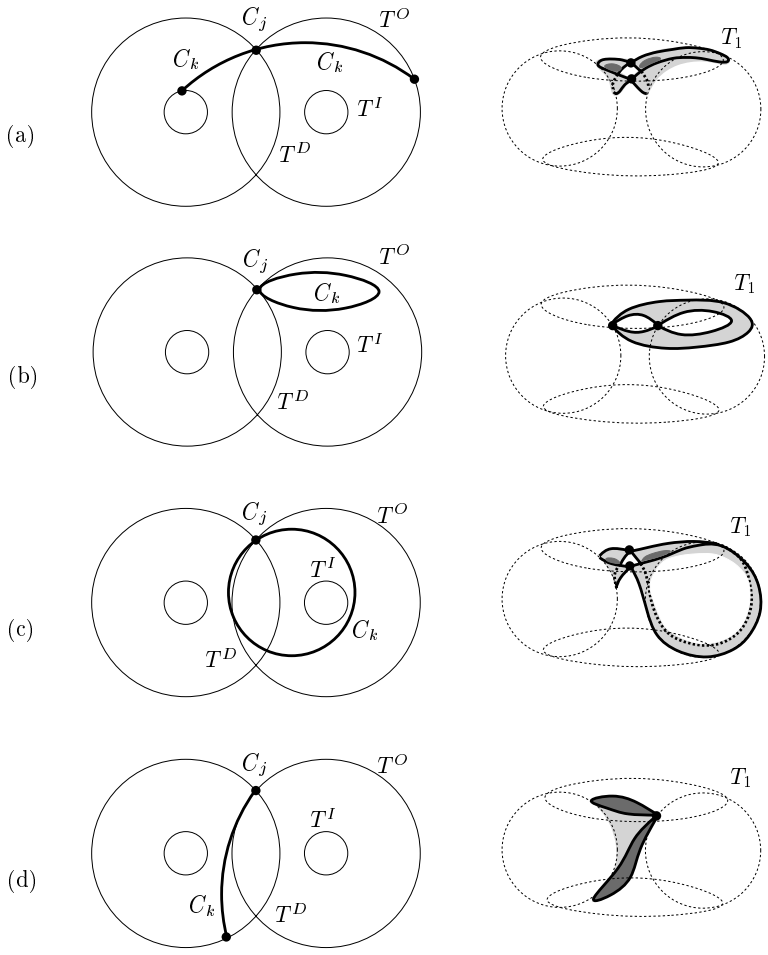

Figure 9.6: $Bdr(\cup B_r(C_i)) \cap T_1$, where C_i includes a C_j of Type I

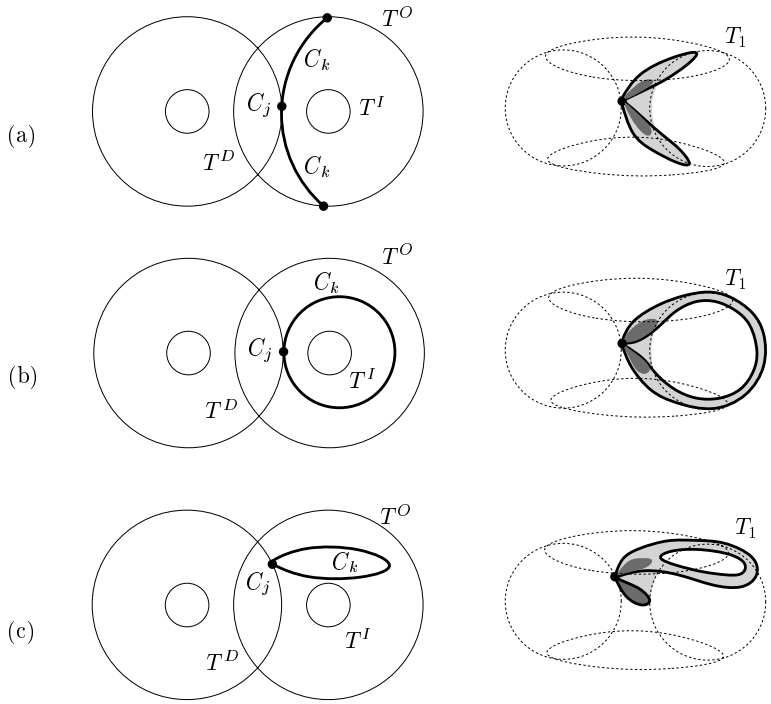

Figure 9.7: $Bdr(\cup B_r(C_i)) \cap T_1$, where C_i includes a C_j of Type II

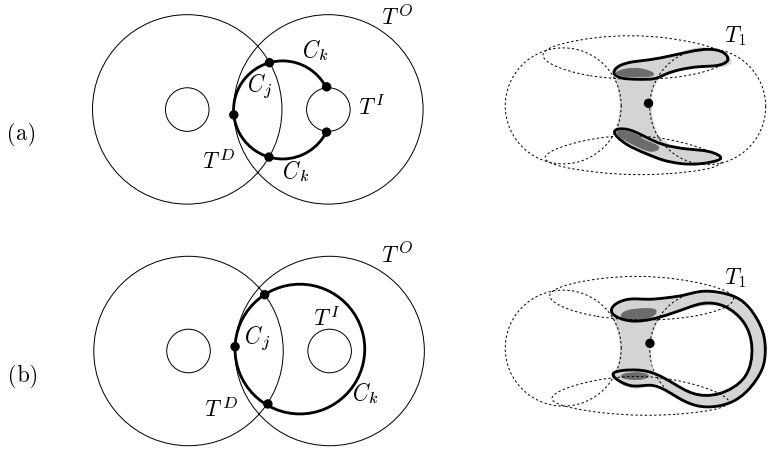

Figure 9.8: $Bdr(\cup B_r(C_i)) \cap T_1$, where C_i includes a C_j of Type III

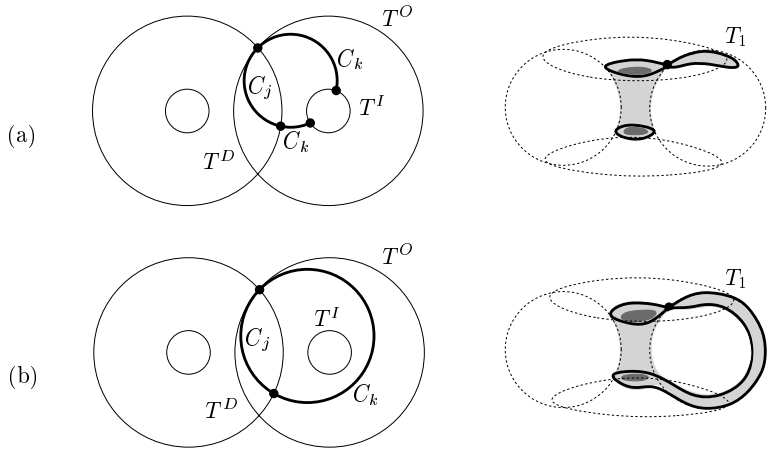

Figure 9.9: $Bdr(\cup B_r(C_i)) \cap T_1$, where C_i includes a C_j of Type IV

$Bdr(\cup B_r(C_i)) \cap T_1$ will consist of a singular point and a closed loop. Figure 9.11(c) shows the case when C_j of Type IV is connected with a C_k of Type 2. In this case, $C_i \cap T_-^D \neq \emptyset$ and C_i passes through a vertex of T^D tangentially; thus $Bdr(\cup B_r(C_i)) \cap T_1$ consists of a singular curve with a singular point on it.

When the number of connected components in $C_i \cap (T_-^D \cup T^D)$ is two, the types of C_j which can be included in C_i are Type I, Type II, and Type V (Figure 9.12). When C_j is of Type III or IV, C_j intersects with T^D at one point of multiplicity two and one or two points of multiplicity one. There are four intersection points between a torus and a circle at most; thus if C_i includes one C_j of Type III or IV, there is only one C_j in C_i.

Two C_js in C_i can be connected with (i) two C_ks of Type 2, or (ii) one C_k of Type 2 and two C_ks of Type 1. We consider the case when two C_js of Type V are included in C_i. Let's assume that C_k has no tangent intersection with $T^I \cup T^O$. Figure 9.13(a) shows two C_js and corresponding intersections $(\cup B_r(C_j)) \cap T_1$. Each $(\cup B_r(C_j)) \cap T_1$ has two closed loops as a boundary curve. When two C_js are connected by two C_ks of Type 2, there are three topological types of $Bdr(\cup B_r(C_i)) \cap T_1$ (Figures 9.13(b)–(d)). Figure 9.13(e) presents the case of two C_js connected by two C_ks of Type 2 which has a tangent intersection point with $T^I \cup T^O$. Figure 9.13(f) presents the case of two C_js connected by two C_ks of Type 1 and one C_k of Type 2. The examples of TTI curves for the case of two C_js of Type V are included in C_i are given in

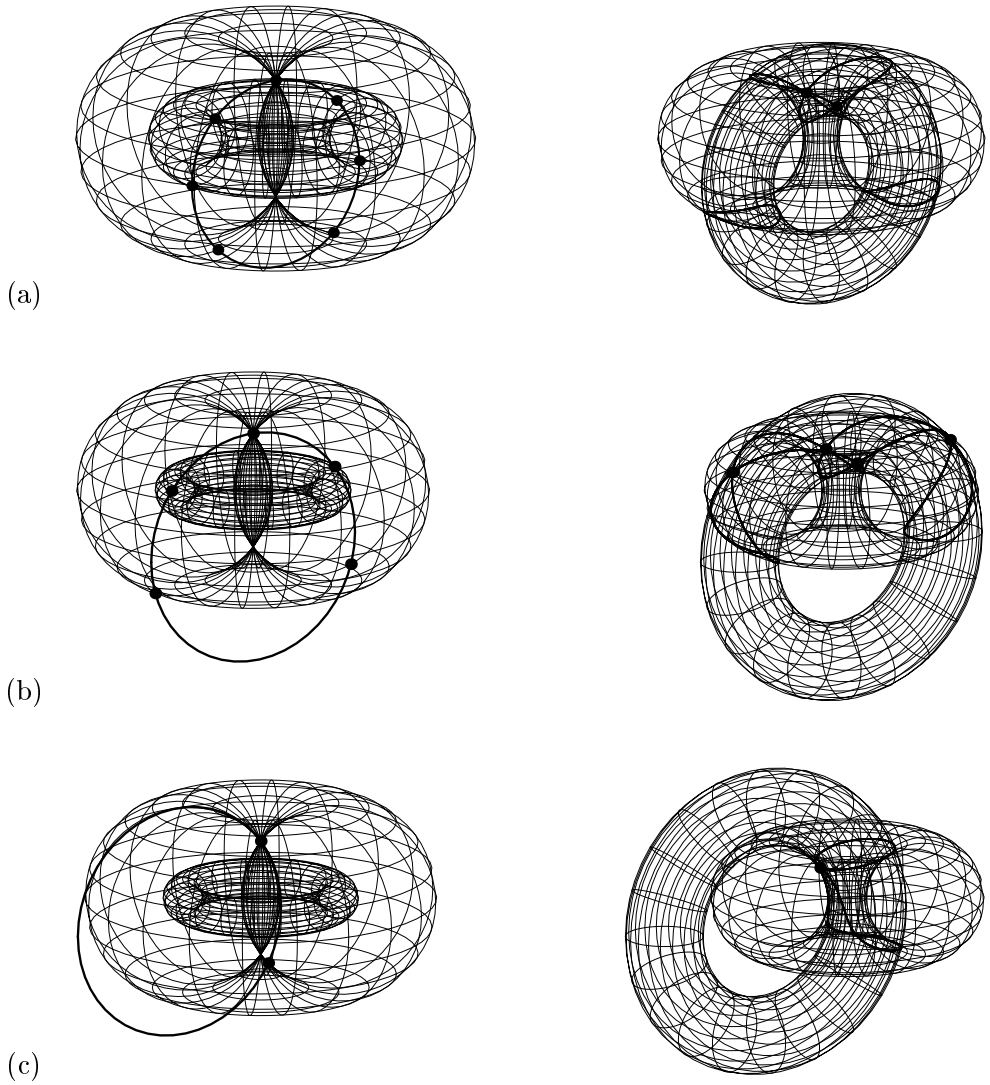

Figure 9.10: The TTI curves when a C_j of Type I is in C_i.

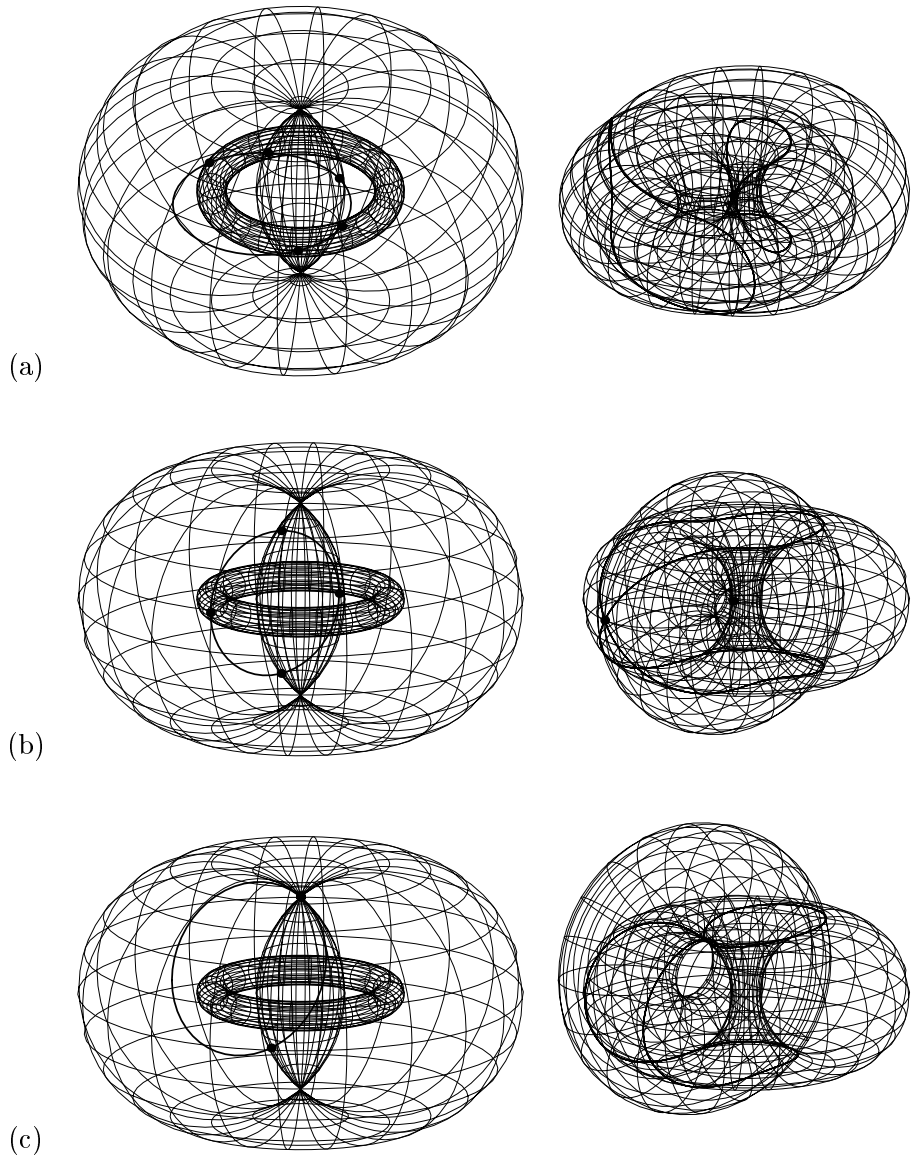

Figure 9.11: The TTI curves when a C_j (of Types II, III, or IV) is in C_i.

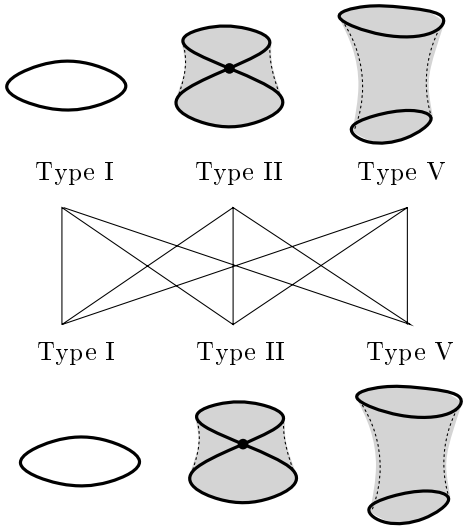

Figure 9.12: Possible pairs of types of $(\cup B_r(C_j)) \cap T_1$, where C_j is a connected component in $C_i \cap (T_-^D \cup T^D)$.

Figure 9.14.

Figure 9.15(a) shows two C_js (Type I and Type V) and corresponding intersections $(\cup B_r(C_j)) \cap T_1$. The topological types of $Bdr(\cup B_r(C_i)) \cap T_1$ when two C_js of Type I and Type V are connected by two C_ks of Type 2 are given in Figures 9.15(b)–(e). The topological type of $Bdr(\cup B_r(C_i)) \cap T_1$ when two C_js of Type I and Type V are connected by two C_ks of Type 1 and a C_k of Type 2 is given in Figure 9.15(f).

Figure 9.16(a) shows two C_js (Type II and Type V) and corresponding intersections $(\cup B_r(C_j)) \cap T_1$. The topological types of $Bdr(\cup B_r(C_i)) \cap T_1$ when two C_js of Type II and Type V are connected by two C_ks of Type 2 are given in Figures 9.16(b)–(e). The topological type of $Bdr(\cup B_r(C_i)) \cap T_1$ when two C_js of Type II and Type V are connected by two C_ks of Type 1 and a C_k of Type 2 is given in Figures 9.16(f).

Similarly, we can determine the topological types of $Bdr(\cup B_r(C_i)) \cap T_1$ when two C_js of Type I and Type I, or Type I and Type II, or Type II and Type II are given (Figures 9.17–9.19).

- If $C_i = C$ and C_i is embedded in T^O, $T_1 \cap T_2$ consists of a singular circle or a singular curve with one or two singular points on it.

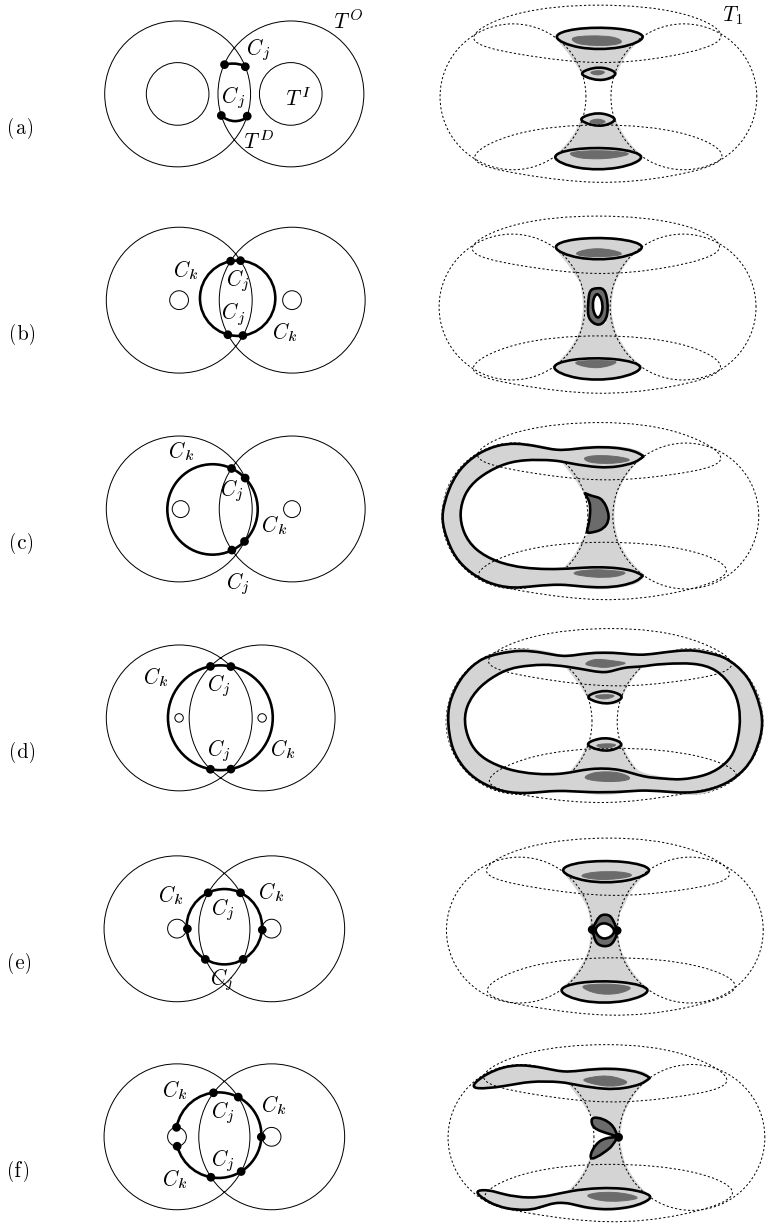

Figure 9.13: Types of $Bdr(\cup B_r(C_i)) \cap T_1$ when two C_js of Type V are connected by two or three C_ks.

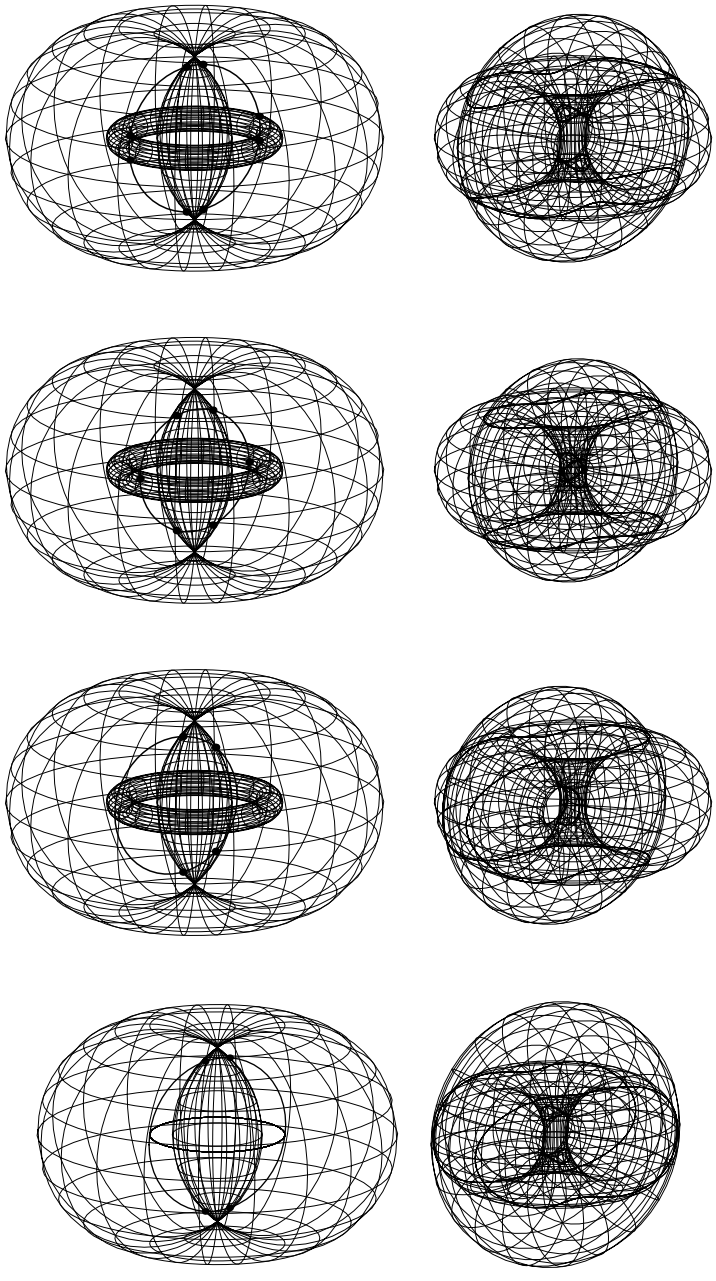

Figure 9.14: The TTI curves when two C_js (of Type V) are in C_i.

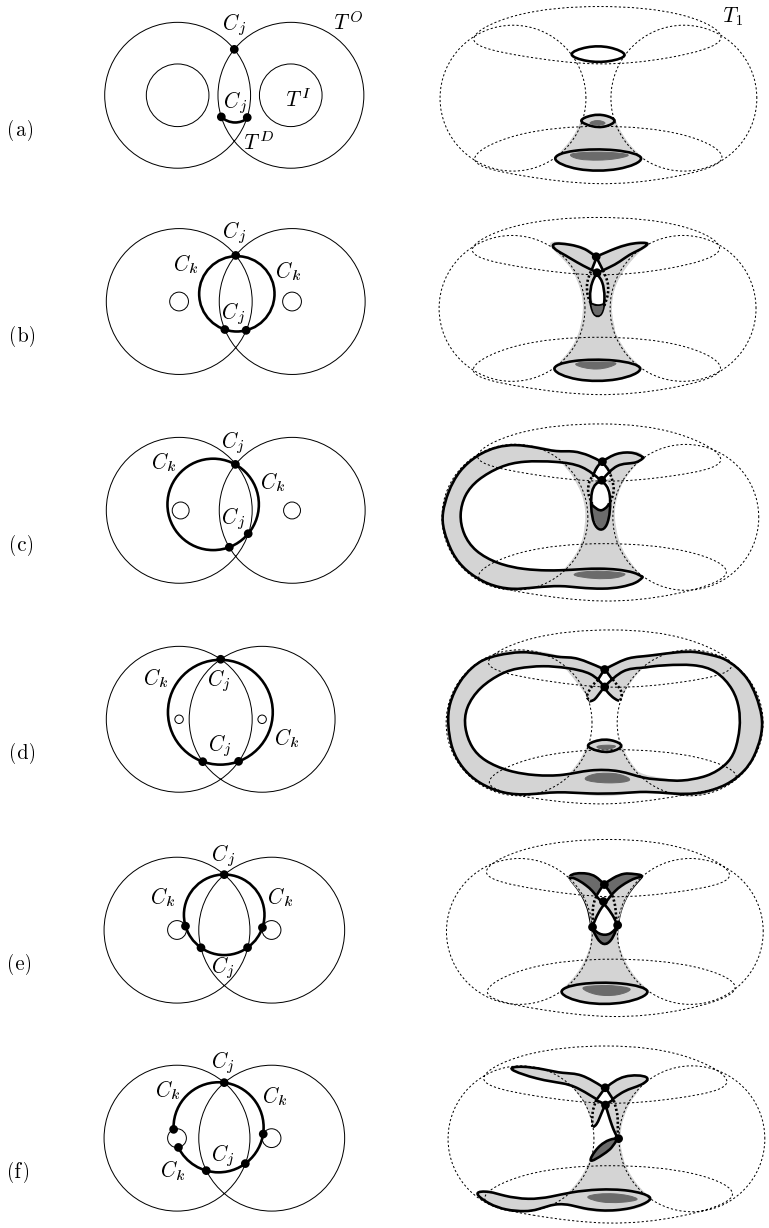

Figure 9.15: Types of $Bdr(\cup B_r(C_i)) \cap T_1$, where C_i includes two C_js (of Type I and Type V) and two or three C_ks.

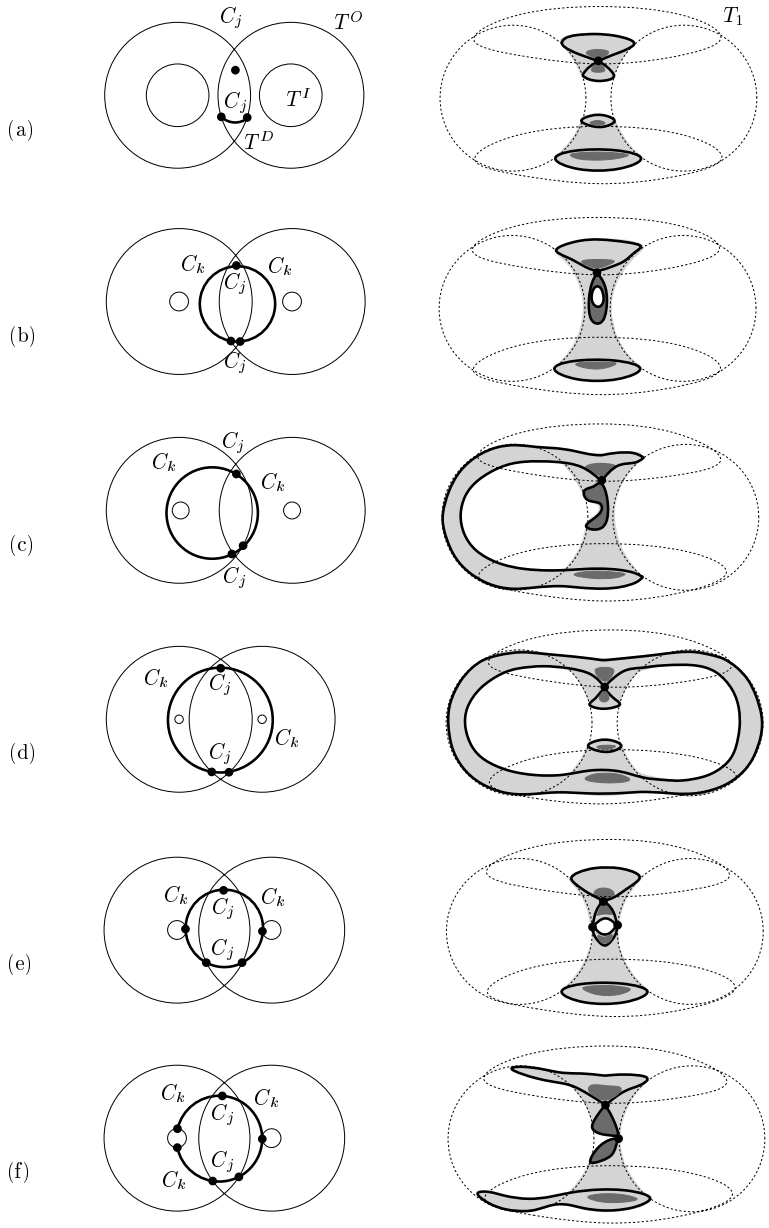

Figure 9.16: Types of $Bdr(\cup B_r(C_i)) \cap T_1$, where C_i includes two C_js (of Type II and Type V) and two or three C_ks.

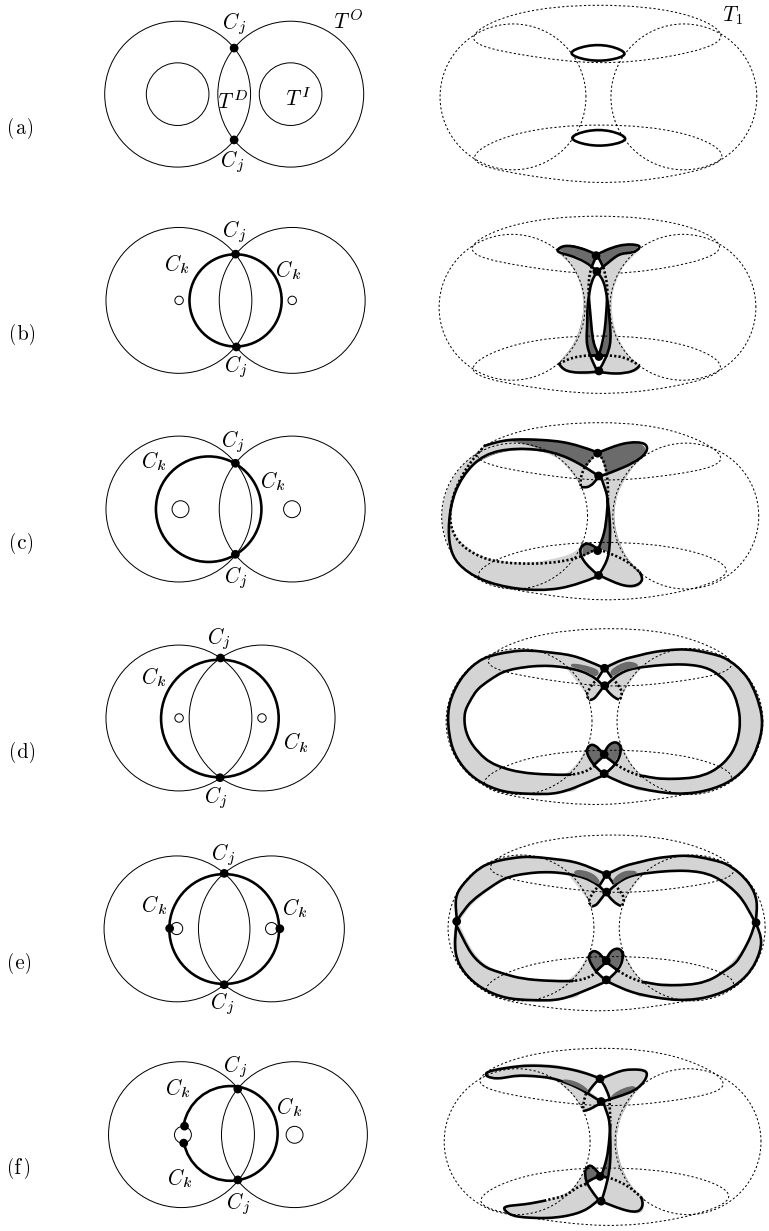

Figure 9.17: Types of $Bdr(\cup B_r(C_i)) \cap T_1$, where C_i includes two C_js (of Type I) and two or three C_ks.

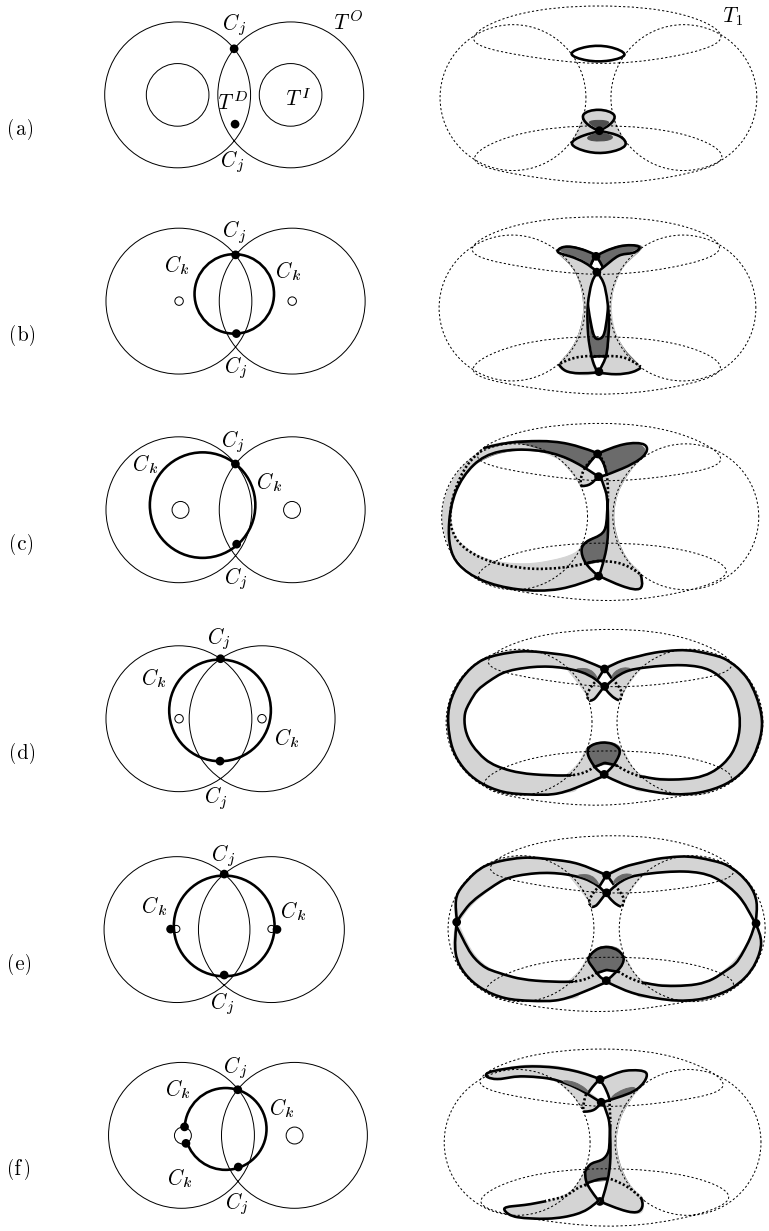

Figure 9.18: Types of $Bdr(\cup B_r(C_i)) \cap T_1$, where C_i includes two C_js (of Type I and Type II) and two or three C_ks.

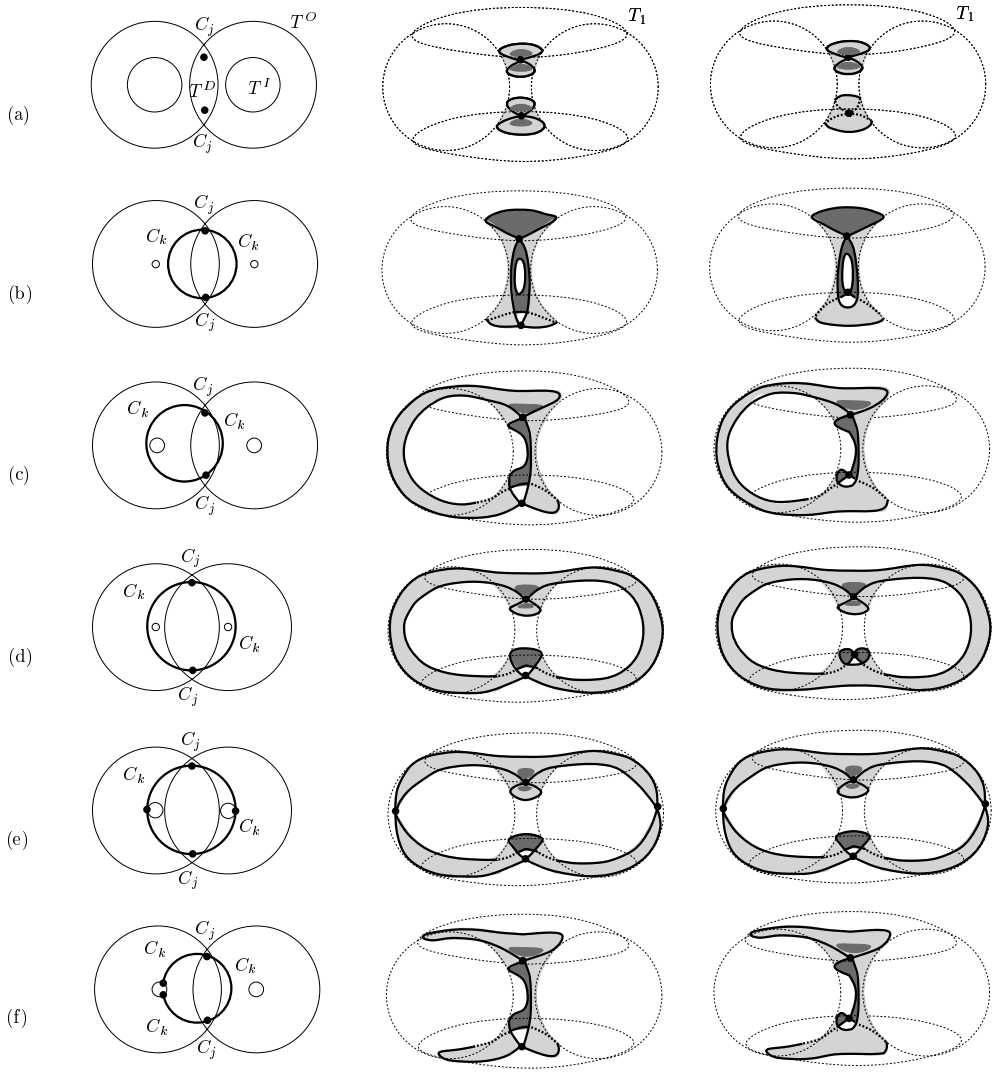

Figure 9.19: Types of $Bdr(\cup B_r(C_i)) \cap T_1$, where C_i includes two C_js (of Type II) and two or three C_ks.

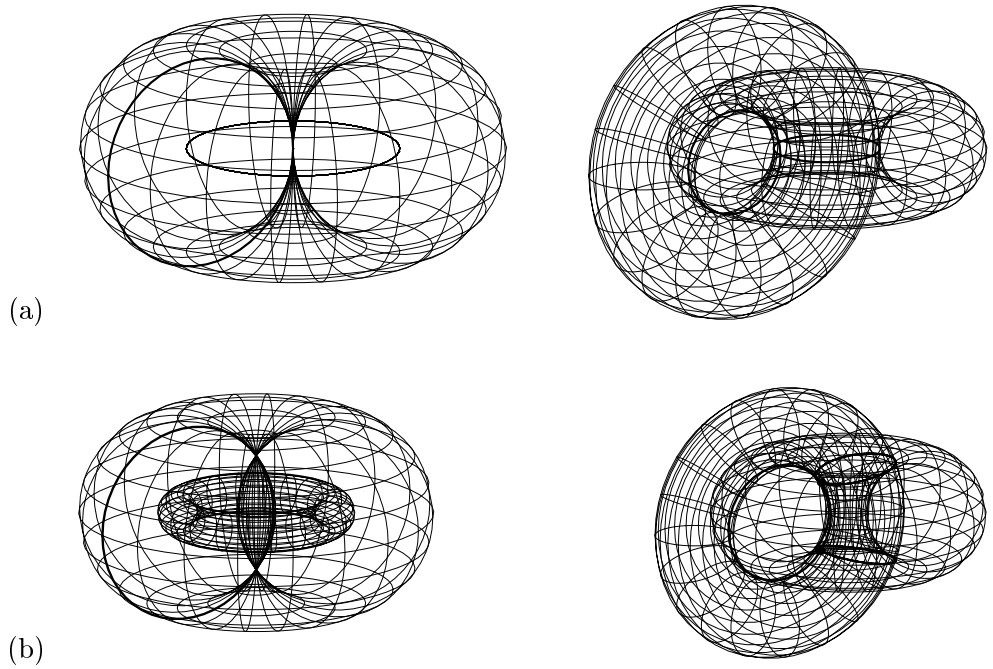

Figure 9.20: The cases when C_i is embedded in T^O.

Let's assume that $C_i = C$. A circle can be embedded in T^O if and only if the circle is a profile circle, a cross-sectional circle, or an Yvone-Villarceau circle of T^O. We consider the case when $C_i \cap (T^D_- \cup T^D) \neq \emptyset$; thus, T^O cannot have an Yvone-Villarceau circle and T^O cannot embed C_i as a profile circle. If C_i is a cross-sectional circle of T^O and T^D is a point, T_2 is outside T_1, and T_2 intersects with T_1 tangentially along a cross-sectional circle and a profile circle of T_1 (Figure 9.20(a)). If C is a cross-sectional circle of T^O and T^D is a volume, T_2 intersects with T_1 at a singular curve which consists of a cross-sectional circle of T_1 and two loops which are connected by two singular points from the cross-sectional circle (Figure 9.20(b)).

9.2 Analysis for the Case of $0 < r = \delta$

When the minor radius of the torus T_1 and the minor radius of the torus T_2 are same, the inner offset surface of T_1 is a circle: $T^I = C_\Delta(\mathbf{0}, \mathbf{e}_3)$. Let C denote the main circle of T_2: $C = C_R(\mathbf{p}, \mathbf{N})$. If there is no intersection point between C and T^I, we can apply the methods for the case of $0 < r < \delta$ to detect the closed loops

and singular curves in the TTI curve (see Section 9.1). Thus, we consider the only cases where C intersects with T^I. Since $C \cap T^I$ is a circle/circle intersection, C intersects with T^I at two intersection points at most. When C intersects with T^I at a point $\mathbf{q}$, the singular points are derived in the TTI curve by intersecting two cross-sectional circles centered at $\mathbf{q}$ on T_1 and T_2. These cross-sectional circles are two great circles contained on the same sphere $S_r(\mathbf{q})$. Thus, there are only two cases: two cross-sectional circles are coincident or they intersect at two points.

Let C_i denote a connected component in $C \cap (T_-^O \cup T^O)$, which intersects with T^I.

- If C_i intersects with T^I at an intersection point $\mathbf{q}$ and the tangent vector of C_i at $\mathbf{q}$ is parallel to the tangent vector of T^I at $\mathbf{q}$, the cross-sectional circle of T_2 at $\mathbf{q}$ intersects with T_1 at a circle, where each point on the circle is a singular point. $Bdr(\cup B_r(C_i)) \cap T_1$ consists of a singular circle and a singular curve which intersect at two singular points: $\mathbf{q} \pm r\frac{\mathbf{e}_3+\mathbf{N}}{||\mathbf{e}_3+\mathbf{N}||}$, if $\mathbf{e}_3 + \mathbf{N} \neq \mathbf{0}$, and $\mathbf{q} \pm r\mathbf{e}_3$, otherwise (see Figure 3.13(d)).

- Otherwise, if C_i intersects with T^I at one or more intersection points, the intersection curve consists of a singular curve (see Figure 9.21).

The figures in the left columns of Figure 9.21 illustrate the relative positions of C in the C-space of the torus T_1; the figures in the right columns of Figure 9.21 illustrate the corresponding relative configurations of $T_1 \cap T_2$.

When C_i intersects with T^I at an intersection point $\mathbf{q}$ and the tangent vector of C_i at $\mathbf{q}$ is parallel to the tangent vector of T^I at $\mathbf{q}$, the cross-sectional circle of T_1 at $\mathbf{q}$ and the cross-sectional circle of T_2 at $\mathbf{q}$ are coincident, and there is no intersection point between C_i and T^D. If such C_i has k tangent intersection points with $T^O \setminus T^D$, $Bdr(\cup B_r(C_i)) \cap T_1$ consists of a singular curve with $2 + k$ singular points on it.

If C_i intersects with T^I at an intersection point $\mathbf{q}$ and the tangent vector of C_i at $\mathbf{q}$ is not parallel to the tangent vector of T^I at $\mathbf{q}$, the cross-sectional circle of T_1 at $\mathbf{q}$ intersects with T at two singular points. When C_i passes through T^I, regardless of the intersection points of C_i and T^O, $Bdr(\cup B_r(C_i)) \cap T_1$ consists of a singular curve. We can trace $Bdr(\cup B_r(C_i)) \cap T_1$ from the singular points on it (see Figure 9.21).

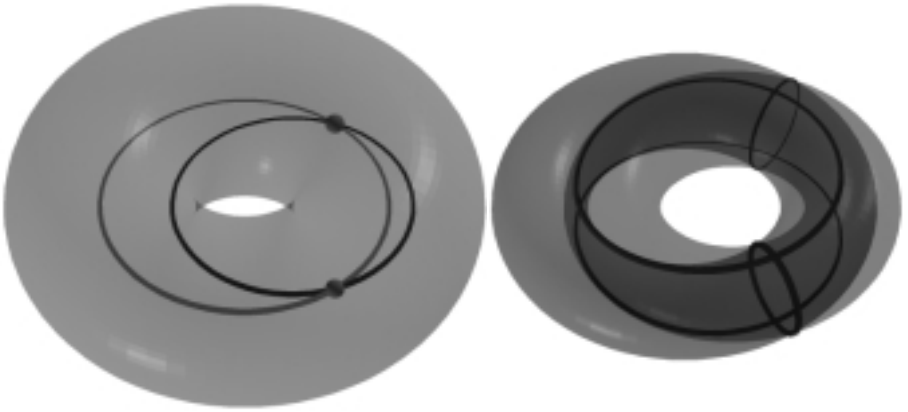

(a)

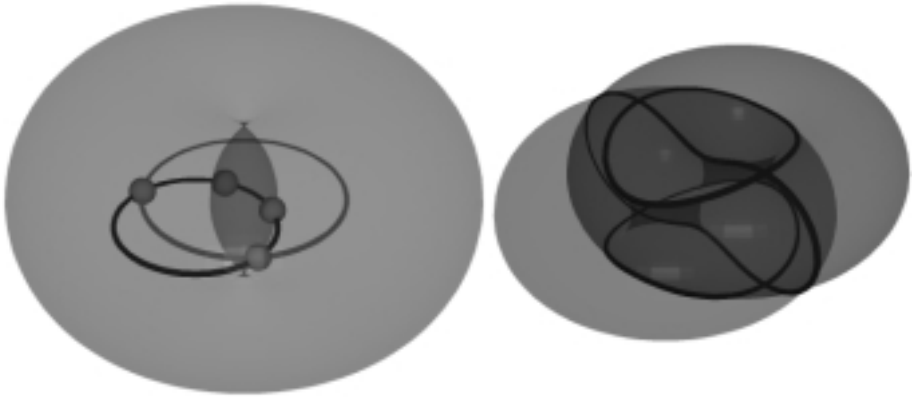

(b)

Figure 9.21: The TTI curve for the case when C_i intersects with T^I, where $T^I = C_R(\mathbf{0}, \mathbf{e}_3)$.

(c)

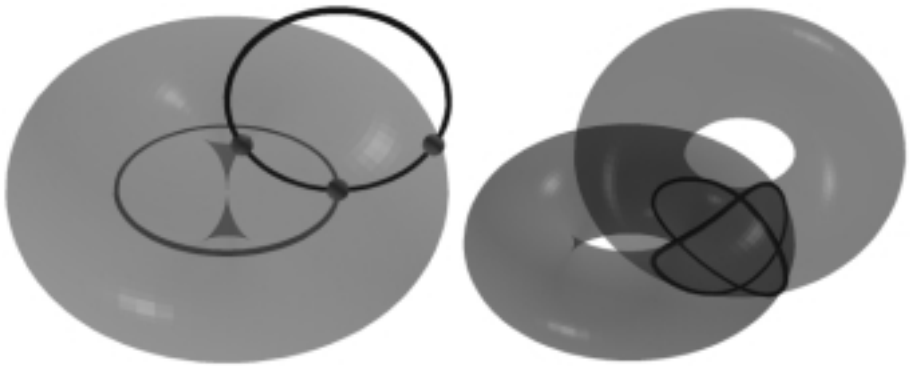

(d)

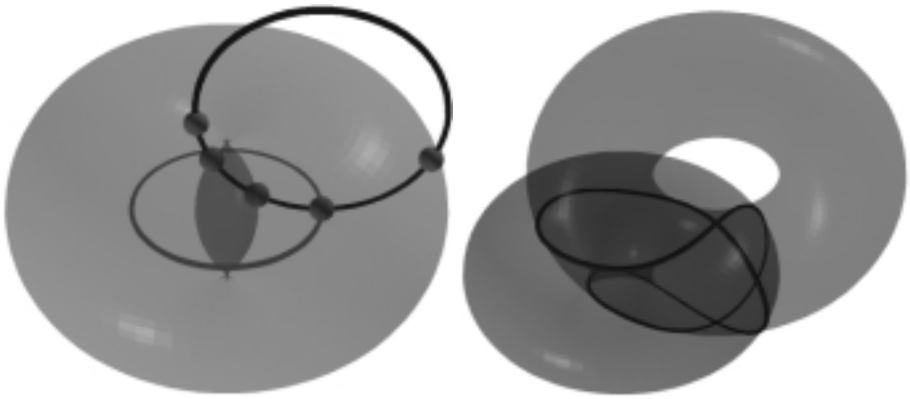

Figure 9.21: (*cont.*)

9.3 Algorithm: Torus_Torus_Intersection

Algorithm: Torus_Torus_Intersection of Appendix A.7 summarizes the TTI algorithm based on the above case analyses. In this algorithm, we assume that cubic curve tracing routines: Trace_Singular_TTI_Curve (T_1, T_2, DP) and Trace_Regular _TTI_Curve (T_1, T_2, IP), are available, where T_1 and T_2 are tori, and IP and DP are a set of starting points and a set of singular points, respectively. Each singular intersection curve can be traced starting from its singular point (see also Piegl [21]), the details of which are given in the routine: Trace_Singular_TTI_Curve. We assume that when a singular curve is traced, if the singular curve passes through a point in IP, that point is removed from IP.

In Line (1), we assume that the routine Detect_Circles_in_TTI(T_1, T_2), which detects and computes all degenerate circles in the TTI curve is available (see Section 3.7). Line (2) computes the starting points for the case where C is included in $T_-^O \cap T_+^I \cap T_+^D$. By intersecting an arbitrary cross-sectional circle of T_2 with T_1, the starting points are computed. Lines (3)–(5) compute the starting points of closed loops in the TTI curve. If C_i is a connected component in $C \cap (T_-^O \cap T_+^I)$ and C_i does not intersect with $T_-^D \cup T^D$, $Bdr(\cup B_r(C_i)) \cap T_1$ is a closed loop. When $\mathbf{q}$ is an end point of C_i, and $\mathbf{q}_T$ denotes a point on T_1 at which $S_r(\mathbf{q})$ touches T_1, let C_T denote the cross-sectional circle of T_1 which passes through $\mathbf{q}_T$. Line (3) detects the closest point from $\mathbf{q}_T$ in the set of points $T_2 \cap C_T$ as a starting point for a closed loop. Line (4) computes the starting points for the closed loop which corresponds to C_i which is a connected component in $T_-^O \cap T_+^I$, where $C_i \cap (T_-^D \cup T^D) \neq \emptyset$. Line (5) computes the starting points for the closed loop which corresponds to C_k which is a connected component in $T_-^O \cap T_+^I \cap T_+^D$, and both end points of C_k are on T^D. In Line (6), all singular curves in the TTI curve are traced from DP which is the set of all singular points in the TTI curve. Line (7) traces all closed loops in the TTI curve.

Chapter 10

Conclusion

Given two arbitrary surfaces, the determination of all possible topological types of surface-surface intersection curve is non-trivial, in general. This is indeed the case even for intersecting two natural quadrics [18]. However, in the case of the torus/simple-surface intersection curve computation considered in this thesis, we demonstrated that the classification can be made considerably easier based on a C-space transformation.

We demonstrated that all topological/geometric classifications (including singular point and/or degenerate circle detection) can be carried out using vector/distance computations and curve/surface intersections (see Table 4.1). All required computations can be implemented efficiently and robustly using floating-point arithmetic. For TPI, TSI, and TYI curves, we showed that exactly one starting point on each closed loop can be generated. We also presented methods that detect all closed loops in TKI and TTI curves, in which given surfaces need be subdivided at most four times.

Given a torus and a simple surface, to apply an intersection algorithm based on a C-space approach, we treated one surface as an obstacle and the other surface as the envelope surface of a moving ball. The problem of intersecting two surfaces was reduced to that of intersecting a C-space obstacle (of one surface) and a moving ball's center trajectory (of the other surface). For given two surfaces (whenever one surface is an envelope surface of a moving ball and the C-space obstacle of the other surface can be computed), the intersection algorithm based on a C-space approach can be applied. The problem of intersecting cyclides or canal surfaces based on a

C-space approach remains as an important problem for further research.

References

[1] Bajaj, C., Hoffmann, C., Hopcroft, J., and Lynch, R., "Tracing Surface Intersections," *Computer Aided Geometric Design*, Vol. 5, pp. 285–307, 1988.

[2] Bajaj, C., and Kim, M.-S., "Generation of Configuration Space Obstacles: The Case of a Moving Sphere," *IEEE J. of Robotics and Automation*, Vol. 4, No. 1, pp. 94–99, 1988.

[3] Bajaj, C., and Xu, G., "NURBS Approximation of Surface/Surface Intersection Curves," *Advances in Computational Mathematics*, Vol. 2, No. 1, pp. 1–21, 1994.

[4] Choi, J.-J., "Local Canonical Cubic Curve Tracing along Surface/Surface Intersections," Ph.D. Thesis, Dept. of Computer Science, POSTECH, February, 1997.

[5] De Pont, J., *Essays on the Cyclide Patch*, Ph.D. Thesis, Cambridge University Engineering Department, Cambridge, 1984.

[6] Farouki, R., Neff, C., and O'Connor, M., "Automatic Parsing of Degenerate Quadric-Surface Intersections," *ACM Trans. on Graphics*, Vol. 8, No. 3, pp. 174–203, 1989.

[7] Guibas, L., Ramshaw, L., and Stolfi, J., "A Kinetic Framework for Computational Geometry," *Proc. of 24th Annual Symp. on Foundations of Computer Science*, pp. 100–111, 1983.

[8] Guillemin, V., and Pollack, A., *Differential Topology*, Prentice-Hall, Inc., Englewood Cliffs, N.J., 1974.

[9] Hoschek, J., and Lasser, D., *Fundamentals of Computer Aided Geometric Design*, A.K. Peters, Wellesley, MA, 1993.

[10] Johnstone, J., "A New Intersection Algorithm for Cyclides and Swept Surfaces Using Circle Decomposition," *Computer Aided Geometric Design*, Vol. 10, No. 1, pp. 1–24, 1993.

[11] Johnstone, J., and Shene, C.-K., "Computing the Intersection of a Plane and a Natural Quadric," *Computers & Graphics*, Vol. 16, No. 2, pp. 179–186, 1992.

[12] Levin, J., "A Parametric Algorithm for Drawing Pictures of Solid Objects Composed of Quadric Surfaces," *Commun. ACM*, Vol. 19, No. 10, pp. 555–563, 1976.

[13] Levin, J., "Mathematical Models for Determining the Intersections of Quadric Surfaces," *Computer Graphics and Image Processing*, Vol. 11, pp. 73–87, 1979.

[14] Lozano-Pérez, T., "Spatial Planning: A Configuration Space Approach," *IEEE Trans. on Computers*, Vol. 32, No. 2, pp. 108–120, 1983.

[15] Martin, R., de Pont, J., and Sharrock, T., "Cyclide Surfaces in Computer Aided Design," *The Mathematics of Surfaces I*, J.A. Gregory (Ed.), Clarendon Press, Oxford, pp. 253–267, 1986.

[16] Miller, J., "Geometric Approaches to Nonplanar Quadric Surface Intersection Curves," *ACM Trans. on Graphics*, Vol. 6, No. 4, pp. 274–307, 1987.

[17] Miller, J., and Goldman, R., "Using Tangent Balls to Find Plane Sections of Natural Quadrics," *IEEE Computer Graphics & Applications*, pp. 68–82, March, 1992.

[18] Miller, J., and Goldman, R., "Geometric Algorithms for Detecting and Calculating All Conic Sections in the Intersection of Any Two Natural Quadric Surfaces," *Graphical Models and Image Processing*, Vol. 57, No. 1, pp. 55–66, 1995.

[19] Patrikalakis, N., "Surface-to-Surface Intersections," *IEEE Computer Graphics & Applications*, pp. 89–95, January, 1993.

[20] Piegl, L., "Geometric Method of Intersecting Natural Quadrics Represented in Trimmed Surface Form," *Computer-Aided Design*, Vol. 21, No. 4, pp. 201–212, 1989.

[21] Piegl, L., "Constructive Geometric Approach to Surface-Surface Intersection," *Geometry Processing for Design and Manufacturing*, R.E. Barnhill (Ed.), SIAM, 1992, Ch. 7, pp. 137–159, 1992.

[22] Pottmann, H., Personal Communication.

[23] Pratt, M., and Geisow, A., "Surface/Surface Intersection Problems," *The Mathematics of Surfaces I*, J.A. Gregory (Ed.), Clarendon Press, Oxford, pp. 117–142, 1986.

[24] Rossignac, J., and Requicha, A., "Constant-Radius Blending in Solid Modeling," *Computer in Mechanical Engineering*, Vol. 3, No. 1, pp. 65–73, 1984.

[25] Rossignac, J., and Requicha, A., "Offsetting Operations in Solid Modelling," *Computer Aided Geometric Design*, Vol. 3, No. 2, pp. 129–148, 1986.

[26] Sarraga, R., "Algebraic Methods for Intersections of Quadric Surfaces in GMSOLID," *Computer Vision, Graphics and Image Processing*, Vol. 22, No. 2, pp. 222–238, 1983.

[27] Sederberg, T. W., Christiansen, H. N., and Katz, S., "Improved test for closed loops in surface intersections", *Computer-Aided Design*, Vol. 21, No. 8, pp. 505-508, 1989.

[28] Shene, C.-K., and Johnstone, J., "On the Lower Degree Intersections of Two Natural Quadrics," *ACM Trans. on Graphics*, Vol. 13, No. 4, pp. 400–424, 1994.

[29] Wilf, I., and Manor, Y., "Quadric-surface Intersection Curves: Shape and Structure," *Computer-Aided Design*, Vol. 25, No. 10, pp. 633–643, 1993.

Appendix A

Torus/Simple-Surface Intersection Algorithms

A.1 TPI Algorithm

Algorithm: Torus_Plane_Intersection

Input: $T = T_{r,R}(\mathbf{0}, \mathbf{e}_3)$; /* Torus */
$L = L(\mathbf{p}, \mathbf{N})$; /* Plane */

begin

DP:={ $S_r(\mathbf{p}_i) \cap L \mid \mathbf{p}_i$ is a tangent intersection point in $C_R(\mathbf{p}, \mathbf{N}) \cap (L^O \cup L^I)$};

if $C_R(\mathbf{0}, \mathbf{e}_3) \subset L^O_+ \cup L^I_-$ **then** /* There is no intersection */
Output($\emptyset$); /* Figure 5.2(a) */

else if $C_R(\mathbf{0}, \mathbf{e}_3) \subset L^O_- \cap L^I_+$ **then**

if $\mathbf{e}_3 \times \mathbf{N} = \mathbf{0}$ **then**

(1) Compute_Profile_Circles (T, L);

else /* Figure 5.2(b) */
Trace_Regular_TPI_Curve(T, L, $L \cap C_r(C(0), \mathbf{N}_{C(0)})$);

else if $|DP| = 1$ **then** /* Figure 5.3 */
Trace_Singular_TPI_Curve(T, L, DP);

else if $|DP| = 2$ **then** /* Figure 5.6 */

(2) Compute_Yvone_Villarceau_Circles(T, L, DP);

else if $C_R(\mathbf{0}, \mathbf{e}_3)$ is embedded in L^I **then**
Output($C_R(\mathbf{q}, \mathbf{e}_3)$), where $\mathbf{q} = \mathbf{0} + r\mathbf{e}_3$;

else if $C_R(\mathbf{0}, \mathbf{e}_3)$ is embedded in L^O **then**
Output($C_R(\mathbf{q}, \mathbf{e}_3)$), where $\mathbf{q} = \mathbf{0} - r\mathbf{e}_3$;

else begin

if there is only one circular arc C_1 in $C_R(\mathbf{0}, \mathbf{e}_3) \cap (L^O_- \cap L^I_+)$ **then begin**

(3) $\mathbf{q}$:= the middle point of C_1;
$\mathbf{p}_i$:= a point in $L \cap C_r(\mathbf{q}, \mathbf{N_q})$, where $\mathbf{N_q} := \mathbf{N} \times \frac{\mathbf{q}-\mathbf{p}}{\|\mathbf{q}-\mathbf{p}\|}$;
Trace_Regular_TPI_Curve(T, L, $\{\mathbf{p}_i\}$); /* Figure 5.4 */

end

else begin

if $\langle \mathbf{p}, \mathbf{N} \rangle = 0$ and $\langle \mathbf{e}_3, \mathbf{N} \rangle = 0$ **then**

(4) Compute_Cross_Sectional_Circles (T, L);

else /* Figure 5.5 */

(5) Trace_Regular_TPI_Curve(T,L,{$L \cap C_{R+r}(\mathbf{0}, \mathbf{e}_3)$});

end

end

end

A.2 TSI Algorithm for the Case of $0 < \delta \leq r$

Algorithm: Torus_Sphere_Intersection_I /* For the case of $0 < \delta \leq r$ */
Input: $T = T_{r,R}(\mathbf{0}, \mathbf{N})$; /* Torus */
$S = S_\delta(\mathbf{p})$; /* Sphere */
begin
if $\mathbf{p} \in T^O \setminus T^D$ **then begin** /* Figure 6.1(a) */
(1) $\mathbf{p}_T := \mathbf{p} + \delta \dfrac{\mathbf{p}_c - \mathbf{p}}{||\mathbf{p}_c - \mathbf{p}||}$, where $\mathbf{p}_c$ is the closest point of $C_R(\mathbf{0}, \mathbf{N})$ to $\mathbf{p}$;
Output($\{\mathbf{p}_T\}$);
end
else if $\mathbf{p} \in T^D$ and $\mathbf{p}$ is a vertex of T^D **then** /* Figure 6.1(b) */
Output($C_\Delta(\mathbf{q}, \mathbf{N})$), where $\Delta = \dfrac{\delta}{\delta + r} R$ and $\mathbf{q} = \dfrac{r}{\delta + r}\mathbf{p}$;
else if $\mathbf{p} \in T^D$ and $\mathbf{p}$ is not a vertex of T^D **then begin** /* Figure 6.1(c) */
(2) $\mathbf{p}_T := \mathbf{p} + \delta \dfrac{\mathbf{p}_f - \mathbf{p}}{||\mathbf{p}_f - \mathbf{p}||}$, where $\mathbf{p}_f$ is the farthest point of $C_R(\mathbf{0}, \mathbf{N})$ from $\mathbf{p}$;
Trace_Singular_TSI_Curve(T, S, $\{\mathbf{p}_T\}$);
end
else if $\mathbf{p} \in T^I$ **then**
if $0 < \delta < r$ **then begin** /* Figure 6.1(d) */
(3) $\mathbf{p}_T := \mathbf{p}_c + r \dfrac{\mathbf{p} - \mathbf{p}_c}{||\mathbf{p} - \mathbf{p}_c||}$, where $\mathbf{p}_c$ is the closest point of $C_R(\mathbf{0}, \mathbf{N})$ to $\mathbf{p}$;
Output($\{\mathbf{p}_T\}$),
end
else if $\delta = r$ **then** /* Figure 6.1(e) */
Output($C_r(\mathbf{p}, \mathbf{N}_\mathbf{p})$), where $\mathbf{N}_\mathbf{p} = \mathbf{N} \times \dfrac{\mathbf{p}}{||\mathbf{p}||}$;
else if $\mathbf{p} \in T^O_+ \cup T^I_-$ **then** /* Figures 6.2(a)–(b) */
Output($\emptyset$);
else if $\mathbf{p} \in T^O_- \cap T^I_+ \cap T^D_+$ **then begin** /* Figure 6.2(c) */
$\mathbf{p}_c :=$ the closest point of $C_R(\mathbf{0}, \mathbf{N})$ to $\mathbf{p}$;
(4) $\mathbf{p}_{SC} :=$ one point of $S \cap C_r(\mathbf{p}_c, \mathbf{N}_{\mathbf{p}_c})$, where $\mathbf{N}_{\mathbf{p}_c} = \mathbf{N} \times \dfrac{\mathbf{p}_c}{||\mathbf{p}_c||}$;
Trace_Regular_TSI_Curve(T, S, $\{\mathbf{p}_{SC}\}$);
end
else if $\mathbf{p} \in T^D_-$ **then** /* Figure 6.2(d) */
if $\mathbf{p} \times \mathbf{N} = \mathbf{0}$ **then**
(5) Compute_Profile_Circles (T, S);
else
(6) Trace_Regular_TSI_Curve(T,S,$S \cap C_r(C(0), \mathbf{N}_{C(0)})$),
end

A.3 TSI Algorithm for the Case of $0 < r < \delta$

Algorithm: Torus_Sphere_Intersection_II /* For the case of $0 < r < \delta$ */
Input: $T = T_{r,R}(\mathbf{p}, \mathbf{N})$; /* Torus */
$S = S_\delta(\mathbf{0})$; /* Sphere */
begin
DP:=$\{S_r(\mathbf{p}_i) \cap S \mid \mathbf{p}_i$ is a tangent intersection point in $C_R(\mathbf{p}, \mathbf{N}) \cap (S^O \cup S^I)$ $\}$;
if $C_R(\mathbf{p}, \mathbf{N}) \subset S^O_+ \cup S^I_-$ **then** /* There is no intersection */
Output($\emptyset$);
else if $C_R(\mathbf{p}, \mathbf{N}) \subset S^O_- \cap S^I_+$ **then** /* Figure 6.5(a) */
if $\mathbf{p} \times \mathbf{N} = \mathbf{0}$ **then**
(1) Compute_Profile_Circles (T, S);
else
Trace_Regular_TSI_Curve(T, S, $S \cap C_r(C(0), \mathbf{N}_{C(0)})$);
else if $|DP| = 1$ **then** /* Figures 6.5(b) and 6.5(e) */
Trace_Singular_TSI_Curve(T, S, DP);
else if $|DP| = 2$ **then** /* Figures 6.6(a)–(b) */
(2) Compute_Yvone_Villarceau_Circles(T, S, DP);
else if $C_R(\mathbf{p}, \mathbf{N})$ is embedded in S^I **then** /* Figure 6.6(c) */
Output($C_\Delta(\mathbf{q}, \mathbf{N})$), where $\Delta = \frac{\delta}{\delta - r} R$ and $\mathbf{q} = \frac{\delta}{\delta - r}\mathbf{p}$;
else if $C_R(\mathbf{p}, \mathbf{N})$ is embedded in S^O **then** /* Figure 6.6(d) */
Output($C_\Delta(\mathbf{q}, \mathbf{N})$), where $\Delta = \frac{\delta}{\delta + r} R$ and $\mathbf{q} = \frac{\delta}{\delta + r}\mathbf{p}$;
else begin
if there is only one circular arc C_1 in $C_R(\mathbf{p}, \mathbf{N}) \cap (S^O_- \cap S^I_+)$ **then begin**
(3) $\mathbf{q}$:= the middle point of C_1; /* Figure 6.5(c) */
$\mathbf{p}_i$:= a point in $S \cap C_r(\mathbf{q}, \mathbf{N_q})$, where $\mathbf{N_q} := \mathbf{N} \times \frac{\mathbf{q}-\mathbf{p}}{||\mathbf{q}-\mathbf{p}||}$;
Trace_Regular_TSI_Curve(T, S, $\{\mathbf{p}_i\}$);
end
else begin /* Figure 6.5(d) */
if $\langle \mathbf{p}, \mathbf{N} \rangle = 0$ and $||\mathbf{p}||^2 = R^2 + \delta^2 - r^2$ **then**
(4) Compute_Cross_Sectional_Circles (T, S)
else
(5) Trace_Regular_TSI_Curve(T,S,$\{S \cap C_{R+r}(\mathbf{p}, \mathbf{N})\}$);
end
end
end

A.4 TYI Algorithm for the Case of $0 < r \leq \delta$

Algorithm: Torus_Cylinder_Intersection_I /* For the case of $0 < r \leq \delta$ */
Input: $T = T_{r,R}(\mathbf{0}, \mathbf{e}_3)$; /* Torus */
$Y = Y_\delta(\mathbf{p}, \mathbf{N})$; /* Cylinder */
begin
if $C_R(\mathbf{0}, \mathbf{e}_3) \subset Y_+^O \cup Y_-^I$ **then** /* there is no intersection */
Output($\emptyset$);
else if $\mathbf{p} \times \mathbf{e}_3 = \mathbf{0}$ and $\mathbf{e}_3 \times \mathbf{N} = 0$ and $R - r \leq \delta \leq R + r$ **then**
Compute_Profile_Circles(T, Y); /* see Figure 3.5 */
else if $\delta = r$ and $\langle \mathbf{p}, \mathbf{e}_3 \rangle = 0$ and $\langle \mathbf{e}_3, \mathbf{N} \rangle = \mathbf{0}$
and $||\mathbf{p}||^2 = R^2 + \langle \mathbf{p}, \mathbf{N} \rangle^2$ **then begin**
Compute_Cross_Sectional_Circles(T, Y); /* see Figure 3.8 */
Trace_Singular_TYI_Curve(T, Y, { $\mathbf{q} \pm r\mathbf{e}_3$ }), where $\mathbf{q} = \mathbf{p} + \langle \mathbf{0} - \mathbf{p}, \mathbf{N} \rangle \mathbf{N}$;
end
else if $\delta = R$ and $\langle \mathbf{e}_3, \mathbf{N} \rangle^2 = \cos^2(\arcsin(r/R))$ and $||\mathbf{p} \times \mathbf{N}||^2 = r^2$ **then begin**
Compute_Yvone_Villarceau_Circles(T, Y); /* see Figure 3.11 */
Trace_Singular_TYI_Curve(T, Y, { $\mathbf{q} \pm R\frac{\mathbf{q}}{||\mathbf{q}||}$ }), where $\mathbf{q} = \mathbf{p} + \langle -\mathbf{p}, \mathbf{N} \rangle \mathbf{N}$;
end
else if $C_R(\mathbf{0}, \mathbf{e}_3) \subset Y_-^O \cap Y_+^I$ **then** /* Figure 7.6 */
(1) Trace_Regular_TYI_Curve(T, Y, $Y \cap C_r(C(0), \mathbf{N}_{C(0)})$);
else begin
for each circular arc C_i in $C_R(\mathbf{0}, \mathbf{e}_3) \cap ((Y_-^O \cap Y_+^I) \cup Y^I \cup Y^O)$ **do begin**
(2) $DP := \{\ C_r(\mathbf{p}_i, \mathbf{N}_{\mathbf{p}_i}) \cap Y \mid \mathbf{p}_i$ is a tangent intersection in $C_i \cap (Y^I \cup Y^O)\}$
$\cup\ \{\ C_r(\mathbf{p}_i, \mathbf{N}_{\mathbf{p}_i}) \cap Y \mid \mathbf{p}_i \in C_i \cap Y^I$ if $Y^I = l(\mathbf{p}, \mathbf{N})\ \}$;
if $|DP| \geq 1$ **then** /* Figures 7.2(c), 7.5, 7.7 */
(3) Trace_Singular_TYI_Curve(T, Y, DP);
else begin /* Figures 7.2(a)–(b) */
(4) $\mathbf{q}$:= an end point of C_i;
(5) $\mathbf{p}_Y := Y \cap B_r(\mathbf{q})$;
(6) l := a profile line of Y that passes through $\mathbf{p}_Y$;
(7) $\mathbf{p}_{TC}$:= the closest point to $\mathbf{p}_Y$ among those in $T \cap l$;
(8) Trace_Regular_TYI_Curve(T, Y, { $\mathbf{p}_{TC}$ });
end
end
end
end

A.5 TYI Algorithm for the Case of $0 < \delta < r$

Algorithm: Torus_Cylinder_Intersection_II /* For the case of $0 < \delta < r$ */
Input: $T = T_{r,R}(\mathbf{0}, \mathbf{e}_3)$; /* Torus */
$Y = Y_\delta(\mathbf{p}, \mathbf{N})$; /* Cylinder */
begin
if $\mathbf{p} \times \mathbf{e}_3 = \mathbf{0}$ and $\mathbf{e}_3 \times \mathbf{N} = \mathbf{0}$ and $R - r \leq \delta \leq R + r$ **then**
Compute_Profile_Circles(T, Y); /* see Figure 3.5 */
else begin
(1) $DP := \{\ C_\delta(\mathbf{q}, \mathbf{N}) \cap T \mid \mathbf{q}$ is a tangent intersection in $l(\mathbf{p}, \mathbf{N}) \cap (T^I \cup T^O \cup T^D)$
or $\mathbf{q}$ is an intersection point of $l(\mathbf{p}, \mathbf{N})$ and the vertices of $T^D\}$;
if $|DP| \geq 1$ **then**
(2) Trace_Singular_TYI_Curve(T, Y, DP);
for each connected line segment $l_i \subset l(\mathbf{p}, \mathbf{N}) \cap ((T^I_+ \cap T^O_-) \cup T^I \cup T^O)$
which does not intersect with $T^I \cup T^O$ tangentially, and $l_i \cap T^D = \emptyset$
do begin
(3) $\mathbf{q}$:= an end point of l_i;
(4) $\mathbf{p}_T := T \cap B_\delta(\mathbf{q})$;
(5) C := a cross-sectional circle of T which passes through $\mathbf{p}_T$;
(6) $\mathbf{p}_{TC}$:= the closest point to $\mathbf{p}_T$ among those in $Y \cap C$;
(7) Trace_Regular_TYI_Curve(T, Y, $\{\ \mathbf{p}_{TC}\ \}$);
end
if $l(\mathbf{p}, \mathbf{N}) \cap T^D_- \neq \emptyset$ **then begin**
if $|DP| = 0$ **then begin**
(8) $\mathbf{q}$:= an end point of $l(\mathbf{p}, \mathbf{N}) \cap T^D_-$;
(9) $\mathbf{p}_T$:= the tangent intersection point between $B_\delta(\mathbf{q})$ and T;
(10) C := the cross-sectional circle of T which passes through $\mathbf{p}_T$;
(11) $IP := \{$ two points in $Y \cap C$ which are minimum and maximum distance
(12) from $\mathbf{p}_T$ in polar coordinate $\}$;
end
else if ($|DP| = 2$ and the z-values of two points in DP have same signs)
or $|DP| = 1$ **then**
(13) $IP := \{$ the closest regular point from $\mathbf{0}$ in $C \cap l(\mathbf{p}, \mathbf{N})\ \}$,
where C is a cross-sectional circle of T which passes through
one of the points in DP;
Trace_Regular_TYI_Curve(T, Y, IP);
end
end
end

A.6 TKI Algorithm

Algorithm: Torus_Cone_Intersection
Input: $T = T_{r,R}(\mathbf{0}, \mathbf{e}_3)$; /* Torus */
$K = K_\theta(\mathbf{p}, \mathbf{N})$; /* Cone */
begin
(1) Detect_Circles_in_TKI (T, K); /* see Figures 3.6, 3.9, and 3.12 */
$DP := \{\ C_r(\mathbf{p}_i, \mathbf{N}_{\mathbf{p}_i}) \cap K \mid \mathbf{p}_i$ is a tangent intersection point
in $C \cap (K^I \cup K^O \cup K^D \cup K^B)$, or the vertex of K^D in $C \cap K^D$,
and $\mathbf{N}_{\mathbf{p}_i} = \frac{\mathbf{e}_3 \times (\mathbf{p}_i - \mathbf{0})}{\|\mathbf{e}_3 \times (\mathbf{p}_i - \mathbf{0})\|}$ $\}$;

if $C \cap (K^O_- \cap K^I_+ \cap K^D_+) = C$ and $|DP| = 0$ **then**
(2) $IP := IP \cup (C_r(C(0), N_{C(0)}) \cap K)$; /* see Figure 8.6 */
else begin
for each connected component $C_i \subset K^O_- \cap K^I_+$ **do begin**
if $C_i \cap (K^D \cup K^D_-) = \emptyset$ **then begin**
$\mathbf{q}$:= an end point of C_i;
$\mathbf{p}_K$:= the tangent intersection point between $B_r(\mathbf{q})$ and K;
l := a profile line of K which passes through $\mathbf{p}_K$;
(3) $IP := IP \cup \{$ the closest point from $\mathbf{p}_K$ in $l \cap T$ $\}$;
end
else begin
l := an arbitrary profile line of K;
(4) $IP := IP \cup \{\ \mathbf{q} \mid \mathbf{q} \in l \cap T\ \}$;
for each connected component $C_k \subset C_i \setminus (K^D_- \cup K^D)$ **do**
if both end points of C_k are on K^D **then**
(5) $IP := IP \cup \{\ \mathbf{q} \mid \mathbf{q} \in C_r(\mathbf{p}_m, \mathbf{N}_{\mathbf{p}_m}) \cap K$, $\mathbf{p}_m$ is the middle point
of C_k and $C_r(\mathbf{p}_m, \mathbf{N}_{\mathbf{p}_m})$ is a cross-section circle of T at $\mathbf{p}_m$ $\}$;
end
end
end

if $|DP| \geq 1$ **then**
(6) Trace_Singular_TKI_Curve(T, K, DP);
if $|IP| \geq 1$ **then**
(7) Trace_Regular_TKI_Curve(T, K, IP);
end

A.7 TTI Algorithm

Algorithm: Torus_Torus_Intersection
Input: $T_1 = T_{\delta,\Delta}(\mathbf{0}, \mathbf{e}_3)$; /* Torus */
$T_2 = T_{r,R}(\mathbf{p}, \mathbf{N})$; /* Torus */
begin
(1) Detect_Circles_in_TTI (T_1, T_2);
$DP := \{\ C_r(\mathbf{p}_i, \mathbf{N}_{\mathbf{p}_i}) \cap T_1 \mid \mathbf{p}_i$ is a tangent intersection point in $C \cap (T^I \cup T^O \cup T^D)$, or a vertex of T^D in $C \cap T^D$, and $\mathbf{N}_{\mathbf{p}_i} = \frac{\mathbf{N} \times (\mathbf{p}_i - \mathbf{p}_2)}{||\mathbf{N} \times (\mathbf{p}_i - \mathbf{p}_2)||}$ \};
if $r = \delta$ **then**
$DP := DP \cup \{\ C_r(\mathbf{p}_i, \mathbf{N}_{\mathbf{p}_i}) \cap T_1 \mid \mathbf{p}_i \in T^I \cap C$ and $\mathbf{N}_{\mathbf{p}_i} = \frac{\mathbf{N} \times (\mathbf{p}_i - \mathbf{p}_2)}{||\mathbf{N} \times (\mathbf{p}_i - \mathbf{p}_2)||}$ \};

if $C \cap (T^O_- \cap T^I_+ \cap T^D_+) = C$ and $|DP| = 0$ **then**
(2) $IP := IP \cup (C_r(C(0), \mathbf{N}_{C(0)}) \cap T_1)$;
else
for each connected component $C_i \subset T^O_- \cap T^I_+$ **do begin**
if $C_i \cap (T^D \cup T^D_-) = \emptyset$ and $C_i \neq C$ **then begin**
$\mathbf{q}$:= an end point of C_i;
$\mathbf{p}_T$:= the tangent intersection point between $B_r(\mathbf{q})$ and T_1;
C_T := the cross-sectional circle of T_1 which passes through $\mathbf{p}_T$;
(3) $IP := IP \cup \{$ the closest point from $\mathbf{p}_T$ in $C_T \cap T_2$ \};
end
else begin
C_1 := an arbitrary cross-sectional circle of T_1;
(4) $IP := IP \cup \{\ \mathbf{q} \mid \mathbf{q} \in T_2 \cap C_1$ \};
for each connected component $C_k \subset C_i \cap (T^O_- \cap T^I_+ \cap T^D_+)$) **do**
if two end points of C_k are on T^D **then**
(5) $IP := IP \cup \{\ \mathbf{q} \mid \mathbf{q} \in C_r(\mathbf{p}_m, \mathbf{N}_{\mathbf{p}_m}) \cap T_1$, $\mathbf{p}_m$ is the middle point of C_k and $C_r(\mathbf{p}_m, \mathbf{N}_{\mathbf{p}_m})$ is a cross-section circle of T_2 at $\mathbf{p}_m$ \};
end
end

if $|DP| \geq 1$ **then**
(6) Trace_Singular_TTI_Curve(T_1, T_2, DP);
if $|IP| \geq 1$ **then**
(7) Trace_Regular_TTI_Curve(T_1, T_2, IP);
end

Appendix B

Torus/Circle Intersection

We introduce a method to compute the intersection between a torus T and a circle C: $T = T_{r,R}(\mathbf{0}, \mathbf{e}_3)$, where $\mathbf{0} = (0,0,0)$ and $\mathbf{e}_3 = (0,0,1)$, and $C = C_\Delta(\mathbf{p}, \mathbf{N})$, where $\mathbf{p} = (p_x, p_y, p_z)$. Firstly, we compute the intersection $T \cap L$, where L is a main plane of C: $L = L(\mathbf{p}, \mathbf{N})$. By computing the intersection of $T \cap L$ and C, we can compute the intersection points between T and C.

We denote the main plane of C as L whose basis vectors are $\mathbf{v}_1$ and $\mathbf{v}_2$, where $\mathbf{v}_1 = (v_{1x}, v_{1y}, v_{1z})$, $\mathbf{v}_2 = (v_{2x}, v_{2y}, v_{2z})$. There are relations between $\mathbf{v}_1$, $\mathbf{v}_2$, and $\mathbf{N}$ as follows: $\langle \mathbf{v}_1, \mathbf{v}_2 \rangle = \langle \mathbf{v}_1, \mathbf{N} \rangle = \langle \mathbf{v}_2, \mathbf{N} \rangle = 0$, and $\langle \mathbf{v}_1, \mathbf{v}_1 \rangle = \langle \mathbf{v}_2, \mathbf{v}_2 \rangle = 1$.

T is in a standard position, thus we may represent T in the implicit equation:

$$T(x,y,z) = (x^2 + y^2 + z^2 + R^2 - r^2)^2 - 4R^2(x^2 + y^2) = 0, \tag{B.1}$$

and we formulate L and C as follows:

$$L(s,t) = \mathbf{p} + s\mathbf{v}_1 + t\mathbf{v}_2, \tag{B.2}$$

$$C(s,t) = s^2 + t^2 - \Delta^2 = 0. \tag{B.3}$$

To compute $T \cap L$, we need to solve the system of Equation (B.1) and Equation (B.2).

We can derive the parametric formula of the intersection curve between T and L by substituting the parameters x, y, z of T with the parameters s, t of L as follows:

$$\begin{aligned} x &= p_x + sv_{1x} + tv_{2x}, \\ y &= p_y + sv_{1y} + tv_{2y}, \\ z &= p_z + sv_{1z} + tv_{2z}. \end{aligned}$$

The terms $x^2+y^2+z^2$ and x^2+y^2 are represented by the parameters s and t as follows:

$$\begin{aligned} x^2+y^2+z^2 &= ||(x,y,z)||^2 \\ &= ||\mathbf{p}+sv_1+tv_2||^2 \\ &= s^2+t^2+2s\langle \mathbf{p},v_1\rangle + 2t\langle \mathbf{p},\mathbf{v}_2\rangle + ||\mathbf{p}||^2, \\ x^2+y^2 &= (p_x+sv_{1x}+tv_{2x})^2+(p_y+sv_{1y}+tv_{2y})^2. \end{aligned}$$

The equation of $T \cap L$ is represented as follows:

$$\begin{aligned} (T\cap L)(s,t) &= (s^2+t^2+2s\langle \mathbf{p},\mathbf{v}_1\rangle + 2t\langle \mathbf{p},\mathbf{v}_2\rangle + ||\mathbf{p}||^2+R^2-r^2)^2 \\ &\quad -4R^2((p_x+sv_{1x}+tv_{2x})^2+(p_y+sv_{1y}+tv_{2y})^2) \qquad \text{(B.4)} \\ &= 0. \end{aligned}$$

The intersection points between C and $T \cap L$ are a solution of Equation (B.3) and Equation (B.4). From Equation (B.3), we derive the equation $s^2+t^2=\Delta^2$. We can replace the term s^2+t^2 in Equation (B.4) by Δ^2, and the term t^2 by Δ^2-s^2, thus, $C \cap (T \cap L)$ is a solution for the following two equations:

$$\begin{aligned} &s^2+t^2-\Delta^2=0, \\ &c_4s^2+c_3st+c_2s+c_1t+c_0=0, \end{aligned}$$

where c_i $(0 \le i \le 4)$ is a constant value. This system is reduced as follows:

$$\begin{aligned} &(c_3^2+c_4^2)s^4+2(c_4c_2+c_3c_1)s^3+(2c_0c_4-c_3^2\Delta^2+c_1^2+c_2^2)s^2 \\ &+2(-\Delta^2c_3c_1+c_0c_2)s+c_0^2-\Delta^2c_1^2=0 \\ &t=-\frac{c_4s^2+c_2s+c_0}{c_3s+c_1} \end{aligned}$$

The quartic polynomial equation is solved in closed form; thus, we can compute the intersection points of $T \cap C$ efficiently and robustly.